ADVANCED TESTING AND CHARACTERIZATION OF TRANSPORTATION SOILS AND BITUMINOUS SANDS

BY

JOSEPH K. ANOCHIE-BOATENG

B.S., University of Science & Technology, 1994
M.S., North Carolina A & T State University, 2002

DISSERTATION

Submitted in partial fulfillment of the requirements
for the degree of Doctor of Philosophy in Civil Engineering
in the Graduate College of the
University of Illinois at Urbana-Champaign, 2007

Urbana, Illinois

Doctoral Committee:

Associate Professor Erol Tutumluer, Chair
Professor Imad L. Al-Qadi
Professor Emeritus Samuel H. Carpenter
Professor Emeritus Marshall R. Thompson
Dr. Liqun Chi, Caterpillar Inc., Peoria, IL

ABSTRACT

New and improved laboratory test procedures have been developed as a suite of tests to characterize the behavior of one fine-grained cohesive soil and three naturally occurring bituminous or oil sand materials. The overall objective was to determine behavior of these geomaterials under field loading conditions of off-road construction and mining equipment. The test procedures were used to conduct a comprehensive laboratory testing program to determine both static and dynamic properties, and deformation characteristics of the cohesive soil and the oil sand materials, with bitumen contents of 8.5%, 13.3% and 14.5% by weight. The soil sample was tested at moisture states chosen at the optimum moisture content, 3% below and 3% above the optimum. The complete test data provided an extensive database of material properties including friction angle and cohesion strength properties, bulk modulus, shear modulus, resilient modulus, dynamic modulus, damping ratio, and permanent deformation characteristics.

Moisture content was the main parameter that affected material properties of the soil sample. The strength and modulus values of the soil generally increased for the 3% below the optimum moisture condition and decreased for the 3% above the optimum. Also, bitumen content commonly affected modulus and permanent deformation properties of the oil sand materials. The oil sand sample with 8.5% bitumen content had the highest modulus values whereas the sample with 14.5% had the lowest. Moreover, permanent deformation accumulation was higher in the oil sand sample with 14.5% bitumen content than the sample with 8.5%. The behavior of the oil sand samples with bitumen contents of 13.3% and 14.5% were similar. Generally, all the three oil sand materials appeared to have stress softening modulus behavior similar to fine-grained soils, and their stiffness trends under different temperatures and loading frequencies were typical of asphalt materials.

Based on the individual databases, material property correlations and characterization models were developed for the soil and oil sand samples using the applied stress states, loading frequency, test temperature and bitumen content as variables. The correlations and models may be used as practical predictive equations to estimate strength and stiffness behavior of fine-grained soils and oil sand materials, and predict the amount of rutting and sinkage in the field.

To Father and Mother

ACKNOWLEDGEMENTS

I am very grateful to Dr. Erol Tutumluer for his immense contribution to my entire doctoral degree studies at the University of Illinois at Urbana-Champaign (UIUC). Dr. Tutumluer served as the director of my research and chairman of my dissertation committee. My sincere thanks go to the dissertation committee members: Dr. Imad Al-Qadi, Dr. Sam Carpenter, Dr. Marshall Thompson, and Dr. Liqun Chi of Caterpillar, Inc., Peoria, Illinois. Their interest in this study and individual efforts to shape this dissertation are commendable. I am grateful to Dr. Barry Dempsey, the immediate past director and Dr. Imad Al-Qadi, the current director of the University of Illinois Advanced Transportation Research and Engineering Laboratory (ATREL), where I conducted this research and many other research projects. I am also grateful to Caterpillar Inc. Technical Division office at Peoria, Illinois, who sponsored this research, and again, acknowledge Dr. Liqun Chi for his help and collaborative efforts in funding this research, providing the oil sand samples and his valuable insights in this study.

Many thanks go to my divine brother, Dr. Francis Kofi Andoh-Baidoo, his wife Rosemarie, a PhD Candidate at the Virginia Commonwealth University, and their family. I would also like to appreciate my uncle Samuel Kyei of Greensboro, North Carolina, my wife Joana, my entire family and loved ones in Ghana, my friend and colleague Dr. Alex Kwame Apeagyei, other friends and all research assistants at ATREL. Each one of these played a key role in my studies at UIUC. I would also like to appreciate the staffs of both ATREL and Civil Engineering Transportation group for their support and assistance during the entire period of my doctoral studies. Finally, I am grateful to the Almighty God for given me the strength and grace to successfully complete my doctoral studies.

TABLE OF CONTENTS

LIST OF TABLES

LIST OF FIGURES

CHAPTER 1 INTRODUCTION

1.1 Background

The routine operations of large capacity off-road construction and mining equipment on fine-grained cohesive soils and naturally occurring bituminous sand materials (oil /tar sands) have become a concern to the construction, mining and equipment manufacturing sectors. A major problem is mobility (trafficability) of large capacity haul trucks and shovels on oil sand materials during the hottest months in spring and summer, and stability of fine-grained cohesive soils. Researchers have extensively investigated the behavior of fine-grained subgrade cohesive soils (Thompson and Robnett 1979, Bejarano and Thompson 1999). Others have also studied the behavior of oil sand materials in the laboratory and field (Dusseault and Morgenstern 1978a-b, Hsu et al. 1985, Samieh and Wong 1997 and1998, Joseph 2002 and 2005). All of these studies indicate that behavior of fine-grained soils and oil sands are primarily influenced by type of loading, nature of applied stresses, and material properties including density, moisture, and grain size distribution.

Fine-grained cohesive soils are commonly dealt with in transportation engineering for preparing the subgrade foundation for transportation facilities. Subgrade soils and aggregates constituting the foundation of highway and airport pavements as well as railroad track often exhibit different and unique responses to loading from construction equipment. The soil composition, grain size and physical properties as well as the type of applied static and dynamic loads and the nature of resulting stresses acting upon them primarily dictate the behavior. Both fine-grained cohesive and cohesionless granular soils referred to here as geomaterials exhibit stress dependent, nonlinear, and elastoplastic (combined elastic and plastic) behavior under the routine operation of construction and mining equipment.

Oil sands, or tar sands are natural deposits of bituminous sand materials that are mined for crude oil production. The world's largest oil sand deposits are found in the Alberta Province in Canada. The typical 8% to 15% by weight of bitumen or asphalt content in the oil sand composition makes these naturally occurring sands low load-bearing materials for haul trucks, shovels and other mining equipment.

Joseph et al. (2003) observed trucks and shovels operating on these soft materials in summer to face with sinkage, rutting and trafficability problems. This is due to the fact that equipment mobility and/or rolling resistance is adversely affected by equipment tire sinkage, which is measured when the wheel is loading the soil as opposed to the permanent deformation or rutting accumulating at an observation point in the soil when the wheel is making a number of passes (Saarilahti 2002). Thus, sinkage could be linked to the permanent strain accumulation in the material during the first few load applications, whereas rutting is the permanent strain accumulated after several thousands of load applications. On the other hand, the rolling resistance of a wheel (or a track) is the force opposing the motion of the wheel as it rolls on a surface of soil. Therefore, rolling resistance is a function of the strength and deformation properties of the soil, and tire size and dimensions.

The relationship between sinkage and rolling resistance is demonstrated in Figure 1.1. Rolling resistance is associated with traction and sinkage. Traction is a measure of the shear stress applied and the contact surface. The deeper a wheel sinks into the surface, the higher is the rolling resistance. The main factors affecting sinkage and rolling resistance are vehicle wheel characteristics, types of soils and strength properties of the soil.

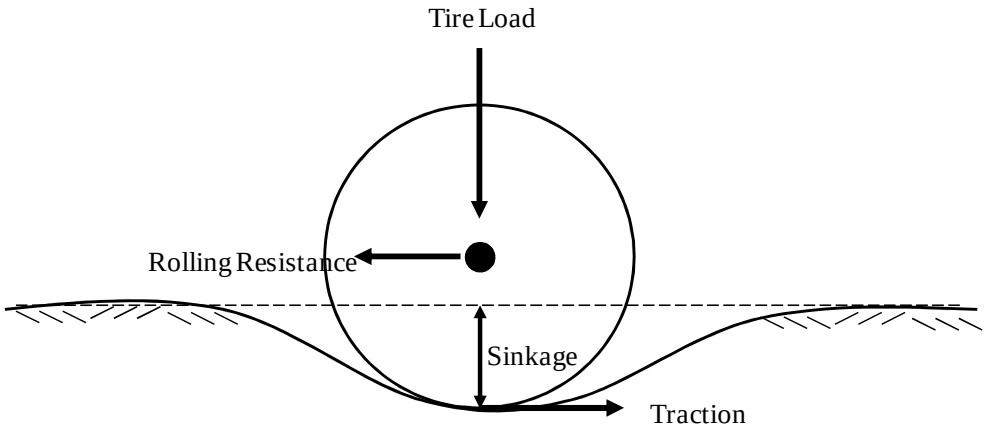

FIGURE 1.1 A Schematic Representation of Sinkage and Rolling Resistance of a Wheel

A detailed review of the research findings by Joseph (2005) also reveals that the modulus and deformation behavior of oil sands are primarily dependent upon the applied load magnitude (wheel load in the field), rate of loading or frequency, and number of load applications. The confinement under the truck wheels are rather large up to 500 kPa in the loose 6 to 8 meters of soil near ground, which are generally unsaturated and not significantly affected by pore pressure development upon loading. The oil sands exhibit stress-softening behavior, which is typically observed instead in fine-grained type silty and clayey soils. The composition governed by the fluid content (bitumen + water), grain size and physical properties as well as the type of applied loading, i.e., static and/or dynamic, and the nature of resulting stresses acting upon them primarily dictate the behavior.

To better understand the behavior of fine-grained soils and oil sand materials under operations of construction and mining equipment, it is important to properly address the actual time and temperature dependent, viscous, elastic and plastic deformation characteristics under both static monotonically increasing and dynamic repeatedly applied or cyclic loading conditions. Further, to characterize behavior of these geomaterials, there is a need to conduct laboratory tests that closely simulate field densities and loading conditions. A comprehensive laboratory testing program should consider experimental designs with full factorials of governing or controlling test parameters and material properties and permit application of a wide variety of stress states on the specimen. Such an experimental study would provide measurements, control, and improvement of in situ properties of the geomaterials during construction and mining activities.

Current laboratory test procedures for characterizing fine-grained cohesive soils and oil sands have certain limitations. They do not, in general: (a) apply combinations of various static and dynamic loading conditions on the specimen; (b) pulse the confining pressures on the specimen; (c) control the horizontal and vertical stresses independently on the sample for applying extension states; and (d) apply different loading frequencies during testing. In addition, the majority of the geomaterial models to date do not adequately predict the behavior of soils and oil sand materials under construction and mining equipment.

This is because most of the available models for geomaterials are based on laboratory stress-strain test data obtained from limited loading conditions. Therefore, improved or new laboratory testing procedures are needed to better study the behavior of these geomaterials.

This research study was intended to develop laboratory test procedures for advance testing and characterization of fine-grained cohesive soils and oil sand materials. The test procedures are based on typical field loading conditions and the loading characteristics of large capacity construction and mining equipment. The study also aimed to provide a better understanding of the behavior of the materials tested, and support efforts to properly model soil and oil sand behavior under both static and dynamic loads. The laboratory test results were also intended to provide both a comprehensive database of geomaterial properties that can be used to improve designs of construction and mining equipment and a set of guidelines for the future development of laboratory testing protocols and material characterization models for predicting the behavior of fine-grained cohesive soils and oil sand materials.

1.2 Problem Statement

There is a growing concern about the routine operations of large capacity off-road compaction, construction and mining trucks and shovels on fine-grained cohesive soils and oil sand materials due to problems with mobility, sinkage and unwanted vibration. The existing laboratory testing and material characterization models do not adequately address the behavior of these problematic geomaterials under field loading conditions of construction and mining equipment.

1.3 Objectives and Scope

The overall research objective in this study is to better understand the behavior of fine-grained cohesive soils and oil sand materials under field loading conditions of off-road construction and mining equipment, and develop performance-based elastic and plastic deformation models for predicting strength, stiffness and deformation characteristics such as initial sinkage and rutting potential of these geomaterials.

Specific objectives pursued are as follows:

(1) Develop laboratory testing procedures to adequately characterize behavior of fine-grained cohesive soils and oil sand materials under dynamic loading conditions of field loading of off-road construction and mining equipment.

(2) Conduct laboratory tests following the developed test procedures on one fine-grained cohesive soil and three types of oil sand samples to determine strength, modulus and damping properties and permanent deformation accumulation under laboratory applied stresses that are representative of field loading conditions.

(3) Establish databases of material properties from the laboratory testing program, and develop material characterization models for the tested soil and oil sand strength, modulus, and damping properties.

(4) Develop permanent deformation models for predicting field sinkage and rutting potentials in oil sand materials.

The scope of this laboratory research effort was limited to testing one fine-grained cohesive subgrade soil and three different oil sand materials. The soil sample was A-6 clay soil, and obtained from Caterpillar Inc. Demonstration Training Center in Edwards, Illinois. The oil sand samples used for the study were one low grade and two high grade material obtained from Suncor Energy Inc. and Syncrude Canada Ltd. oil sand mines in Canada. Laboratory tests performed on these geomaterials are (1) hydrostatic loading tests, (2) monotonic loading shear strength test, (3) repeated load triaxial modulus and permanent deformation test, (4) pure shear loading tests, and (5) damping property tests.

1.4 Outline of Dissertation

This dissertation is divided into nine chapters. Chapter 1 consists of a detailed discussion of the research background and the motivation and anticipated contribution of the entire study to the research community.

Chapter 2 presents a review of the existing laboratory test procedures and characterization models for fine-grained cohesive soils and oil sand materials. A brief description of the existing test procedures and discussions of state-of-the-art advanced testing equipment selected for this study is presented.

In addition, Chapter 2 discusses the existing material characterization models including wheel and soil interaction models for fine-grained cohesive soils and oil sand materials. The limitations of the existing test procedures and the characterization models are also summarized in this chapter.

In Chapter 3, new and/or improved laboratory test procedures are developed for fine-grained soils and oil sand materials. Some of these new innovative and comprehensive test procedures provide improved testing protocols for determining strength, modulus and deformation characteristics of soils and oil sand materials. Results of the preliminary laboratory tests conducted on one fine-grained soil and three oil sand samples are presented, and various laboratory testing equipment suitable for standard and advanced testing are described. The methods of sample preparation and detailed elaborations of the significance and use of the developed test procedures are also given in this chapter.

Chapter 4 focuses on characterizing bulk moduli of the soil and oil sand samples using the hydrostatic compression testing procedure. The test results are used to develop material property correlations and bulk modulus characterization models for the soil and oil sand samples.

In Chapter 5, shear strength properties are determined using triaxial and direct shear tests. The triaxial shear strength test is used to determine the properties of the soil sample, while both the triaxial and direct shear tests are used for determining the properties of the oil sand samples. The Mohr-Coulomb criterion is used to characterize the strength of the soil and oil sand samples. The effects of various test parameters and loading conditions on the shear strength properties are also discussed in this chapter.

Chapter 6 focuses mainly on permanent deformation behavior of the three oil sand materials. This chapter describes comprehensive laboratory tests conducted in this study. A newly developed repeated load test procedure is used to determine permanent deformation characteristics and the resilient behavior of the three oil sand materials. The test data are then analyzed to develop permanent deformation models. The resilient behavior of the oil sand materials is also characterized using existing stress-dependent modulus models.

Chapter 7 presents shear modulus characterization of the soil and oil sand samples using a newly developed pure shear loading test procedure. In this chapter, the standard cyclic triaxial test procedure for determining shear modulus of soils is also employed to conduct tests on the oil sand samples at selected loading conditions. In addition to the shear modulus property, the phase angles of the tested materials are reported. Comparisons of the obtained shear moduli are made between the standard cyclic and the newly developed pure shear tests. Test results obtained from the two procedures are used to develop shear modulus characterization models.

A new laboratory test procedure developed for determining the damping properties of fine-grained soils and oil sand materials are presented in Chapter 8. Based on the test results, various characterization models are developed for the dynamic modulus and damping ratio properties. The sigmoidal model used for characterizing asphalt materials is also employed to model dynamic modulus of the oil sand samples. The effects of various loading conditions on dynamic modulus and damping ratio properties are also discussed in this chapter.

Chapter 9 summarizes the research findings and recommendations for future work. The general findings are outlined, and separate findings are grouped according to individual tests. Recommendations are made on how to effectively evaluate the responses and behavior of fine-grained cohesive soils and oil sand materials under large capacity construction and mining equipment.

CHAPTER 2 REVIEW OF GEOMATERIALS TEST PROCEDURES AND CHARACTERIZATION MODELS

2.1 Introduction

Over the years, considerable progress has been made to develop laboratory test procedures and material characterization models to enhance the understanding of the behavior of soils and oil sands under cyclic and monotonic loading conditions. The major limitation is how these laboratory test procedures can effectively reproduce field stress conditions, and simulate the combined effects of both static and cyclic/dynamic loading, which typically occur in an element of a foundation geomaterial during construction and mining activities of mobile equipment. Another difficulty is to accurately predict the damaging field loading effects of large mobile equipment including haul trucks and shovels. When the limitations of existing testing procedures and characterization models are properly addressed for fine-grained soils and oil sand materials, reliable test results and accurate models could be developed to characterize their engineering behavior.

2.2 Current Laboratory Testing for Material Characterization

Current laboratory test methods used to determine soils/geomaterial properties mostly include (a) direct shear, (b) simple shear test, (c) cyclic triaxial test, (d) repeated load triaxial test, (e) true triaxial test, and (f) hollow cylinder tests. These test procedures, under various conditions have been extensively used to investigate both static and dynamic loading behavior of soils/geomaterials. Recently, triaxial compression tests have been extended for performance-based testing of bituminous materials (AASHTO TP7-94). A brief description of each test procedure is presented under this section, including a discussion of the limitations and advantages of the various testing devices.

2.2.1 Direct Shear Testing

Direct shear test is commonly used to determine the shear strength properties of soils in the laboratory. The current standard procedure for direct shear test is ASTM D3080. In the direct shear test, a normal load is first applied to the specimen in a shear box, and shear load is applied to fail the specimen. The data collected are used to determine friction angle and cohesion properties of the sample. The principle behind direct shear test is quite simple, and the test is easy to perform.

The direct shear test equipment is commercially available, and it is not expensive. The specimen failure is forced to occur on or near a horizontal plane at the middle of the specimen. Also the shear stresses and specimen deformations are not uniformly distributed within the specimen.

2.2.2 Simple Shear Testing

In the simple shear test device for soils, a cyclic horizontal shear stress is applied at the top or bottom of a laterally constrained specimen after consolidating it under an initial vertical stress. The loading condition of this test results in zero to +/- 90 degree principal stress axis rotation and accompanying reversal of shear stress. The simple shear tests can determine permanent deformation accumulation in the specimen during testing due to its capabilities to simulate shear stress reversal in the field. Problems in performing this test include the difficulties in the application of uniform shear stress at the top of the specimen and the development of uniform shear deformations throughout the specimen. Further, it is often difficult to prevent slippage along the top and bottom loading plates and to simulate a continuous rotation of the principal stresses, which occurs in a soil element during dynamic loading.

2.2.3 Cyclic Triaxial Testing

Owing to the availability of test equipment, the cyclic triaxial test has been commonly used to determine modulus and damping properties of soils. During the test, cylindrical specimens are subjected to a cyclic variation in the axial stress, which is intended to simulate the cyclic shear stresses experienced by an element of soil/geomaterial in the field during dynamic type of loading. As illustrated in Figure 2.1, the cyclic deviator stress $\Delta\sigma$ is applied such that the specimen is subjected to alternating cycles of vertical compression and extension about an all-around effective consolidation stress of $\sigma_c^{'}$. A corresponding cyclic shear stress is produced on the 45 degree plane. One of the major shortcomings of the cyclic triaxial shear test is that unlike in the field where stresses vary in both radial and vertical directions, an equal all-around pressure is assumed for confinement.

The stress path of the applied cyclic load is not oriented vertically (see Figure 2.1) but it is rather in the direction of axial compression and does not provide a good representation of the shear stresses induced in the ground as a result of dynamic loading. Due to the isotropic confinement, the variation in the shear stress on any plane is not symmetric throughout the cyclic loading.

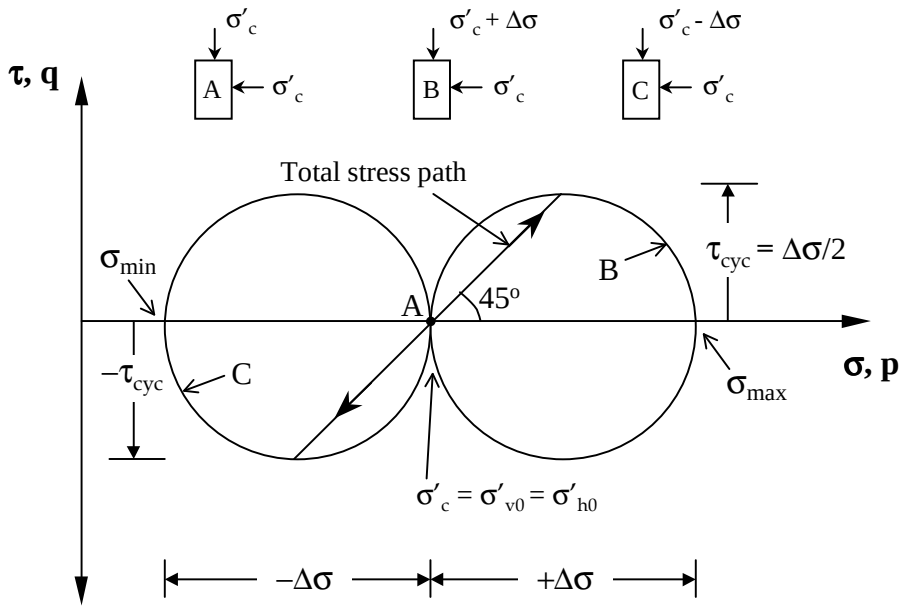

FIGURE 2.1 Stress Components in Cyclic Triaxial Tests: An Isotropically Consolidated Specimen.

2.2.4 Repeated Load Triaxial Testing

The principles of cyclic triaxial test have been extended to the field of pavement engineering to perform the repeated load triaxial test to simulate highway or airport type of loading. The major difference is that in the repeated load triaxial test, transient loads which are well below failure stresses are applied on the specimen. The AASHTO T307 is the current test procedure to perform standard repeated load triaxial test to determine the resilient properties for unbound materials and subgrade soils. The initial conditioning stage of this test is used for permanent deformation characterization of geomaterials in a limited capacity. The test has been mainly used to simulate highway loading conditions in the laboratory.

During testing, cylindrical specimens are subjected to different repeated/pulsed stress states under different constant all-around confining pressures to simulate lateral stress caused by the overburden pressure and dynamically applied wheel loadings. The test device is commercially available, and the size of the specimen required is reasonable for field representation and laboratory preparation. However, the current repeated load triaxial test procedure is unable to simulate horizontal dynamic stresses applied on a pavement element under a wheel load in a constant confining pressure triaxial test. In addition, the highest confining pressure and axial stress applied during laboratory testing is limited, and cannot simulate field situations where confining pressure exceeds the applied axial stress, i.e., extension loading. The maximum stress ratio is also limited to 2.0 in the standard AASHTO T307 test procedure, which is not enough to simulate higher field stress ratios.

2.2.5 True Triaxial Testing

The true triaxial test is used to include the effects of applied intermediate principal stress, which is often different than the major and minor principal stresses, to investigate anisotropy or directional dependency in material properties. The test allows the application of three principal stresses independently on six faces of a cubical specimen compared to the only two normal stresses applied in the standard triaxial and simple shear tests. The setup for true triaxial device is often complex, and preparation of the cubical specimen is extremely difficult. This characteristic makes the true triaxial test setup somewhat unsuitable for routine laboratory testing.

2.2.6 Hollow Cylinder Testing

The hollow cylinder test allows for both isotropic and anisotropic initial stress conditions to be applied on the specimen. Chan and Brown (1984), and Alavi (1992) reported hollow cylinder test to closely simulate all the field complex stress conditions including principal stress axis rotation to which geomaterial element is subjected during testing. The hollow cylinder test is flexible to applying different stress path loading for characterizing granular material and soil behavior. The test procedure is particularly suitable to investigate permanent deformation accumulation under various stress states applied by moving wheel loads.

However, torsional shear equipment used for this test is not widely available, and specimen preparation procedure can be very difficult due to the placement of two membranes both internally and externally on the specimen. Another limitation is that interpretation of test results is rather complicated and may not permit correlation with other tests (Ishibashi and Sherif 1974). Furthermore, the shape of the specimen makes the device impractical for use in conventional practice.

2.3 Advanced Testing Equipment and Capabilities

In this study, state-of-the art laboratory specimen preparation and testing equipment for soils/geomaterials and asphalt material characterizations are selected to address the limitations of current laboratory test procedures and testing equipment. All the specimen preparation and testing equipment to be discussed are currently used for characterizing transportation materials including bituminous materials, unbound granular materials and soils at the Advanced Transportation Research and Engineering Laboratory (ATREL) located at University of Illinois. Detailed descriptions and capabilities of five selected devices are presented next.

2.3.1 Advanced Triaxial Testing Equipment (UI-FastCell and RaTT cell)

Two advanced cyclic/repeated load triaxial testing devices at ATREL, University of Illinois FastCell (UI-FastCell), and the Industrial Process Controls (IPC), Ltd rapid triaxial testing cell (RaTT cell) can be conveniently used for soils and bituminous materials testing. In addition to pulsing stresses in the vertical direction, these testing devices offer the extra capability to apply dynamic stresses in the radial/horizontal direction to better simulate field stress states under traffic/moving wheel loads and measure anisotropic material stiffness properties if needed. Both the UI-FastCell and RaTT cell use a one to one (1:1) specimen height to diameter ratio in their setups with no need for specimen trimming and gluing to end plates. Compared to RaTT cell, the UI-FastCell system also allows the more rapid application of higher static radial stresses through the use of hydraulic oil-filled confining chamber. The test setup for UI-FastCell also enables measuring shear stress reversals due to dynamic loading that involves a change in total shear stress direction (Tutumluer and Thompson, 1997a-b).

2.3.1.1 Description of UI-FastCell

The UI-FastCell device was custom-designed and manufactured by the Industrial Process Controls (IPC), Ltd. Company in Australia. The device was designed based on concepts which resulted from successful research findings by Tutumluer (1995), Tutumluer and Thompson (1997a-b). UI-FastCell uses a fluid/air interface to minimize compressibility effects when conducting tests in which the horizontal stress on a specimen must be cycled. Figure 2.2a shows the UI-FastCell with the confinement cell lowered down on the specimen for the testing position. An air actuator is used to apply the axial pressure to the specimen, and the confining pressures are cycled through a hydraulic fluid within a rubber membrane. The driving cylinders on the back of the confining *cell* (not shown here) include an air-fluid interface, which provides *fast* application and switching of the dynamic loading. Figure 2.2b is an illustration of the cylindrical specimen, 150-mm in diameter by 150-mm (approximately 6-in diameter by 6-in) high under independently applied vertical and radial stresses and the instrumentation consisting of linear variable displacement transducers (LVDTs) measuring axial and radial specimen deformations.

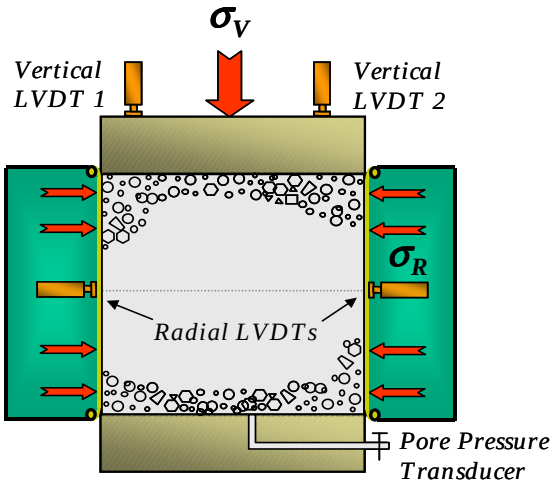

(a) Photo of UI-FastCell (b) Instrumentation and Cylindrical Specimen

FIGURE 2.2 University of Illinois's Advanced Triaxial Testing Device (UI-FastCell).

The UI-FastCell specifically offers the following highly beneficial capabilities in laboratory geomaterial characterization, (a) measurement of on sample vertical and radial displacements, and axial force and displacement external to cell; (b) a bladder type horizontal confinement chamber with a built-in membrane which is inflated to apply variable confining pressures during vertical cyclic loading; (c) independently cycling either vertical or radial stress in phase or out of phase, or cycling both vertical and radial stresses simultaneously at different stress levels, in compression or extension type loading; and (d) applying shear stress reversals by changing principal load/stress direction on the same specimen with applied radial pulse stresses exceeding the vertical one. Since its inception, the UI-FastCell has been used to perform several geomaterial characterization tests (Tutumluer and Seyhan 1999, Seyhan 2002, Kim 2005, Kim and Tutumluer 2006).

2.3.1.2 Description of RaTT Cell

The RaTT cell device uses IPC's universal testing machine series, UTM-5P system, with an environmental chamber, which is temperature controlled, to apply loading to test specimens. The instrumentation and specimen configuration is the same as UI-FastCell (Figure 2.2b), except that RaTT cell has additional transducer for temperature measurement of the specimen. The system provides automated control of cell movement to simplify specimen handling, and computer control of both confining and axial stress. Figure 2.3 is a photograph of RaTT cell setup used in permanent deformation testing of bituminous specimens in ATREL.

In this study, the test procedures designed for the RaTT cell testing allowed varying sine load pulses in the axial and radial directions to apply on the specimen at multiple frequencies, multiple stress states, and different temperatures. These capabilities enable the test setup to determine both time-dependent and stress-dependent specimen responses, two features that are important for bituminous materials characterization. The ATREL RaTT cell is installed in a 5 kN load-frame fitted with a pneumatic actuator, and mounted in a -15 to + 60^{o}C temperature environmental chamber.

FIGURE 2.3 RaTT Cell Setup in the Temperature Controlled Environmental Chamber.

Curtis et al. (1999) and Gould et al. (2003) found RaTT cell to be appropriate for characterizing the behavior of asphalt concrete mixes for mechanistic modeling applications. The RaTT cell setup in ATREL has been extensively used to characterize bituminous and granular materials. Adu-Osei (2000) used the RaTT cell to characterize resilient behavior of unbound granular materials for flexible pavement use. Carpenter and Vavrik (2001) used the RaTT cell for HMA performance evaluation tests.

2.3.2 IPC Servopac Gyratory Compactor

The IPC Servopac gyratory type compactor is recommended for compaction of bituminous materials in Superpave volumetric mixture design. This compaction method allows fabricating specimens at field density levels and compaction properties. The IPC Servopac compactor at ATREL is a servo-controlled pneumatic loading system used to produce 150 mm in diameter by 150 mm high specimens for fitting into UI-FastCell and the RaTT cell for testing. The compactor operates by applying constant vertical pressure of 600 kPa, standard gyration angle of 1.25 degrees, and rotational speeds up to 30 rpm to the specimen during compaction process. Compaction is achieved by the simultaneous action of static compression and shearing resulting from the motion of the center line of the specimen. Figure 2.4 shows the gyratory compaction setup used for this study.

FIGURE 2.4 IPC Servopac Gyratory Compactor at the University of Illinois ATREL.

The ability of gyratory compactor to simultaneously apply a vertical pressure in addition to a self regulated kneading action enables a reasonable simulation of field traffic loading of flexible pavement system. Adu-Osei (2000) found that gyratory compaction better replicate field compaction properties than other compaction methods including impact hammer (Proctor) and vibratory compaction.

2.3.3 Universal Testing Machine (UTM-5P)

The IPC's UTM-5P setup at ATREL for conventional triaxial testing offers a simple and convenient way to perform modulus and triaxial shear strength tests for soils and sand size granular materials. The current setup has the capability of testing cylindrical specimens of diameters ranging from 38 to 76-mm (1.5 to 3-in.). A vertical actuator applies an axial monotonic load to the specimen, and the all-around confining pressures are applied inside the triaxial chamber. The 1700-kPa capacity plexiglass allows the application of constant confining pressures from a dry compressible air source to consolidate the sample before testing. Specimen responses from load cell and axial displacement transducers are recorded and stored in binary files of a personal computer. Figure 2.5 shows a picture of the triaxial cell with a 50.8-mm (2-in) diameter soil specimen seen inside the confinement chamber.

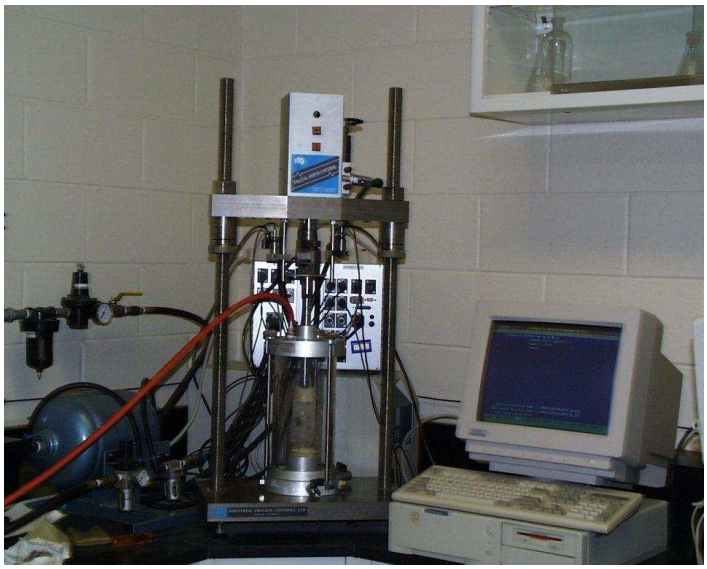

FIGURE 2.5 Photograph Showing Small Triaxial Test Setup at ATREL.

Several researchers (Garg and Thompson 1997, Bejarano and Thompson 1999, Anochie-Boateng and Tutumluer 2003) used the UTM-5P setup at ATREL to characterize resilient modulus and triaxial shear strength properties, and permanent deformation characteristics of soil samples.

2.3.4 Pneumatic Direct Shear Testing Device

The most recent addition to the soil/geomaterials laboratory at ATREL is Humboldt's automated pneumatic direct shear testing device. This is an advanced device which utilizes pneumatic loading to apply vertical loads to the specimen. Apart from improving the accuracy of test results, the pneumatic loading system of this device eliminates the need for numerous weights used in the dead weight-type direct shear loading system and can apply both light and heavy loads on the specimen.

The horizontal loads are measured with a 10 kN capacity S-type load cell, and the vertical loads are measured with 1400 kPa capacity in-built pressure transducer. Two linear strain transducers are used to measure the vertical and shear displacements during testing. The device is integrated with a stepping drive motor and a controller which permits and maintains the desired rate of strain in the range of 0.0001 to 10.0 mm/min

(0.0001 to 0.40 in/min). Figure 2.6 shows a picture of the pneumatic shear device with shear box assembly held between the motor (left) and load cell (right).

FIGURE 2.6 Assembly of Humboldt Pneumatic Direct Shear Testing Device.

A complete laboratory test setup of direct shear testing comprises of the direct shear device, an integrated computer system for data acquisition and air supply facilities. The Humboldt pneumatic direct shear testing device used for this study is quite new and automated.

2.4 Current Characterization Models for Soils and Oil Sands

Material characterization models and constitutive relationships are often developed to properly describe the behavior of materials as they are subjected to field stresses in the laboratory. Soils are elastoplastic materials and thus undergo both elastic (recoverable) and plastic (permanent) deformation during loading. Oil sand materials, however, exhibit viscous behavior in addition to undergoing elastic and plastic deformations under field loading (Joseph 2005). The current characterization models for soils and oil sand materials are mainly based on stress-strain relationships. Typical stress-strain curves presented by Bejarano and Thompson (1999), as well as typical material properties obtained from stress-strain relationships are shown in Figure 2.7.

Two significant modulus properties related to Figure 2.7 are the initial tangent and secant moduli. The initial tangent modulus or the maximum elastic modulus is the slope of the tangent to the curve passing through the origin, and the secant modulus is the

slope of a line connecting the origin of the curve to a specific stress level on the stress-strain curve. The material modulus decreases with increasing strain.

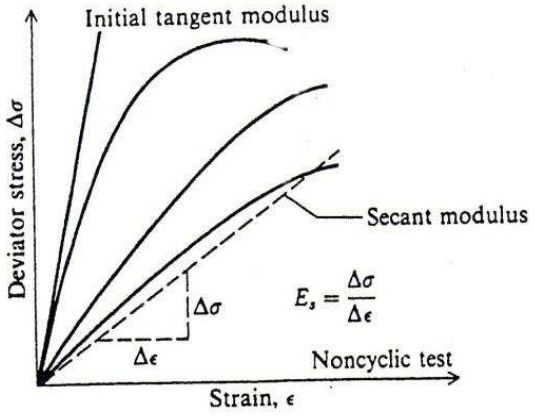

FIGURE 2.7 Typical Stress-Strain Relationships of Soils (Bejarano and Thompson 1999).

2.4.1 Fine-Grained Soil Characterization Models

2.4.1.1 Mohr-Coulomb Failure Criterion

The Mohr-Coulomb failure criterion is a widely known strength definition which has been successfully used for soils/geomaterials stability analysis in geotechnical engineering. The model is expressed as follows:

$$\tau_{max} = c + \sigma_n \tan \phi \qquad (2.1)$$

where, τ_{max} = shear strength; σ_n = normal stress at failure; c = cohesion intercept, $\tan \phi$ = slope of the failure envelope (ϕ is friction angle).

This model has been extended to pavement engineering to characterize subgrade soils and unbound materials in pavement layers. The Mohr-Coulomb criterion states that the shear stress in a plane at failure is a function of the normal stress in the plane. The two properties that define failure line are the friction angle and the cohesion. This model assumes that the soil material behaves linearly elastic and perfectly plastic until failure occurs. However, soils are often stress-dependent, inelastic and nonlinear in behavior, over a wide range of stresses. The use of Mohr-Coulomb's model or envelope clearly falls short in describing the entire behavior of a soil, particularly during dynamic loading.

2.4.1.2 Hyperbolic Stress-Strain Models

Kondner (1963) has shown that the nonlinear stress-strain behavior of soils can be approximated reasonably by hyperbolic stress-strain models. These models have been widely used for modeling behavior of many soils because it is versatile and simple. Kondner (1963) proposed that a hyperbolic relationship given by Equation 2.2 could be used to describe the soil stress-strain response as a function of the initial tangent modulus, axial strain and the ultimate deviator stress expressed as follows:

$$\frac{\varepsilon}{\sigma_1-\sigma_3}=\left[\frac{1}{E_i}+\frac{\varepsilon}{(\sigma_1-\sigma_3)_u}\right] \tag{2.2}$$

where, E_i = initial tangent modulus, $(\sigma_1 - \sigma_3)_u$ = maximum or ultimate stress difference, σ_1 and σ_3 are major and minor principal stresses, respectively and ε = axial strain. The ultimate stress difference is related to the compressive strength, or stress difference at failure, $(\sigma_1 - \sigma_3)_f$, by the failure ratio, R_f, which is defined as follows:

$$R_f = \frac{(\sigma_1-\sigma_3)_f}{(\sigma_1-\sigma_3)_u} \tag{2.3}$$

The variation of $(\sigma_1 - \sigma_3)_f$ with confining pressure, σ_3 can be expressed by means of the Mohr Coulomb criterion as follows:

$$(\sigma_1-\sigma_3)_f = \frac{2c\cos\phi}{1-\sin\phi}+\frac{2\sin\phi}{1-\sin\phi}\sigma_3 \tag{2.4}$$

Duncan and Chang (1970), and Duncan (1980) later reported that for most soils, the value of R_f ranges between 0.5 and 1.0. R_f is independent of the confining pressure.

Janbu (1963) proposed a stress-dependent hyperbolic model for soils in which E_i varied with σ_3. The model was based on primary loading data from triaxial tests.

It is expressed as follows:

$$E_i = k\, P_a \left(\frac{\sigma_3}{P_a}\right)^n \tag{2.5}$$

where, P_a = atmospheric pressure expressed in the same units as E_i and σ_3, k = Young's modulus number, and n = Young's modulus exponent, which determines the rate of variation of E_i with σ_3. The parameters k and n may be determined from the results of standard laboratory triaxial tests by plotting E_i against σ_3 on a log-log scale.

Duncan and Chang (1970) combined Kondner and Janbu models to develop a hyperbolic model, which is mainly confining pressure dependent. The Duncan and Chang hyperbolic model is obtained by substituting equations 2.3 and 2.4 into the derivative of Equation 2.2 with respect to strain. The model is expressed in terms of the tangent modulus E_t, of the soil material as follows:

$$E_t = \left[1 - \frac{R_f (1-\sin\phi)(\sigma_1 - \sigma_3)}{2\, c \cos\phi + 2\, \sigma_3 \sin\phi}\right]^2 k P_a \left(\frac{\sigma_3}{P_a}\right)^n \tag{2.6}$$

The tangent modulus in this expression can be used in incremental stress analyses of soils. All the parameters in this model may be determined from laboratory test results. In addition, Duncan and Chang (1970) proposed another hyperbolic stress-strain model to show the variation of modulus with confining pressure, using unloading or reloading triaxial tests data of sand material. In this model, the modulus of the material was related to confining pressure as follows:

$$E_{ur} = k_{ur}\, P_a \left(\frac{\sigma_3}{P_a}\right)^n \tag{2.7}$$

where, E_{ur} = unloading/reloading Young's modulus, k_{ur} = unloading/reloading Young's modulus number. Duncan (1980) reported that for stiff soils the value of k_{ur} could be 20% greater than the value of k in Equation 2.5.

For soft soils, he reported k_{ur} to be three times as large as k. According to Duncan, the value of n was assumed to be the same in the hyperbolic relations for both primary loading and unloading/reloading conditions.

Duncan (1980) also suggested that for a conventional triaxial test, in which the deviator stress ($\sigma_1 - \sigma_3$) increased from zero at constant confining pressure, there was a nonlinear relationship between the bulk modulus, the deviator stress and the volumetric strain. This relationship is represented as follows:

$$K = \left(\frac{\sigma_1 - \sigma_3}{3\varepsilon_v} \right) \tag{2.8}$$

where, K = bulk modulus and ε_v = volumetric strain of soil material.

For modeling volumetric responses of soils, Duncan (1980) proposed a hyperbolic model for the variation of bulk modulus as a function of confining pressure. The model is expressed as follows:

$$K = k_b \, P_a \left(\frac{\sigma_3}{P_a} \right)^m \tag{2.9}$$

where, k_b = bulk modulus number and m = bulk modulus exponent. For most soils, Duncan reported the value of m to be between 0 and 1.

The hyperbolic stress-strain models presented have certain limitations when describing the behavior of soils. The majority of the models do not include volume changes due to shear stress. This could limit the models to accurately predict deformations that take place in dilatant soils such as dense sands. The hyperbolic are also limited to static loading conditions. Besides, the parameters in the hyperbolic models are empirically based. These limitations would not allow the hyperbolic stress-strain models to properly characterize soils during construction activities. The field loading conditions of soils due to vehicular loading during construction are both static and dynamic. Therefore, models must be based on static and dynamic loadings to properly account for the behavior.

2.4.1.3 Shear Modulus and Damping Ratio Models

The cyclic triaxial and resonant column tests are the most commonly used laboratory tests for determining shear modulus and damping ratio properties of soils. The test procedures and calculations of modulus and damping properties are described in ASTM D 3999 for cyclic triaxial test, and ASTM D 4015 for resonant column test. The major difference between the two tests is that the cyclic triaxial test measures material properties at high strain levels whereas the resonant column test measures the material properties at low strain levels.

In the cyclic triaxial test, the shear modulus G is indirectly computed from the elastic modulus E of the material using an assumed value of Poisson's ratio. The material damping ratio is computed from hysteresis loop of deviator stress graphed with axial strain. The slope of the secant line connecting the extreme points on the hysteresis loop is used to define the material's elastic modulus. The material damping ratio D is computed as the ratio of the energy dissipated in one cycle to the maximum strain energy stored by the sample. Equations 2.10 to 2.13 are used to compute shear modulus and damping ratio properties from the cyclic triaxial tests.

$$E = \frac{\sigma_d}{\varepsilon_1} \tag{2.10}$$

$$\gamma = (1+\nu)\varepsilon \tag{2.11}$$

$$G = \frac{E}{2(1+\nu)} \tag{2.12}$$

$$D = \frac{A_L}{4\pi A_T} \text{ x } 100 \tag{2.13}$$

where, σ_d = deviator stress, γ = shear strain, ε_1 = axial strain and ν = Poisson's ratio, A_L = area of hysteresis loop, which is equivalent to total energy dissipated in one cycle, A_T = total area representing the maximum strain energy.

In the resonant column test, the soil sample is excited to longitudinal or torsional vibration by means of an excitation device.

Once the resonant frequency is established during testing, the velocity of wave propagation and the degree of material damping are derived. The shear modulus is then obtained from the derived velocity and the density of the sample. The damping ratio is computed from Equation 2.13 while the shear modulus is obtained from Equation 2.14.

$$G = \rho (2\pi L)^2 (f_T/F_T)^2 \tag{2.14}$$

where, f_T = system resonant frequency for torsional motion, L = length of specimen, ρ = density of sample, F_T = dimensionless frequency factor. The value of F_T is obtained from charts provided in ASTM D 4015.

The maximum shear modulus, G_{max} is a key property in small strain dynamic analyses, such as those used for predicting soil behavior and soil structure interaction during earthquakes, explosions or machine and traffic vibrations. According to elastic theory, G_{max} can be computed from the known shear wave velocity as follows:

$$G_{max} = V_s^2 . \rho \tag{2.15}$$

where, Vs = shear wave velocity, and ρ = known soil density.

A normalized shear modulus concept has been used by Hardin and Black (1968) to develop an empirical equation to compute the maximum shear modulus of soils. The equation is expressed as follows:

$$\frac{G_{eq}}{G_{max}} = \frac{1}{1 + (\Delta \gamma_{SA}/0.0012)} \tag{2.16}$$

where, G_{eq} = equivalent shear modulus, defined as the ratio of single amplitude shear stress to shear strain and $\Delta\gamma_{SA}$ = single amplitude shear strain.

Hardin and Drnevich (1972) related the G/G_{max} ratio to the damping ratio D of soil materials. The relationship is expressed as follows:

$$D = D_{max} \left[1 - (G/G_{max})\right] \tag{2.17}$$

Based on shear modulus data obtained from resonant column tests, Seed and Idriss (1970) suggested various empirical equations for the maximum shear modulus, which is mainly dependent on the relative density of the soil.

It can be seen that shear modulus and damping properties have not been modeled using the applied stress states or field loading conditions in the laboratory. Generally, the applied stresses are the most important factors that affect behavior of soils under dynamic loading conditions. Shear modulus and damping ratio properties should be modeled as stress dependent.

2.4.1.4 Resilient Modulus Models

Resilient modulus properties of fine-grained cohesive soils are determined in the laboratory from repeated load triaxial tests, in which cylindrical specimens are subjected to a number of repeated deviator stresses under different constant confining stress conditions. The resilient behavior of soils is affected by several factors including magnitude of stress level, stress history, number of load applications and conditioning sequence. Other soil properties such as liquid limit, plasticity index, specific gravity, water content, density and organic carbon contents have also been linked to the resilient modulus of soils (Bejarano and Thompson 1999). The applied stresses and the specimen moisture content significantly influence the resilient behavior of fine-grained soils.

Studies conducted by Hicks and Monismith (1971), Boyce (1980), Thompson and Elliot (1985), Uzan (1985), Lade and Nelson (1987), O'Reilly and Brown (1991), Uzan et al. (1992) have all shown that the resilient response of soils/geomaterials can be characterized by using stress dependent models which express the modulus as nonlinear power functions of stress states. Fine-grained cohesive soils are stress-softening whereas granular soils harden with increasing stress states.

The popular K-theta model (Equation 2.18) proposed by Hicks and Monismith (1971) has been widely used to characterize resilient modulus of granular materials although it neglects the effects of shear stress on the resilient modulus. For a more accurate representation of the soil/geomaterials behavior, Uzan (1985) modified the K-theta model to include shear stress effects in modeling. Witczak and Uzan (1992) modified the Uzan model, and presented the universal model.

The universal model considers in three-dimensions the dilation effect that take place when an element of the material is subjected to a large principal stress ratio, such as would occur under large mobile construction and mining equipment in soils. Recently, the National Cooperative Highway Research Program (NCHRP) has modified the Witczak and Uzan models for determining resilient modulus of geomaterials. The K-theta, Uzan, the universal and the NCHRP (1-37A 2004) Mechanistic Empirical Pavement Design Guide (MEPDG) models are expressed as follows:

K-theta: $$M_R = k_1\theta^{k_2} \tag{2.18}$$

Uzan (1985): $$M_R = k_1\theta^{k_2}\ \sigma_d{}^{k_3} \tag{2.19}$$

Universal Model: $$M_R = k_1\ P_a \left(\frac{\theta}{P_a}\right)^{k_2}\left(\frac{\tau_{oct}}{P_a}\right)^{k_3} \tag{2.20}$$

MEPDG Model: $$M_R = k_1\ P_a \left(\frac{\theta}{P_a}\right)^{k_2}\left(\frac{\tau_{oct}}{P_a}+1\right)^{k_3} \tag{2.21}$$

where, θ = bulk stress (sum of principal stresses), σ_d = deviator stress, τ_{oct} = octahedral shear stress, k_1, k_2, and k_3 are model parameters obtained from multiple regression analyses of triaxial data.

For fine-grained cohesive soils, Fredlund et al. (1977) also proposed a semi-log model that relates resilient modulus with the applied deviator stress. The model is expressed by the following equation:

$$\text{Log}\, M_R = k - n\,\sigma_d \tag{2.22}$$

where, k, and n are model parameters.

Brown (1979) proposed a resilient response model from repeated load triaxial testing of fine-grained cohesive subgrade soils. This model accounts for the effects of mean normal stress caused by overburden and the deviator stress caused only by the wheel loading.

The model is expressed as follows:

$$M_R = A\left(\frac{p'_0}{q_R}\right)^b \tag{2.23}$$

where, p'_0 = effective mean normal stress caused by overburden, q_R = deviatoric stress caused by wheel loading, A and b are material constants.

Thompson and Robnett (1979) proposed the arithmetic model for resilient response modeling of fine-grained soils. The arithmetic model relates resilient modulus with repeated deviator stress. This is a bilinear approximation of resilient modulus with breakpoint modulus represented as the intersection point of the two lines. Since its inception, the model has been the most commonly used in the US to describe the stress softening behavior of fine-grained soils. The arithmetic or bilinear model is usually expressed as follows:

$$M_R = k_1 + k_3 (k_2 - \sigma_d) \text{ when } \sigma_d < k_2 \tag{2.24a}$$

$$M_R = k_1 - k_4 (\sigma_d - k_2) \text{ when } \sigma_d > k_2 \tag{2.24b}$$

where k_1 = breakpoint modulus, k_2, = breakpoint deviator stress, and k_3, k_4 are material constants obtained from laboratory repeated load tests.

Moossazadeh and Witczak (1981) used resilient response data for fine-grained cohesive soils to propose the power model, which is expressed as follows:

$$M_R = k\ \sigma_d^n \tag{2.25}$$

where, k and n are model parameters.

Boateng-Poku and Drum (1989) proposed a hyperbolic model to account for the stress softening behavior of fine-grained cohesive soils.

The model is written as follows:

$$M_R = \frac{a' + b'\sigma_d}{\sigma_d} \tag{2.26}$$

where, a' *a*nd b' are hyperbolic parameters.

2.4.1.5 Permanent Deformation Models

Laboratory data obtained from repeated load triaxial tests are used to model the permanent deformation behavior of fine-grained cohesive soils. Previous studies by Lashine et al. (1971), Barksdale (1972), Monismith et al. (1985), and Lekarp (2000) documented that load characteristics and moisture content are the most important factors affecting the permanent deformation (plastic) behavior of fine-grained soils. Consequently the majority of permanent deformation models found in the literature are based on loading characteristics such as number of load repetitions, stresses and strains. Using laboratory test data, curve-fitting procedures have been successfully used to model permanent deformation characteristics of soils. Barksdale (1972) used the hyperbolic model given Duncan and Chang (1970) and derived the variation of permanent axial strain with applied stresses in repeated load tests as follows:

$$\varepsilon_p = \frac{(\sigma_d)/k_1\sigma_3^{k_2}}{1 - \left[\frac{(R_f\ \sigma_d)/(2c\cos\phi + 2\sigma_3\sin\phi)}{(1-\sin\phi)}\right]} \tag{2.27}$$

where, ε_p = permanent axial strain, σ_d = repeated deviator stress, σ_3 = constant confining pressure, ϕ = friction angle, c = cohesion, R_f = the failure ratio, k_1, k_2 are material constants.

Several subgrade soil models have been used to represent permanent strain accumulation with number of load applications.

Monismith et al. (1985) proposed the phenomenological power model as follows:

$$\varepsilon_p = A N^b \quad (2.28)$$

where, N = number of load applications, A and b are experimentally determined model parameters obtained from simple regression analysis of the test data.

A permanent strain accumulation model was developed at Ohio State University to describe permanent deformation in pavement layers including asphalt, granular base and subbase courses and the subgrade soil (Khedr 1985). The model is expressed as follows:

$$\varepsilon_p/N = A N^m \quad (2.29)$$

where, A = experimental constant which depends on the applied stresses, and m is an experimental constant which depends on material properties.

Thompson and Nauman (1993) proposed rutting rate model, which is comparable to the Ohio State University model. The rutting rate model was used to predict rutting in AASHO Road Test pavement s (Thompson and Nauman 1993). The model is expressed as follows:

$$RR = RD/N = A N^b \quad (2.30)$$

where, RR = rutting rate, RD = rut depth (in.) and A, b are model parameters developed from field calibration testing data.

The new Mechanistic-Empirical Pavement Design Guide (MEPDG, NCHRP 1-37A 2004) recommends the form of the permanent deformation model developed by Tseng and Lytton (1989) to estimate the permanent deformation of granular and subgrade materials.

The MEPDG permanent deformation model is expressed as:

$$\delta_a = \left(\frac{\varepsilon_0}{\varepsilon_r}\right) \cdot e^{-\left(\frac{\rho}{N}\right)^{\beta}} \cdot \varepsilon_v \cdot h \qquad (2.31)$$

where, δ_a = permanent deformation for the layer/sublayer

N = number of load applications

ε_0, β and ρ are material properties

ε_r = resilient strain imposed in laboratory test to obtain material properties ε_0, β and ρ

ε_v = average vertical strain in the layer/sublayer as obtained from the primary response model

h = thickness of layer/sublayer

The limitations of resilient modulus and permanent deformation characterization models may be attributed to the deficiencies in the current laboratory test procedures. For instance, the current repeated load test procedure for soils (AASHTO T 307) can only apply maximum confining stress of 41.4 kPa (6 psi), and cyclic/deviator stresses of 69 kPa (10 psi). Such small stresses are obviously inadequate to account for the high loading conditions experienced by fine grained soils under heavy construction equipment. As a result, modulus and permanent deformation models, which are mainly based on these test procedures cannot properly account for field loading conditions.

2.4.2 Oil Sand Characterization Models

The current laboratory characterization models for oil sands are predominantly based on stress-strain data obtained from experimental studies. Many researchers (Dusseault and Morgenstern 1978a-b, Scot and Kosar 1984, Scot and Hsu 1986, Kosar et al. 1987, Samieh and Wong 1997 and 1998, Wong 1993 and 1999, and Joseph 2002a) have used such data to model behavior of oil sands. In the laboratory, triaxial compression tests were mainly used to characterize oil sand behavior. In the field, limited data of simple plate load tests have been used to characterize oil sands. Unconfined uniaxial compressive strength test data obtained by Dusseault and Morgenstern (1978b) yielded no correlation between peak stress and strain values.

Using the same data, Joseph (2004) obtained a weak correlation between the modulus of elasticity and axial strain. Although significantly large amount of triaxial strength data have been reported for oil sands, the majority of these data is based on static loading conditions. Material models developed from these data are limited to static confining stresses and shear strength parameters. The following subsections describe the existing oil sand characterization models.

2.4.2.1 Laboratory Characterization Models of Oil Sands

Joseph (2005) described oil sand as elastoplastic materials, and reported that oil sand behavior was similar to clay with little frictional characteristics and high cohesion. It should be noted that fine-grained soils and oil sand materials have different compositions. Oil sand is a bituminous material. Therefore, the behavior may be different from soils under similar loading conditions. Dusseault (1977), Dusseault and Morgenstern (1978b) developed several Mohr-Coulomb relations for oil sands using both triaxial strength and direct shear test data. Based on several test data obtained from Athabasca oil sand studies, they demonstrated that the Mohr-Coulomb failure envelopes of oil sands could be expressed as generalized power-law relationships given by:

$$\tau_{max} = A\,\sigma_n^b \tag{2.32}$$

where, τ_f = shear strength of oil sand, σ_n = applied normal stress during test, and A, b are model constants. Equation 2.32 indicates that oil sand materials have little or no cohesion between grains. Optical and scanning electron microscope studies conducted by Wong (1999) supported findings by Dusseault and Morgenstern (1978b). The power-law model has been used to describe the strength behavior of oil sands at varying temperatures and oil contents.

The laboratory data of oil sands have also been described by hyperbolic models used for soil materials. Agar et al. (1987) used the hyperbolic model developed by Duncan et al. (1980) to fit triaxial compression test data to model the behavior of Athabasca oil sands. For up to approximately 80% of peak deviatoric stress, the hyperbolic model could reasonably model the stress-strain behavior of the oil sands.

Samieh and Wong (1997) used the model proposed by Janbu (1963) to evaluate the initial Young's modulus of Athabasca oil sand, and correlated the friction angle ϕ and confining pressure σ_3 of Athabasca oil sands by the following equation:

$$\phi = F\phi_0 \left(\frac{\sigma_3}{Pa}\right)^{-n} \tag{2.33}$$

where, ϕ_o = reference friction angle, ($\phi_o = 30^o$), and F and n are constants. The friction angle is an important shear strength property, which is defined for cohesionless soils by the following equation:

$$\phi = \sin^{-1}\left(\frac{\sigma_1 - \sigma_3}{\sigma_1 + \sigma_3}\right) \tag{2.34}$$

where, σ_1 and σ_3 are major and minor principal stresses, respectively.

The hyperbolic model for a soil's bulk modulus proposed by Duncan (1980) is currently used to describe oil sand volumetric response properties. This clearly indicates that continued research for oil sand characterization is essential. As stated earlier, the presence of bitumen in oil sands make the material behave differently from soils. Hence, models such as the hyperbolic model used to describe soil behavior may not adequately describe oil sand behavior.

Based on the analysis performed on laboratory triaxial test data, Joseph (2005) proposed a constitutive model to define the elastic-plastic behavior of oil sands. The constitutive model for the oil sand was represented by the following equation:

$$E_{ps} = 1.37\,\sigma_3\,\varepsilon_1^{-1.43}\ \text{MPa} \tag{2.35}$$

where, E_{ps} = Oil sand modulus of elasticity, σ_3 = confining pressure, and ε_1 = axial strain.

Joseph's elastoplastic model for oil sands is also based on static loading, and only accounts for applied confining pressure and axial strain measured.

Joseph (2005) also suggests that triaxial strength test data could be conveniently evaluated by empirically relating the principal stress ratio with axial strain such that the principal stress ratio is an inverse function of the axial strain. He supported this assertion by observing a convergence of σ_1/σ_3 using data from historical triaxial data. Other empirical characterization models were proposed by Li and Chalaturnyk (2005) to characterize oil sand behavior (Equations 2.36 to 2.39). Equations 2.36 and 2.37 represent the modulus of elasticity behavior of oil sands, in which the modulus is expressed as a function of the applied confining pressure. Equations 2.38 and 2.39 show the relationships proposed by Li and Chalaturnyk (2005) for maximum friction and dilation angles, respectively.

$$E = 950\ P_a \left(\frac{\sigma_3}{P_a}\right)^{0.5} \tag{2.36}$$

$$E = 343\ \sigma_3^{\,0.875} \tag{2.37}$$

$$\phi_p = 55 - 14.93 \log\left(\frac{\sigma_3}{P_a}\right) \tag{2.38}$$

$$\psi_p = 25.8 - 12.05 \log\left(\frac{\sigma_3}{P_a}\right) \tag{2.39}$$

where, E = elastic modulus, P_a = atmospheric pressure, σ_3 = confining pressure, ϕ_p = peak friction angle, and ψ_p = peak dilation angle.

Although these laboratory characterization models presented for oil sands have been reported to perform adequately, several limitations certainly need to be addressed. For example, majority of oil sand models are based on triaxial compression tests with constant confining pressures used as major model variables. It is noteworthy to mention that the dynamic properties including shear, dynamic and resilient moduli, damping ratio and phase angle, and permanent deformation characteristics of oil sand materials have not been modeled to date. Such models would be useful to account for oil sand dynamic properties especially under field loading conditions of large capacity mining equipment.

In addition, most oil sand models do not account for varying stress levels, temperature, loading duration, and bitumen content.

2.4.2.2 Field Characterization Models for Oil Sands

Joseph (2002a) used data obtained from the Oil sands-Equipment Interactions Program (OsEIP) study to predict the stiffness and deformation behavior of oil sands under loading of mining equipment. One of the main observations from the OsEIP studies was the effect of equipment duty cycles on ground deformation. An empirical stiffness-deformation model obtained from the study is presented in Equation 2.40. This equation computes the ground stiffness of oil sands using large haul truck and electrical shovel. Joseph (2005) used the experimental data obtained from the study to show that oil sand ground stiffness is a function of deformation. A general relationship obtained from the study is expressed as follows:

$$\left(\frac{k D_f}{P}\right)\left(\frac{1-\nu}{\nu}\right) = C\left(\frac{d}{D_f}\right)^{-b} \tag{2.40}$$

where, k = ground stiffness of the oil sands, P = external load exerted by the equipment at certain depth of influence, (D_f), ν = Poisson ratio for oil sands ($0.29 < \nu < 0.33$), and d = ground deformation due to equipment loading, b and C are empirical constants which depend on oil sand behavior. The depth of influence is related to the loading footprint of equipment, A, as follows:

$$D_f = 3 * \sqrt{A} \tag{2.41}$$

The loading footprint A of equipment is the volume of material that is directly subjected to the ground softening process.

Joseph (2002a) reported that seismic Rayleigh waves generated as a result of moving truck or shovel on oil sands could cause a wave-dictated deformation in the oil sand material.

Joseph related the generated Rayleigh wave velocities to the stiffness behavior of oil sands to obtain the following empirical equation:

$$k = \frac{2\rho\,(1+\nu)}{D_f}\,\frac{V_R^2}{0.95^2} \tag{2.42}$$

where, ρ = density of oil sand material, and V_R = Rayleigh wave velocity.
Using both equations 2.40 and 2.42, the ground deformation of oil sand material due to equipment loading can be estimated.

Joseph (2005) indicated that the oil sand ground is softened with increasing number of duty cycles of mining equipment. Such an observation suggests that oil sand models must include the vehicular number of passes in order to accurately evaluate rutting potential (sinkage) of oil sand materials in mining pit. However, laboratory test procedures that closely simulate this loading condition do not exist for oil sands. Consequently, there are no rutting models that include vehicular number of passes or number of load applications in the oil sand material. The presence of such a test procedure would provide test data to model permanent deformation characteristics of oil sand materials in the field.

2.5 Review of Wheel-Soil Interaction Models

Mobility (trafficability) of off-road trucks and shovels on weak fine-grained cohesive soils and high grade oil sand materials during construction or mining activities largely depend on the behavior of these materials and the climatic effects of the environment. Early research work by Bekker (1956) and Reece (1964) focused on developing models to describe interaction between the truck wheels or shovel tracks of off-road vehicles and soil. Harnisch et al. (2005) and Tao et al. (2006) recently noted the deformations that occurred under wheel interactions with soils in both vertical and horizontal directions. The vertical deformation was used to describe pressure-sinkage characteristics of the soil whereas the horizontal deformation described the shear stress-displacement characteristics. A review of some of the existing wheel-soil interaction models is presented in the following subsections.

2.5.1 Vertical Stress-Displacement (Pressure-Sinkage) Models

The concept of rut depth (rutting) measurement in pavements is similar to sinkage in the study of off-road vehicle and soil interactions. Saarilahti (2002) suggested that for practical purposes, there is no difference between sinkage and rutting. Sinkage is measured when the wheel is loading the soil, and rutting is measured when the wheel is making a number of passes at an observation point in the soil. Rolling resistance of a wheel has also been associated with sinkage in mobility studies (McRae 1967 and Kraft et al. 1969). The rolling resistance is a measure of the force that opposes the motion of a wheel (or a track) as it rolls on the surface of the soil. The deeper a wheel sinks into the surface, the higher is the rolling resistance. Factors such as applied load, friction and tire deflection affect rolling resistance. Over the years, several empirical and analytical models have been developed for estimating sinkage and rolling resistance of off-road vehicles as they interact with soils (Bekker 1956, 1960 and 1969, Richmond, et. al. 1965, McRae 1967, Kraft, et al. 1969, Wong 1989 and 2001, Al-Qadi and Rivera-Ortiz 1991). The majority of these models have been based on wheel (tire) characteristics, types of soils, and their strength properties.

The classical empirical plate sinkage model is the Bernstein (1913) formula, which relates the pressure underneath a plate to the depth of sinkage. It is expressed as follows:

$$p = k z^n \tag{2.43}$$

where, p = contact pressure, z = sinkage, k = soil deformation modulus and n = sinkage exponent.

Bekker (1956) modified Bernstein's formula and presented a semi-empirical pressure-sinkage model by introducing soil property constants to account for friction angle and cohesion of the soil. Bekker's model is perhaps the most commonly used formula in off-road vehicle trafficability to define vertical stress-displacement relationships.

The model assumes that a rolling wheel on the surface of homogeneous soil is equivalent to a plate which is continuously pushed vertically into the soil to a depth equal to the rut depth produced by the wheel load. Bekker's pressure-sinkage model is expressed as follows:

$$p = \left(\frac{k_c}{b} + k_\varphi \right) z^n \tag{2.44}$$

where, p = contact pressure between soil and tire, z = vertical soil deformation (sinkage), n = sinkage exponent, b = width of the wheel (related to the width of the contact surface area), and k_c , k_ϕ = cohesive and frictional moduli of deformation, respectively. To obtain the model constants (n, k_c, k_ϕ) a set of sinkage tests are normally performed using different size loading plates. From Equation 2.44, log p is plotted against log z to obtain a series of straight lines of slope n and intercept ($k_c/b + k_\phi$) on the log p axis. The intercept values are then plotted against 1/b to obtain k_c and k_ϕ. Bekker (1960) used an analytical approach to modify the pressure-sinkage model (Bekker 1956) to include the applied wheel load and the tire diameter. The resultant relationship is expressed as follows:

$$z = \left[\frac{3P}{b\,(3-n)(k_c/b + k_\varphi)\sqrt{D_m}} \right]^{(2/(2n+1))} \tag{2.45}$$

where, P = tire (wheel) load, D_m = tire diameter. The remaining symbols are defined in Equation 2.44.

Using curve fitting technique of laboratory test data, Reece (1964) modified Bekker's (1960) model. Reece's model is given by:

$$p = \left(c\,k_c + \gamma_s b k_\varphi \right) \left(\frac{z}{b} \right)^n \tag{2.46}$$

where, n, k_c, and k_ϕ are pressure-sinkage parameters, c = soil cohesion and γ_s = unit weight of the soil.

Based on experimental test data, Al-Qadi and Rivera-Ortiz (1991) developed analytical pressure-sinkage model to predict runaway tire sinkage in granular materials used as arrester bed. The model was found to satisfactorily predict sinkage in the materials. Moreover, this model had a better fit for dynamic data compared with Bekker's (1956) equation. Al-Qadi and Rivera-Ortiz (1991b) model is expressed as follows:

$$p = A + Bz + Cz^2 \tag{2.47}$$

where, p = contact pressure between granular material and truck tire, z = sinkage, A, B, C are polynomial regression constants.

Using test data obtained from aircraft studies by the US Army corps of Engineers Waterways Experiment Station (WES), Richmond et al. (1965) developed empirical models to predict sinkage. First, Richmond et al. used the cone index and wheel characteristics to calculate a dimensionless clay mobility number (MN). Based on the mobility number, an empirical relationship was established to estimate sinkage. This relationship is expressed as:

$$\frac{z}{D_m} = 0.003 + (CMN)^{-2.6} \quad \text{for} \quad 3 \le CMN \le 10 \tag{2.48}$$

$$\text{where, } CMN = \frac{(CI)\, b\, D_m}{P}\left(\frac{\delta_t}{h_t}\right)^{1/2}$$

b = tire width, δ_t = tire deflection, h_t = tire section height, CI = average cone index value over the first six inches.

Based on the analysis of aircraft wheel data, Kraft et al. (1969) developed empirical equations to predict sinkage for cohesive and cohesionless soils.

The equations for cohesive soils are:

$$\frac{z}{L} = -0.03 + 0.19\frac{\alpha}{CI} \quad \text{for} \quad 0.20 \le \frac{\alpha}{CI} \le 0.60 \tag{2.49a}$$

$$\frac{z}{L} = -0.11 + 0.33\frac{\alpha}{CI} \quad \text{for} \quad 0.60 \le \frac{\alpha}{CI} \le 0.90 \tag{2.49b}$$

L = tire footprint, CI and P are defined in Equation 2.48, α = P/A (A = contact area), and term (α/CI) represents stress due to tire loading and the strength of the soil.

Wong (2001) used Bekker's pressure-sinkage relationship to develop sinkage model for track vehicles. Wong indicated that the normal reaction exerted on a track by the soil is similar to the reaction beneath a sinkage plate in the plate-sinkage test. For a track with a uniform contact pressure p, the sinkage z is given by:

$$z = \left(\frac{p}{k_c/b + k_\varphi}\right)^{1/n} = \left(\frac{P/bL}{k_c/b + k_\varphi}\right)^{1/n} \tag{2.50}$$

where, p = normal (contact) pressure, P = normal load on the track (wheel load), b = width of the track in contact with the soil, and L = length of track.

Other authors, including Turnage (1972c) and Maclaurin (1990, 1997) have presented different types of sinkage (rutting) models which used WES-parameters as input variables. These empirical models permit analyses of sinkage or rutting by using single and multiple pass wheels at an observation point in the soil. Wong et al. (1984) and Wong (1989) also proposed other sinkage models to characterize the response to repetitive loading for wheeled and tracked vehicles. Particularly, Wong's models were used to calculate sinkage during soil loading and unloading.

Sinkage and rolling resistance of wheels have been correlated by some authors. McRae (1967) proposed empirical models to correlate sinkage and rolling resistance. McRae's model was based on a database established from comprehensive field tests performed on heavy clay and sand.

The model is given by:

$$\frac{R}{P} = 0.85\left(\frac{z}{L}\right)^{0.77} \tag{2.51}$$

where, R = rolling resistance, L = the horizontal projection of the length of the effective tire contact area. Kraft et al. (1969) also developed empirical models for rolling resistance-sinkage relations. These models are based on single wheel loads and are applicable to all soil types including cohesive soils. The wheel loads used to develop these models were considered to be similar to those of earth-moving equipment. A wide range of tire diameters were also considered for developing the models. It should be noted that Kraft et al. (1969) used data from aircraft studies conducted by Ladd et al. (1967) to develop rolling resistance models. The models are expressed as follows:

$$\text{All soils}: \frac{R}{P} = 0.018 + 3.23\left(\frac{z}{D_m}\right) \tag{2.52a}$$

$$\text{Cohesive soils}: \frac{R}{P} = 3.85\left(\frac{z}{D_m}\right) \tag{2.52b}$$

$$0.01 \le z/D_m \le 0.12$$

Macmillan (2002) reported that when a wheel rolls over a soft surface, it causes rutting or creates a compacted track. He indicated that the rolling resistance R, for such a surface is given by:

$$R = \frac{b}{(n+1)\left(\frac{k_c}{b} + k_\varphi\right)} \cdot p^{(n+1)/n} \tag{2.53}$$

where, p = vertical pressure on the surface, k_c and k_ϕ are soil sinkage moduli for cohesive and frictional materials, respectively, b = width of the wheel (related to the width of the contact surface area), and n = soil sinkage exponent.

It was observed that the various pressure-sinkage models are mainly based on static loading conditions and do not account for dynamic loading conditions of the soils.

In addition, based on their application these models do not account for the number of vehicle passes, which are important to properly model rutting in geomaterials under vehicular loading.

2.5.2 Horizontal Shear Stress-Displacement Relations

The soil shear stress-displacement relationships are used to model the tractive force developed by tracks over a contact surface. Wong (2001) indicated that the maximum tractive force under a track may be determined by soil shear strength properties ϕ and c, and the contact area. Experimental data from different shear strength tests including shear box, shear ring, rectangular shear plate and rigid track are usually used to express the shear stress of a surface as a function of shear strength parameters. This implies that the shear stress mobilized at any point along the wheel-soil contact surface can be conveniently described by the Coulomb's rule (see Equation 2.1).

Based on considerable field data, Wong (2001) suggested three types of shear stress-displacement relationships for different soils. For loose sand and saturated clay, Wong suggested that the stress-displacement relationship proposed by Janosi and Hanamoto (1961) could be used to describe the characteristics of the soil materials. The relationship is expressed as follows:

$$\tau = \tau_{max}(1 - e^{-j/K_s}) \;;\; \tau = c + p\tan\phi(1 - e^{-j/K_s}) \tag{2.54}$$

where, τ = the shear stress, p =normal pressure, j = shear displacement, c = cohesion, ϕ = friction angle of the soil and K_s = shear deformation modulus. The value of K_s was found to be in the range of 1cm for firm sandy terrain to 2.5 cm for loose sand.

For organic terrain with saturated peat beneath it, Wong (2001) noted that the shear stress-displacement relationship can be described as follows:

$$\tau = \tau_{max}(j/K_w)\exp(1 - j/K_w) \tag{2.55}$$

where, K_w = shear displacement at the maximum shear stress τ_{max} occurs. The values of K_w and τ_{max} may be obtained directly from a plot of τ against j.

Based on field data collected for various types of organic terrain tested in some parts of Canada, the value of K_w was found to vary from 14.4 cm to 16.4 cm (Wong 2001).

Wong (2001) reported that for compact sand, silt and loam soils, the shearing behavior can be characterized by the following relationship:

$$\tau = \tau_{max} K_r \left\{ 1 + \left(\frac{1}{K_r\ (1\text{-}1/e)} - 1 \right) \exp\left(1 - j/K_w\right) \right\} .\ [1 - \exp(-j/K_w)] \qquad (2.56)$$

where, K_r = ratio of the residual shear stress (τ_{max}) to the maximum shear stress. A plot of shear stress against displacement can be used to obtain τ_{max}. The filed data collected on various types of soils show that K_w varies from 2.7 cm to 7.1 cm, and K_r varies from 0.38 cm to 0.72 cm.

Wong's (2001) proposed shear stress-displacement models are based on generalized field static data of specific soil types, and developed mainly to account for shear strength properties of the soil. Therefore, it may not be adequate to characterize soil and oil sand materials under dynamic loading conditions.

2.6 Summary

A general review of the existing laboratory test procedures and material characterization models including rutting or sinkage models for soils and oil sand materials was presented. The state-of-the-art testing devices which address some of the limitations of the existing soils/geomaterials laboratory testing equipment were described. These advanced testing devices have the capabilities for applying on the specimen, field stress conditions at various loading frequencies and temperatures in the laboratory.

The review indicate that dynamic loading conditions of soils and oil sand materials under mobile construction and mining equipment have not been studied thoroughly in the laboratory. Therefore, limited data are available to characterize the dynamic behavior of soils and oil sand materials. New or improved laboratory test procedures are needed to address some of the existing shortcomings of current test procedures and characterization models.

The review also showed that field tests for soils and oil sand materials under off-road vehicle loading conditions were not commonly conducted possibly due to high cost of effectively conducting some of those tests.

The detailed review of existing soil and oil sand material models showed that static loading conditions have mostly been used to characterize the behavior of these materials. It was found that confining pressure, instead of dynamic stress states was the main stress variable for modeling behavior of soils and oil sands. As a result, material dynamic properties including shear, dynamic and resilient moduli, damping ratio and permanent deformation characteristics have not been modeled properly. It was also observed that majority of the existing models including soil-vehicle interaction models were empirical based, and could be only used under specific test conditions. Therefore, they were only effective under the prevailing conditions under which they were developed. Studies that address some of these shortfalls of laboratory testing and characterization of soils and oil sand materials under large equipment loading conditions are needed.

CHAPTER 3 DEVELOPMENT OF ADVANCED TEST PROCEDURES AND GEOMATERIALS TESTED

3.1 Introduction

The purpose of laboratory test procedures is to subject a representative material sample to conditions that closely simulate field loading conditions. Field loadings on an element of soil or oil sand could be static and/or dynamic. Static loading is mainly provided by the overburden weight and stopped vehicle load, whereas the dynamic loading could be originated from sources such as earthquakes, activities of mining and construction equipment, and traffic wheel loads. Typically, soil or oil sand element under haul truck or shovel experiences a combination of static and dynamic stresses. For example, the roll and bounce motion of the trucks, and the rocking motion of the shovels during construction and mining activities result in both static and dynamic loading in soils and oil sand materials. At any time the wheels impose varying magnitudes of vertical, radial, and shear stresses on the materials. The dynamic vertical stresses always become higher underneath the wheels where shear stresses do not exist. However, at some radial distance away from the wheel, there exist shear stresses which may be higher than the applied vertical stresses. Not only must laboratory testing procedures be able to reproduce these complex field conditions, but they should also be simple and repeatable for user agencies to perform. Moreover, test equipment selected for laboratory test procedures must have capabilities of applying the expected field loading conditions on specimens and should have loading systems that are capable of measuring the magnitude of the applied loads as well as recording accurate responses of the materials tested. The testing devices must also be simple enough for researchers and agencies to use routinely and quickly to acquire the necessary material parameters.

This chapter presents advanced triaxial test procedures developed to properly characterize fine-grained cohesive soils and oil sand materials under typical field loading conditions of construction and mining equipment. Prior to developing the test procedures, preliminary laboratory tests were conducted on four geomaterials, one type of fine-grained soil and three oil sands to determine physical properties. Based on the preliminary test results and some data from previous studies on the fine-grained soil and oil sands, five different test procedures are developed for these geomaterials.

3.2 Factors Considered for Developing Laboratory Test Procedures

Factors that affect engineering behavior of geomaterials such as compaction characteristics were taken into account for the developed laboratory test procedures. Other factors considered include loading and stress conditions, i.e., load pulse characteristics, loading frequency, temperature, and number of load applications. For the purpose of this study, it was important to also consider the field loading characteristics of large capacity off-road haul trucks and shovels. The subsequent subsections discuss all the factors considered in developing the laboratory test procedures for the fine-grained soil and three oil sand materials selected for testing in this study.

3.2.1 Compaction Characteristics

The main compaction characteristics for geomaterials are the maximum dry density and optimum moisture content. Compaction curves primarily dictate a target moisture range in designing experimental program. An extensive soil testing study conducted by Thompson and Robnett (1979) showed that for most silty and clayey soils, a change in gravimetric water content of up to 3 to 4% above the optimum water content is often enough to saturate the soil. It is well documented that density affects the strength and deformation characteristics of geomaterials.

An increase in the soil density improves its strength and stiffness properties. The compaction characteristics of oil sand materials have also been extensively studied in the field and laboratory by Lord and Cameron (1985, 1988). Their investigation suggested that an optimal amount of bitumen content of oil sand materials is required to achieve maximum field density and optimum water content for construction purposes. This study uses compaction characteristics of the materials tested to support the development of the developed laboratory test procedures.

3.2.2 Loading and Stress Conditions

3.2.2.1 Pulse Load Characteristics

Barksdale (1971) investigated the vertical stress pulses from traffic loading in flexible pavements. He reported that vehicle speed and depth beneath wheel load affect the duration and magnitude of the vertical stress pulse.

For low to moderate vehicle speeds, 24 to 72 km/h, the stress pulse is between 0.05 and 0.4 sec, corresponding to frequency between 20 and 2.5Hz, i.e, MEPDG conversion of time (t in sec) to transform load pulse duration into frequency (f in Hz) using the relation t = 1/f . Barksdale (1975) and Huang (1993) indicated that sinusoidal or haversine pulse shapes could be used to simulate actual stress states in pavement structure. Recently, Loulizi et al (2002) found that haversine or normalized bell-shaped equations may be used to represent the measured normalized compressive stress load pulse for a moving truck. Seed (1979) reported that typical duration of strong ground motion of earthquakes ranges from 5 to 40 seconds during which there are about 5 to 30 significant shear stress cycles. The current repeated load triaxial test procedure (AASHTO T 307) recommends a haversine load pulse with load duration of 0.1-second and cycle duration of 1-second for a typical highway loading. However, for construction and mining activities, longer load durations would be required considering that loads are applied by slow moving wheels of the vehicles. Recently, Bejarano and Thompson (1999), Kim (2005), Kim and Tutumluer (2006) found that longer load duration produces larger permanent deformations in geomaterials than lower durations. Based on the above studies a practical pulse load characteristics are selected for the new laboratory test procedures developed in this study.

3.2.2.2 Loading Frequency and Temperature

Studies by Boyce (1976), Sousa and Monismith (1987), and Sweere (1990) concluded that frequency has little to no effect on the modulus properties of granular materials. Also, no correlation was found between dynamic modulus and frequency when loading frequency was varied from 0.5 to 10Hz in a repeated loading hollow cylinder test performed on uniform sand samples (Sousa and Monismith 1987). However, the effect of frequency on different moisture conditions of fine-grained cohesive soils, and bitumen content in oil sand materials needs to be investigated.

The main reason for including temperature effect in the test procedure is to investigate seasonal variation of temperature on the behavior of oil sand materials. As mentioned earlier, typical oil sands compose of high amount of bitumen content.

Similar to asphalt materials, the high percentage of bitumen content would make oil sands sensitive to both temperature and loading frequency. Therefore, it was essential to include temperature effects in the laboratory test procedures for oil sands.

3.2.2.3 Number of Load Applications

The number of load applications (repetitions) is one of the most important variables in repeated load test procedures. Barksdale (1972) concluded from laboratory tests that permanent deformation in granular soils accumulates linearly with the logarithm of number of load applications. Brown and Hyde (1975) noted that an equilibrium state of permanent deformation can be established after 1,000 load applications. Boyce (1976) reported a maximum of 10% decrease in the resilient strain between 200 and 1,000 load repetitions in granular soils. However, some authors, Morgan (1966), Barksdale (1972) and Sweere (1990) applied significant number of load applications to describe permanent deformation in granular materials. In this study, number load applications were one of the major factors considered in all the developed laboratory test procedures.

3.2.2.4 Stress Magnitudes

The applied stress magnitude is a significant factor among all the variables that affect the stress-strain behavior of soils and unbound materials. Morgan (1966) indicated from repeated load triaxial tests of granular materials that deviator stress and confining pressure relate to accumulation of axial strain in the specimen. Other researchers such as Hicks (1970), Smith and Nair (1973), Uzan (1985), and Sweere (1990) have all shown that resilient modulus of cohesionless soils increase considerably with an increase in both the confining and bulk stresses. Studies by Kim (2005) also indicated that higher stress ratios give higher permanent deformation accumulation in unbound granular materials. In this study, higher stress ratios corresponding to field loading of heavy construction and mining equipment were considered in the developed test procedures for realistic determination of soils and oil sand materials behavior in the laboratory.

3.2.3 Field Loading Characteristics of Large Capacity Off-Road Vehicles

The loading characteristics and vehicle travel speeds of construction and mining equipment are often provided in manuals or handbooks of the equipment manufacturing companies, e.g. Caterpillar Inc., Komatsu, etc. The world's largest haul truck for construction and mining activities is Caterpillar truck 797B. This equipment has a maximum nominal payload capacity of approximately 363 metric tonnes (400 tons) with maximum operating speed of 67 kph (42 mph). CAT 797B has tire dimension of 3.8 m (12.5 ft) in diameter, nominal width of 1.5 m, with tire pressure in the range of about 621 to 690 kPa (90-100 psi). The gross vehicle weight of CAT 797B is 623,690 kg with an average of 104 000 kg loads on each of the six tires. On the other hand, Pawling and Harnischfeger shovel, P&H 4100 BOSS has nominal payload of about 91 metric tonnes (100 tons) with a bucket capacity that ranges between about 30 to 61 cubic meters. This series of shovels weighs about 1.4 million kilograms (~3 million pounds) with track length of about 3.51 m (11.5 ft). Joseph (2005) notes that a Caterpillar 797B truck would produce vertical stress of about 800 kPa with confining pressure between 250 and 300 kPa. Further, Joseph observed that the P & H 4100 BOSS shovels generate static ground loading of up to 220 kPa, and induce a ground confinement of about 70 kPa. Therefore, developed laboratory test procedures will need to be mainly based on the loading characteristics of this equipment for proper characterization of fine-grained cohesive soils and oil sand materials.

3.3 Materials and Preliminary Tests

Approximately, 455 kg (1000 lbs) of a fine-grained cohesive soil from Caterpillar Inc. (CAT) Demonstration Training Center in Edwards, Illinois was shipped to the University of Illinois Advanced Transportation Research and Engineering Laboratory (ATREL) for testing. In addition, three types of oil sand materials used in this study were obtained from Suncor Energy Inc. and Syncrude Canada Ltd. oil sand mines in Canada. Suncor Energy Inc. provided two types, SE low and high grades with respect to the bitumen contents, whereas Syncrude Canada Ltd. provided one sample of the Aurora (AU) high grade oil sand. All the three oil sand materials were also shipped by CAT in Peoria, Illinois, to ATREL in separate barrels for the laboratory tests.

3.4 Preliminary Laboratory Testing

The main purpose of the preliminary laboratory tests was to obtain information on applicable laboratory loading conditions for the developed test procedures. Gradation and index properties tests were conducted to classify the fine-grained soil. The standard Proctor compaction tests were also conducted on the soil sample to identify the maximum dry density and optimum moisture content. The other preliminary test conducted on the soil sample was the specific gravity test. Similarly, compaction and gradation tests were performed on the three oil sand samples. Other preliminary tests performed on the oil sand materials include bitumen content determination tests and strength and stiffness tests. Detailed test procedures and results of the preliminary tests are presented in the following subsections.

3.4.1 Preliminary Tests for Fine-Grained Soil

Index properties tests were first performed on the soil sample in accordance with AASHTO T89 and T90 specification to obtain Atterberg's limits, i.e., liquid limit (LL), plasticity limit (PL) and plasticity index (PI). This was followed by the specific gravity test, which was performed in accordance with AASHTO T 100 specifications. The specific gravity tests were conducted for determining the degree of saturation. Particle size analysis test was also performed on the soil sample according to AASHTO T88 to establish the grain size distribution of the material. Table 3.1 shows the test results for the physical properties of the soil. Figure 3.1 indicates the grain size distribution curve for the soil. Based on the Atterberg limits and gradation results, the soil sample was classified as CL according to Unified Soil Classification or as A-6 according to AASHTO classification. The soil sample is hereon referred to as CAT A-6 sample.

TABLE 3.1 Physical Properties of CAT A-6 Soil

Specific Gravity	Atterberg limits, %			Gradation, %		
	LL	PL	PI	Sand	Silt	Clay
2.72	27.8	16.3	11.5	27.5	43.7	27.4

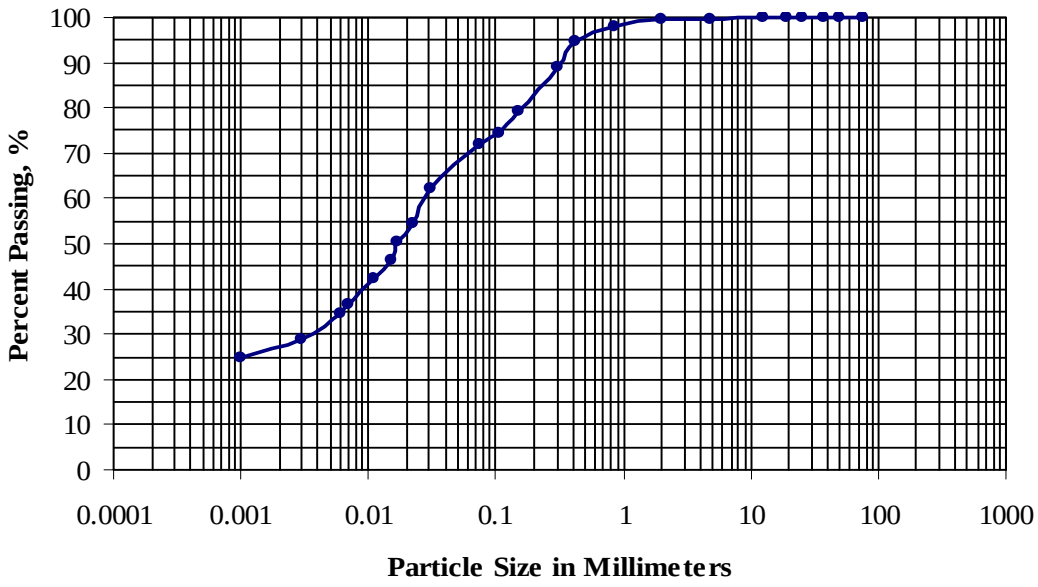

FIGURE 3.1 Particle Size Distribution of CAT A-6 Soil Sample.

In addition, moisture-density tests were performed on CAT A-6 soil in accordance with AASHTO T 99 (standard Proctor) to establish the maximum dry density and the optimum moisture content of the sample. Compaction curve obtained from five standard Proctor tests was used to define a target moisture range in which the soil specimens were prepared for testing. Figure 3.2 shows the maximum dry density, optimum water content and the lines of equal degree of saturation at 80, 90, and 100%. The maximum dry density (MDD) obtained was 18.4 kN/m^3 (117.1 pcf) at optimum water content (OWC) of 14.3 %. The degree of saturation at maximum dry density and optimum water content was found to be approximately 87%, and the degree of saturation at 3% above optimum water content is about 90%.

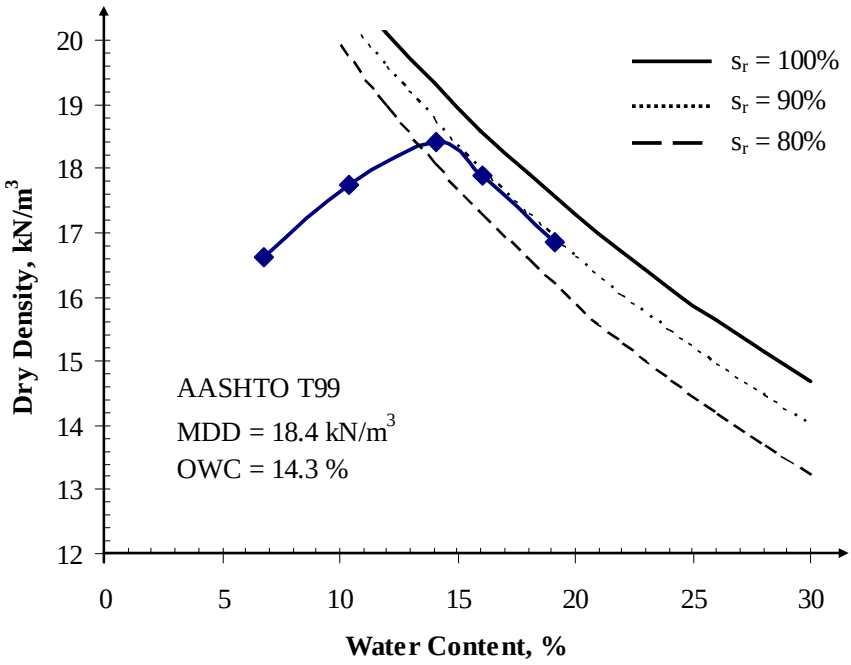

FIGURE 3.2 Standard Proctor Moisture-Density Characteristics of Fine-Grained Soil

3.4.3 Preliminary Tests for Oil Sand Samples

The oil sand samples were initially tested for water and bitumen content by drying in the oven and burning the bitumen content in the ignition oven. The water contents were determined in accordance with AASHTO T 265 (Laboratory Determination of Moisture Content of Soils) and the bitumen contents were determined using AASHTO T 308 test procedures (Determining the Asphalt Binder Content of Hot Mix Asphalt by Ignition Method). Table 3.2 shows the water, bitumen and fluid contents of the three oil sand samples. Based on the bitumen contents, the Suncor Energy low and high grades were designated as SE-09 and SE-14, respectively, and the Aurora high grade oil sand material was designated as AU-14. The water contents were obtained at the temperature of 110^{o}C. To obtain the bitumen contents, an average of 1500g of each sample was placed in the ignition oven, which was preheated at the temperature of 482^{o}C (900^{o}F). The bitumen contents were obtained after ignition, i.e. when constant weight of the sample is achieved. An average maximum temperature achieved for ignition was about 526^{o}C, 552^{o}C, and 569^{o}C for SE-09, SE-14 and AU-14, respectively.

TABLE 3.2 Water and Bitumen Contents of Oil Sand Samples

Oil Sand ID	Water Content (%)	Bitumen Content (%)	Fluid Content* (%)
SE-09	1.4	8.5	9.9
SE-14	3.2	13.3	16.5
AU-14	2.2	14.5	16.7

*: Fluid Content = Water Content + Bitumen Content

After separating bitumen from the oil sands through burning in the oven, washed sieve analysis tests were conducted on the sand ingredients to determine particle size distributions of the three oil sands using AASHTO T 27 test procedure. Table 3.3 shows gradation properties, and Figure 3.3 shows the grain size distributions for the three oil sand materials. All the three oil sand samples are uniformly graded fine to medium sands with the smallest to largest size particles ranging from 0.6 mm to 2.36 mm and the fines contents, i.e., passing No. 200 sieve or 0.075 mm, ranging from 7% to 15%. Similar grain size distributions for oil sand materials were reported by Cameron and Lord (1988).

TABLE 3.3 Gradation Properties for Oil Sand Samples

Oil Sand ID	D_{10}	D_{30}	D_{50}	D_{60}	Cu	Cc
SE-09	0.065	0.12	0.17	0.19	2.9	1.17
SE-14	0.075	0.14	0.18	0.21	2.8	1.24
AU-14	0.090	0.17	0.22	0.27	3.0	1.19

D_i = grain size (in mm) corresponding to *i-percent* passing by mass;

Cu = coefficient of uniformity;

Cc = coefficient of curvature.

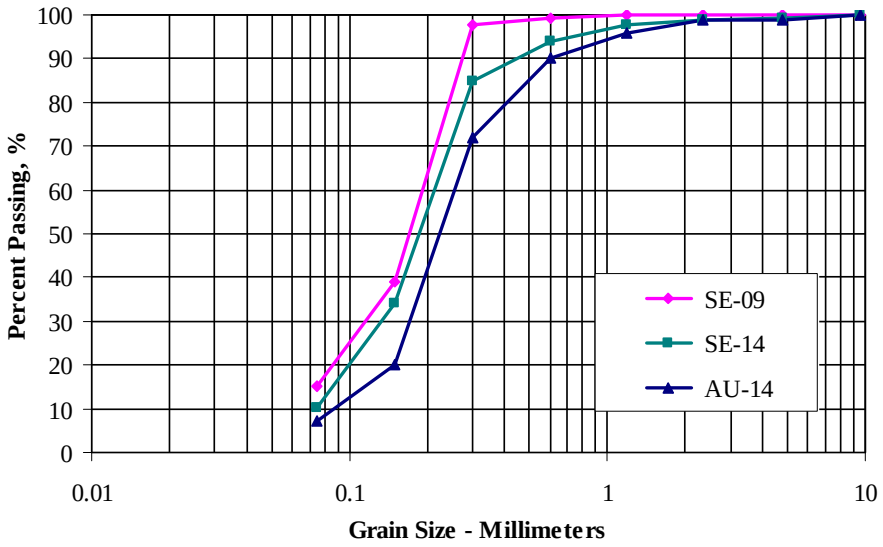

FIGURE 3.3 Particle Size Distributions of Oil Sand Samples.

Field density levels and compaction properties of the oil sands were next studied in the laboratory using a gyratory compaction device. Three replicate specimens for each oil sand sample were produced at room temperature and tested directly in the Superpave gyratory compactor. The number of gyrations to reach the specific 150-mm specimen height and the actual bulk (wet) density to achieve this height were recorded for the preparation of test specimens. During compaction, changes in bulk density of the specimen were recorded. Figure 3.4 shows the bulk density levels varying with the number of gyrations for the three oil sand materials. A considerably higher number of gyrations was needed to compact the lower bitumen content SE-09 oil sand (see Figure 3.4) when compared to the higher grade ones. The typical bulk densities achieved for SE-09 and SE-14 were 2,000 kg/m^3 at 100 gyrations and 2,050 kg/m^3 at 40 gyrations, respectively. The density achieved for AU-14 was 2,050 kg/m^3 at 25 gyrations. These achieved densities were very close to field values reported by Joseph (2005) and computed from the following equations:

$$\text{Dry density (kg/m}^3\text{)} = 2{,}150 - 37*(\%\text{ bitumen content}) \quad (3.1a)$$

$$\text{Bulk density (kg/m}^3\text{)} = 804 + 0.7*(\text{dry density in kg/m}^3\text{}) \quad (3.1b)$$

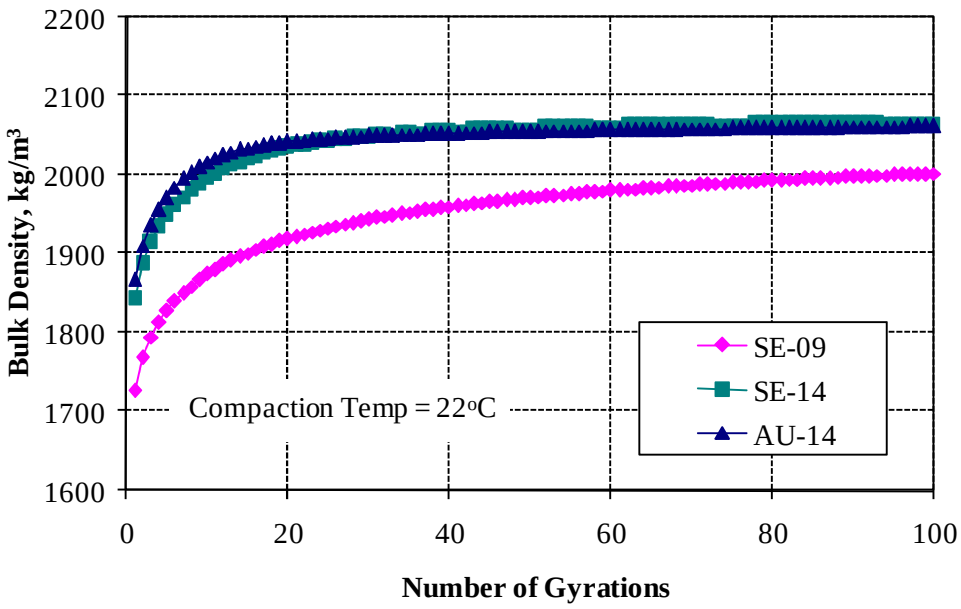

FIGURE 3.4 Gyratory Compaction Properties of Oil Sand Samples.

One preliminary strength test was conducted on the gyratory compacted specimens of the three oil sands. This test was of an investigative nature to determine the uniformity and strength profile with depth in the gyratory compacted specimens. Two replicate specimens of each sample were used for the test. A dynamic cone penetrometer (DCP) was used to penetrate the specimen in the middle of the top circular face with the 8-kg (17.6-lb) standard hammer dropped from 575-mm (22.6- in). The strength profile expressed in terms of penetrations per blow is shown in Figure 3.5 for the oil sand samples. All three oil sand samples indicated similar penetration profiles with an initial high penetration on top of the specimen followed by much stiffer sample response at depths greater than 40 mm. A penetration of 9 mm corresponds to approximately a California Bearing Ratio (CBR) of 25.

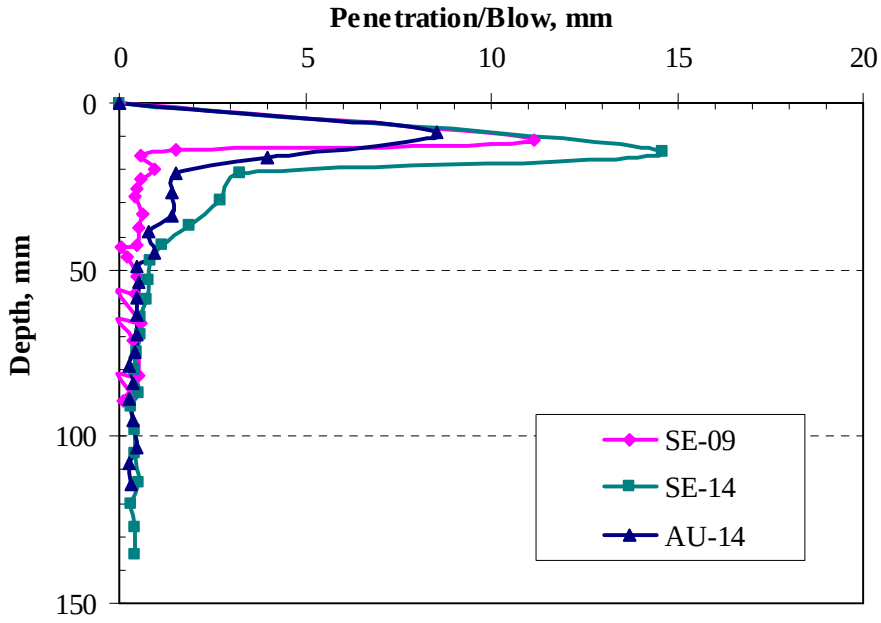

FIGURE 3.5 Strength Profiles of the Oil Sand Samples.

The second test conducted on the gyratory compacted specimens was the standard resilient modulus test (AASHTO T307) to determine the variation of the modulus properties of the oil sands with deviator stress at 5 different confining stresses, 20.7, 34.5, 69.0, 103.5, and 138.0 kPa (1 psi = 6.9 kPa). Figure 3.6 presents the test results for the SE 09 oil sand. More of a stress-softening behavior can be observed from Figure 3.6 especially at higher confining pressures. This trend was very significant for the 14% bitumen content SE-14 and AU-14 specimens although not all the stress states could be applied. Joseph (2005) reported considerably higher confining pressures under the loaded truck tires, as high as 500 kPa, for which the oil sands exhibited stress-softening behavior similar to those of the fine-grained type silty or clayey soils.

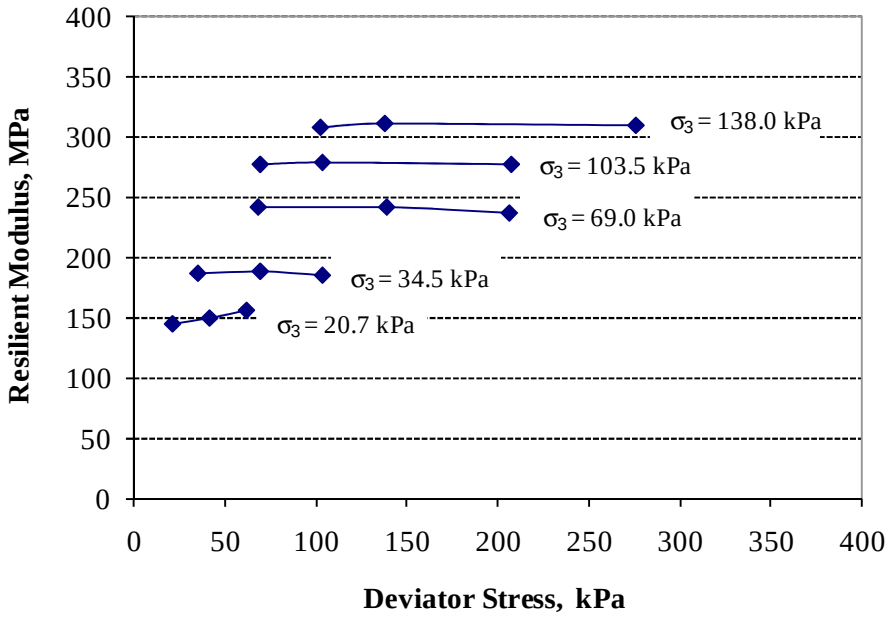

FIGURE 3.6 Resilient Modulus Test Results obtained for SE-09 Oil Sand Sample.

3.5 Suite of Laboratory Test Procedures Conducted

One of the main objectives of this study was to develop new laboratory test procedures to properly characterize field loading behavior of fine-grained cohesive soils and oil sand materials. For the various viscous, elastic and plastic material models to be developed, five different test procedures are developed for determining corresponding material properties for fine-grained soils and oil sand materials. The developed test procedures mainly are based on field loading conditions of the construction and mining haul trucks and shovels, existing laboratory tests, and the preliminary tests performed on the soil and oil sand samples used for this study. The test procedures conducted in this study include: (1) hydrostatic loading tests, (2) monotonic loading shear strength tests, (3) repeated load triaxial modulus and permanent deformation tests (4) pure shear loading tests, and (5) damping ratio tests.

3.5.1 Experimental Design Parameters

The selection of experimental design parameters for the developed test procedures was based on field and laboratory conditions.

The preliminary laboratory test results and field loading characteristics of the construction and mining equipment described in previous sections in this chapter were properly considered in the test procedures. Parameters included in the soil test program were applied stresses and loading frequency. Three moisture states from the standard Proctor tests, i.e., one moisture state chosen at the optimum moisture content, the second at 3% below the optimum for a dry soil condition, and finally, the third at 3% above the optimum for a wet/saturated condition, were key design parameters for the soil test program.

The main experimental design parameters for the oil sand materials were applied stress levels, load duration (or loading frequency) and test temperature. The selection of these parameters was based on field conditions of oil sand mining pits. Joseph (2005) reports that oil sand materials could experience extreme temperatures of $+40^{o}$C and -40^{o}C during summer and winter, respectively. This was found to be typical for oil sand materials within the top 1 to 3 meters from the ground surface. He indicated that oil sand is more problematic to construction and mining equipment during summer months than winter. Joseph (2005) also observed that oil sand materials become very soft at ambient temperature of 28^{o}C (82.4^{o}F). Based on these findings, laboratory tests for oil sand materials can reasonably be performed at two temperatures, 20 degrees Celsius (68^{o}F) and 30 degrees Celsius (86^{o}F), to account for spring and hotter summer periods, respectively.

3.5.2 Significance and Use of Developed Test Procedures

The developed test procedures are intended to provide the user with strength, modulus, damping and deformation properties needed for developing material behavior models for fine-grained cohesive soils and oil sands under field loading conditions of typical haul trucks and other construction, and mining equipment.

The hydrostatic loading test procedure provides data to determine bulk modulus and volumetric strain properties of the materials. Material's bulk modulus relates directly to the volume change of the material, and it may be used to model the volumetric deformation due to hydrostatic loadings.

The monotonic loading shear strength tests provide shear strength properties of the soil and oil sand materials. Geomaterials shear strength properties are important inputs to finite element models that incorporate Mohr-Coulomb failure criteria. The shear strength properties obtained from the developed test procedure may be used by equipment designers to model friction angle and cohesion of the ground surface affecting the design of tires/ tracks of construction and mining equipment.

The repeated load triaxial test provides laboratory data to define permanent deformation characteristics and resilient behavior of materials tested. The deformation response of the soil and oil sand material under off-road haul trucks, shovels and other construction and mining equipment loading can be conveniently characterized by plastic (permanent) and elastic (resilient) strains. The material's permanent deformation characteristics are important for developing characterization models to predict sinkage (rutting) potential, and the resilient characteristics may be used to characterize the stiffness behavior of the soil and oil sand.

The newly developed pure shear test provides static and dynamic data in both axial and radial directions to evaluate shear modulus of soils and oil sand materials. The shear modulus values obtained from the developed test procedure can be used to characterize the shear stress induced in the materials by the wheel/track loading of construction and mining haul trucks and shovels.

The damping properties test provides data to calculate damping ratio, dynamic modulus and phase angle of soil and oil sand materials. The material damping properties provide knowledge about its ability to reduce vibration. Damping ratio values may be used for tire mobility and vibration analysis of construction and mining equipment. The values of dynamic modulus and phase angle may be used as performance criteria of soils and oil sand materials over a range of loading frequencies and temperatures. Generally, dynamic modulus is used to characterize viscous and elastic properties of bituminous materials.

3.5.3 Testing Equipment

The Industrial Process Controls Limited (IPC)'s servo-pneumatic testing device, Universal Testing Machine (UTM) is suitable for the developed test procedures.

The IPC UTM is a closed-loop servo control loading system. The main part of the system consists of loading frame, triaxial cell, Control and Data Acquisition System (CDAS) and integrated software package and personal computer (PC). The IPC UTM has large loading frames that allow the use of a triaxial cell to test 150-mm diameter by 150-mm high specimens. The nature of the frame limits deflection and vibrations which could influence the accuracy of measurements especially when both axial and radial dynamic repeated loadings are applied on the sample at the same time. The UI-FastCell and the RaTT cell are two main cells selected for the developed triaxial test procedures. The selection of these advanced triaxial testing equipment was based on their unique capabilities described in Chapter 2.

The CDAS directly controls the servo valve to apply the requested loading rate or waveform for testing. The CDAS is linked to the PC through a standard serial communications link. While the specimen is being subjected to loading forces, the CDAS captures data from the transducers and transfers these data, using the serial link, to the PC for processing, display and storage. The load and specimen deformation are measured by load cells and linear variable displacement transducers (LVDTs), respectively. The current UI-FastCell setup uses 20 kN capacity load cell whereas the RaTT cell setup is limited to 5 kN capacity load cell. Other testing equipment selected for the test procedures are the UTM-5P small triaxial cell and the Humboldt pneumatic loading direct shear device for shear strength tests.

3.5.4 Test Specimens and Sample Preparation

With the exception of the triaxial shear strength tests, all the triaxial tests were performed on 150 mm in diameter by 150 mm high test specimens. The fine grained soil specimens for the triaxial tests were prepared from split mold assembly whereas oil sand specimens were obtained from gyratory compaction machine (Figure 2.4). The triaxial shear strength test was performed on 50.8 or 71-mm diameter (approximately 2 or 2.8-in diameter) cylindrical specimens. The diameter to height ratio is 1:2. The direct shear tests were performed on square prismatic specimens of size 100 mm. The thickness of the prismatic sample is between 25 and 40 mm.

All the oil sand test specimens were conditioned at a minimum of six hours in an environmental temperature chamber at the desired temperatures. The following subsection presents sample preparation for fine-grained soils and oil sands.

3.5.4.1 Fine-Grained Soil Specimen Preparation

The soil samples were oven dried and sieved through the 4.75 mm sieve (No.4 sieve) to break up larger aggregations to facilitate the distribution of water through the soil during mixing. The prepared samples were mixed with the required amount of water to bring the moisture content to the target value. Cylindrical specimens were prepared to fit in the confinement chamber of the UI-FastCell or RaTT cell. The soil sample was prepared at the required water content and maximum dry density using a split aluminum compaction mold specifically manufactured for use with the UI-FastCell. A latex membrane, 0.6-mm (0.025-in.) thick, was attached to the bottom platen with an o-ring and the platen was placed in an assembly of a split mold for compaction. The soil material mixed with the required amount of water was placed in the mold in three lifts, and each lift was rodded 25 times using a standard rod for concrete testing. A pneumatic vibratory compactor was used for compaction. Specimen density was controlled by measuring the weight of material and compacted thickness of each lift, referenced to the top of the mold. The surface of each lift was scarified up to a depth of approximately 12-mm, and the next lift was placed, and compacted. After compaction, the final height and density of specimen were noted, and a loading platen was placed at the top of the specimen. The split mold was then removed and a second membrane (latex membrane) was placed on the specimen and secured to the top and bottom platens with o-rings. The specimen was placed centered in the UTM test frame, and the UI-FastCell or RaTT cell was lowered for testing to start.

For triaxial shear testing, soil specimens were mechanically compacted in a mold by a standard Proctor compaction hammer in lifts of three to the target density. Similarly, the surface of each lift was scarified to effect compaction at required number of lifts (usually 3 or 5 lifts). After compaction, specimen density was calculated and the specimen was placed in a small triaxial cell confinement chamber for testing.

3.5.4.2 Oil Sand Specimen Preparation

All specimens except for shear strength test specimens were prepared using IPC Servopac gyratory compactor. Cylindrical specimens were compacted at different density levels depending on the applied number of gyrations at the approximate density states in the field using the gyratory compactor. A 150-mm diameter filter paper was placed at the bottom of a gyratory compaction mold. The required amount of oil sand material to achieve the expected density is placed in the mold. Another filter paper was placed on top of the sample for compaction. Compaction was initiated by an integrated personal computer, and achieved by simultaneous action of static compression and shearing action resulting from the motion of specimen. During compaction, a vertical compression force was applied using servo controlled pneumatic actuator to initiate the gyratory motion. When the compaction process was completed, the specimen was ejected from the mold by a pneumatic system setup. The achieved specimen density was recorded in the computer program, and final compaction data were retrieved and stored in the form of readable ASCII test files on the PC. After compaction, specimens were placed in 0.6 mm thick latex membrane for testing. Following this, specimens are conditioned in the temperature chamber before testing at the desired temperature.

The triaxial shear strength test specimens were mechanically prepared using the procedure described for soils triaxial shear strength testing in subsection 3.5.4.1. The direct shear test specimens were prepared from gyratory compacted specimens (see 3.5.4.2). Using a masonry saw, the gyratory compacted specimens were cut to the required size for testing.

3.5.5 Developed Test Procedures

The suites of tests were performed to determine strength, modulus, and damping and deformation properties using hydrostatic, shear, and repeated/cyclic loading techniques. These test procedures were applicable to soils and oil sand materials, and other geomaterials subjected to construction and mining equipment loading conditions. The UI-FastCell and RaTT cell setups described in Chapter 2 were used to conduct the hydrostatic loading, repeated loading, pure shear loading and damping ratio tests.

The shear strength tests were performed with a conventional triaxial cell in UTM-5P loading system, and direct shear testing device described in Chapter 2. Specimen preparations for various test procedures are described in section 3.5.2. Overall, five different test procedures were followed in this study. Each test procedure is described in the following subsections.

3.5.5.1 Procedure A - Hydrostatic Loading Test

The hydrostatic loading test procedure provides data to determine the bulk modulus and volumetric deformation properties of soils and oil sand materials under isotropic (hydrostatic) loading. A pulsed wave shape with 60 seconds loading and 60 seconds unloading is applied on the specimen. The complete applied stress states/path and the required measurements are as follows:

- Applied stresses: 0 → 20.7 kPa 0 → 41.4 kPa → 0 → 69 kPa → 0 → 138 kPa → 0 → 276 kPa (static all-around stresses, $\sigma_1 = \sigma_3$ in triaxial states; 1 psi = 6.9 kPa). Specimen undergoes load-unload-reload until the last load cycle is applied;
- Properties measured: Continuous record of axial and radial strains, ε_1 and ε_3, in the vertical and radial directions, respectively.

The sample's bulk modulus (K) and volumetric strains (ε_v) may be computed using the following equation:

$$K = \frac{\Delta\sigma_1 + \Delta\sigma_2 + \Delta\sigma_3}{\Delta\varepsilon_v} = \frac{\Delta p}{\Delta\varepsilon_v} \tag{3.2}$$

where,

Δp = incremental hydrostatic pressure (stress), $\Delta\varepsilon_v$ = incremental volumetric strain.

$\varepsilon_v = \varepsilon_1 + \varepsilon_2 + \varepsilon_3 = \varepsilon_1 + 2\varepsilon_3$ for cylindrical specimen in triaxial tests and

$p = (\sigma_1 + \sigma_2 + \sigma_3)/3 = (\sigma_1 + 2\sigma_3)/3$

3.5.5.2 Procedure B - Shear Strength Test

Shear strength tests are performed to determine friction angle ϕ and cohesion c properties. Both triaxial and direct shear tests are conducted in this study. The triaxial test is conducted under different constant confining pressures while vertical deviator stress is monotonically increased until the sample fails. For the direct shear test, at constant normal stresses, a horizontal stress (shear stress) is applied to the sample until it is sheared. The following are the loading conditions and measurements taken from this test procedure:

- Confining pressure σ_3 levels: 0, 20.7, 41.4, 69.0, 138.0, and 276.0 kPa (1 psi = 6.9 kPa). For direct the shear tests, higher normal stress of 552.0 kPa may be used to simulate high tire pressures of large capacity construction and mining trucks;
- Displacement controlled test corresponding to a loading strain rate of approximately 1 % strain/minute (typical loading strain rate for soils strength testing);
- Properties measured: Continuous record of strain, ε, in the vertical/horizontal direction, maximum deviator stress σ_d (or shear stress) attained at or until specimen failure;

Initial modulus may be obtained from the stress-strain curve, and the shear strength properties, ϕ and c are generally computed from the Mohr-Coulomb criterion given by Equation 2.1. For the triaxial shear test the strength properties may conveniently be computed from the least squares regression equation in the form of $\sigma_1 = a + b\sigma_3$ (see Figure 3.7), where, a and b are regression constants determined from curve fit in the experimental data. The values of ϕ and c are computed from Equations 3.3.

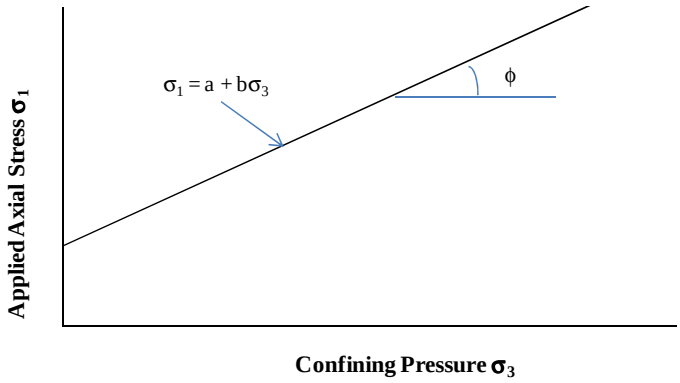

FIGURE 3.7 Relationship between Axial Stress and Confining Pressure.

$$\phi = \sin^{-1}\left(\frac{b-1}{b+1}\right) \quad ; c = \frac{a}{2\cdot\sqrt{b}} \tag{3.3}$$

3.5.5.3 Procedure C - Repeated Load Triaxial Test

The repeated load triaxial test procedure for the fine-grained cohesive soil and oil sand testing is similar to the current AASHTO T307 test procedure used for determining resilient modulus of soils and aggregate materials or geomaterials. However, from the initial conditioning stage of the AASHTO T307 test procedure, permanent deformation properties of granular materials are often obtained at only one stress state using equal confining and deviator stresses of 103.5 kPa (15 psi), or a total vertical stress (σ_1) to horizontal confining stress (σ_3) ratio of 2. A haversine load pulse with 0.1-second loading and 0.9-second rest period is applied on the specimen for 1,000 load cycles. Thus, the AASHTO T307 test procedure is limited in terms of applied stress states. In this study, newly developed repeated load triaxial test procedure for soils and oil sand materials considers higher stress states (stress ratios). Further, two different haversine load pulse durations of 0.1 and 0.5 seconds are also included in the laboratory testing program to consider the effects of different trafficking speeds of haul trucks and other construction and mining equipment on the soil and oil sand sinkage and rut development in the field. A major consideration in the developed test procedure is the ability to measure both resilient modulus and permanent deformation in the same test. In addition, each test specimen is subjected to *only* one stress state or loading condition.

The use of a new specimen for each stress state eliminates the effect of stress history on permanent deformation. The stress levels and other loading conditions applied on the specimen are as follows:

- Confining pressure σ_3 levels: 0, 20.7, 41.4, 138 and 276 kPa (1 psi = 6.9 kPa);
- Vertical deviator stress σ_d levels: 20.7, 41.4, 69, 138 and 276 kPa;
- Load pulse duration: 0.1 and 0.5 sec;
- At different number of load applications, permanent deformations (δ_p) are recorded for each cycle and the corresponding plastic strains (ε_p) and elastic strains (ε_r) are computed;
- The resilient modulus M_R of the sample is computed as follows:

$$M_R = \frac{\sigma_d}{\varepsilon_r} \tag{3.4}$$

3.5.5.4 Procedure D - Pure Shear Loading Test

The pure shear tests are performed for obtaining the shear modulus of the materials as a function of the applied stress states. The applied stresses due to construction and mining equipment loads acting on an element of soil or oil sand beneath a level ground surface can best be represented by using Mohr circles and stress paths as illustrated in Figure 3.8. An element of soil or oil sand under at-rest stress conditions (vertical and horizontal stresses, σ_v' and σ_h') and the subsequent cyclic ground shaking due to shear stress τ, are shown in Figure 3.7a. The corresponding Mohr circles and stress paths are also plotted in Figures 3.8b and 3.8c, respectively. Upon application of the pure shear loading, the radius of the Mohr circle representing at-rest conditions increases to result in a larger circle (shown by dashed line). The center point of the new circle, however, does not move since the vertical and horizontal stresses remain constant. The stress path, therefore, moves vertically upward to point D. When the shear loading reverses direction in the next cycle, the stress path moves this time vertically downward to point B and that the principal stress axes rotate.

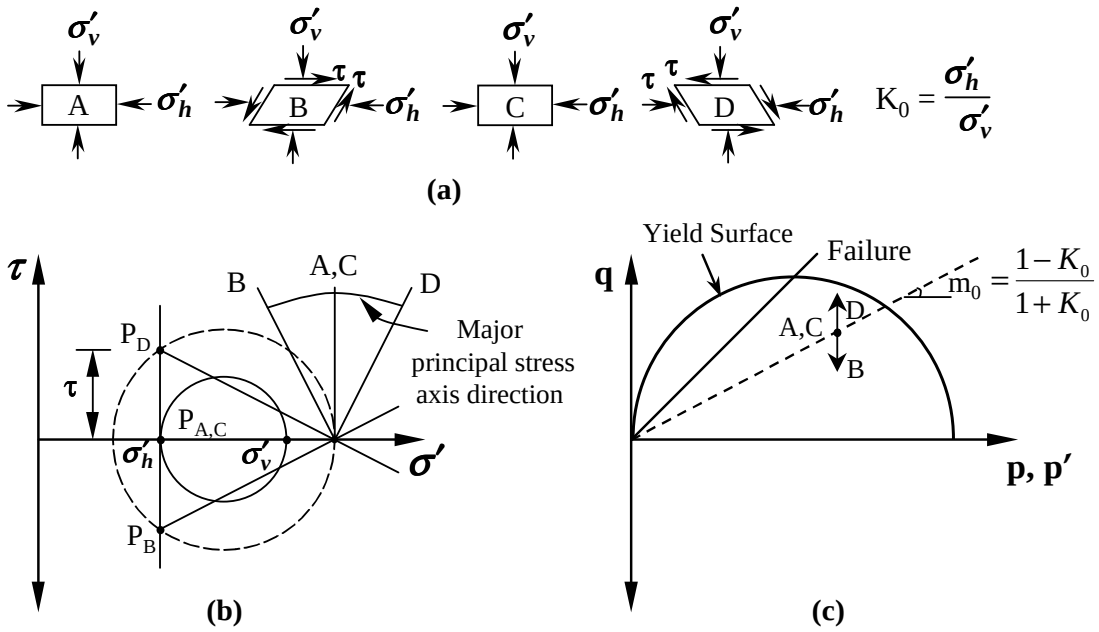

FIGURE 3.8 Stress Conditions Imposed on Element of Soil below Level Ground Surface by Vertically Propagating Shear Waves, and the Corresponding Mohr Circles and Stress Paths (Kramer 1996).

This type of continuous rotation of principal stresses corresponding to field stress conditions on a soil or oil sand element can closely be simulated in the laboratory. For the application of the pure shear stresses, two alternating pulses of the same magnitude are applied at the same time in the vertical and radial directions. Figure 3.9 shows the 90-degree out of phase cyclic stresses, $\Delta\sigma/2$, applied on the specimen by decreasing (or increasing) the lateral pressure by the same amount $\Delta\sigma/2$, by which the vertical stress is increased (or decreased). The corresponding Mohr circle is then made to expand and contract about a constant center point and the resulting stress oscillates by the magnitude of $\Delta\sigma/2$ ($= \tau_{cyc}$) for the compression and extension loadings. The applied stress path is then in the vertical direction similar to that of the pure shear loading induced by a vertically propagating shear wave. The pure shear loading is indicated in Figure 3.8 by the vertically oriented stress path, $\pm\tau_{cyc}$, on a shear stress q ($=\sigma_1-\sigma_3$) - effective mean pressure p [$= (\sigma_1+2\sigma_3)/3$] plot. Figure 3.9 shows the specimen first loaded with a total normal stress for hydrostatic statue of σ_3. The stresses on the specimen are applied such that axial stress is equal to $\sigma_3 + \frac{1}{2}\sigma_d$ and the radial stress is $\sigma_3 - \frac{1}{2}\sigma_d$.

Next, the specimen is loaded so that the axial stress is $\sigma_3 - \frac{1}{2}\sigma_d$ and the radial stress becomes $\sigma_3 + \frac{1}{2}\sigma_d$. It can be observed that at any time, a cyclic normal stress of $\frac{1}{2}\sigma_d$ are applied on the specimen simultaneously in the vertical and horizontal directions to achieve pure shear loading condition.

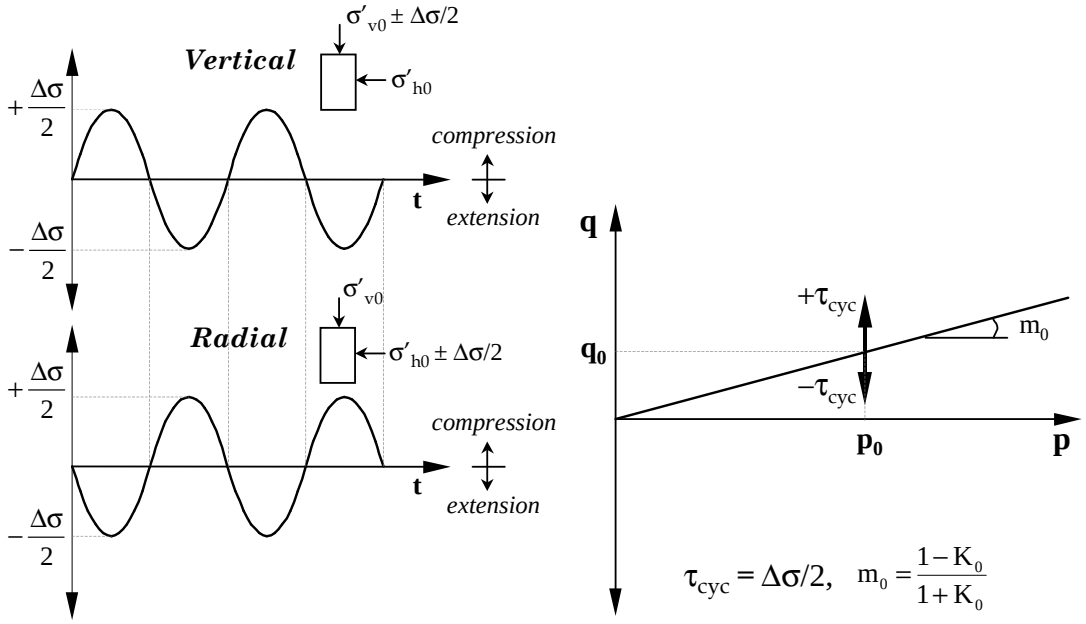

(a) Applied cyclic stresses (b) Corresponding stress path

FIGURE 3.9 Pure Shear Loading Applied on the Specimen.

The loading conditions and measurements to obtain pure shear characteristics due to the applied static and dynamic field loading conditions are as follows:

- Confining pressure levels: 20.7, 41.4, 69 and 138 kPa (1 psi = 6.9 kPa);
- Shear stress levels: 20.7, 41.4, 69 and 138 kPa (a maximum value of applied σ_3);
- Loading frequencies: 2 and 10Hz;
- At different stress levels strains in vertical and radial directions are recorded. The Shear modulus, G is calculated using the measured shear strain and the applied shear stress as follows:

$$\tau = \sigma_1 - \sigma_3 \qquad (3.5a)$$

$$\gamma = \frac{2}{3}(\varepsilon_1 - \varepsilon_3) \quad (3.5b)$$

$$G = \frac{\tau}{\gamma} \quad (3.6)$$

where, τ = applied shear stress, σ_1, σ_3 = axial and radial (confining) stresses, respectively, γ = shear strain, ε_1 and ε_3 are axial and radial strains, respectively.

3.5.5.5 Procedure E – Damping Property Test

The main objective of this test procedure is to provide data to measure damping ratio of fine-grained cohesive soils and oil sand materials. Damping ratio is defined as the ratio of total energy dissipated per cycle by test specimen to the maximum strain energy stored by the sample during cyclic loading. The energy dissipated per cycle in a specimen is proportional to area of hysteresis loop as shown in Figure 3.10. The current test procedures used for determining damping ratio of soils are the cyclic triaxial (ASTM D3999) and the resonant column procedures (ASTM D4015). As mentioned earlier, these test procedures have limited loading conditions. For instance, in the cyclic axial tests for soils, a limited frequency range of 0.1 to 2Hz is suggested for the loading equipment. In the resonant column test procedure, material properties are obtained at limited small strains. However, soil and oil sand materials experience moderate to large strains under heavy construction and mining equipment in the field. Test procedures used for materials under such heavy equipment should be able to account for the large strains and other field loading conditions.

The newly developed damping ratio test procedure for the fine-grained soils and oil sand materials is simple and considers high stresses and loading frequencies. Damping properties of oil sand materials are obtained at two different test temperatures to simulate prevailing field temperatures. In addition, the test configuration allows dynamic modulus and phase angle of tested materials to be computed. The new Mechanistic-Empirical Pavement Design Guide (NCHRP 1-37A 2004) uses the dynamic modulus as the stiffness parameter for hot-mix asphalt characterization. The dynamic modulus is defined as the absolute value of the complex modulus (see Equation 3.10), and the phase angle of the material is the amount by which strain response lags the applied stress.

The value of the phase angle is an estimate of the material's viscous or elastic behavior under specified loading conditions.

The loading conditions proposed for damping property tests are as follows.

- Confining pressure levels: 0, 20.7, 41.4, 69, 138 and 207 kPa (1 psi = 6.9 kPa)
- Vertical deviator stress levels of 41.4 kPa
- Complete sine load waveform applied at the loading frequencies of 2, 5, 10, and 20Hz with no rest between the sinusoidal waves
- At different stress levels strains in vertical and radial directions are recorded to compute damping ratio and dynamic modulus of the material. Damping ratio, D dynamic modulus $|E^*|$ and phase angle δ are computed from the test data.

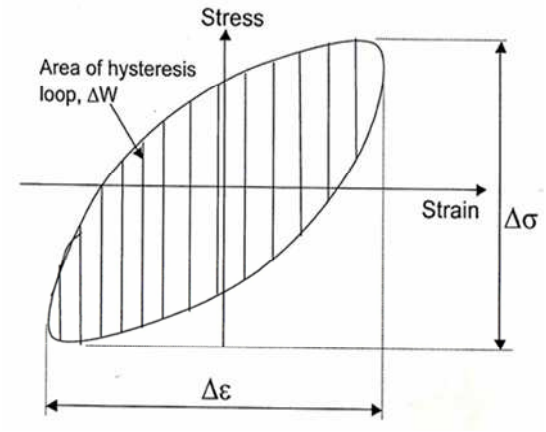

FIGURE 3.10 Typical Hysteresis Loop used for Damping Ratio Computations.

The damping ratio and the dynamic modulus of the soil or oil sand material are computed from Equations 3.7 and 3.10, respectively.

$$D = \frac{2}{\pi} \frac{\Delta W}{\Delta\sigma \text{ x } \Delta\varepsilon} \tag{3.7}$$

where, ΔW = area of the hysteresis loop = the amount of energy dissipated by the material during one cycle of loading at angular frequency ω. The angular frequency in rad/s is found based on the test frequency f, in Hz.

$\Delta\sigma$ = incremental axial stress, and $\Delta\varepsilon$ = incremental axial strain.

The maximum applied peak stress (σ_0) and maximum measured peak strain (ε_0) values for a material subjected to a sinusoidal loading can be conveniently obtained by using a generalized mathematical curve fit function given in Equation 3.8. The parameters used to compute the maximum values of stress and strain could also be used to calculate the phase angle of the materials.

$$F(t) = a_0 + a_1 t + b\cos(\omega t) + c\sin(\omega t) \tag{3.8}$$

$$\text{Amplitude} = \sqrt{b^2 + c^2} \tag{3.9a}$$

$$\text{Phase Angle} = \tan^{-1}\left(\frac{c}{b}\right) \tag{3.9b}$$

The dynamic modulus of the material is computed by the following equation:

$$|E^*| = \frac{\sigma_0}{\varepsilon_0} \tag{3.10}$$

where, $|E^*|$ = dynamic modulus;

σ_0 = applied stress amplitude (peak stress);

ε_0 = measured strain amplitude (peak strain);

$\omega = 2\pi f$ = angular frequency; $f = 1/T$ = frequency,

T = period, and a_0, a_1, b and c are regression constants.

3.6 Summary

Five new and improved laboratory triaxial test procedures were developed to determine strength, modulus and damping properties, and permanent deformation characteristics of fine-grained soils and oil sand materials. The tests procedures were based on field loading characteristics of off-road haul trucks and shovels, and other construction and mining equipment. The results from preliminary laboratory test program performed on one fine-grained soil sample and three oil sand samples, and field loading and stress conditions were considered in the development of the test procedures. These advanced test procedures are simple and rational, and can reasonably simulate behavior of fine-grained cohesive soils and oil sand materials under typical field loading conditions of compaction, construction and mining equipment. Detailed sample preparation methods for suitable specimen sizes were suggested for all the test procedures. The test procedures utilize testing equipment and devices capable of simulating in the laboratory, wide range of stress conditions, i.e., low to high stresses experienced by the materials in the field. Detailed discussions were provided for the use and significance of the individual test procedures. Data obtained from these test procedures can conveniently be used to develop performance characterization models to account for distresses faced by off-road vehicles during construction and mining activities.

CHAPTER 4 BULK MODULUS OF FINE-GRAINED COHESIVE SOIL AND OIL SAND MATERIALS

4.1 Introduction

An element of soil subjected to hydrostatic (isotropic) loading condition experiences an all-around uniform normal stresses and zero shear stresses. The bulk modulus is a material property that describes the resistance of the soil to volume change when the element is subjected to hydrostatic loading. In this study, bulk modulus is determined in the laboratory for one fine-grained cohesive soil and three oil sand materials using a newly developed hydrostatic compression test procedure. Details of the developed test procedure are described in Chapter 3. The results from the hydrostatic compression tests are analyzed, and used to develop empirical equations and material characterization models for the soil and oil sand samples.

4.2 Testing Program and Procedure

The hydrostatic loading test developed in section 3.5.4 (Procedure A) was used to conduct the entire laboratory testing on the soil and oil sand samples. A series of hydrostatic loading cycles described in test Procedure A were applied on CAT A-6 soil specimens at three moisture states: (1) dry of optimum w = 11.3%, (2) optimum w_{opt} = 14.3% and (3) wet of optimum w = 17.3%. Tests on the oil sand materials were performed on SE-09, SE-14, and AU-14 samples with bitumen contents of 8.5%, 13.3% and 14.5%, respectively at temperatures of 20^{o}C and 30^{o}C. Two replicate specimens were tested for all the samples. Thus, a total of 6 hydrostatic compression tests were performed on the soil sample at the three water contents or moisture states whereas 12 tests were performed on the three oil sand samples.

The UI-FastCell test setup was used for applying the hydrostatic stresses on both the soil and oil sand samples. A pulsed wave shape with 60 second loading and 60 second unloading was applied on the test specimens. The axial static loading was measured by the load cell, and the radial loading was measured by a pressure transducer. Both axial and radial strains were measured by two symmetrical LVDTs.

4.3 Test Data Analyses

The applied hydrostatic stresses and measured volumetric strains obtained from hydrostatic compression tests are used to calculate bulk modulus. A plot of the applied isotropic compression stress against volumetric strain of soils gives a nonlinear curve (Terzaghi and Peck 1967, Vesic and Clough 1968, and Quabain et al., 2003). Vesic and Clough (1968) suggested that the soil's elastic properties could conveniently be obtained from the nonlinear curve by straight line approximations that linearly relate increments of both the isotropic stress and volumetric strains. In this study, the straight line approximation concept was used for analyzing the test results of the samples. The bulk moduli (K) of the soil and oil sand samples were calculated from the ratio of the incremental hydrostatic stress ($\Delta\sigma$) to the incremental volumetric strain ($\Delta\varepsilon_v$). Equation 4.1 is used to define the bulk modulus of the tested samples.

$$K = \frac{\Delta\sigma}{\Delta\varepsilon_v} \tag{4.1}$$

The volumetric strain ε_v is computed from the axial strain ε_1 and the radial strain ε_3 as $\varepsilon_v = \varepsilon_1 + 2\varepsilon_3$. For triaxial compression tests, hydrostatic stress $\sigma = \sigma_1 = \sigma_2 = \sigma_3$.

4.3.1 Analyses of Fine-Grained Soil Test Results

A total of about 270 stress-strain data sets for each test were analyzed for the bulk modulus of the soil sample at one moisture state. Each data set represents an average value from two replicate specimens. Figure 4.1 shows a plot of the applied hydrostatic stress against the total volumetric strain for CAT A-6 soil sample at the three moisture states. A polynomial regression curve was fit into individual data sets of the soil sample at optimum, dry of optimum and wet of optimum, and straight line approximation was used to obtain the incremental hydrostatic stresses and corresponding volumetric strains. The bulk modulus was then computed at each hydrostatic loading stress using Equation 4.1.

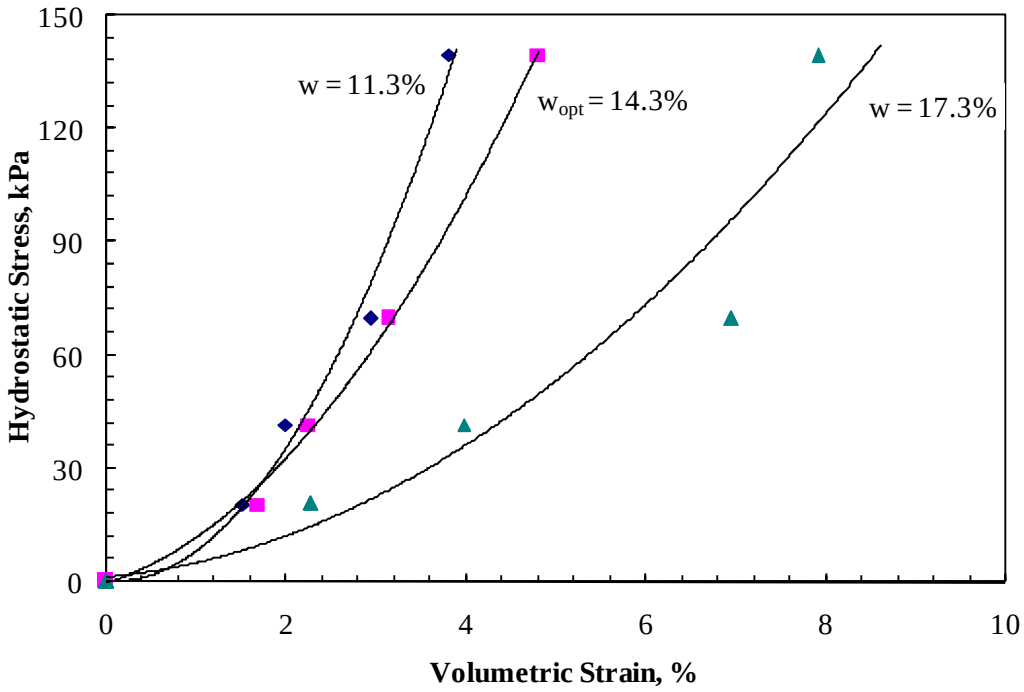

FIGURE 4.1 Hydrostatic Loading Test Results for CAT A-6 Soil at three Water Contents.

Table 4.1 lists summarized test results of the soil sample at the three moisture states. As expected, the soil sample at dry of optimum gave the highest bulk modulus values whereas the lowest bulk modulus values were obtained at wet of optimum. The average bulk modulus value increases by 0.3 MPa from optimum to dry of optimum, and decreases by 0.92 MPa from optimum to wet of optimum. Thus, a change in water content of 3% below the optimum resulted in about 15% increase in the bulk modulus of the soil sample, whereas a change in water content of 3% above the optimum resulted in about 45% decrease in the modulus values. The high lubrication of soil particles at wet of optimum water content weakens the soil sample. Therefore, the modulus of the sample becomes low at wet of optimum compared to dry of optimum, or the soil becomes less sensitive at dry of optimum.

TABLE 4.1 Test Results for CAT A-6 Soil at Three Moisture States

$\Delta\sigma$ (kPa)	w =11.3%		w_{opt} = 14.3%		w = 17.3%	
	$\Delta\varepsilon_v$ (%)	K (MPa)	$\Delta\varepsilon_v$ (%)	K (MPa)	$\Delta\varepsilon_v$ (%)	K (MPa)
20.7	1.50	1.38	1.50	1.38	2.90	0.71
41.4	2.18	1.90	2.38	1.74	4.25	0.97
69	2.80	2.46	3.20	2.16	5.90	1.17
138	3.80	3.63	4.80	2.88	8.50	1.62

4.3.1.1 Regression Equations for CAT A-6 Soil Sample

Figure 4.2 shows empirical equations of bulk modulus as power functions of hydrostatic stress for the soil sample at the three moisture states. The significantly high coefficients of correlation values ($R^2 > 0.99$) indicate that the straight line approximation concept (Equation 4.3) used for the analyses performed well for the soil sample at all the three moisture states.

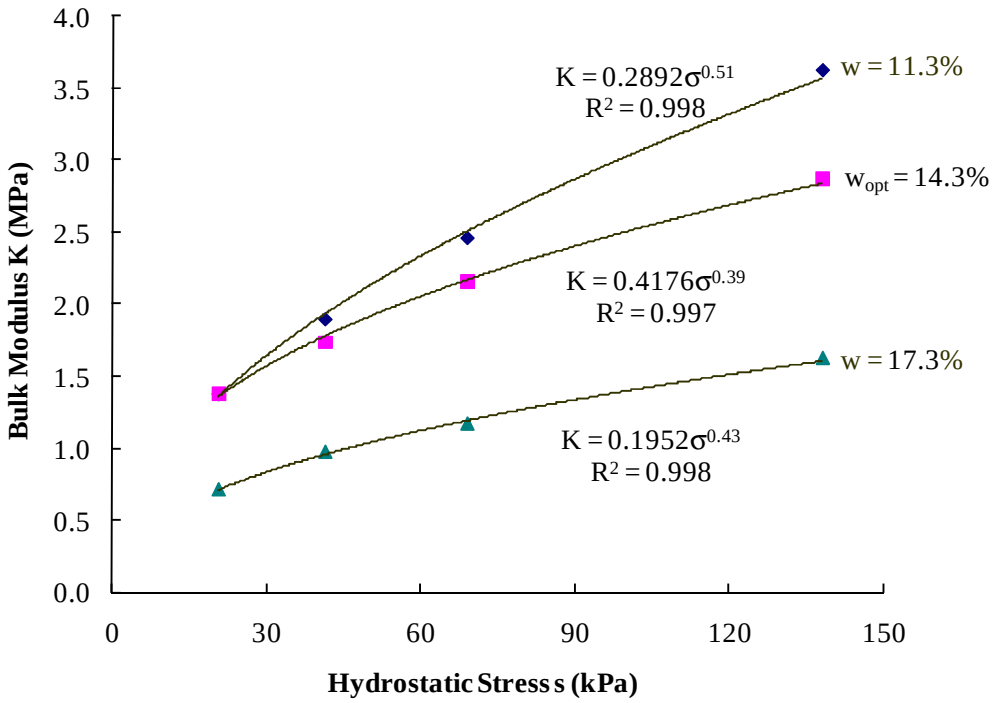

FIGURE 4.2 Correlations between Bulk Modulus and Hydrostatic Stress for CAT A-6 Soil at three Moisture States.

4.3.2 Analyses of Oil Sand Test Results

For each oil sand sample a total of about 270 stress-strain data points were obtained from testing one specimen. Thus, about 540 data points were analyzed for each oil sand sample at the two test temperatures. Note that each data set represents an average value from the two replicate specimens. Similar analysis performed to obtain the bulk modulus values of the CAT A-6 soil sample was used to determine the bulk modulus values of the oil sand samples (section 4.3.1). A polynomial function was fit into test data of the SE-09, SE-14 and AU-14, and the incremental hydrostatic stresses and volumetric strains obtained were used to calculate the bulk modulus values. Figures 4.3 and 4.4 show the variation of hydrostatic stress with volumetric strain for the three oil sand samples at 20°C and at 30°C, respectively.

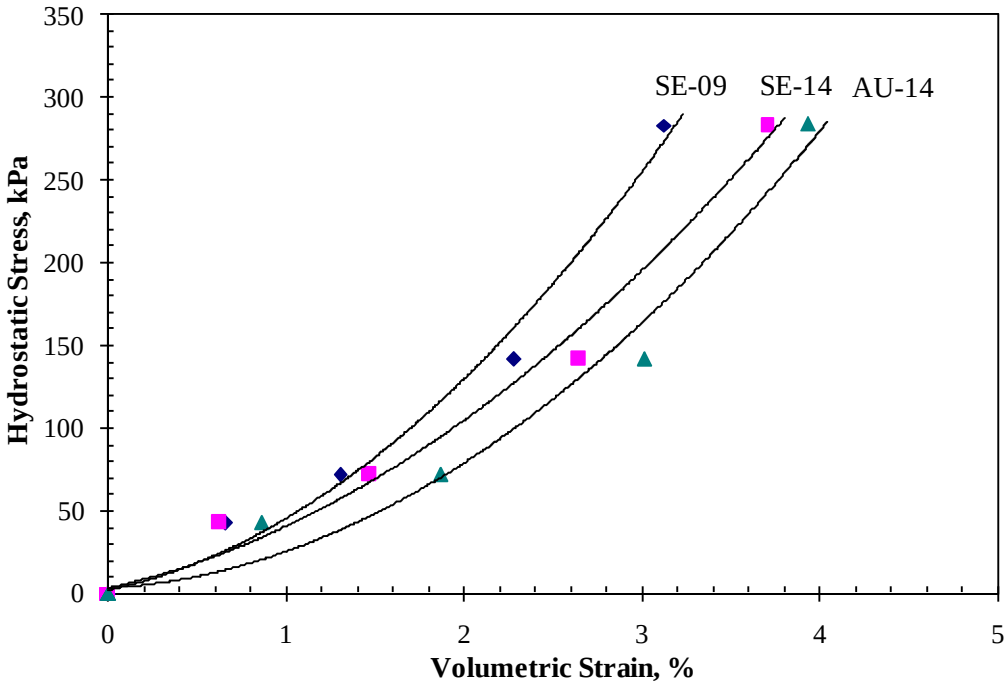

FIGURE 4.3 Variation of Hydrostatic Stress with Volumetric Strain for the Oil Sands at 20°C.

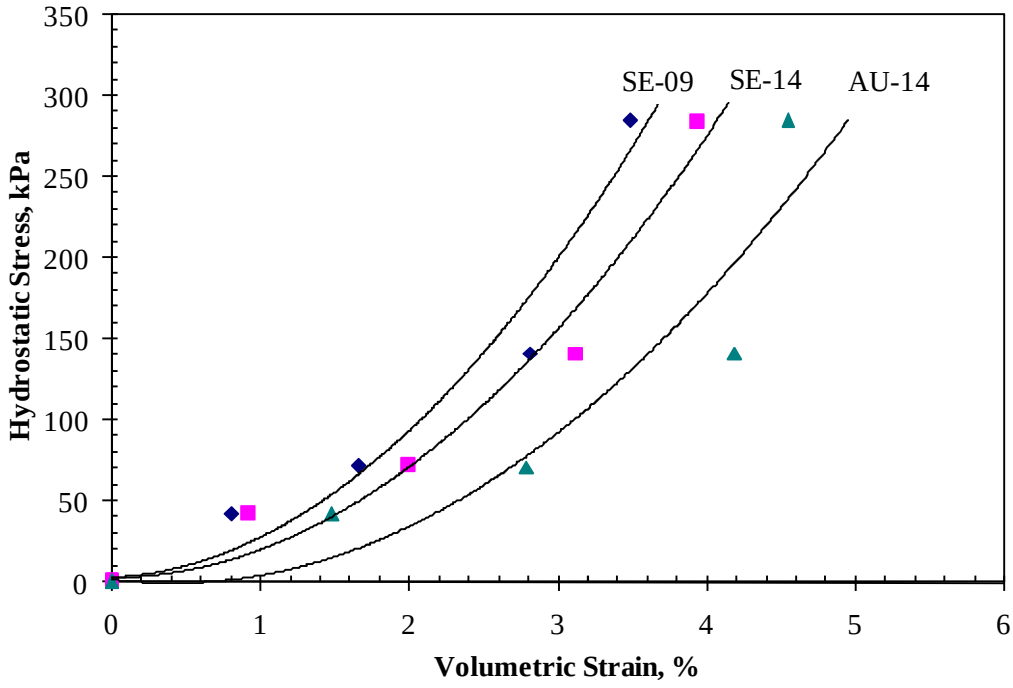

FIGURE 4.4 Variation of Hydrostatic Stress with Volumetric Strain for the Oil Sands at 30°C.

Tables 4.2 and 4.3 list the test results for all the oil sand samples at 20°C and 30°C, respectively. As expected, higher bulk modulus values were obtained at 20°C than at 30°C for all the oil sand samples. The SE-09 sample gives the highest bulk moduli while AU-14 sample gives the lowest values. At 20°C, the difference in magnitude between the average bulk modulus of SE-09 and AU-14 samples is 1.61 MPa, i.e., about 26% difference, and the difference between SE-09 and SE-14 is 0.78 MPa, representing about 12.5%. The average bulk modulus of SE-14 and AU-14 samples are close to each other although the bulk modulus of SE-14 is a little higher than AU-14. Similar trend in bulk modulus at 20°C is observed for the samples at 30°C. That is, the SE-09 sample has the highest bulk modulus values whereas AU-14 sample has the lowest bulk modulus. However, it is interesting to note that the magnitude of the bulk modulus of SE-14 and AU-14 samples were comparable at the two test temperatures. The average bulk modulus of SE-14 at 20°C is about 1.2 times of the bulk modulus of AU-14 compared to about 1.3 times at 30°C. The amount of bitumen content and the test temperature appear to be the factors that influenced the overall stiffness of the oil sand materials.

The AU-14 sample with high bitumen content has lower bulk modulus, whereas the SE-09 sample with low bitumen content has the highest bulk modulus. Also, for all the oil sand samples the average bulk modulus at 20°C was higher than the average bulk modulus at 30°C.

TABLE 4.2 Test Results for Oil Sand Samples at 20°C

$\Delta\sigma$ (kPa)	SE-09		SE-14		AU-14	
	$\Delta\varepsilon_v$ (%)	K (MPa)	$\Delta\varepsilon_v$ (%)	K (MPa)	$\Delta\varepsilon_v$ (%)	K (MPa)
41.4	0.88	4.70	1.02	4.06	1.40	2.96
69.0	1.35	5.11	1.52	4.54	1.90	3.63
138.0	2.10	6.57	2.43	5.68	2.78	4.96
276.0	3.18	8.68	3.60	7.67	3.90	7.08

TABLE 4.3 Test Results for Oil Sand Samples at 30°C

$\Delta\sigma$ (kPa)	SE-09		SE-14		AU-14	
	$\Delta\varepsilon_v$ (%)	K (MPa)	$\Delta\varepsilon_v$ (%)	K (MPa)	$\Delta\varepsilon_v$ (%)	K (MPa)
41.4	1.30	3.18	1.50	2.76	2.18	1.90
69.0	1.65	4.18	1.95	3.54	2.60	2.65
138.0	2.30	6.00	2.80	4.93	3.70	3.73
276.0	3.58	7.71	4.00	6.90	4.90	5.63

4.3.3 Bulk Modulus Characterization Models

Statistical regression analyses were performed on the oil sand test results to develop empirical equations for each sample at 20°C and at 30°C. Figures 4.5 and 4.6 indicate the relationships between bulk modulus and hydrostatic stress at 20°C and at 30°C, respectively, and the resulting correlation equations for the three oil sand samples. The high R^2 values indicate that good approximations were achieved with Equation 4.1. Therefore, strong correlations exist between the bulk modulus and hydrostatic stress for all the oil sand samples tested at the two temperatures.

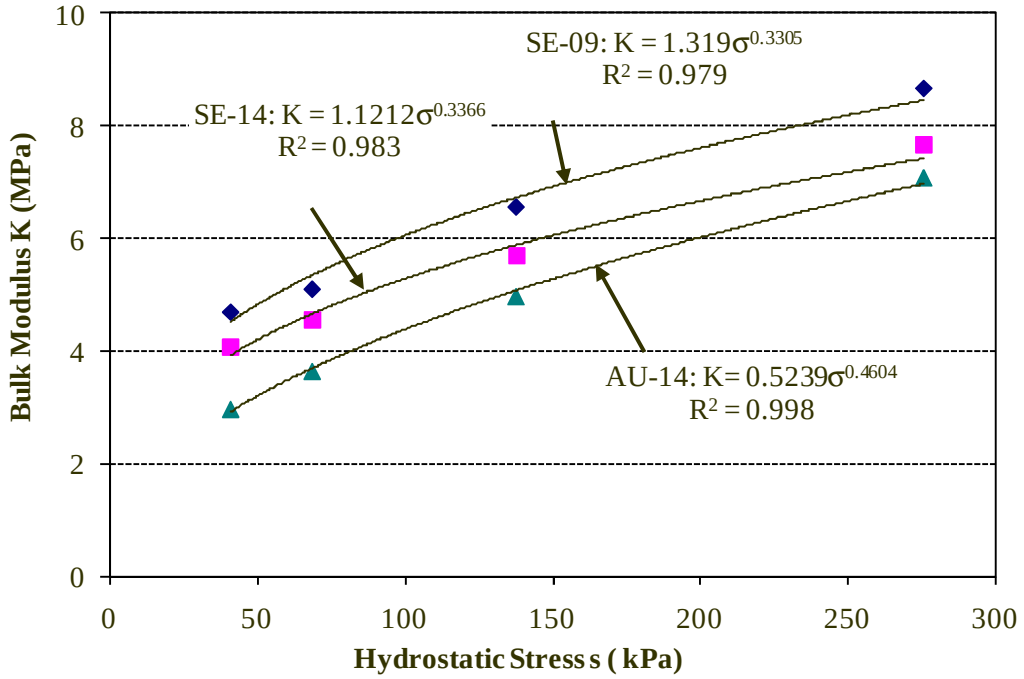

FIGURE 4.5 Variation of Bulk Modulus with Hydrostatic Stress for Oil Sands at 20°C.

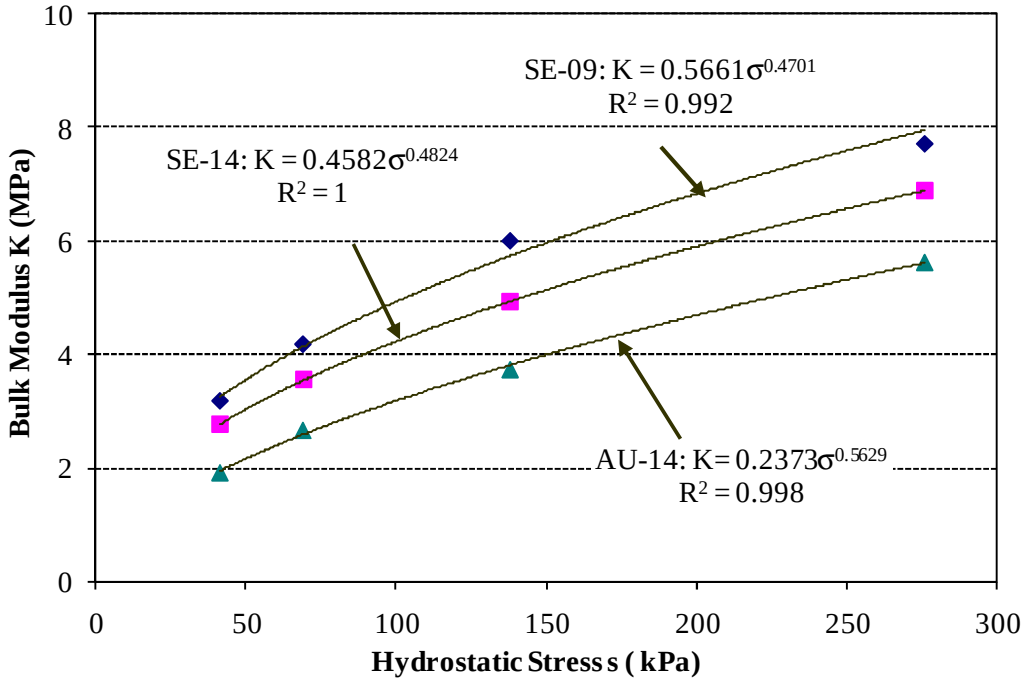

FIGURE 4.6 Variation of Bulk Modulus with Hydrostatic Stress for Oil Sands at 30°C.

To evaluate other important loading conditions and physical properties that might affect the behavior of oil sand materials, the SAS statistical software was used to perform multiple regression analyses on the test data to include variables such as temperature, bitumen content and three gradation properties (Cu, Cc and D_{50}). However, the initial statistical analyses to determine variables affecting bulk modulus showed that no significant correlation exist between the bulk modulus and all the three gradation properties ($R^2 < 0.2$). Therefore, the gradation properties were not included in the SAS multiple regression analyses.

The data set of each oil sand sample (SE-09, SE-14 and AU-14) was first analyzed separately, and a combined test data set of all the three oil sand samples was also analyzed to develop models of bulk modulus as dependent variable and hydrostatic compression stress (σ), temperature (T) and bitumen content (w_b) as independent variables. Among other mathematical forms including linear, nonlinear, and hyperbolic, the power function was most suitable for modeling bulk modulus of the oil sand materials. The model parameters and the coefficient of correlations obtained for the individual oil sands (see Table 4.4a) indicated that a generalized bulk modulus models could be developed using the combined data sets of the three oil sand samples. Table 4.4a lists the bulk modulus (K) models and the model parameters obtained for each oil sand sample while Table 4.4b lists characterization models and parameters obtained for the combined test data set of the three oil sand samples. Note that additional variable (bitumen content) is included in the models when the combined data set is used.

It can be seen that parameter A has the greatest influence on the bulk moduli of the samples as the hydrostatic stresses increase. Both Tables 4.4a and 4.4b show high R^2 for all the models. The difference in R^2 values obtained as a result of subsequent inclusion of independent variables is an indication of the contribution of the variables. The change in R^2 observed in models 2 and 3 indicates high dependency of bulk modulus on hydrostatic stress (see Table 4.4b). However, the improvement in the R^2 value observed in model 3 indicates that there are significant contributions of temperature and bitumen content in the model. Recall that temperature and bitumen content are important factor that affect field loading behavior of oil sand materials. This suggests that model 3 would be more practical to characterize the oil sands than models 1 and 2.

Model 3 was used to fit into the individual oil sand test data at 20°C and at 30°C. There is a very good fit overall, for all the three oil sand test data at the two test temperatures (see Figures 4.7 and 4.8). Therefore model 3 can be used for future studies on bulk modulus characterization of oil sand materials.

TABLE 4.4a Bulk Modulus Characterization Models for Oil Sand Samples

Model 1: $K = A * \sigma^{k_1}$

Model 2: $K = A * \sigma^{k_1} T^{k_2}$

Model	Model Parameters				
	log A	k_1	k_2	R^2	*RMSE**
		SE-09 Sample			
1	-0.0640	0.4005		*0.859*	*0.058*
2	0.6204	0.4005	-0.4927	*0.963*	*0.033*
		SE-14 Sample			
1	-0.1446	0.4095		*0.848*	*0.062*
2	0.6107	0.4095	-0.5437	*0.968*	*0.031*
		AU-14 Sample			
1	-0.4527	0.5116		*0.833*	*0.082*
2	0.6356	0.5116	-0.7835	*0.990*	*0.023*

TABLE 4.4b Bulk Modulus Characterization Models for Combined Oil Sand Data

Model 1: $K = A * \sigma^{k_1}$

Model 2: $K = A * \sigma^{k_1} T^{k_2}$

Model 3: $K = A * \sigma^{k_1} w_b^{k_2} T^{k_3}$

Model	Model Parameters					
	log A	k_1	k_2	k_3	R^2	*RMSE*
1	-0.2204	0.4406			*0.690*	*0.096*
2	0.4068	0.4406	-0.5853		*0.821*	*0.075*
3	1.2494	0.4406	-0.5853	-0.6066	*0.926*	*0.049*

*: Root Mean Square Error

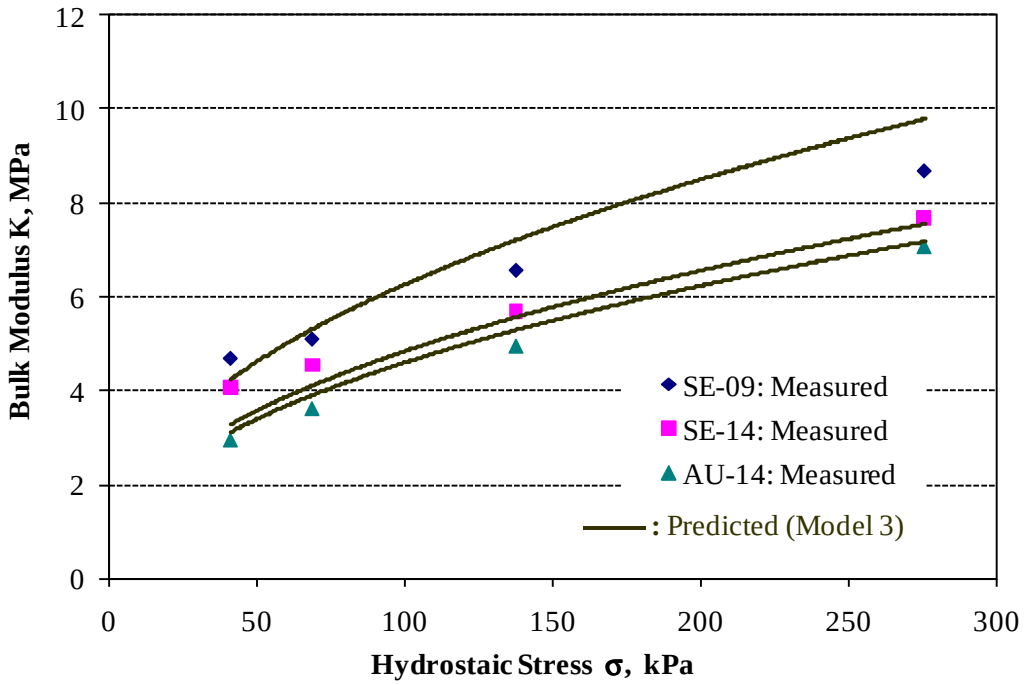

FIGURE 4.7 Bulk Modulus Model 3 Performances for Oil Sand Samples at 20°C

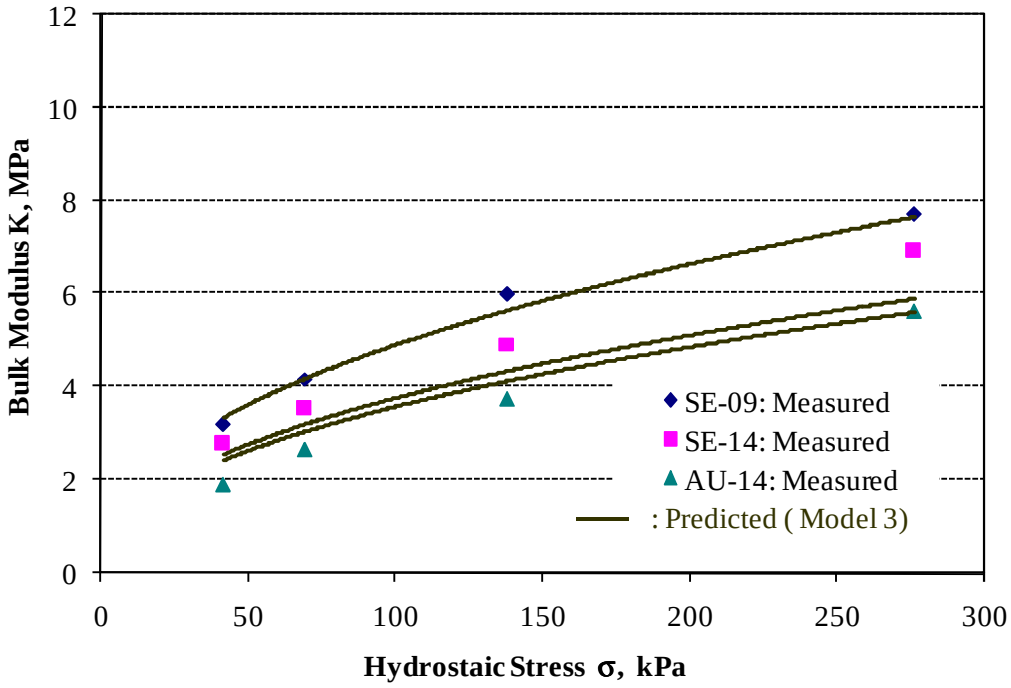

FIGURE 4.8 Bulk Modulus Model 3 Performances for Oil Sand Samples at 30°C.

4.4 Summary

Hydrostatic triaxial compression tests were performed on one fine-grained cohesive soil and three oil sand materials in the laboratory using a newly developed hydrostatic loading test procedure. For the soil sample, the laboratory tests were performed to determine bulk modulus at water contents of 11.3%, 14.3% and 17.3%, representing dry of optimum, optimum and wet of optimum, respectively. Tests were also performed on three oil sand samples with bitumen contents 8.5%, 13.3% and 14.5% to determine bulk modulus at temperatures of 20^{o}C and 30^{o}C.

Based on the test results, empirical equations of bulk modulus as a function of the applied hydrostatic stress were obtained for the soil and oil sand samples. In addition, material characterization models that consider all the field loading conditions were developed for the tested oil sand materials. The results from the bulk modulus models show that the oil sand samples can properly be characterized by temperature and bitumen contents. There was considerable improvement in the coefficient of correlation values when temperature and bitumen contents were included in the initial model, which has only hydrostatic stress as independent variable. Also, the model parameters obtained for individual oil sand samples suggested that all the data could be combined to develop one representative model for the three oil sand samples. The empirical equations and characterization models would be useful in evaluating behavior of fine-grained soils and oil sand materials in the field. The following are the summary of observations derived from the tests results:

1. For the soil sample, the highest bulk modulus values were obtained at dry of optimum, and the lowest values were obtained at wet of optimum. It was found that a change in water content of 3% below the optimum resulted in about 15% increase in the bulk modulus or stiffness of the soil sample, whereas a change in water content of 3% above the optimum resulted in about 45% decrease in the stiffness of the sample.
2. Results of the oil sand tests gave higher bulk moduli at 20^{o}C than at 30^{o}C. Comparisons of the bulk modulus values indicate that at both test temperatures, SE-09 sample had the highest bulk modulus while the AU-14 sample had the lowest.

At 20^{o}C, the difference in magnitude between the average bulk modulus of SE-09 and AU-14 samples was about 26%, and the difference between SE-09 and SE-14 was about 12.5%. The average bulk modulus of SE-14 and AU-14 samples was found to be comparable at the two temperatures although the bulk modulus of SE-14 was about 1.2 and 1.3 times of the bulk moduli of AU-14 at 20^{o}C and 30^{o}C, respectively. The amount of bitumen content appeared to be the main factor that influenced the bulk modulus values of the oil sand materials. The SE-09 sample, with lowest bitumen content, was found to be the sample with the highest stiffness, whereas the AU-14 sample with the highest bitumen content appeared as the least stiff sample.

CHAPTER 5 SHEAR STRENGTH OF FINE-GRAINED COHESIVE SOIL AND OIL SAND MATERIALS

5.1 Introduction

Shear strength of soils and granular materials are usually determined from laboratory tests performed on prepared specimens or on in-situ undisturbed samples. For several decades, the triaxial compression and direct shear tests have been recognized as the standard laboratory tests for determining shear strength properties of soils and granular materials. The results from these tests are commonly used for analyzing the bearing capacity and stability of slopes and foundations of structures and pavements. These tests have also been successfully used during the past 40 years to determine shear strength properties of oil sands. For instance, Round (1960), Dusseault and Morgenstern (1978b) and Agar et al. (1987) conducted extensive studies on shear strength of Athabasca oil sands using both the triaxial compression and direct shear testing procedures.

This chapter presents the results of both triaxial compression and direct shear tests performed to characterize one cohesive soil and three oil sand materials. The test procedures used for this study are similar to those of the traditional shear strength tests (ASTM D 2166, 2850, 3080 and 4767). However, in this study, the selected testing conditions are particularly based on the field loading conditions of large capacity off-road construction and mining equipment. In addition, advanced testing equipment and data acquisition systems were used to simulate close to field loading conditions of such large capacity equipment. Details of the new test procedure are presented in Chapter 3. The laboratory testing conditions and procedures used for analyzing the test results are presented in this chapter. The test results are used to develop Mohr-Coulomb failure models for each tested material. Detailed analyses and discussions of test results are also presented.

5.2 Laboratory Testing and Test Conditions

The fine-grained soil and oil sand specimens were tested in accordance with the developed test procedure described in section 3.5.4 (Test Procedure B).

For the soil sample (CAT A-6), five triaxial strength tests were conducted at optimum (w_{opt} = 14.3%), dry of optimum (w = 11.3%), and wet of optimum (w = 17.3%) to obtain the friction angle ϕ, and cohesion c properties. Each test was carried out on cylindrical specimens, 50.8mm (2 inches) in diameter and 101.6mm (4 inches) high and at five confining stress levels, i.e., 0, 20.7, 41.4, 69 and 138 kPa. The test specimens were monotonically loaded at a strain rate of 1% strain/min using the UTM-5P pneumatic testing system, and pressurized in a triaxial chamber with air pressure. The load was measured through the load cell, whereas, the deformations were measured using the actuator LVDT.

For the oil sands, tests were conducted on three samples with bitumen contents of 8.5% (SE-09), 13.3% (SE-14) and 14.5% (AU-14) using both triaxial and direct shear test procedures. The triaxial tests were performed on cylindrical specimens, 71 mm (2.8 in.) in diameter and 142 mm (5.6 in.) high, and at five confining stress levels, i.e., 20.7, 41.4, 69, 138 and 276 kPa. Specimens were conditioned and tested at temperatures of 20^{o}C and 30^{o}C, using the same loading conditions of the soil sample. Direct shear tests were performed on the oil sand samples to compare test results with the triaxial compression tests. The same test conditions for the triaxial tests were used to perform the direct shear except that confining stresses were increased to 552 kPa. Square prismatic specimens, 100 mm size and 25-40 mm high, were prepared and tested in the Humboldt pneumatic direct shear test setup using a strain rate of 1% strain/min. The shear stress was measured through the load cell, whereas, the horizontal and vertical deformations were measured using horizontal and vertical LVDTs.

5.3 Background for Analyses of Shear Strength Test Results

Shear strength of a geomaterial is mobilized due to two components; cementing action or cohesion and grain interlock from applied loads (friction angle). Typical shear strength tests, either triaxial compression or direct shear require testing specimens at three or more confining stress levels to accurately develop a failure envelope. In triaxial tests, an all-round confining pressure is initially applied on the specimen before an axial monotonic load is gradually applied an increased to shear it.

On the other hand, in the direct shear test, the confining pressure is applied by a vertical load on the specimen followed by a gradual application of a horizontal shear load to shear the specimen.

The Mohr-Coulomb equation has been successfully used to characterize shear strength behavior of soils or geomaterials within limited stress ranges. The results from such characterization provide parameters, which are employed in analyzing the stability of the tested materials. In this study, the linear Mohr-Coulomb model was used to analyze test data of both the soil and oil sand samples. The values of the Mohr-Coulomb strength properties were used to develop shear strength models for the individual samples at different moisture states or bitumen contents. The Mohr-Coulomb failure envelope is defined by Equation 2.1.

For the triaxial tests, Mohr's circles were first constructed using the applied confining stresses and the corresponding maximum shear stresses at failure. The Mohr-Coulomb failure envelope was then constructed for determining the strength parameters for each sample tested. For the direct shear test data, the following procedure was used to obtain the shear strength parameters:

(a) Peak deviator stresses are determined from the results as the maximum shear stresses at failure;

(b) Maximum shear stresses are graphed as a function of the applied normal stresses;

(c) Friction angle and cohesion are determined from the graph in (b).

For all the tests, where no clear peak is observed in the stress-strain plots, the deviator stress corresponding at 5 % axial strain was adopted to define the shear strength of the specimen (Garg and Thompson, 1998).

5.3.1 Analyses of CAT A-6 Soil Test Results

The results for five tests performed on the soil sample at three different moisture states are reported in Table 5.1, and the effect of water content on shear strength properties, i.e., friction angle ϕ and cohesion c of CAT A-6 soil sample. Generally, higher shear strengths were obtained at dry of optimum states.

As expected, increasing confining pressure resulted in increasing deviator stress (shear stress) at failure for all the three moisture states. The results at w = 17.3% and confining stress of 138 kPa, were not included in the analysis due to difficulties encountered during testing. This should not have significant effect on the shear strength properties since the remaining 4 tests are enough to obtain the strength properties. Comparison of the test data shows that the differences in cohesion are higher than the differences in friction angle of the soil sample at the three moisture states (see Table 5.1). The highest difference in cohesion was found between dry of optimum and wet of optimum, i.e., 215 kPa. At the same time, the difference in friction angle between the two moisture states is 8.3 degrees. Thus, a change in water content of 3% above or below the optimum water content resulted in considerable change in cohesion but a little change in the friction angle of the soil sample. This suggests that the strength behavior of CAT A-6 soil could greatly be influenced by increasing or decreasing the water content above or below the optimum. Higher c values are associated with high resistance of the soil material to shearing stresses, and higher ϕ values implies greater capacity of the soil to develop strength and resist permanent deformation in the field. The effect of water content on the shear strength properties of CAT A-6 soil is clearly shown in Figure 5.1.

TABLE 5.1 Triaxial Shear Strength Test Results for CAT A-6 Soil

Water Content	Peak Shear Stress @ Confining Stress (kPa)					Strength Properties	
	0	20.7	41.4	69	138	ϕ (Deg)	c (kPa)
w = 11.3%	971.6	1129.8	1355.9	1401.4	1629.6	42.0	250
w_{opt} = 14.3%	472.5	528.5	641.9	764.3	973.0	39.5	112
w = 17.3%	121.7	152.8	141.2	299.5	-	33.7	35

Figures 5.2 to 5.4 show the test results represented by Mohr circles at failure for five tests of CAT A-6 soil at w = 11.3%, w_{opt} = 14.3% and w = 17.3%. The five tests are labeled as test numbers 1 through 5 in the figures. Figures 5.2 to 5.4 also show Mohr-Coulomb failure envelopes obtained for the sample at the three moisture states.

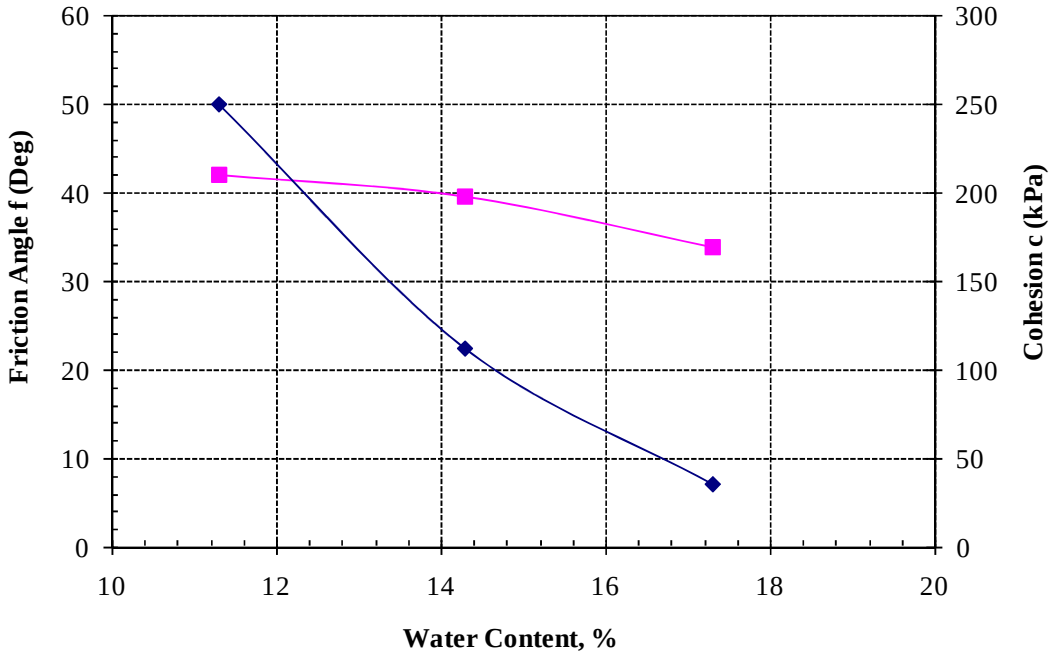

FIGURE 5.1 Effect of Water Content on Friction Angle and Cohesion Properties.

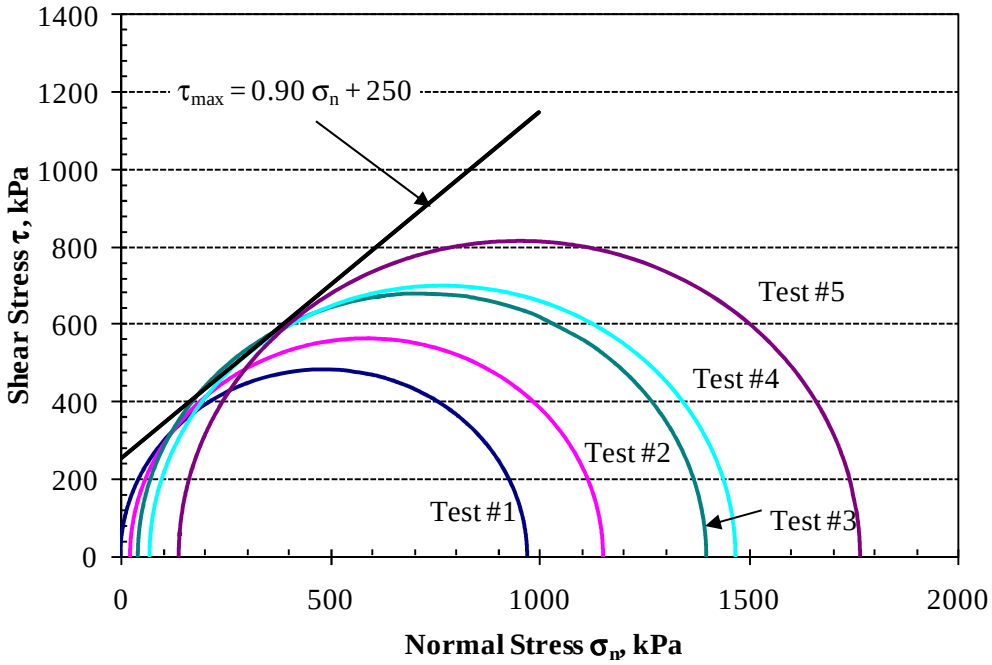

FIGURE 5.2 Mohr Circles and Failure Envelope for CAT A-6 Soil at w = 11.3%.

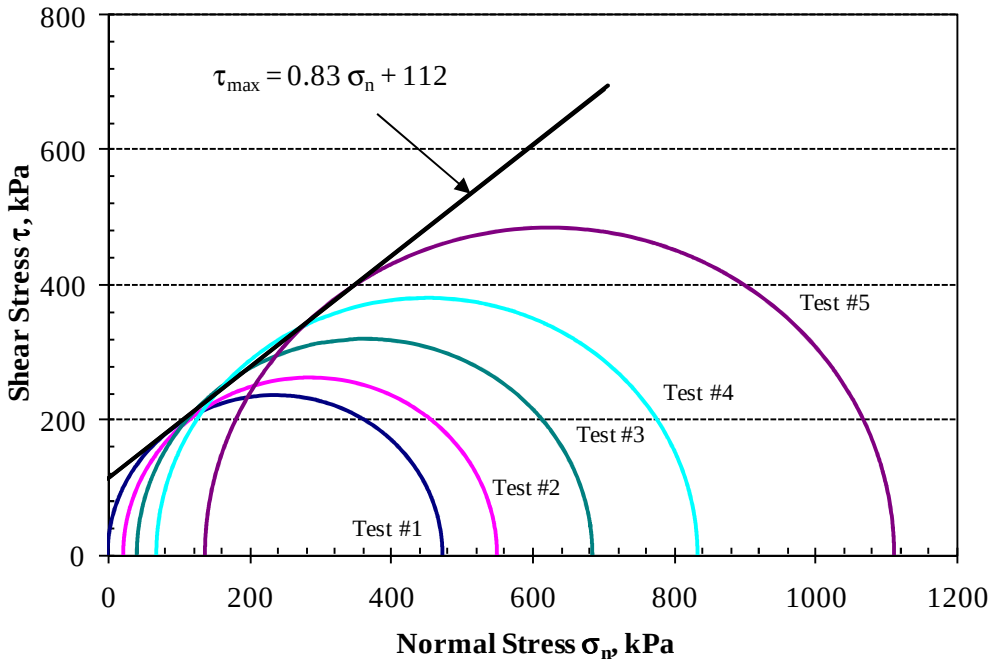

FIGURE 5.3 Mohr Circles and Failure Envelope for CAT A-6 Soil at w_{opt} = 14.3%.

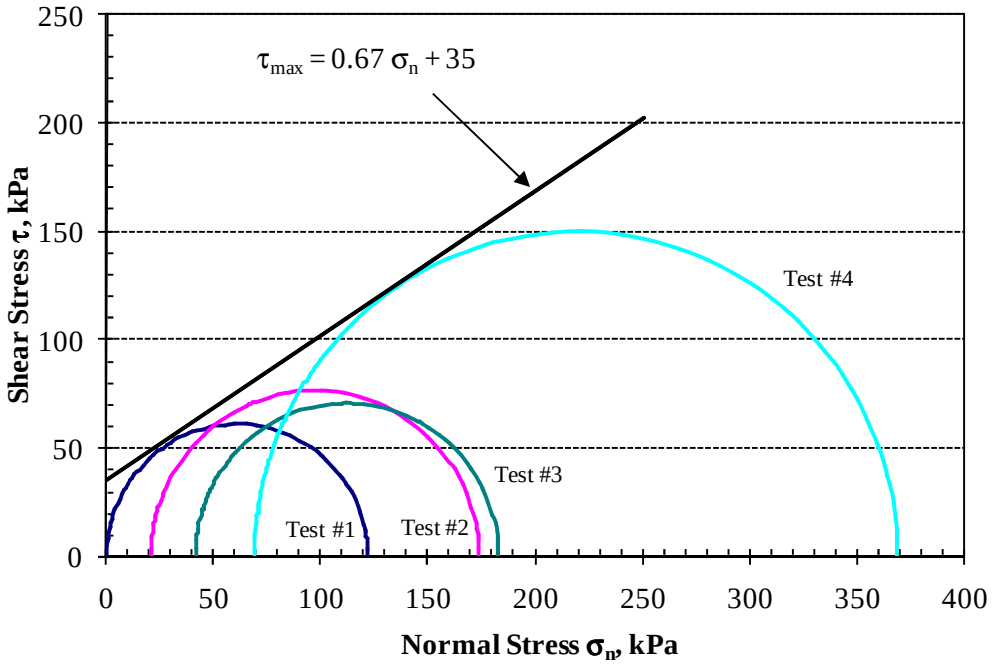

FIGURE 5.4 Mohr Circles and Failure Envelope for CAT A-6 Soil at w = 17.3%.

5.3.2 Analyses of Oil Sand Test Results

5.3.2.1 Analysis of Triaxial Test Data

The results of the triaxial shear strength tests of the three oil sands are presented in Mohr's circles. Tables 5.2 and 5.3 shows the test results for all the three oil sand samples at 20^{o}C and at 30^{o}C, and Figures 5.5 and 5.6 present the test results in Mohr circles. These figures indicate that the oil sand samples have essentially the same shear strength. Apparently, the oil sand materials did not densify as confining pressure increased, hence the shear strength did not increase. It is worth mentioning that none of the specimens tested failed by shear, rather all the test specimens bulged when the applied shear stress reached the peak value. This failure mode resulted in zero friction angles for all the oil sand samples, i.e., there is no or negligible interlock between the sand grains of the materials. The zero friction angles obviously are not reflective of the dense nature of the tested oil sand materials.

Dusseault and Morgenstern (1978b) and Agar et al. (1983), reported that oil sand derives its strength from the dense interlocking grain structure it exhibits. Therefore, the test results obtained from this study show that there was no significant contact between the grains of the oil sands tested, which resulted in zero friction angle. In a related case, Dusseault and Morgenstern (1978b) abandoned triaxial tests in favor of direct shear test for Athabasca oil sands. One of the reasons was that sample uniformity and the required number of similar specimens to describe Mohr-Coulomb envelopes could not be obtained from triaxial testing.

In this study, the direct shear tests were performed to verify the ambiguity in the triaxial test results obtained for the oil sand samples. However, the small cohesion values obtained for all the samples appear to reasonably agree with findings by Round (1960), Morgenstern and Dusseault (1978b) and Agar et al. (1987). Generally, no significant difference was found between cohesion of the three oil sand samples at 20^{o}C and at 30^{o}C. Cohesion was found to be relatively higher at 20^{o}C than at 30^{o}C for all the oil sands with the AU-14 sample giving the highest cohesion value of 24.8 kPa at 20^{o}C. Note that in Figure 5.5c, the Mohr circles lying above the failure envelope (test # 1 and test #3) were not considered for determining the cohesion property of AU-14 sample.

TABLE 5.2 Triaxial Shear Strength Test Results for Oil Sand Samples at 20°C

Sample ID	Peak Shear Stress @ Normal Stress (kPa)					Strength Properties	
	20.7	41.4	69	138	276	ϕ (Deg)	c (kPa)
SE-09	32.5	26.7	35.5	33.9	27.0	0	15.7
SE-14	40.6	43.9	43.9	41.6	50.9	0	22.3
AU-14	62.7	51.1	69.0	41.3	41.9	0	24.8

TABLE 5.3 Triaxial Shear Strength Test Results for Oil Sand Samples at 30°C

Sample ID	Peak Shear Stress @ Normal Stress (kPa)					Strength Properties	
	20.7	41.4	69	138	276	ϕ (Deg)	c (kPa)
SE-09	24.5	33.3	34.0	31.3	21.5	0	15.0
SE-14	22.2	20.7	24.5	25.9	21.4	0	13.0
AU-14	28.7	22.9	22.9	28.7	30.2	0	15.4

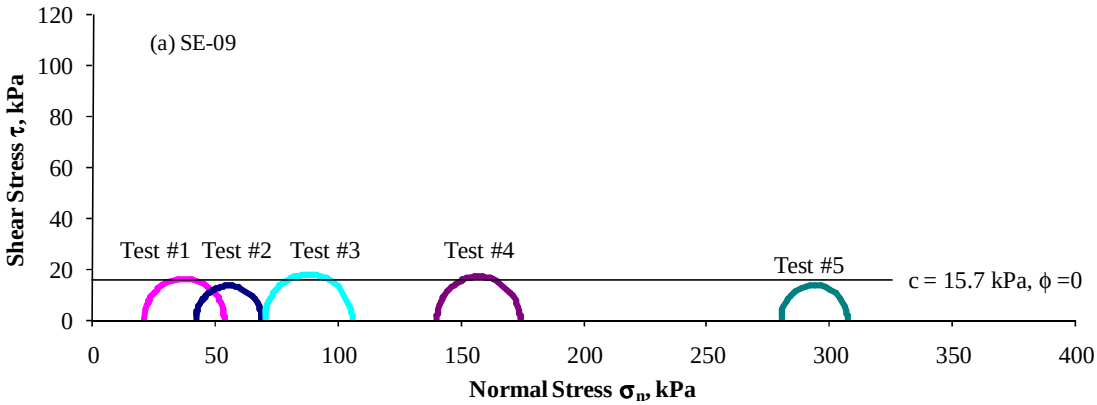

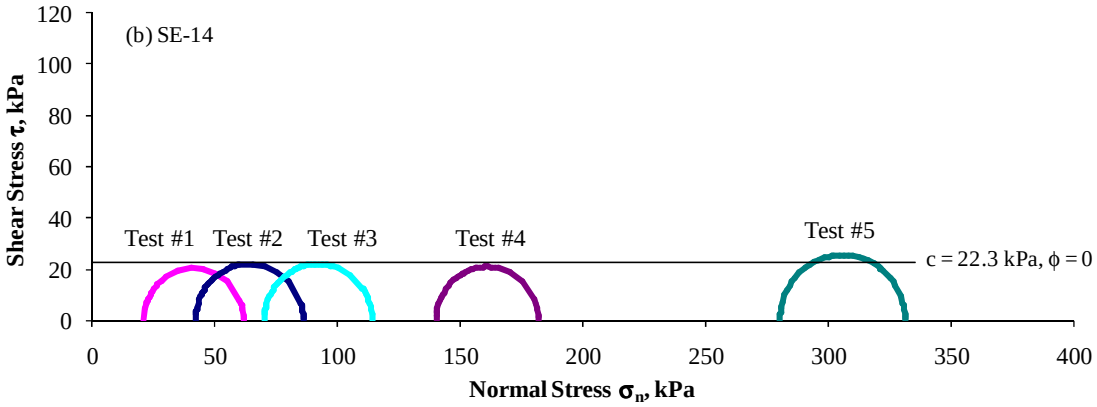

(b)

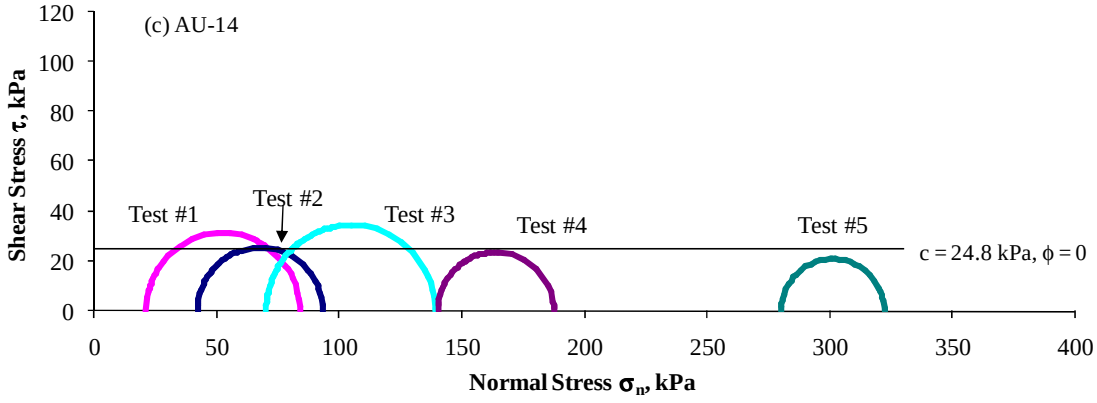

(c)

FIGURE 5.5 Mohr Circles for Oil Sand Samples at 20°C.

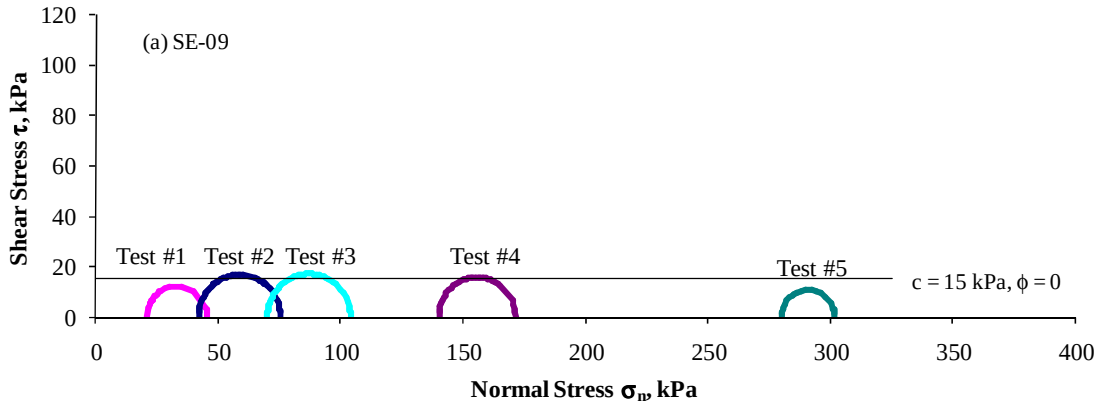

(a)

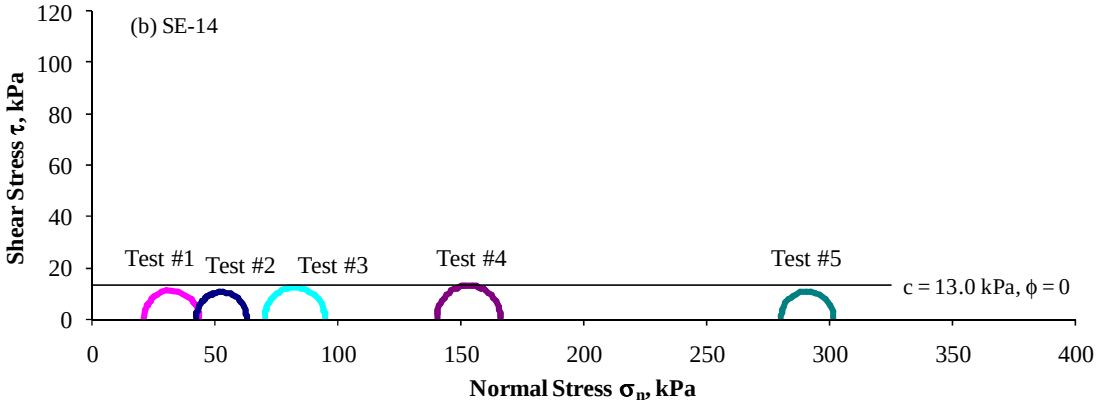

(b)

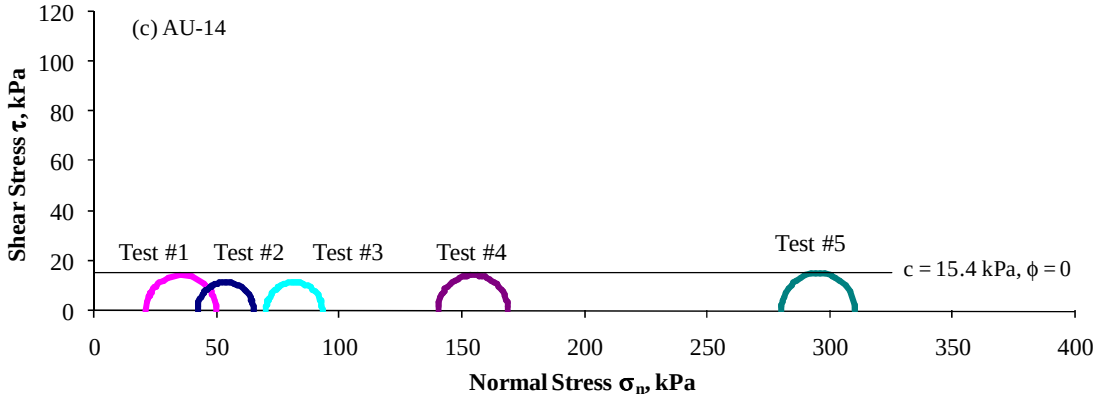

(c)

FIGURE 5.6 Mohr Circles for Oil Sand Samples at 30°C.

5.3.2.2 Analysis of Direct Shear Test Data

The results for the direct shear tests for all three oil sand samples are reported in Tables 5.4 and 5.5. In these tables, the maximum deviator stress at failure, the applied normal stresses, and shear strength properties are summarized for test temperatures of 20°C and 30°C. Note that only 4 direct shear tests were performed for the oil sand samples at 30°C. There were insufficient oil sand samples to conduct the tests at all the six confining stresses.

TABLE 5.4 Direct Shear Strength Test Results for Oil Sand Samples at 20°C

Sample ID	Peak Shear Stress @ Normal Stress (kPa)						Strength Properties	
	20.7	41.4	69.0	138.0	276.0	552.0	ϕ (Deg)	c (kPa)
SE-09	27.3	45.7	59.8	126.3	218.3	473.4	39.4	6.2
SE-14	26.2	52.1	77.6	94.1	223.1	417.9	35.7	15.2
AU-14	32.2	41.8	61.2	123.0	210.2	365.9	32.1	22.9

TABLE 5.5 Direct Shear Strength Test Results for Oil Sand Samples at 30°C

Sample ID	Peak Shear Stress @ Normal Stress (kPa)				Strength Properties	
	69.0	138.0	276.0	552.0	ϕ (Deg)	c (kPa)
SE-09	63.8	113.5	190.6	384.4	33.0	17.6
SE-14	56.6	120.4	209.7	355.2	30.7	29.5
AU-14	65.0	98.8	210.1	332.4	29.0	31.4

Comparisons between the test results indicate that the oil sand materials exhibit higher friction angles at 20°C than at 30°C. On the other hand, the cohesion parameter was found to be higher at 30°C than at 20°C. Overall, the SE-09 sample has the highest friction angle and the lowest cohesion, whereas AU-14 has the lowest friction angle and highest cohesion. The SE-09 sample has the highest friction angle and the lowest cohesion at 30°C.

There is apparently no significant difference between friction angle and cohesion values of SE-14 and AU-14 samples. Both AU-14 and SE-14 samples have higher cohesion intercepts compared to SE-09 sample.

As mentioned previously, high ϕ values implies ability of the geomaterial to develop strength under confinement and resist permanent deformation, and high c values means high resistance of the geomaterials to shearing stresses. Although, the differences between the test parameters are not large, the SE-09 sample is expected to have greater potential to resist field sinkage or permanent deformation when compared to SE-14 and AU-14 samples. The behavior of SE-14 sample appears to be close to the AU-14 sample. This could be expected since the difference between their bitumen contents is not significant. It appears bitumen content has effect on shear strength of oil sand materials. This effect could be explained in more detail if the characteristics of the bitumen were better known.

Generally, the high friction angles and low cohesion exhibited by the three oil sand samples are in agreement with research findings of Round (1960) and Dusseault and Morgenstern (1978b). All these studies reported low or negligible cohesion and high friction angles for oil sand materials in direct shear tests. Typical "c" values for oil sand materials from direct shear tests under different test conditions are less than 20 kPa; whereas typical "ϕ" values range mostly between 30 and 60^{o} (Round 1960, Dusseault and Morgenstern 1978b). These researchers also noted that oil sand with high quartz content or highly coarse-grained in nature have high shear strength properties.

Based on the test results, shear strength models were developed for each oil sand sample using Mohr-Coulomb failure envelopes. Figures 5.7 and 5.8 show the Mohr-Coulomb failure envelopes developed from the cohesion c and angle of internal friction ϕ for the three oil sand materials. It can be observed from Figures 5.7 and 5.8 that high normal stress has a significant influence on the shear strength properties of the oil sand samples.

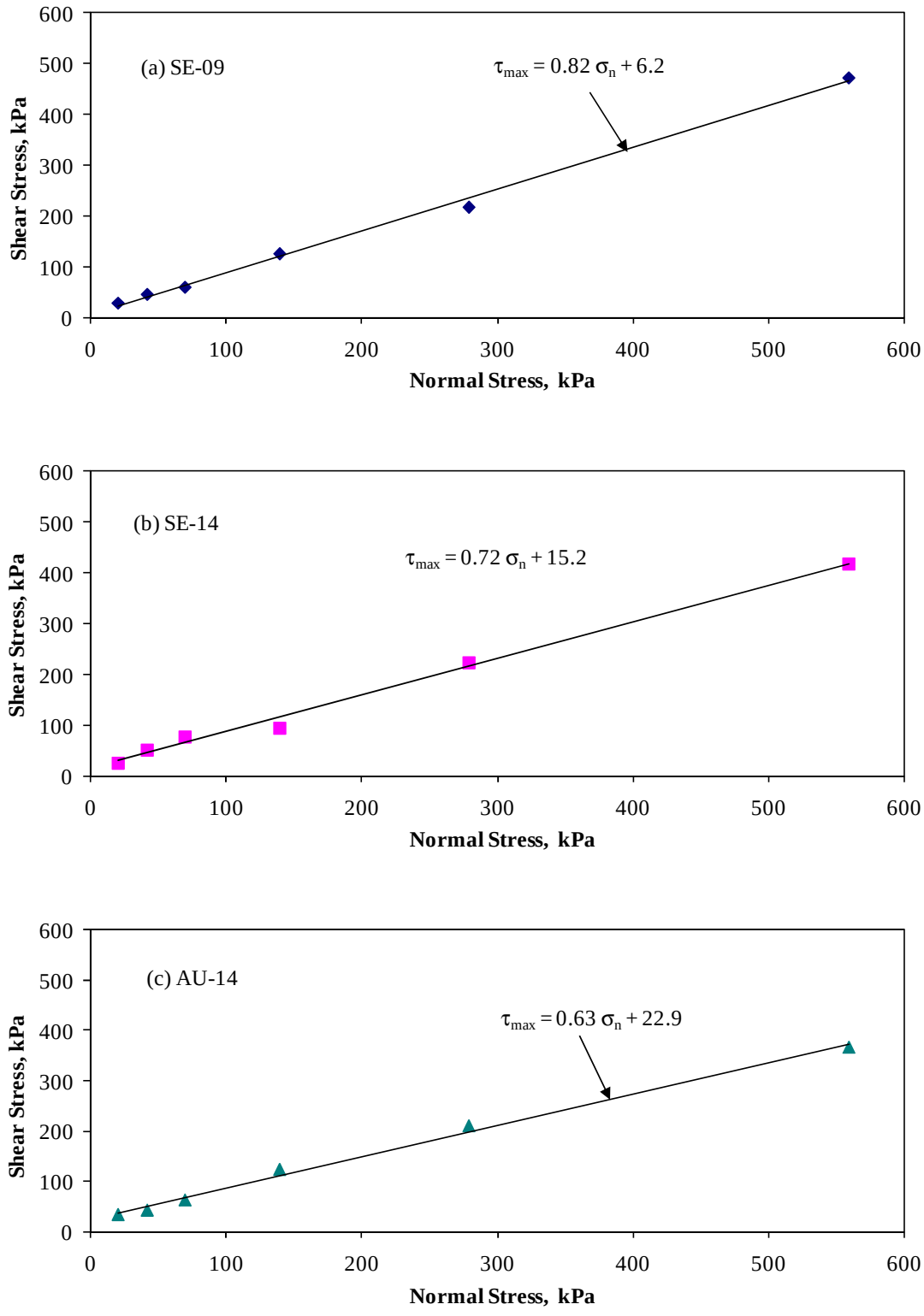

FIGURE 5.7 Mohr-Coulomb Failure Envelopes for Oil Sand Samples at 20°C.

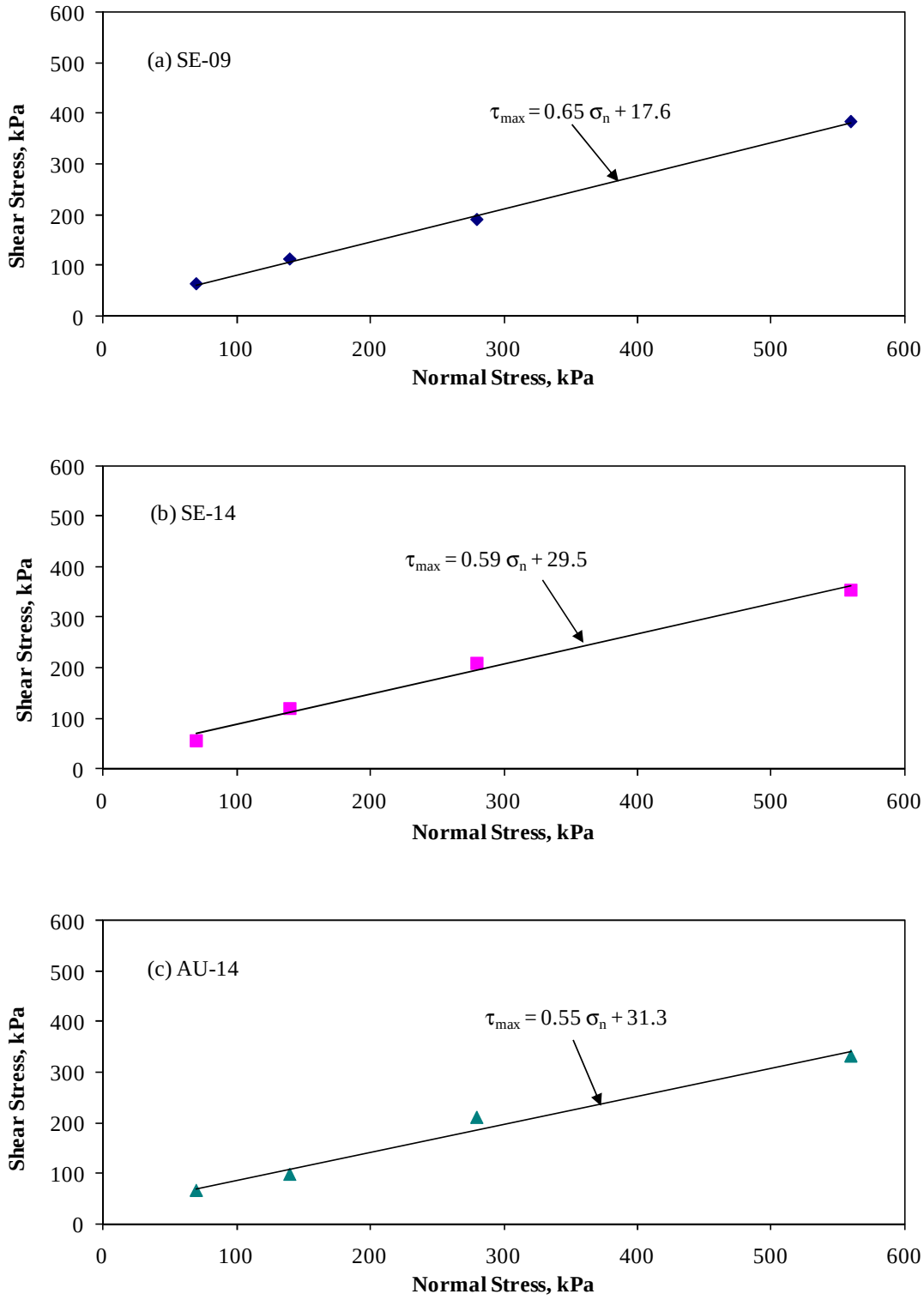

FIGURE 5.8 Mohr-Coulomb Failure Envelopes for Oil Sand Samples at 30°C.

5.4 Summary

Shear strength tests to allow application of somewhat high confining or normal stresses were used to determine strength properties of one fine-grained soil and three types of oil sand samples. Triaxial compression tests were performed on the soil sample at optimum water content, w_{opt} = 14.3%, dry of optimum, w = 11.3% and wet of optimum, w = 17.3%. Both triaxial compression and direct shear tests were performed on the oil sand materials with bitumen contents of 8.5%, 13.3% and 14.5% at test temperatures of 20^{o}C and 30^{o}C. Results from the two test procedures could not be effectively compared since the triaxial tests produced zero friction angles for all the oil sand materials. However, the results from the direct shear tests were comparable to other laboratory tests performed on similar oil sand samples. Based on the test results Mohr-Coulomb failure models were developed to characterize the soil sample at each moisture state, and each of the three oil sand samples at the two test temperatures. The test results for both the soil and oil sand samples showed that the soil sample at dry of optimum and the oil sand sample with lowest bitumen content would have greater ability to resist potential rutting (sinkage) in the materials. This observation was evident from high friction angles obtained for the soil sample at dry of optimum and the oil sand sample with less bitumen content. The major findings derived from the shear strength tests are as follows:

1. Both cohesion and angle of friction of the soil sample were higher at dry of optimum than optimum and wet of optimum water contents. Also, the shear strength properties were higher at optimum than wet of optimum water content. A change in water content of the soil sample by 3% below optimum resulted in about 1.06 times of friction angle and about 2.23 times of cohesion at dry of optimum. On the other hand, a change in water content by 3% above optimum resulted in 0.85 times of friction angle and about 0.3 times of cohesion at wet of optimum.
2. The triaxial compression tests performed on the three oil sand materials gave zero friction angles. All specimens failed by specimen mid-height budging, which suggests that there were apparently no interparticle contacts between the sand grains in the oil sand samples.

The results obtained for cohesion intercept was rather reasonable and agreed with results reported in the literature for similar oil sand samples.

3. Direct shear tests were performed to obtain friction angle and cohesion strength properties of the oil sand materials. The test results indicated that the oil sand samples had higher friction angles at 20^{o}C than at 30^{o}C, and lower cohesion values were obtained at 20^{o}C. Generally, SE-09 sample had the highest friction angle and lowest cohesion, whereas AU-14 had the lowest friction angle and highest cohesion at the two test temperatures. The differences in friction angle and cohesion between SE-14 and AU-14 sample were insignificant.

CHAPTER 6 MODULUS AND PERMANENT DEFORMATION BEHAVIOR OF OIL SAND MATERIALS

6.1 Introduction

Deformation of geomaterials is generally divided into two parts: elastic (recoverable) and plastic (permanent) deformations. The plastic deformation measures the rutting potential of the geomaterial, whereas the elastic deformation the resilient behavior of the geomaterial. Current field studies on oil sand materials characterized total deformation behavior under heavy construction and mining equipment. However, it is important that the elastic and plastic deformations of oil sands are studied separately in order to adequately describe field loading responses of these materials under equipment wheel loads to develop various stiffness, sinkage and rutting models.

In comparison to strength characteristics, less research has been devoted to resilient and permanent deformation behavior of oil sand materials in the laboratory. One plausible reason is that oil sands behavior under haul trucks or shovels are still far from advanced. Another reason is the lack of laboratory test procedures or equipment capable of simulating field loading conditions, and providing data to characterize resilient and permanent deformation behavior of oil sands. The repeated load triaxial test has been the well accepted test method in analyzing the elastic and plastic deformations in geomaterials. The current procedure applies typical highway loading conditions on samples to obtain data for resilient modulus and permanent deformation (AASHTO T307). In this chapter a newly developed repeated load triaxial test procedure, which applies higher stress ratios than the current AASHTO T307 test procedure, is used to characterize resilient modulus and permanent deformation behavior of three types of oil sand materials in the laboratory.

6.2 Deformation Behavior of Oil Sand Materials

6.2.1 Permanent Deformation Behavior

The majority of permanent deformation behavior models for geomaterials are based on the applied stress states and the number of load repetitions.

Recently, Thompson (1984a), Lekarp, et al. (2000) have shown from laboratory studies that load pulse duration or frequency of loading linked to field trafficking speeds has a significant influence on the permanent deformation accumulation in geomaterials. Studies on rutting potential of paving and bituminous base mixes in general indicate that permanent deformation is closely related to asphalt content (Barksdale 1973, 1987). Vehicular loading characteristics are one of the major factors affecting permanent deformation in the field (Kim and Tutumluer, 2006).

It is recognized that the considerable amount of bitumen in the oil sands, high applied loads from the mining equipment, seasonal changes in temperature, and the number of truck passes or load applications are major factors that control deformation behavior of oil sands (Joseph, 2005). The field loading characteristics of large capacity mining equipment is another major factor that could affect permanent deformation behavior of oil sands due to the large nominal payloads and high tire pressures. These mining equipment, particularly, haul trucks could produce high vertical stress to confining stress ratio of 3.20 in the field. To date, no comprehensive laboratory test procedure discusses the individual permanent deformation behavior of oil sand materials. Instead, several research studies on oil sands have traditionally been focused on obtaining laboratory stress-strain test data to describe shear strength and elastic behavior of oil sands (Dusseault and Morgenstern 1978b, Agar et al. 1987, Samieh and Wong 1997, Morgenstern and Scott 1997, Wong 2001, 2003 and 2005)

To study permanent deformation behavior of oil sands in the laboratory, typical loading conditions of mining equipment should be simulated using proper laboratory test procedures and testing equipment. Test results could be used for developing permanent deformation prediction models to better understand mobility and equipment sinkage related problems in oil sands.

6.2.2 Resilient Behavior

Resilient modulus is widely used as a key input property of pavement foundation geomaterials for pavement design. Under the repeated application of dynamic loads, the recoverable strains are used to evaluate the resilient properties of pavement foundation geomaterials.

Traditionally, resilient modulus (M_R) used for the elastic stiffness of pavement materials is defined as the repeatedly applied wheel load stress divided by the recoverable strain determined after shakedown of the material.

Field plate load tests conducted on oil sand materials have indicated that oil sands exhibit stress-softening type deformation behavior, that is, resilient modulus decreases with increasing deviator stress. Joseph (2005) reports that oil sand is currently used as subgrade materials for the construction of permanent and temporary roads in oil sand fields for hauling activities. According to Joseph, coarse-grained gravels and crushed limestone are used as layers above the oil sand subgrade materials, thereby providing a somewhat full pavement structure for the mining activities. Joseph (2005) observed that during Summer, deformation and stiffness problems were prevalent in pavements with high-grade oil sand subgrade compared with those with low-grade oil sand subgrade materials. The low-grade oil sands performed significantly better as subgrade material than high-grade oil sands (Joseph, 2005). In this study, the elastic properties obtained from the repeated load tests are used to characterize modulus behavior of the three oil sand materials tested. Nonlinear resilient modulus models are developed, and used to describe the resilient behavior of the oil sand materials. These models would support the on-going oil sand field studies to assess the possibility of utilizing different grades of oil sands as subgrade materials for mining road structures.

6.3 Laboratory Testing

The newly developed test procedure in section 3.5.5.3 (Procedure C) was used to conduct permanent deformation tests on the three oil sand samples. This test procedure is based on the field loading characteristics of the haul trucks and mining equipment for oil sands considers stress ratios ranging from 1.15 to as high as 7.67 and total vertical stresses (σ_1) as high as 552 kPa (80 psi) (see Table 6.1). Permanent deformation tests were conducted at two temperatures, 20^{o}C and 30^{o}C, to account for spring and hotter summer periods, respectively. Further, two different haversine load pulse durations of 0.1 and 0.5 seconds were also included in the laboratory testing program to consider the effects of different trafficking speeds of haul trucks and other mining equipment on the oil sand sinkage and rut development in the field.

The UI-FastCell integrated with IPC Universal Testing Machine (UTM) loading device, was used for applying stresses on the specimen. During testing, gyratory compacted oil sand specimens were subjected to different applied stress states and principal stress ratios (σ_1/σ_3) as listed in Table 6.1. Each deviator stress σ_d (= σ_1-σ_3) and constant confining stress σ_3 pair was applied on one specimen with the deviator stress repeatedly pulsed in the vertical direction for a total of 1,000 load cycles except for the replicate tests, which were performed at σ_d = 138 kPa (20 psi) and σ_3 = 138 kPa (20 psi) only for a total of 10,000 load cycles and later used to check permanent deformation model performances. The specimen's vertical displacement was determined by averaging readings of the two axial linear vertical displacement transducers (LVDTs). Permanent deformations (δ_p) were recorded for each cycle and the corresponding plastic strains (ε_p) were computed. A total of 36 tests were designed for each type of bituminous sand material, i.e., SE-09, SE-14, and AU-14, to establish a full factorial test matrix. That is, nine applied stress states with the σ_1 to σ_3 stress ratios listed in Table 6.1 were repeated at 20^{o}C and 30^{o}C, and two load pulse durations of 0.1 and 0.5 seconds with 0.9- and 0.5-second rest periods, respectively.

6.4 Analysis of Permanent Deformation Test Results

Permanent deformation test data obtained for all three oil sand materials showed that permanent strains typically accumulated as power functions with increasing number of load applications. Figures 6.1a and 6.1b show the permanent strain accumulations for the three oil sand samples recorded at the applied confining stress of 41.4 kPa (6 psi) and deviator stress of 138 kPa (20 psi) for σ_1/σ_3 = 4.33. As expected, higher permanent deformations accumulated at 30^{o}C when compared to the results at 20^{o}C. Similar trends of higher permanent deformation accumulations were observed for the higher grade SE-14 with 13.3% bitumen content (w_b) when compared to SE-09 results and for the tests conducted with the longer 0.5-second load pulse duration (P_d). In regard to load pulse duration effects on permanent deformation, these ε_p test results were in very good agreement with the test data on granular base materials reported earlier by Kim and Tutumluer (2006).

As shown in Figures 6.1a and 6.1b, the AU-14 sample (w_b = 14.5%) had the highest permanent strain accumulations, followed by the SE-14 sample (w_b = 13.3%) and SE-09 (w_b = 8.5%). These laboratory findings also agree very well with the observed field behavior of oil sand materials (Joseph 2005). It should be noted that rheological properties of bitumen in the oil sands were not considered in detail. However, because the three oil sands samples were obtained from the same deposit, it can reasonably be assumed that the rheological properties should be similar. Further, no information was found from the most recent field study conducted on these oil sand materials in relation to the rheological properties of the bitumen (Joseph 2005).

TABLE 6.1 Applied Stress States in the Permanent Deformation Test Procedure

Specimen Number	Stress States[a] (kPa)			Stress Ratio (σ_1/σ_3)
	Confining Stress (σ_3)	Deviator Stress (σ_d)	Total Vertical Stress (σ_1)	
1	41.4	41.4	82.8	2.00
2	41.4	138	179.4	4.33
3[b]	41.4	276	317.4	7.67
4	138	41.4	179.4	1.30
5	138	138	276	2.00
6	138	276	414	3.00
7	276	41.4	317.4	1.15
8	276	138	414	1.50
9	276	276	552	2.00

[a]: 1 psi = 6.9 kPa

[b]: Specimens did not survive this high principal stress ratio

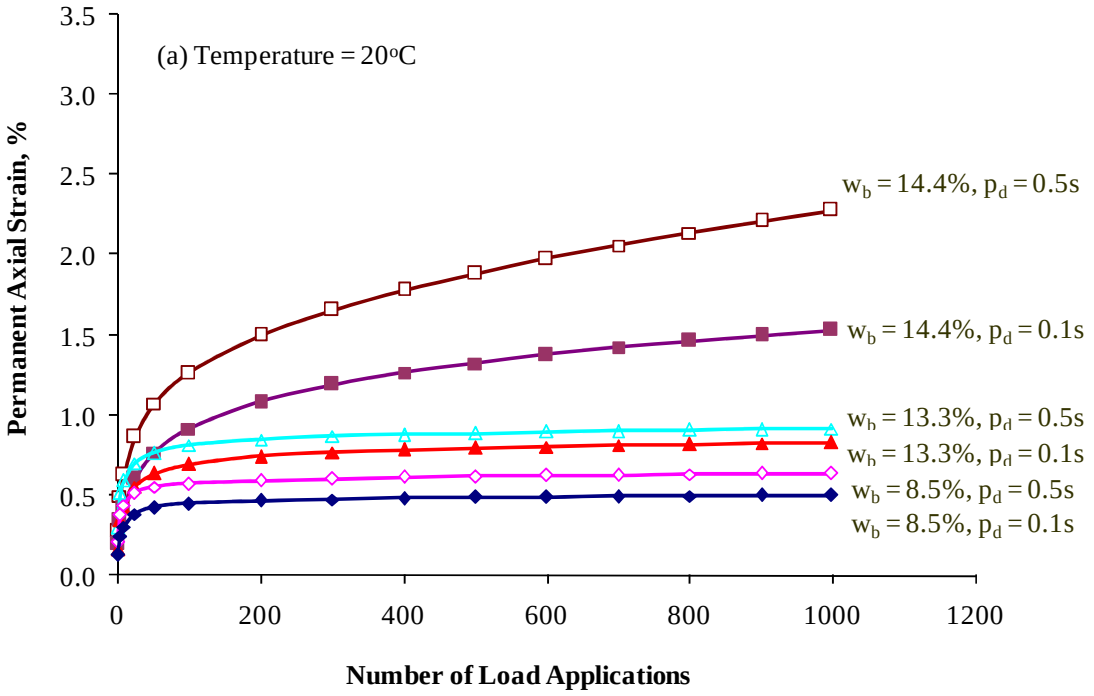

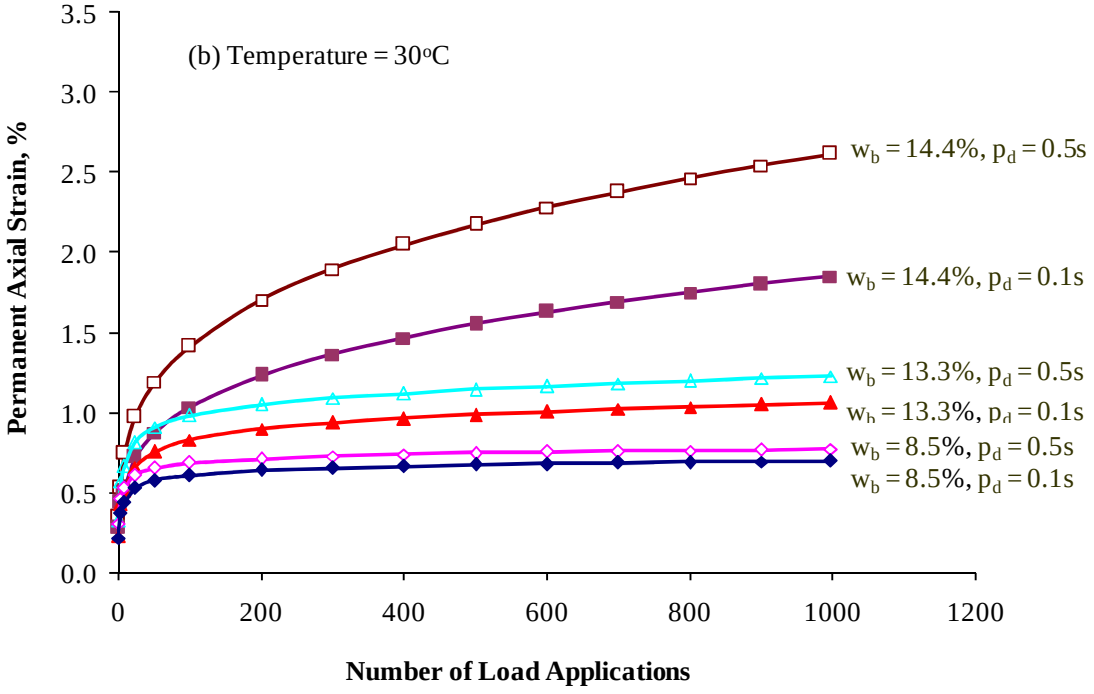

FIGURE 6.1 Permanent Axial Strain Accumulations at Principal Stress Ratio, σ_3/σ_3 = 4.33

6.4.1 Effects of Applied Stress States

6.4.1.1 Effect of Principal Stress Ratio

Effects of applied stress levels on permanent deformation were further investigated for the three oil sand materials tested at different load pulse durations and temperatures. Figures 6.2a and 6.2b show permanent strains recorded at the 1,000th load cycle (@ N=1,000 cycles) graphed with the applied principal stress ratios (σ_1/σ_3) for the test temperatures of 20^{o}C and 30^{o}C, respectively. Note that 1,000th load cycle permanent strains are generally higher at 30^{o}C than at 20^{o}C. Joseph (2002a) reported a similar situation from the field studies, where oil sands experienced higher permanent deformations under heavy mining equipment during summer than winter seasons. At low principal stress ratios, i.e., $\sigma_1/\sigma_3 < 2.00$, there was a gradual accumulation of permanent strain in the oil sand samples compared with the significantly higher accumulations when the stress ratio was greater than 2.00 (see Figure 6.2). It appears that there is no significant difference in permanent strains between the two load pulse durations, and between the three oil sand materials when the stress ratio is below 2.00. However, for principal stress ratios greater than 2.00 ($\sigma_1/\sigma_3 = 7.67$ in Table 6.1 could not be applied since specimens did not survive this high principal stress ratio), the effect of principal stress ratio on permanent strain accumulation becomes quite significant. There is a clear difference in the trend lines of permanent strain accumulation between the two load pulse durations (P_d = 0.5 seconds and 0.1 seconds) supported by the exponential curve-fitting in the combined test data. Overall, the permanent strains in the AU-14 sample were significantly higher at the large stress ratios than those of the SE samples. At a principal stress ratio of 4.33, the 1,000th load cycle permanent strains in AU-14 were found to be about 1.8 to 2.5 times higher than those of the SE-14, and 3.0 to 3.5 times higher than those of the SE-09 for the two test temperatures, whereas at a principal stress ratio of 3.0, permanent strains in AU-14 were found to be in the range of 1.2 to 1.4 times higher than those of the SE-14 and 2 to 2.8 times higher than those of the SE-09. There is a significant impact of applied stresses, especially the principal stress ratios, and the bitumen content on the permanent deformation behavior of naturally occurring bituminous sands.

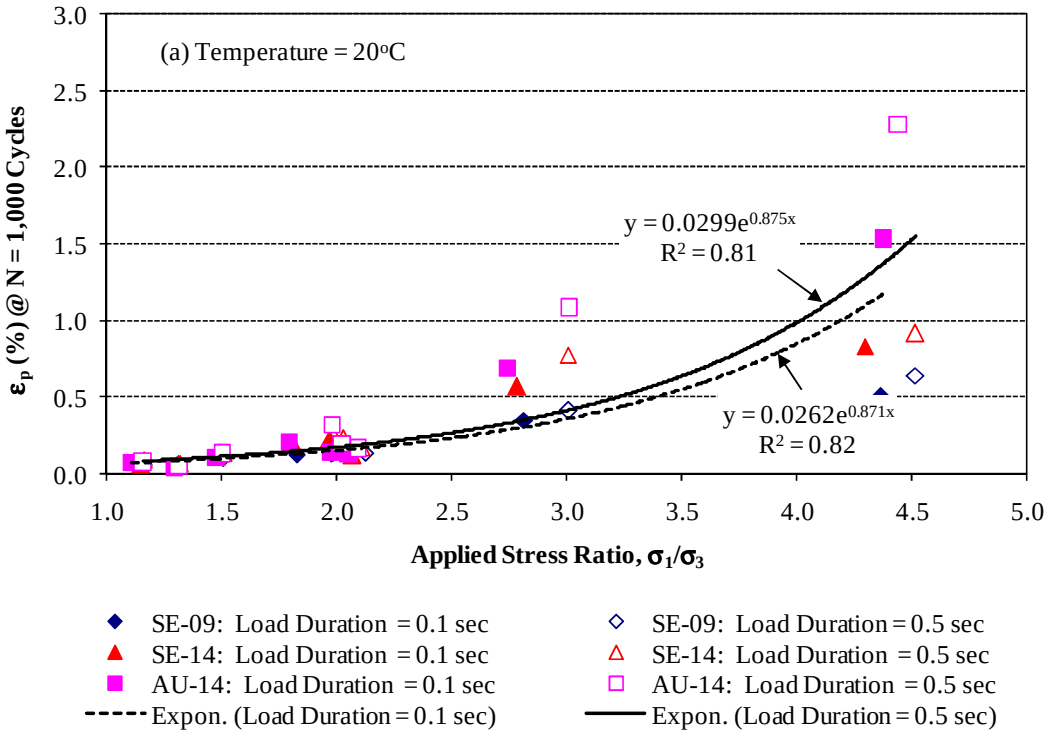

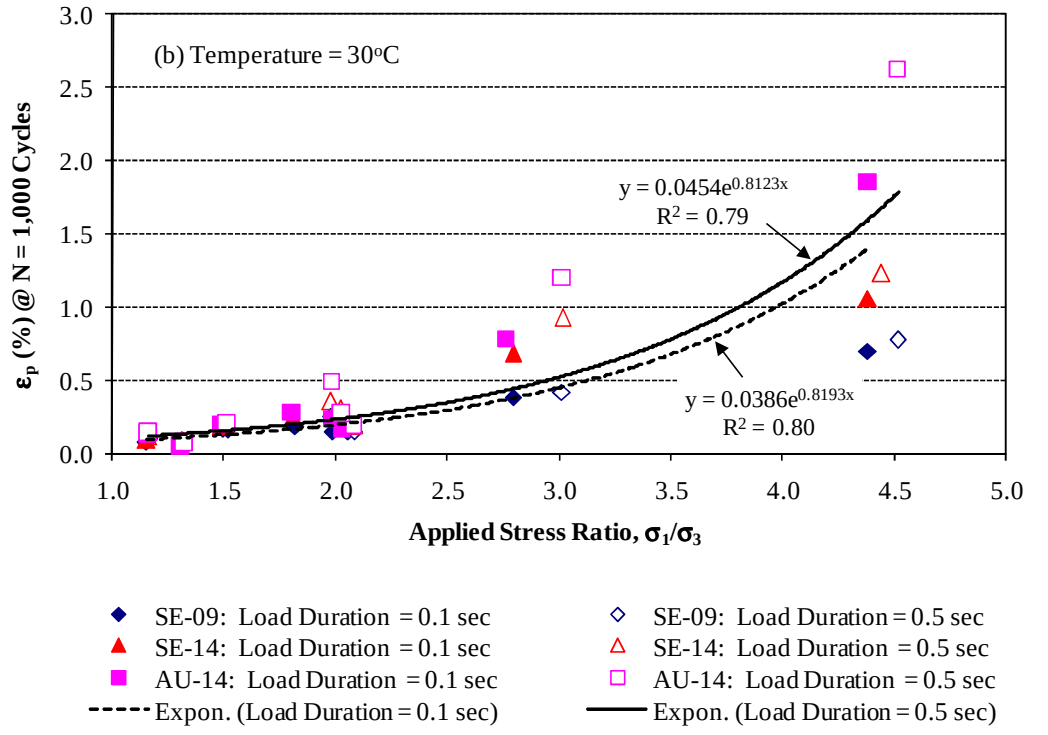

FIGURE 6.2 Permanent Axial Strains Recorded at the 1,000th Load Cycle as a Function of Applied Stress Ratios.

6.4.1.2 Effect of Deviator Stress

The effects of deviator stress on permanent deformation were studied at 30 degrees Celsius and load duration of 0.5 seconds for the oil sand materials at different confining stresses (pressures). Note that from the previous discussions, permanent deformation in all the oil sand materials at 30^{o}C and 0.5 seconds represents the worse condition. Figures 6.3 to 6.5 show typical effects of increasing deviator stress on permanent strain accumulation of the oil sand materials tested at three confining stress, 41.4, 138, and 276 kPa. For all the three oil sand materials tested, the trend found between permanent strain and the number of load applications is that as the applied deviator stress increased, the magnitude of the axial permanent strain accumulation increased. The increase in strain was very significant at high deviator stress-low confining stress pair stress states. Thus, permanent strains are significantly lower at low confining stress (41.4 kPa) compared with the high confining pressures of 138 kPa and 276 kPa. The permanent strains at deviator stress of 138 kPa are also lower than those for 276 kPa. This implies that oil sand materials would experience considerable amount of permanent deformation under dynamic applied load of construction and mining equipment in the field. In other words, the wheel/track loads from haul trucks or shovels tracks will induce more sinkage and rutting as the vertical stress increases in the oil sand materials.

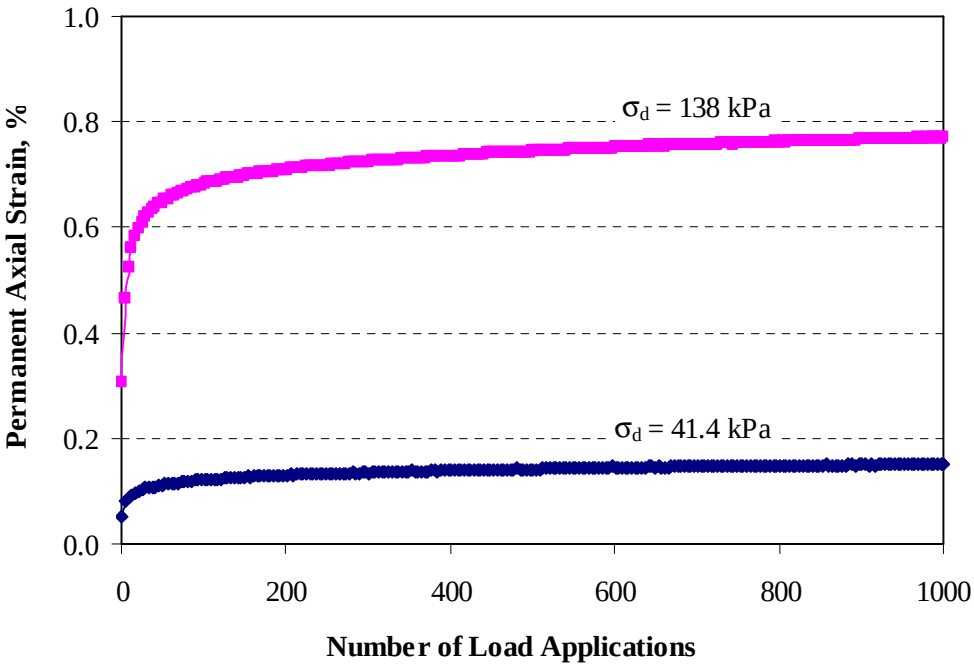

(a) Confining Pressure = 41.4 kPa

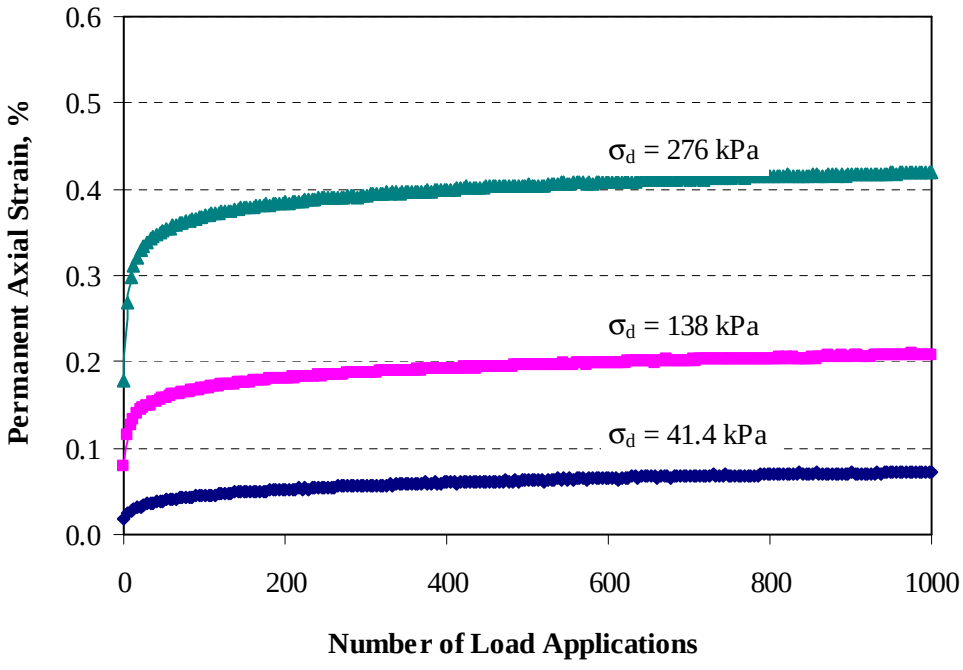

(b) Confining Pressure =138 kPa

FIGURE 6.3 Effect of Deviator Stress on Permanent Strain Accumulation in SE-09 Sample: (a) Confining Pressure = 41.4 kPa, (b) Confining Pressure = 138 kPa and (c) Confining Pressure = 276 kPa.

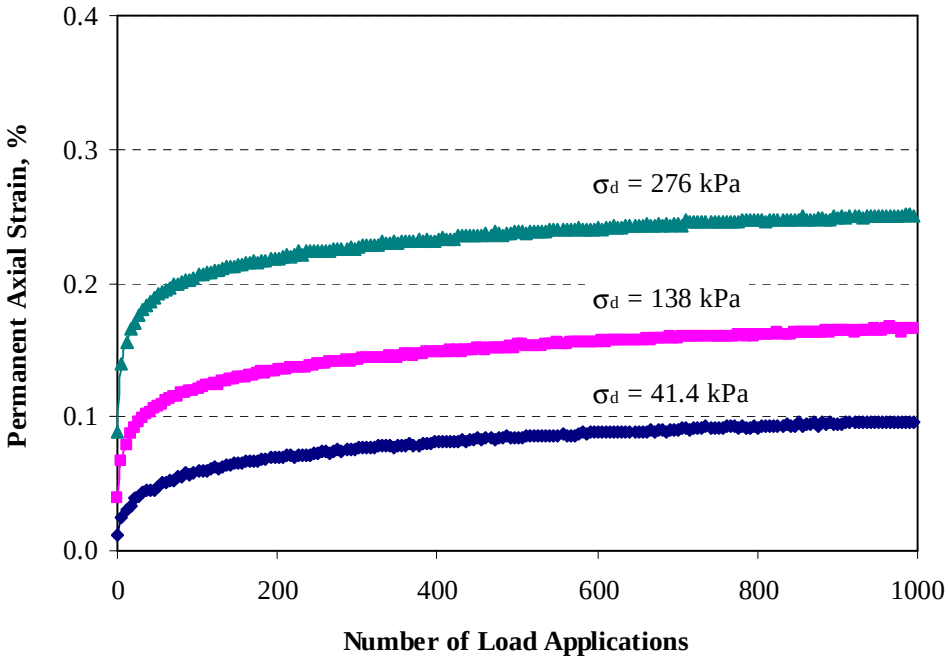

(c) Confining Pressure = 276 kPa

FIGURE 6.3 Effect of Deviator Stress on Permanent Strain Accumulation in SE-09 Oil Sample: (a) Confining Pressure = 41.4 kPa, (b) Confining Pressure = 138 kPa and (c) Confining Pressure = 276 kPa.

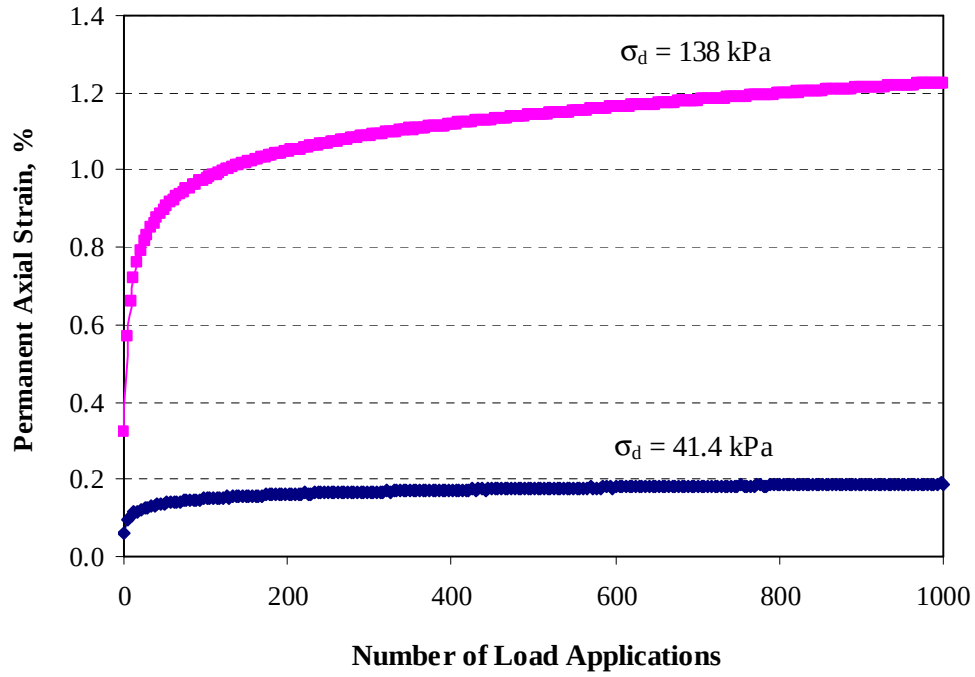

(a) Confining Pressure = 41.4 kPa

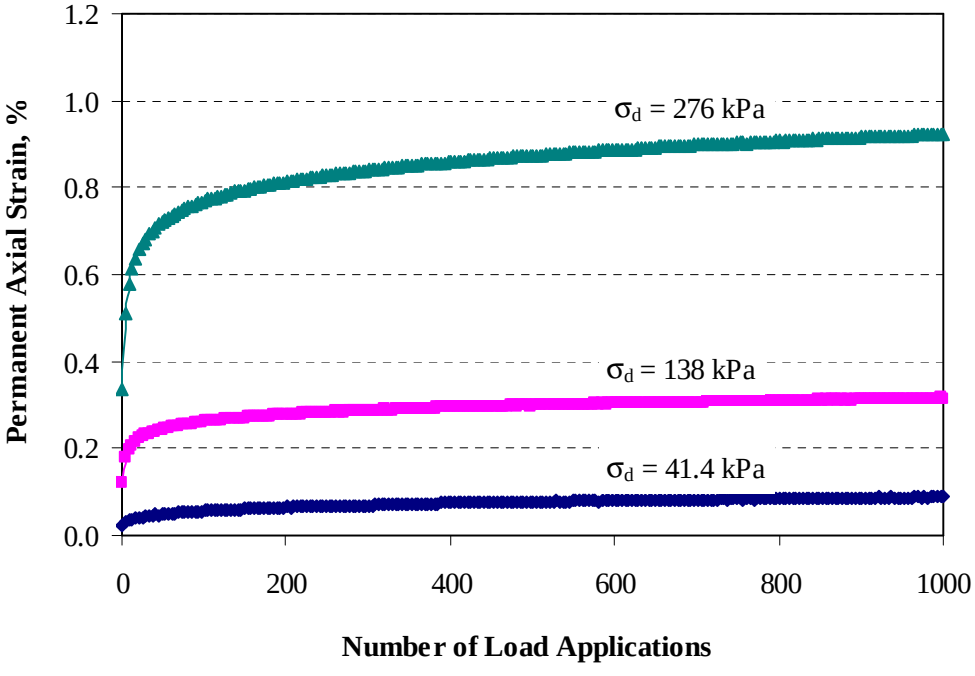

(b) Confining Pressure =138 kPa

FIGURE 6.4 Effect of Deviator Stress on Permanent Strain Accumulation in SE-14 Sample: (a) Confining Pressure = 41.4 kPa, (b) Confining Pressure = 138 kPa and (c) Confining Pressure = 276 kPa.

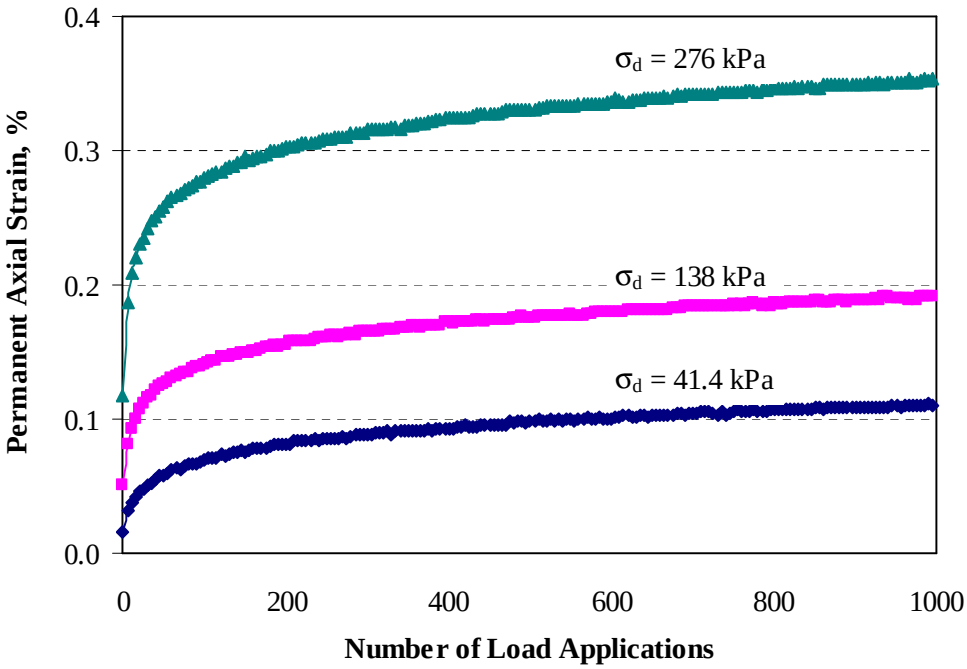

(c) Confining Pressure = 276 kPa

FIGURE 6.4 Effect of Deviator Stress on Permanent Strain Accumulation in SE-14 Sample: (a) Confining Pressure = 41.4 kPa, (b) Confining Pressure = 138 kPa and (c) Confining Pressure = 276 kPa.

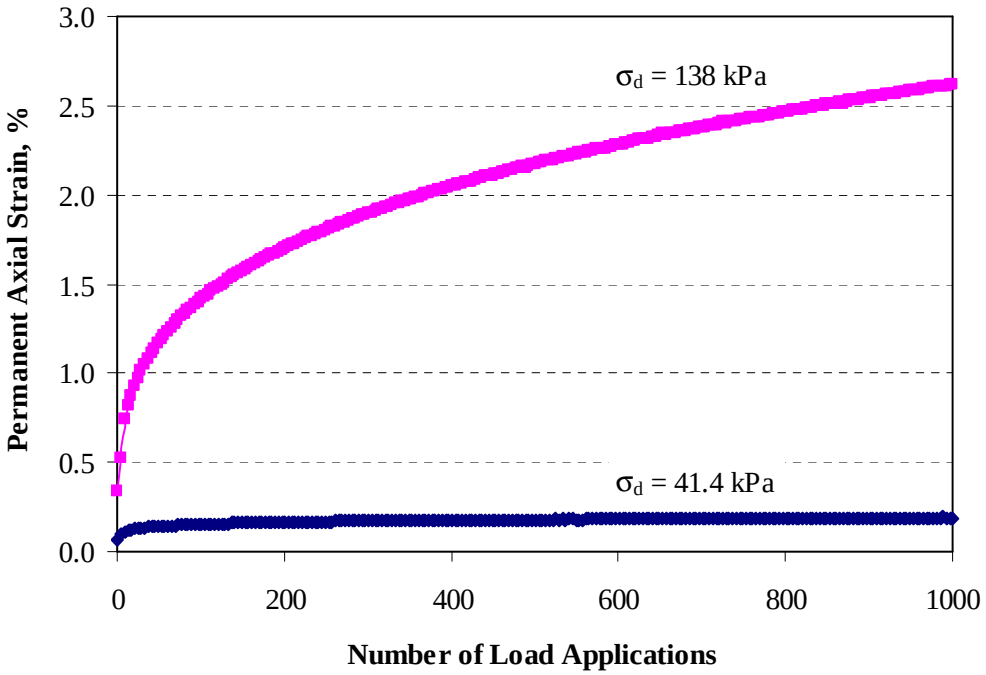

(a) Confining Pressure = 41.4 kPa

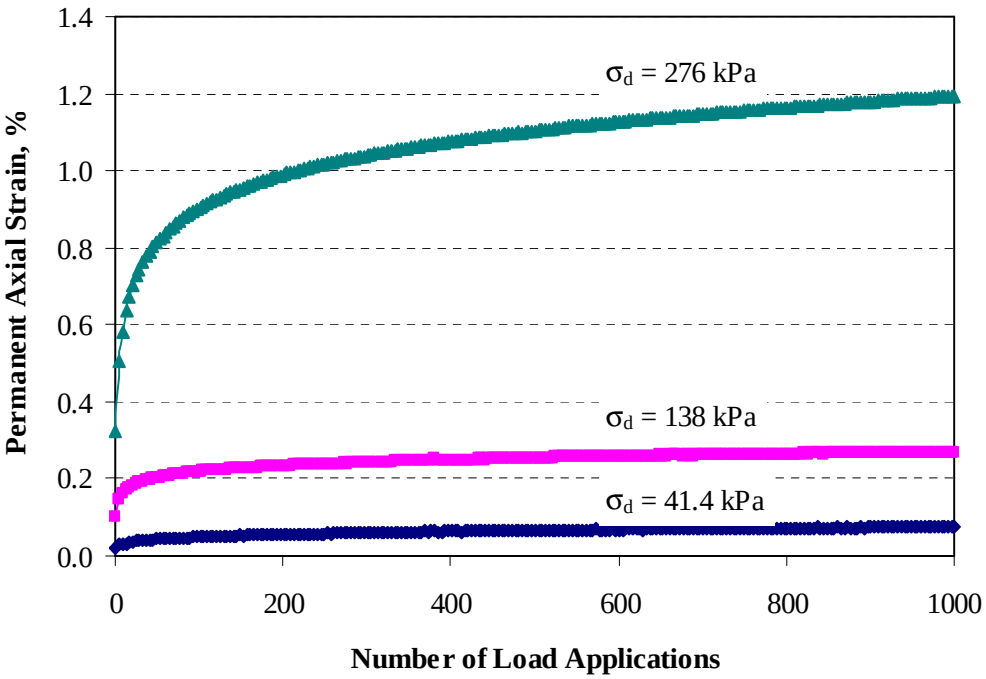

(b) Confining Pressure =138 kPa

FIGURE 6.5 Effect of Deviator Stress on Permanent Strain Accumulation in AU-14 Sample: (a) Confining Pressure = 41.4 kPa, (b) Confining Pressure = 138 kPa and (c) Confining Pressure = 276 kPa.

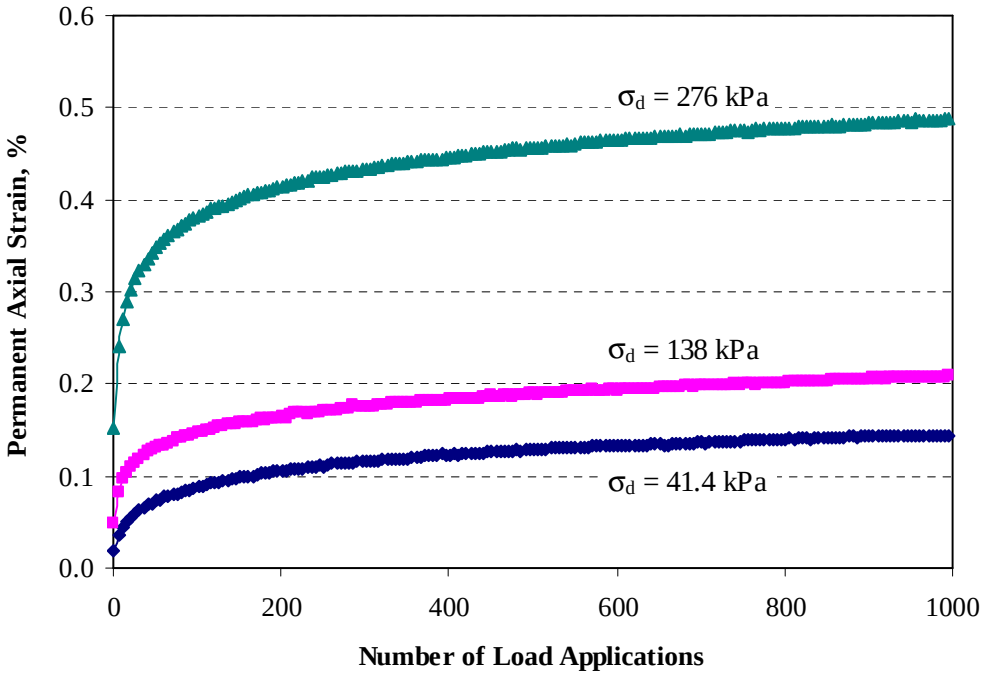

(c) Confining Pressure = 276 kPa

FIGURE 6.5 Effect of Deviator Stress on Permanent Strain Accumulation in AU-14 Sample: (a) Confining Pressure = 41.4 kPa, (b) Confining Pressure = 138 kPa and (c) Confining Pressure = 276 kPa.

6.4.1.3 Effect of Confining Stress

The effect of confining pressure is also studied for the oil sand samples at a temperature of 30^{o}C and load duration of 0.5 seconds. Figures 6.6 to 6.8 show the combined effects of confining pressure and deviator stress on permanent deformation at a temperature of 30^{o}C and load duration, 0.5 seconds for the three oil sand materials. The figures show the rate of permanent strain accumulation at 1,000th load cycle for each of the three confining pressure levels 41.4, 138, and 276 kPa. Permanent strain accumulation rates (i.e., slope of the lines) generally decreased as the magnitude of the confining pressure increased. The observed rate of accumulation indicates that the oil sand samples would resist permanent deformation buildup under higher confinement in the field.

Thus, at low confining pressures, oil sand materials located directly under construction and mining equipment wheel/track would be more vulnerable for sinkage and rutting. Previous authors have reported similar behavior on pavement geomaterials under highway and aircraft wheel loads (Barksdale 1972, Lekarp et al. 2000, Kim 2005).

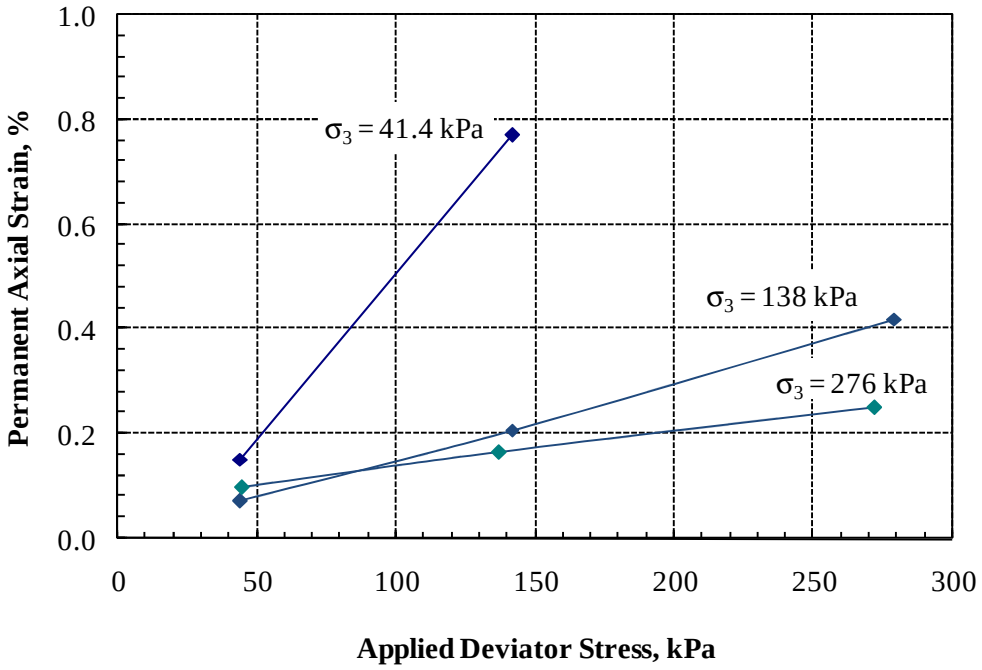

FIGURE 6.6 Effect of Confining Stress on SE-09 Permanent Deformation Development.

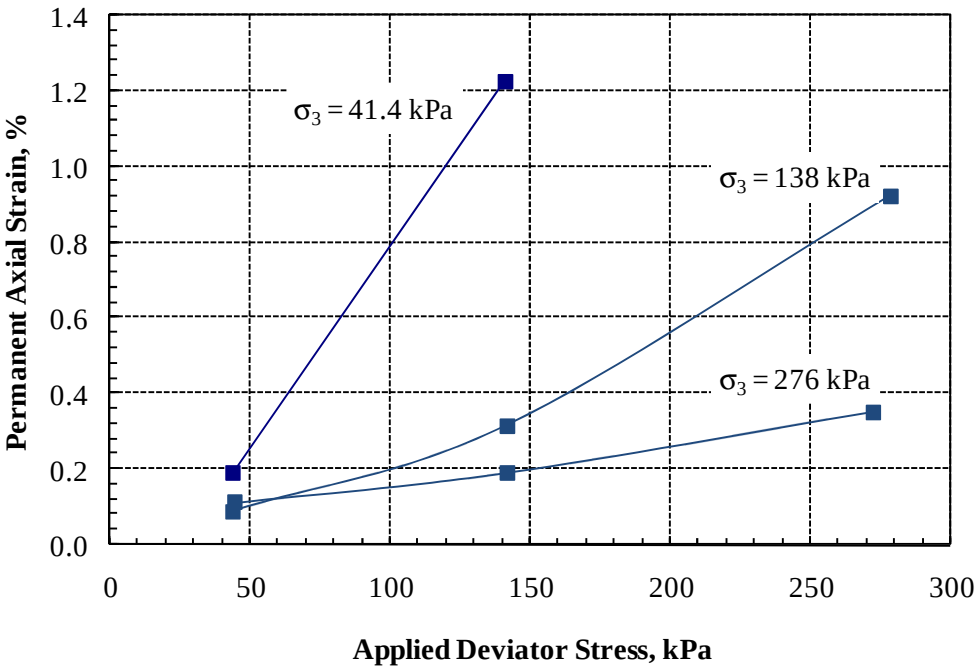

FIGURE 6.7 Effect of Confining Stress on SE-14 Permanent Deformation Development.

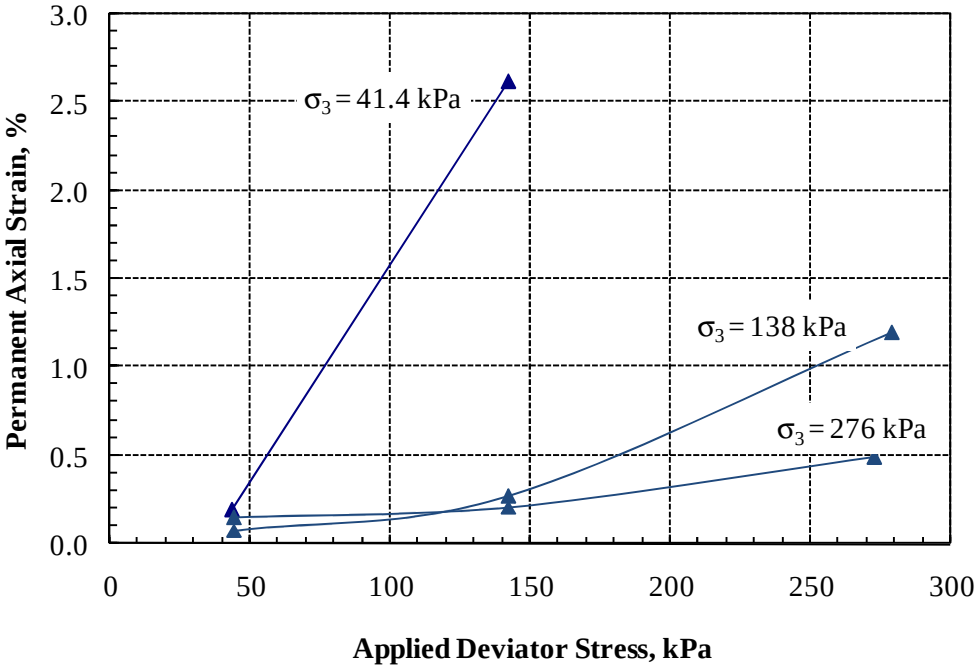

FIGURE 6.8 Effect of Confining Stress on AU-14 Permanent Deformation Development.

6.5 Permanent Deformation Model Development

6.5.1 Development of Power Models

A total of 32 test results corresponding to 32 different applied stress states (see Table 6.1 with the exception of $\sigma_1/\sigma_3 = 7.67$) were obtained from the experimental program for each oil sand material at two temperatures and two load pulse durations. Overall, 96 test results were therefore obtained for the three oil sands. A single test data set consisted of about 250 stress-strain data points giving 8,000 data points for each material and therefore 24,000 data points for all the three oil sands.

The phenomenological power model, expressed by ε_p (%) = $A*N^b$, was used to evaluate the permanent strain accumulation of the oil sand materials with number of load applications N. Statistical regression analyses were performed using this power model to obtain the model parameters A and b. Tables 6.2 through 6.4 present a summary of the model parameters obtained for individual tests conducted at 20^{o}C and at 30^{o}C. The power model adequately predicts the permanent strain accumulations from individual tests as observed from the generally high correlation coefficients (R^2 values) also given in Tables 6.2, through 6.4. The model parameters A and b were investigated to identify their dependence on the applied stress states, temperature, load pulse duration, bitumen content and three gradation properties (Cu, Cc and D50). The parameter A accounts for the permanent strain accumulated at the first load cycle and parameter b describes the rate (slope) of permanent strain accumulation when linear graph of logarithm of ε_p is plotted against logarithm of N. This was recently affirmed by Kim and Tutumluer (2006). As indicated in Tables 6.2 through 6.4, parameter A generally increased with increasing deviator stresses, thus indicating higher immediate sinkage and permanent strain development under heavier wheel loading, whereas parameter b had a slight decreasing trend not affecting notably the rate of permanent strain accumulation with increasing load applications.

TABLE 6.2a Permanent Deformation $\varepsilon_p = A*N^b$ Model Parameters: SE-09 at Temperature 20°C, and Load Duration 0.1sec

σ_3	σ_d	A	b	R^2	*RMSE*
40.4	42.5	0.051	0.129	*0.979*	*0.015*
40.4	135.9	0.250	0.109	*0.869*	*0.033*
138.8	42.0	0.012	0.221	*0.997*	*0.009*
138.8	135.3	0.064	0.107	*0.970*	*0.014*
138.2	250.8	0.189	0.091	*0.957*	*0.015*
279.1	42.0	0.011	0.254	*0.991*	*0.018*
278.6	140.8	0.025	0.203	*0.998*	*0.007*
278.0	229.2	0.051	0.138	*0.971*	*0.019*

TABLE 6.2b Permanent Deformation $\varepsilon_p = A*N^b$ Model Parameters: SE-09 at Temperature 20°C, and Load Duration 0.5sec

σ_3	σ_d	A	b	R^2	*RMSE*
39.8	44.7	0.068	0.105	*0.966*	*0.015*
40.4	141.9	0.376	0.081	*0.899*	*0.021*
139.3	43.6	0.015	0.199	*0.997*	*0.009*
139.3	143	0.095	0.090	*0.980*	*0.010*
138.8	278.4	0.279	0.058	*0.935*	*0.012*
278	44.2	0.020	0.165	*0.990*	*0.012*
278.6	135.9	0.041	0.172	*0.994*	*0.010*
278	272.8	0.051	0.146	*0.976*	*0.017*

TABLE 6.2c Permanent Deformation $\varepsilon_p = A*N^b$ Model Parameters: SE-09 at Temperature 30°C, and Load Duration 0.1sec

σ_3	σ_d	A	b	R^2	*RMSE*
40.4	42.5	0.067	0.115	*0.983*	*0.012*
40.4	136.4	0.356	0.103	*0.919*	*0.024*
138.2	42.5	0.013	0.224	*0.998*	*0.008*
138.2	135.9	0.077	0.097	*0.950*	*0.017*
138.8	248.6	0.219	0.083	*0.931*	*0.017*
278.6	42.5	0.010	0.303	*0.987*	*0.026*
278.0	142.5	0.053	0.164	*0.989*	*0.013*
277.5	227.0	0.073	0.139	*0.982*	*0.014*

TABLE 6.2d Permanent Deformation $\varepsilon_p = A*N^b$ Model Parameters: SE-09 at Temperature 30°C, and Load Duration 0.5sec

σ_3	σ_d	A	b	R^2	*RMSE*
40.4	43.6	0.070	0.114	*0.991*	*0.008*
40.4	141.9	0.447	0.083	*0.935*	*0.017*
138.2	43.6	0.018	0.203	*1.000*	*0.003*
138.8	141.4	0.102	0.104	*0.990*	*0.008*
138.8	279.0	0.255	0.075	*0.962*	*0.011*
278.0	44.7	0.017	0.256	*0.991*	*0.018*
278.0	137.0	0.054	0.167	*0.985*	*0.015*
278.6	271.7	0.122	0.107	*0.984*	*0.010*

TABLE 6.3a Permanent Deformation $\varepsilon_p = A*N^b$ Model Parameters: SE-14 at Temperature 20°C, and Load Duration 0.1sec

σ_3	σ_d	A	b	R^2	*RMSE*
40.4	43.1	0.039	0.165	*0.992*	*0.011*
40.9	134.8	0.324	0.145	*0.920*	*0.033*
138.2	42.5	0.016	0.213	*0.998*	*0.007*
138.8	134.8	0.106	0.110	*0.969*	*0.015*
138.8	247.5	0.297	0.099	*0.922*	*0.022*
278.6	41.4	0.009	0.288	*0.946*	*0.050*
278.0	135.9	0.024	0.239	*0.997*	*0.010*
277.5	223.7	0.076	0.146	*0.990*	*0.011*

TABLE 6.3b Permanent Deformation $\varepsilon_p = A*N^b$ Model Parameters: SE-14 at Temperature 20°C, and Load Duration 0.5sec

σ_3	σ_d	A	b	R^2	*RMSE*
40.4	44.7	0.074	0.121	*0.980*	*0.013*
40.4	141.9	0.494	0.095	*0.926*	*0.021*
138.2	43.6	0.023	0.170	*0.999*	*0.004*
138.2	141.9	0.130	0.090	*0.983*	*0.009*
138.8	277.9	0.450	0.082	*0.931*	*0.017*
278.0	44.7	0.023	0.203	*0.974*	*0.024*
278.6	141.4	0.040	0.183	*0.960*	*0.027*
278.0	272.8	0.117	0.119	*0.964*	*0.017*

TABLE 6.3c Permanent Deformation $\varepsilon_p = A*N^b$ Model Parameters: SE-14 at Temperature 30°C, and Load Duration 0.1sec

σ_3	σ_d	A	b	R^2	*RMSE*
40.4	43.1	0.077	0.127	*0.987*	*0.011*
40.4	136.4	0.376	0.156	*0.959*	*0.025*
138.2	43.1	0.019	0.217	*0.999*	*0.005*
138.2	137	0.103	0.131	*0.985*	*0.013*
138.2	247.5	0.322	0.111	*0.968*	*0.015*
278.0	42.5	0.013	0.281	*0.979*	*0.030*
278.0	135.9	0.053	0.182	*0.989*	*0.014*
278.0	224.3	0.092	0.149	*0.982*	*0.016*

TABLE 6.3d Permanent Deformation $\varepsilon_p = A*N^b$ Model Parameters: SE-14 at Temperature 30°C, and Load Duration 0.5sec

σ_3	σ_d	A	b	R^2	*RMSE*
40.4	43.6	0.082	0.123	*0.987*	*0.011*
40.9	140.8	0.509	0.131	*0.968*	*0.018*
138.2	43.6	0.023	0.197	*0.999*	*0.004*
138.8	141.4	0.160	0.100	*0.982*	*0.010*
138.2	278.4	0.467	0.101	*0.973*	*0.013*
278.0	44.2	0.022	0.238	*0.993*	*0.015*
278.0	141.4	0.064	0.162	*0.990*	*0.012*
278.6	272.3	0.158	0.119	*0.990*	*0.009*

TABLE 6.4a Permanent Deformation $\varepsilon_p = A*N^b$ Model Parameters: AU-14 at Temperature 20°C, and Load Duration 0.1sec

σ_3	σ_d	A	b	R^2	*RMSE*
40.4	42.5	0.042	0.166	*0.958*	*0.027*
40.4	136.4	0.245	0.272	*0.991*	*0.020*
138.8	40.9	0.008	0.225	*0.999*	*0.004*
138.8	135.3	0.061	0.119	*0.964*	*0.018*
138.2	240.8	0.241	0.155	*0.976*	*0.019*
278.6	30.4	0.008	0.303	*0.999*	*0.006*
278.6	133.1	0.022	0.227	*0.998*	*0.007*
278.6	222.1	0.097	0.112	*0.971*	*0.015*

TABLE 6.4b Permanent Deformation $\varepsilon_p = A*N^b$ Model Parameters: AU-14 at Temperature 20°C, and Load Duration 0.5sec

σ_3	σ_d	A	b	R^2	*RMSE*
40.4	44.2	0.070	0.130	*0.966*	*0.019*
40.9	140.8	0.344	0.275	*0.996*	*0.014*
138.8	43.6	0.016	0.160	*0.993*	*0.010*
138.8	141.9	0.091	0.112	*0.969*	*0.016*
138.5	278.4	0.419	0.143	*0.971*	*0.019*
278.6	43.6	0.016	0.219	*0.999*	*0.004*
278.6	140.8	0.050	0.145	*0.995*	*0.008*
278.6	272.8	0.152	0.108	*0.990*	*0.008*

TABLE 6.4c Permanent Deformation $\varepsilon_p = A*N^b$ Model Parameters: AU-14 at Temperature 30°C, and Load Duration 0.1sec

σ_3	σ_d	A	b	R^2	*RMSE*
40.9	42	0.064	0.140	*0.979*	*0.016*
40.4	136.4	0.301	0.264	*0.998*	*0.009*
138.2	42.2	0.012	0.196	*0.999*	*0.005*
138.2	135.3	0.104	0.118	*0.984*	*0.011*
138.2	243.6	0.279	0.155	*0.950*	*0.027*
278.0	43.1	0.019	0.288	*0.995*	*0.014*
278.6	135.3	0.054	0.188	*0.990*	*0.014*
277.5	222.6	0.096	0.158	*0.985*	*0.015*

TABLE 6.4d Permanent Deformation $\varepsilon_p = A*N^b$ Model Parameters: AU-14 at Temperature 30°C, and Load Duration 0.5sec

σ_3	σ_d	A	b	R^2	*RMSE*
40.4	43.6	0.086	0.118	*0.983*	*0.012*
40.4	141.9	0.371	0.285	*0.994*	*0.017*
138.2	44.2	0.021	0.186	*0.999*	*0.005*
138.8	141.9	0.128	0.110	*0.984*	*0.011*
138.8	279.0	0.428	0.153	*0.982*	*0.016*
278.0	44.2	0.025	0.262	*0.990*	*0.019*
278.0	141.9	0.064	0.175	*0.992*	*0.011*
278.0	272.8	0.201	0.132	*0.986*	*0.011*

6.5.2 Permanent Strain Models

To better evaluate the main factors controlling permanent deformation/strain behavior of the oil sand materials, statistical correlation analyses were conducted to establish those noteworthy dependencies between the model parameters A and b and the applied stress states. Equations 6.1a to 6.1e and Figure 6.9 summarize the correlation results between the model parameters and the applied stress levels for the entire database of all oil sand material test results. Generally, Parameter A in the power model $\varepsilon_p = A*N^b$ is known to be primarily a function of applied stress states whereas b largely depends on the soil or geomaterial type (Bejarano and Thompson 1999). As shown in Figure 6.9, the strongest correlation obtained for parameter A was with the principal stress ratios (σ_1/σ_3) giving a considerably high correlation coefficient of $R^2 = 0.84$. This indicates that parameter A is a function of stress ratios and its values increased exponentially with the increasing σ_1/σ_3 ratios. High stress ratios would induce large permanent deformation in the oil sand materials, especially at the initial load application. A relatively strong correlation was also obtained between parameter A and the applied deviator stress but not with the confining stress σ_3 (see Equations 6.1a and 6.1b). On the other hand, weaker correlations were typically found between parameter b and the applied stress levels (see Equations 6.1c to 6.1e) indicating that applied stresses had little effect on parameter b. These are all in agreement with others who reported in general that confining stress had little impact on parameter A, and the applied stress states did not influence much the b parameter (Barksdale 1971, Garg and Thompson 1998).

$$A = 0.0003\,\sigma_d^{1.1667} \quad ; \qquad R^2 = 0.54 \tag{6.1a}$$

$$A = 2.0719\,\sigma_3^{-0.6857} \quad ; \qquad R^2 = 0.19 \tag{6.1b}$$

$$b = 0.2042 \cdot \left(\sigma_1 / \sigma_3\right)^{-0.4581} \quad ; \quad R^2 = 0.26 \tag{6.1c}$$

$$b = 0.5091\ \sigma_d^{-0.2636} \quad ; \qquad R^2 = 0.27 \tag{6.1d}$$

$$b = 0.0779\,\sigma_3^{0.1338} \quad ; \qquad R^2 = 0.07 \tag{6.1e}$$

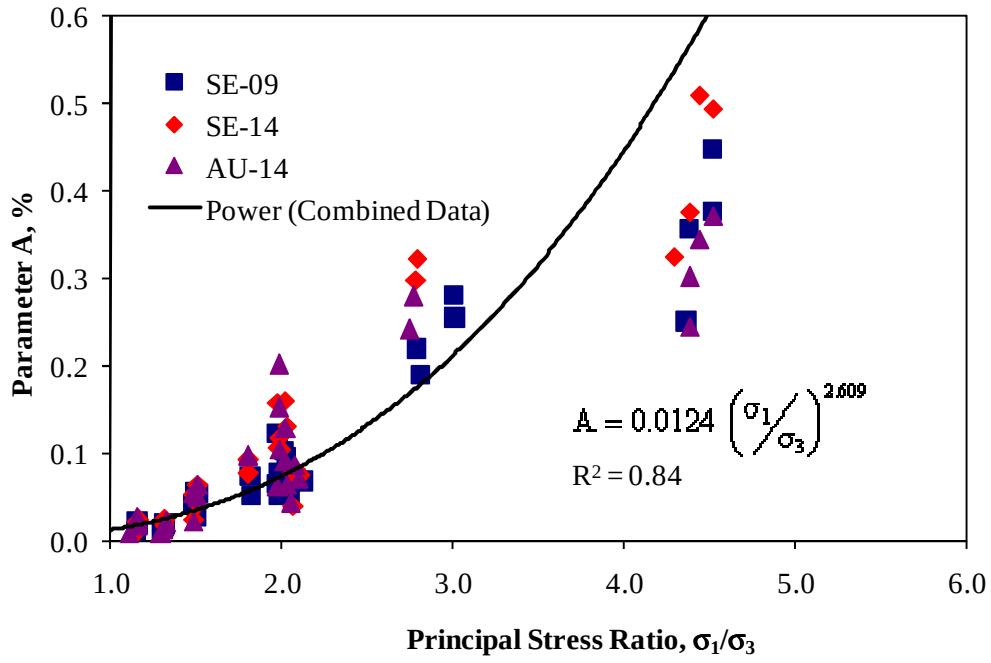

FIGURE 6.9 Model Parameter A as a Function of Principal Stress Ratio, σ_1/σ_3.

No significantly strong or noteworthy correlations, such as shown in Figure 6.9 for parameter A, were obtained individually between parameters A and b and the other test variables, i.e., test temperature, load pulse duration and bitumen content. Detailed statistical analyses conducted using the SAS software package, however, indicated that parameter b had somewhat stronger correlations with bitumen content and load pulse duration than parameter A. On the other hand, parameter A could be more significantly linked to test temperature than parameter b suggesting that temperature, in relation to the applied stress states, could influence oil sand permanent deformation at the initial load application.

6.5.3 Laboratory Validation of Permanent Deformation Models

Additional laboratory tests were conducted on newly prepared specimens of all the three oil sand materials to check performances of the permanent deformation models. These tests were limited to only the 0.1-second load pulse duration, one applied stress state of 138 kPa (20 psi) equal confining and deviator stresses, and the two test temperatures of 20°C and 30°C.

This time, a total of 10,000 load cycles were applied on the replicate specimens in order to adequately validate the permanent deformation model performances for up to 1,000 load cycles and further, check their prediction abilities at larger number of load applications.

Figures 6.10a and 6.10b show both the experimental and model prediction results of permanent axial strain with number of load applications obtained at 20 and 30 degrees Celsius, respectively. Note that unlike in Figure 6.1, due to different stress states applied, AU-14 specimens did not yield the highest plastic strains. In general, the close agreements between the laboratory measured and predicted results demonstrate the good repeatability of the test data and likewise good performances of the individually developed permanent deformation models for predicting plastic strains beyond 1,000 cycles, for up to 10,000 load applications.

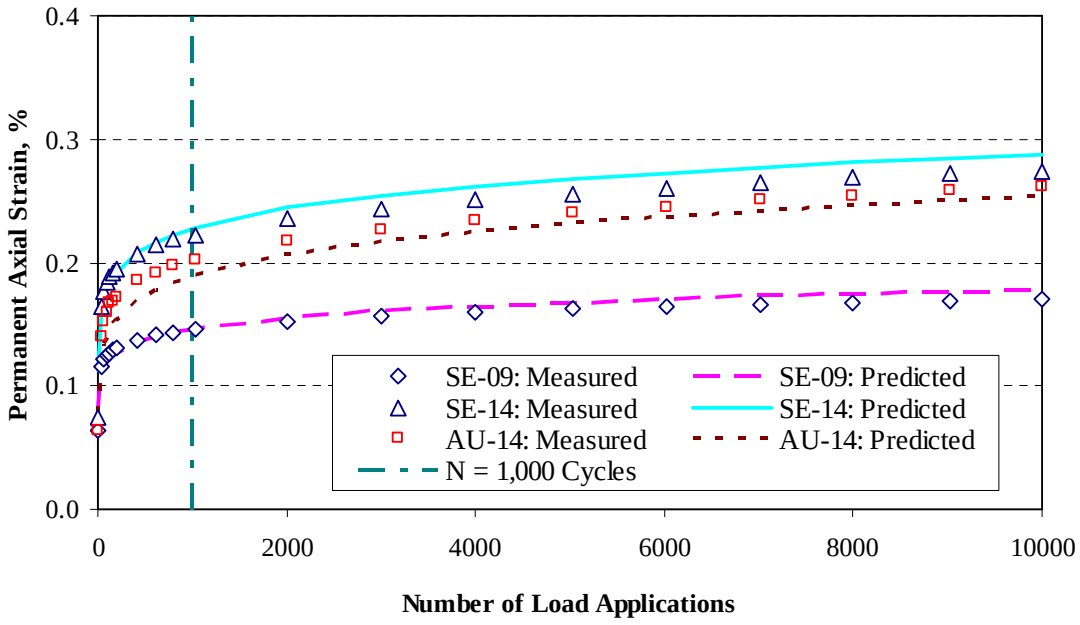

(a) 20°C

FIGURE 6.10 Permanent Strain Model Predictions for Additional Test Specimens: (a) Temperature = 20°C and (b) Temperature = 30°C.

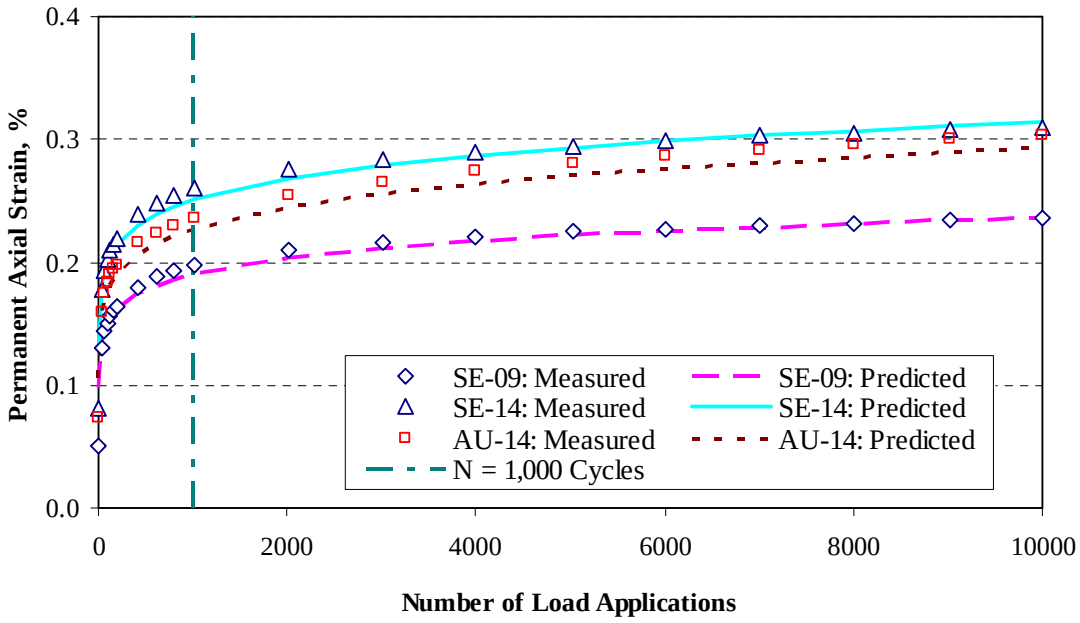

(b) 30°C

FIGURE 6.10 Permanent Strain Model Predictions for Additional Test Specimens: (a) Temperature = 20°C and (b) Temperature = 30°C.

6.5.4 Unified Permanent Deformation Model Development

Since the overall objective was to develop a better basic understanding as well as to come up with practical predictive equations to estimate field sinkage and permanent deformation behavior of oil sands, the stress-strain data sets were combined to create individual databases of the three oil sand materials. A close examination of the physical properties of the three oil sands; particle size distribution, density, and water content suggested that the individual databases could also be combined for analysis.

The correlation coefficient R-square selection method in the SAS software was first used to determine which independent variables were potential candidates for the models. The variables used in the selection include principal stress ratio, deviator stress, confining pressure, number of load applications, bitumen content, temperature, load pulse and three gradation properties (Cu, Cc and D_{50}). It was found that permanent strain strongly depended on the principal stress ratio and the number of load applications.

There was relatively weak dependency of permanent strain on the applied deviator stress, temperature and bitumen content, and little or no correlation was found between the permanent strain and all the three gradation properties. Therefore, principal stress ratio, number of load applications, applied deviator stress, temperature and bitumen content were selected as independent variables of the models. Various mathematical forms such as linear, nonlinear, logarithmic, and hyperbolic were investigated using multiple regression analyses. Considering the typical exponential growth of permanent strains with respect to number of load applications in the triaxial tests, the power or logarithmic functions were found to be most suitable for the models. Based on this result, five models were selected to study oil sand permanent deformation behavior.

Table 6.5a lists three unified permanent strain models developed for each oil sand material and the model parameters obtained from multiple regression analyses. No significant differences were found among the model parameters for the three oil sands. Therefore, it was reasonable to combine the test data to develop a generalized model for oil sands. The combined data allowed bitumen content to be included as a variable in the analyses assuming similar bitumen properties among the three oil sands. Table 6.5b lists the generalized permanent strain models developed using the combined test data and gives the model parameters obtained from stepwise multiple regression analyses. Note that high coefficient of correlation (R^2) values were obtained for all the models, including models 1 through 3, thus indicating stress dependency had the predominant role in predicting permanent strain accumulation. Since a comprehensive but yet practical model should also account for the additional effects of temperature and bitumen content in the oil sand, slightly improved models of 4 and 5 in Table 6.5b can be proposed for routine use in the estimation of field sinkage and permanent deformation behavior of oil sands.

TABLE 6.5a Unified Permanent Strain Models Developed for Each Oil Sand Material

Model 1 $\varepsilon_p = \left(\sigma_1 / \sigma_3\right)^{\beta}$

Model 2 $\varepsilon_p = A \cdot N^{\alpha} \cdot \left(\sigma_1 / \sigma_3\right)^{\beta}$

Model 3 $\varepsilon_p = A \cdot N^{\alpha} \cdot \left(\sigma_1 / \sigma_3\right)^{\beta} \cdot \sigma_d^{\gamma}$

Model 4 $\varepsilon_p = A \cdot N^{\alpha} \cdot \left(\sigma_1 / \sigma_3\right)^{\beta} \cdot \sigma_d^{\gamma} \cdot T^{\lambda}$

Model	Model Parameters						
	Log A	α	β	γ	λ	R^2	*RMSE*
SE-09 Sample							
Model 1	-1.487	-	1.968	-	-	*0.758*	*0.198*
Model 2	-1.845	0.169	1.973	-	-	*0.896*	*0.130*
Model 3	-2.325	0.168	1.711	0.276	-	*0.929*	*0.107*
Model 4	-3.125	0.168	1.711	0.276	0.576	*0.945*	*0.094*
SE-14 Sample							
Model 1	-1.420	-	2.189	-	-	*0.755*	*0.222*
Model 2	-1.808	0.183	2.195	-	-	*0.886*	*0.151*
Model 3	-2.533	0.183	1.800	0.417	-	*0.947*	*0.103*
Model 4	-3.345	0.183	1.800	0.417	0.585	*0.960*	*0.089*
AU-14 Sample							
Model 1	-1.518	-	2.554	-	-	*0.740*	*0.270*
Model 2	-1.954	0.206	2.562	-	-	*0.858*	*0.200*
Model 3	-2.752	0.206	2.113	0.462	-	*0.913*	*0.156*
Model 4	-3.876	0.206	2.115	0.458	0.816	*0.932*	*0.139*

TABLE 6.5b Unified Permanent Strain Models Studied for Oil Sand Materials

Model 1 $\varepsilon_p = A \cdot \left(\sigma_1 / \sigma_3\right)^{\beta}$

Model 2 $\varepsilon_p = A \cdot N^{\alpha} \cdot \left(\sigma_1 / \sigma_3\right)^{\beta}$

Model 3 $\varepsilon_p = A \cdot N^{\alpha} \cdot \left(\sigma_1 / \sigma_3\right)^{\beta} \cdot \sigma_d^{\gamma}$

Model 4 $\varepsilon_p = A \cdot N^{\alpha} \cdot \left(\sigma_1 / \sigma_3\right)^{\beta} \cdot \sigma_d^{\gamma} \cdot W_b^{\eta}$

Model 5 $\varepsilon_p = A \cdot N^{\alpha} \cdot \left(\sigma_1 / \sigma_3\right)^{\beta} \cdot \sigma_d^{\gamma} \cdot W_b^{\eta} \cdot T^{\lambda}$

Model	Model Parameters							
	Log A	α	β	γ	η	λ	R^2	*RMSE*
1	-1.475	-	2.237	-	-	-	*0.726*	*0.244*
2	-1.869	0.186	2.244	-	-	-	*0.850*	*0.196*
3	-2.537	0.186	1.875	0.385	-	-	*0.898*	*0.188*
4	-1.942	0.186	1.874	0.387	0.645	-	*0.918*	*0.185*
5	-2.857	0.186	1.875	0.386	0.650	0.661	*0.933*	*0.185*

6.5.5 Modified Permanent Strain Models Including Shear Strength

Although the unified permanent strain models presented in Table 6.5b would give good prediction of rutting in the oil sand materials, it is important to incorporate the allowable shear strength property into these models to properly study the effect of shear strength in the field. Figure 6.11 shows Mohr-Coulomb representation of a typical stress state applied on a specimen during triaxial testing and the corresponding shear strength properties of the material. The Mohr-Coulomb envelope defines for the limiting maximum stress at failure or shear strength, τ_{max}, and is given by $\tau_{max} = c + \sigma_n * \tan\phi$, where c and ϕ are the cohesion and friction angle, respectively, and σ_n is the normal stress acting on the failure plane. Note that the failure plane makes an angle of $(45^o + \phi/2)$ with the horizontal plane (see Figure 6.11).

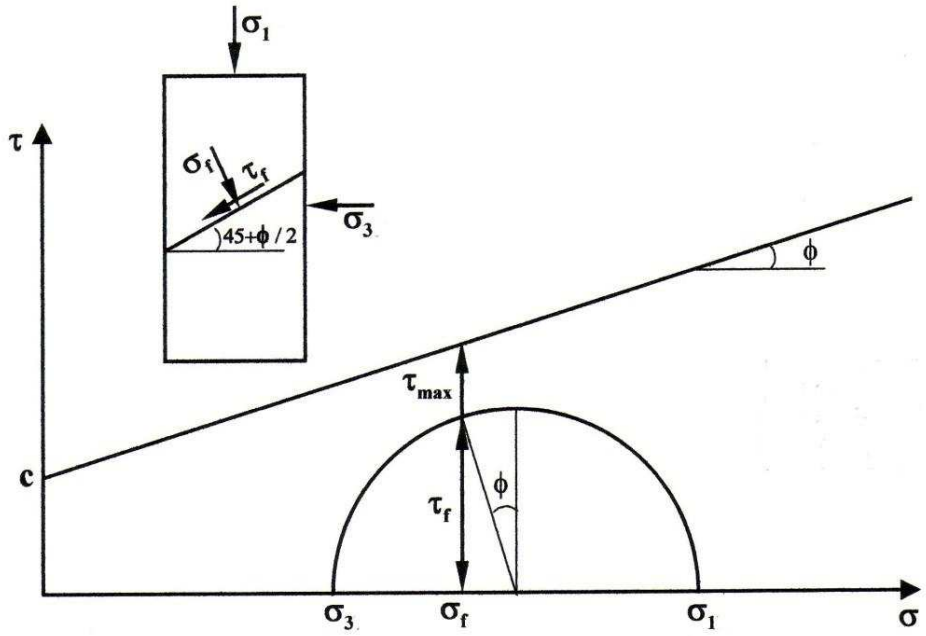

FIGURE 6.11 Mohr-Coulomb Representation of Shear Strength and Applied Stress States.

The applied stress states on the failure plane to compute a shear stress ratio of (τ_f / τ_{max}) indicated in Figure 6.11 can be derived from the following equations:

$$\sigma_f = \frac{2\sigma_3 + 2\tan^2\phi \cdot \sigma_3 + \sigma_d + \tan^2\phi \cdot \sigma_d - \sqrt{(\tan^2\phi \cdot \sigma_d^2 + \tan^4\phi \cdot \sigma_d^2)}}{2(1+\tan^2\phi)} \tag{6.2}$$

$$\tau_f = \sqrt{(\sigma_d/2)^2 - [\sigma_f - (\sigma_3 + \sigma_d/2)]^2} \tag{6.3}$$

where, $\sigma_d = \sigma_1 - \sigma_3$ and, ϕ = friction angle in degrees.

The triaxial compression test is one of the most common methods of determining friction angle ϕ and is the source of most of the existing data on friction angle of soils and granular materials. Other test methods including direct shear and plain strain test have also been successfully used to determine ϕ for soils and granular materials. For practical purposes, it is assumed that both triaxial compression and direct shear tests give similar values of friction angle.

A comparison of direct shear and conventional drained triaxial compression tests showed similar friction angles for residual soils derived from gneiss rock (Maccarini 1993). Accordingly, in this study, friction angles obtained from the direct shear tests were used in the shear stress ratio concept for modeling the permanent deformation behavior of the three oil sand materials. Note that undrained triaxial shear tests performed on the oil sand specimens did not result in shear failure in this study.

During permanent deformation testing of an individual sample, a total of 8 different stress states were applied on the specimens (see Table 6.1). These stress states are generally represented by Mohr circles that are positioned well below the Coulomb envelope. For an individual stress state, the normal and shear stresses acting on the failure plane are also represented in Figure 6.11 as denoted by σ_f and τ_f, respectively. Therefore, at any applied stress state, a *shear stress ratio* of τ_f / τ_{max} will have to give a certain fraction of the shear strength τ_{max} of the material that is acting on the failure plane due to the applied total stresses. A limiting value of this shear stress ratio is believed to control the permanent deformation behavior of the oil sands. This is similar in concept to the subgrade stress ratio (ratio of deviator stress to unconfined compressive strength) approach proposed by Thompson (NCHRP 1-26, 1990) for controlling rutting behavior of subgrade soils. Anisotropic modular ratios of different types of aggregates have also been correlated with shear stress ratios using Mohr-Coulomb approach (Seyhan and Tutumluer 2002).

Note that it is fundamentally more correct to correlate permanent deformation to the shear strength properties using the test results obtained from the triaxial tests. A decrease in shear strength as a result of lower friction angle would result in higher shear stress ratio for the same stress level and vice versa. Thus, the shear stress ratio would be a good indicator of the oil sand performance under varying stress states. In addition, the shear stress ratio would also determine the maximum allowable working stress to control sinkage and rutting potentials. Therefore, a new set of characterization models for the permanent deformation behavior of oil sands were also developed to include shear strength. Table 6.6 lists permanent strain models that incorporate shear stress ratio τ_f / τ_{max}.

Stepwise multiple regression analyses were performed in the development of the modified permanent deformation models except that in this case, permanent strain had strong correlation with load pulse duration instead of deviator stress. It can be seen that the effect of principal stress ratio in the unified permanent deformation models is similar to the shear stress ratio formulated in the modified model. This is observed from the R^2 and RMSE trends for the two sets of models (Tables 6.5a and 6.6). Thus, it can be concluded that an increase in the applied principal stress ratio is directly proportional to an increase in the applied shear stress ratio (τ_f / τ_{max}) of the material.

TABLE 6.6 Modified Permanent Strain Models Studied for Oil Sand Materials

Model 1 $\varepsilon_p = A \cdot \left(\tau_f / \tau_{max} \right)^{\beta}$

Model 2 $\varepsilon_p = A \cdot N^{\alpha} \cdot \left(\tau_f / \tau_{max} \right)^{\beta}$

Model 3 $\varepsilon_p = A \cdot N^{\alpha} . \left(\tau_f / \tau_{max} \right)^{\beta} \cdot P_d^{\gamma} \cdot$

Model 4 $\varepsilon_p = A \cdot N^{\alpha} . \left(\tau_f / \tau_{max} \right)^{\beta} P_d^{\gamma} \cdot W_b^{\eta}$

Model 5 $\varepsilon_p = A \cdot N^{\alpha} . \left(\tau_f / \tau_{max} \right)^{\beta} \cdot P_d^{\gamma} \cdot W_b^{\eta} \cdot \sigma_d^{\lambda}$

Model	Model Parameters							
	Log A	α	β	γ	η	λ	R^2	*RMSE*
1	-0.247	-	1.282	-	-	-	*0.700*	*0.225*
2	-0.636	0.185	1.285	-	-	-	*0.823*	*0.196*
3	-0.531	0.185	1.285	0.161	-	-	*0.837*	*0.188*
4	-0.235	0.185	1.276	0.161	0.323	-	*0.843*	*0.185*
5	-0.413	0.185	1.214	0.152	0.339	0.081	*0.844*	*0.185*

6.6 Analysis of Resilient Modulus Test Results

At each stress level, the resilient modulus was calculated using the applied deviator stress and the corresponding recoverable strains.

The resilient modulus values computed from the 96th to 100th load cycles were averaged for each specimen at every stress state. Tables 6.7 to 6.9 show the applied stresses and resilient modulus values obtained for the three oil sand samples at temperatures of 20^{o}C and at 30^{o}C. Resilient moduli for all the three samples were higher at 20^{o}C than at 30^{o}C. This trend is common to bituminous materials, which become stiffer at low temperatures than high temperatures. At the load duration of 0.1 seconds, the average resilient modulus of SE-09 sample at 20^{o}C was about 28% higher than the resilient modulus at 30^{o}C, and at 0.5- seconds, the resilient modulus at of SE-09 sample at 20^{o}C was about 31% higher than the resilient modulus at 30^{o}C. For the SE-14 sample, resilient modulus at 0.1-second was about 26% higher at 20^{o}C than the resilient modulus at 30^{o}C, and at 0.5-seconds, the resilient modulus at 20^{o}C was about 32% higher than the resilient modulus at 30^{o}C. The AU-14 sample had the lowest differences in resilient modulus between 20^{o}C and 30^{o}C. At 0.1-second, the modulus was about 15% higher at 20^{o}C than the resilient modulus at 30^{o}C, and at 0.5 seconds, the resilient modulus at 20^{o}C was about 16% higher than the resilient modulus at 30^{o}C. The data also indicate that there was virtually no difference between resilient modulus at 0.1 second and 0.5 second load durations for all the samples at the two test temperatures.

The difference at 20^{o}C and 30^{o}C for the SE-09 sample was about 0.5% and 2.7%, respectively, whereas that of SE-14 samples was nearly zero percent at 20^{o}C, and 2% at 30^{o}C. The AU-14 sample has the highest percentage difference of 4.7% and 5% at 20^{o}C and 30^{o}C, respectively. This trend is in agreement with other studies (Boyce et al. 1976, Sousa and Monismith 1987, Sweere 1990) that reported the loading frequency or load duration has little to no effect on the modulus or stiffness properties of granular materials.

Generally the SE-09 sample had the highest resilient modulus, and the AU-14 had the lowest. The SE-14 also had higher resilient modulus values than AU-14, although at some stress states the moduli of the two samples were comparable. In general, the low grade oil sand material was stiffer than the high grade oil sands. This may explain why the low grade oil sand materials are the preferred subgrade materials for the haul roads in the mining fields.

TABLE 6.7a Resilient Modulus Test Results: SE-09 at Temperature = 20°C

Load Duration = 0.1 seconds			Load Duration = 0.5 seconds		
Applied Stress		Resilient Modulus (MPa)	Applied Stress		Resilient Modulus (MPa)
σ_3 (kPa)	σ_d (kPa)		σ_3 (kPa)	σ_d (kPa)	
40.4	42.5	98.1	39.8	44.7	97.4
40.4	135.9	104.3	40.4	141.9	105.9
138.8	42.0	200.6	139.3	43.6	183.0
138.8	135.3	206.3	139.3	143.0	193.6
138.2	250.8	194.2	138.8	278.4	209.0
279.1	42.0	290.4	278.0	44.2	283.8
278.6	140.8	274.4	278.6	135.9	302.1
278.0	229.2	292.1	278.0	272.8	285.2

TABLE 6.7b Resilient Modulus Test Results: SE-09 at Temperature = 30°C

Load Duration = 0.1 seconds			Load Duration = 0.5 seconds		
Applied Stress		Resilient Modulus (MPa)	Applied Stress		Resilient Modulus (MPa)
σ_3 (kPa)	σ_d (kPa)		σ_3 (kPa)	σ_d (kPa)	
40.4	42.5	70.9	40.4	43.6	65.9
40.4	136.4	65.5	40.4	141.9	72.2
138.2	42.5	160.4	138.2	43.6	151.5
138.2	135.9	173.5	138.8	141.4	158.0
138.8	248.6	167.8	138.8	279.0	170.5
278.6	42.5	240.8	278.0	44.7	216.9
278.0	142.5	221.2	278.0	137.0	222.4
277.5	227.0	232.8	278.6	271.7	234.3

TABLE 6.8a Resilient Modulus Test Results: SE-14 at Temperature = 20°C

Load Duration = 0.1 seconds			Load Duration = 0.5 seconds		
Applied Stress		Resilient Modulus (MPa)	Applied Stress		Resilient Modulus (MPa)
σ_3 (kPa)	σ_d (kPa)		σ_3 (kPa)	σ_d (kPa)	
40.4	43.1	70.9	40.4	44.7	86.1
40.9	134.8	91.2	40.4	141.9	94.8
138.2	42.5	175.0	138.2	43.6	177.9
138.8	134.8	153.1	138.2	141.9	176.3
138.8	247.5	176.0	138.8	277.9	165.4
278.6	41.4	241.0	278.0	44.7	251.7
278.0	135.9	260.1	278.6	141.4	247.6
277.5	223.7	262.6	278.0	272.8	249.6

TABLE 6.8b Resilient Modulus Test Results: SE-14 at Temperature = 30°C

Load Duration = 0.1 seconds			Load Duration = 0.5 seconds		
Applied Stress		Resilient Modulus (MPa)	Applied Stress		Resilient Modulus (MPa)
σ_3 (kPa)	σ_d (kPa)		σ_3 (kPa)	σ_d (kPa)	
40.4	43.1	61.9	40.4	43.6	62.4
40.4	136.4	60.0	40.9	140.8	64.0
138.2	43.1	136.3	138.2	43.6	127.4
138.2	137.0	131.2	138.8	141.4	131.9
138.2	247.5	131.9	138.2	278.4	128.0
278.0	42.5	219.6	278.0	44.2	199.0
278.0	135.9	202.8	278.0	141.4	201.0
278.0	224.3	215.2	278.6	272.3	205.2

TABLE 6.9a Resilient Modulus Test Results: AU-14 at Temperature = 20°C

Load Duration = 0.1 seconds			Load Duration = 0.5 seconds		
Applied Stress		Resilient Modulus (MPa)	Applied Stress		Resilient Modulus (MPa)
σ_3 (kPa)	σ_d (kPa)		σ_3 (kPa)	σ_d (kPa)	
40.4	42.5	82.8	40.4	44.2	69.7
40.4	136.4	50.3	40.9	140.8	49.1
138.8	40.9	166.8	138.8	43.6	165.6
138.8	135.3	161.1	138.8	141.9	158.9
138.2	240.8	157.8	138.5	278.4	149.3
278.6	30.4	209.8	278.6	43.6	196.1
278.6	133.1	197.9	278.6	140.8	194.3
278.6	222.1	195.5	278.6	272.8	195.0

TABLE 6.9b Resilient Modulus Test Results: AU-14 at Temperature = 30°C

Load Duration = 0.1 seconds			Load Duration = 0.5 seconds		
Applied Stress		Resilient Modulus (MPa)	Applied Stress		Resilient Modulus (MPa)
σ_3 (kPa)	σ_d (kPa)		σ_3 (kPa)	σ_d (kPa)	
40.9	42.0	67.0	40.4	43.6	60.9
40.4	136.4	47.1	40.4	141.9	45.1
138.2	42.2	132.1	138.2	44.2	129.8
138.2	135.3	135.1	138.8	141.9	124.6
138.2	243.6	130.2	138.8	279.0	121.2
278.0	43.1	192.6	278.0	44.2	188.1
278.6	135.3	180.7	278.0	141.9	176.8
277.5	222.6	189.5	278.0	272.8	178.5

6.7 Effects of Stress States on Resilient Behavior

Based on the average values of resilient modulus at the two load durations (0.1 and 0.5 seconds), analyses were performed to characterize the three oil sand samples at the two test temperatures. Figures 6.12 through 6.14 show graphically the variations of resilient moduli of SE-09, SE-14 and AU-14 samples with the applied deviator stresses at each of the three confining pressure levels (41.4, 138, and 276 kPa) . At constant confining pressure, an increase in deviator stress resulted in little or no change in the resilient modulus values for all the three oil sands materials. Only the AU-14 sample at confining stress of 41.4 kPa shows a clear decrease in resilient modulus with increasing deviator stress. These general trends support the findings from the field that oil sand is a stress softening material (Joseph 2002). Also, these results verify the AASHTO T 307 preliminary tests performed on the SE-09 sample, which showed stress softening behavior of the material (section 3.4.3). As expected, resilient moduli generally increased with increasing confining stress for all the three oil sand materials.

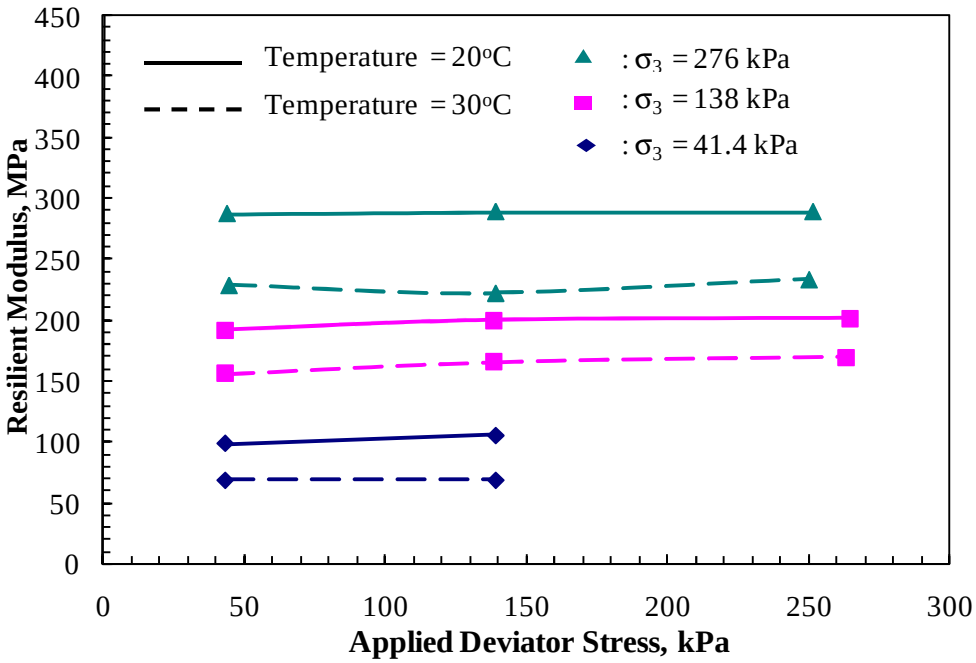

FIGURE 6.12 Variation of Resilient Modulus with Applied Deviator Stress at Two Test Temperatures for SE-09 Sample.

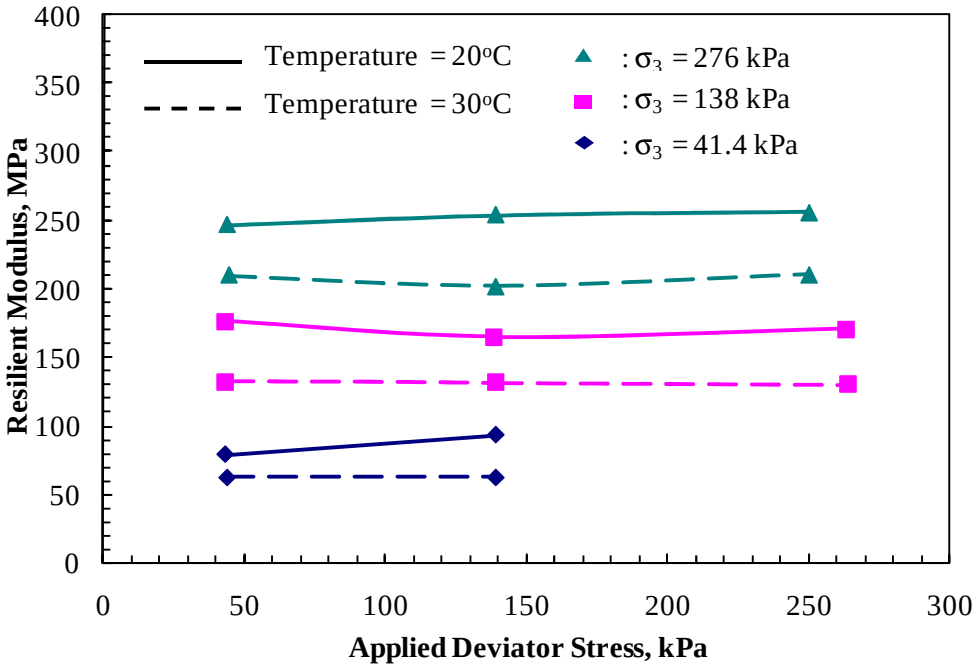

FIGURE 6.13 Variation of Resilient Modulus with Applied Deviator Stress at Two Test Temperatures for SE-14 Sample.

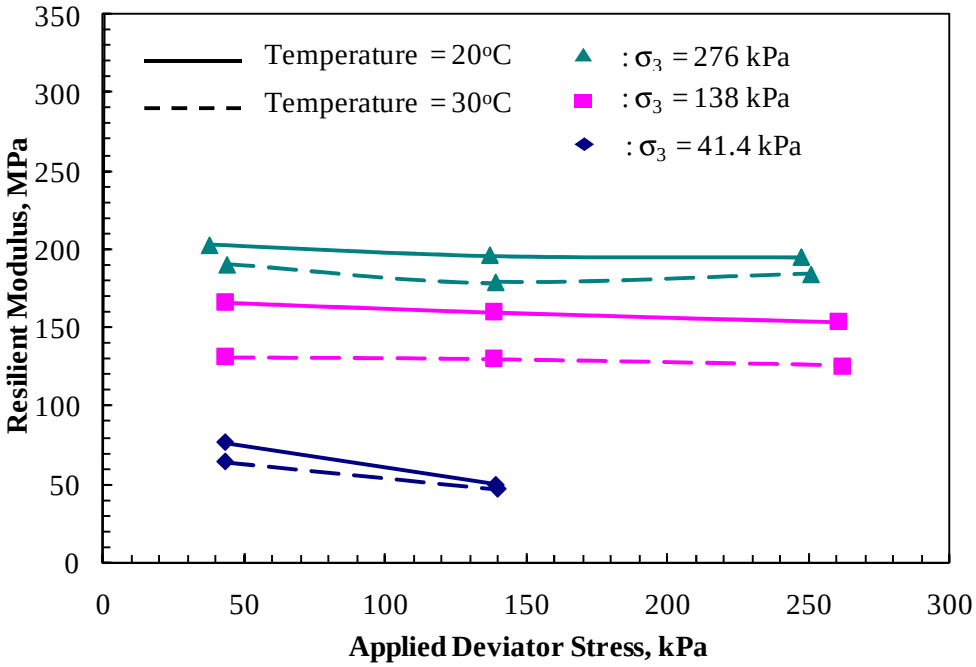

FIGURE 6.14 Variation of Resilient Modulus with Applied Deviator Stress at Two Test Temperatures for AU-14 Sample.

6.8 Resilient Modulus Model Development

Resilient modulus models, such as the Hicks and Monismith K-theta model (1971), Uzan model (1985), Witczak-Uzan universal model (1992), MEPDG model (NCHRP 1-37A, 2004) and Thompson and Robnett model (1979) consider the effects of stress dependency for modeling the nonlinear behavior of geomaterials. These models are commonly used to estimate the resilient modulus of soils and granular materials as a function of stress state, and handle very well the modulus or stiffness increase/decrease with increasing applied stresses in these geomaterials. The K-theta model considers the effects of bulk stress in axisymmetric analysis and the Witczak-Uzan universal and MEPDG models include an octahedral shear stress component instead of deviator stress, which makes them also applicable to three-dimensional finite element analysis. On the other hand, the bilinear or arithmetic model, (Thompson and Robnett 1979), and MEPDG model (NCHRP 1-37A, 2004) are used to characterize resilient behavior of fine-grained subgrade soils. In this study, the resilient responses of the oil sand samples were characterized by analyzing the characteristics of the regression model parameters of the K-theta, the universal, and the MEPDG models. It can be seen from Figures 6.11 to 6.13 that only the high stress regimes of the bilinear model (Thompson and Robnett 1979) were considered in the tests. Therefore, the bilinear model would not give complete behavior including those at lower stress states.

The nonlinear model parameters, k_1, k_2 and k_3 were determined by first, expressing the resilient modulus models in logarithmic relationships to transform the power functions into linear expressions having separate terms (Equations 6.4, 6.5, and 6.6). Multiple linear regression analyses were then performed to determine the model parameters, which were used to develop the resilient modulus prediction models for the three oil sand materials.

K-theta Model: $$\log M_R = \log k_1 + k_2 \log \theta \tag{6.4}$$

Universal Model: $$\log M_R = \log (k_1 \cdot P_a) + k_2 \log\left(\frac{\theta}{P_a}\right) + k_3 \log\left(\frac{\tau_{oct}}{P_a}\right) \tag{6.5}$$

MEPDG Model: $\log M_R = \log(k_1 \cdot P_a) + k_2 \log\left(\frac{\theta}{P_a}\right) + k_3 \log\left(\frac{\tau_{oct}}{P_a} + 1\right)$ (6.6)

where,

M_R = resilient modulus,

θ = bulk stress = $\sigma_1 + \sigma_2 + \sigma_3$,

σ_1 = major principal stress,

$\sigma_2 = \sigma_3$ for triaxial test on cylindrical specimen,

σ_3 = minor principal stress or confining stress in the triaxial cell

τ_{oct} = octahedral shear stress,

$$= \frac{1}{3}\sqrt{(\sigma_1 - \sigma_2)^2 + (\sigma_1 - \sigma_3)^2 + (\sigma_2 - \sigma_3)^2}$$

$$= \frac{\sqrt{2}}{3}(\sigma_1 - \sigma_3)$$ for cylindrical specimen in triaxial tests,

P_a = normalizing stress atmospheric pressure = 101.3 kPa (14.7 psi), and

k_1, k_2, k_3 = model parameters obtained from regression analyses.

Tables 6.10 to 6.12 show the overall summary of model parameters (k_i) obtained from the analyses of the different nonlinear resilient modulus models selected for the study. Strong correlations were obtained for the three models as observed in the R^2 values for all the three models. However, relatively low R^2 values ($R^2 < 0.9$) were observed for AU-14 oil sand sample in the K-theta model. The R-square values improved when both the Universal and MEPDG models were used for the analyses. The overall R^2 values were comparatively higher in the Universal model than the K-theta and the MEPDG models. Also, higher k_1 values were generally achieved at 20^{o}C compared with 30^{o}C. The model parameter k_1 is proportional to the elastic property of the materials, whereas k_2 and k_3 contribute to the terms that involve bulk stress and octahedral shear stress, respectively.

TABLE 6.10 Oil Sand Resilient Modulus Model Parameters of K-theta Model

Oil Sand ID	Temperature °C	Model Parameters		R^2	*RMSE*
		k_1 (MPa)	k_2		
SE-09	20	3.530	0.636	*0.952*	*0.041*
SE-09	30	1.483	0.733	*0.932*	*0.057*
SE-14	20	2.543	0.665	*0.945*	*0.046*
SE-14	30	1.374	0.723	*0.927*	*0.059*
AU-14	20	1.988	0.673	*0.752*	*0.112*
AU-14	30	1.380	0.709	*0.827*	*0.094*

TABLE 6.11 Oil Sand Resilient Modulus Model Parameters of the Universal Model

Oil Sand ID	Temperature °C	Model Parameters			R^2	*RMSE*
		k_1 (MPa)	k_2	k_3		
SE-09	20	0.550	0.694	-0.115	*0.986*	*0.023*
SE-09	30	0.353	0.800	-0.131	*0.964*	*0.043*
SE-14	20	0.448	0.726	-0.121	*0.980*	*0.029*
SE-14	30	0.294	0.807	-0.168	*0.982*	*0.030*
AU-14	20	0.318	0.773	-0.210	*0.842*	*0.093*
AU-14	30	0.254	0.821	-0.225	*0.918*	*0.067*

TABLE 6.12 Oil Sand Resilient Modulus Model Parameters of the MEPDG Model

Oil Sand ID	Temperature °C	Model Parameters			R^2	*RMSE*
		k_1 (MPa)	k_2	k_3		
SE-09	20	0.697	0.696	-0.348	*0.985*	*0.024*
SE-09	30	0.461	0.798	-0.376	*0.960*	*0.046*
SE-14	20	0.576	0.729	-0.375	*0.980*	*0.029*
SE-14	30	0.416	0.809	-0.502	*0.979*	*0.033*
AU-14	20	0.489	0.777	-0.628	*0.830*	*0.096*
AU-14	30	0.401	0.819	-0.645	*0.906*	*0.072*

The performances of the three models were further investigated at a selected temperature of 20^{o}C for the three oil sand samples. The results of measured and predicted resilient moduli are presented in Figures 6.15, through 6.17 for the SE-09, SE-14 and AU-14 samples. Overall, the K-theta model predicted resilient modulus quite well for all the three oil sand materials, especially the low grade oil sand material (SE-09). Also, the Universal model predicted resilient modulus better in SE-09 than SE-14 and AU-14 samples even though performances of the models were better in the SE-14 sample than in the AU-14 sample. The explanation to the relatively weak performances of the selected models is that they perform better with stress-hardening granular materials such as clean sands, gravels, and crushed limestone compared to the stress-softening oil sand materials. Recall that, at constant confining pressure, resilient moduli of all the oil sand materials were statistically the same when the applied deviator stress was increased. It is reasonable to suggest that the amount of bitumen in the oil sand materials affected the model predictions. However, since the properties of the bitumen in the three samples are not known, no firm conclusions can be established.

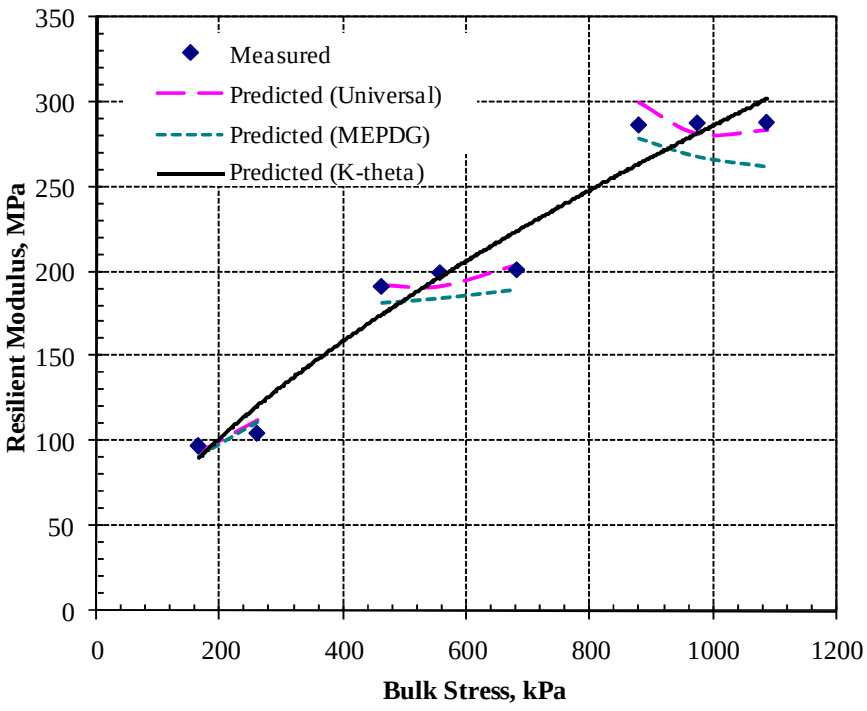

FIGURE 6.15 Performances of the SE-09 Oil sand Sample Resilient Modulus Models.

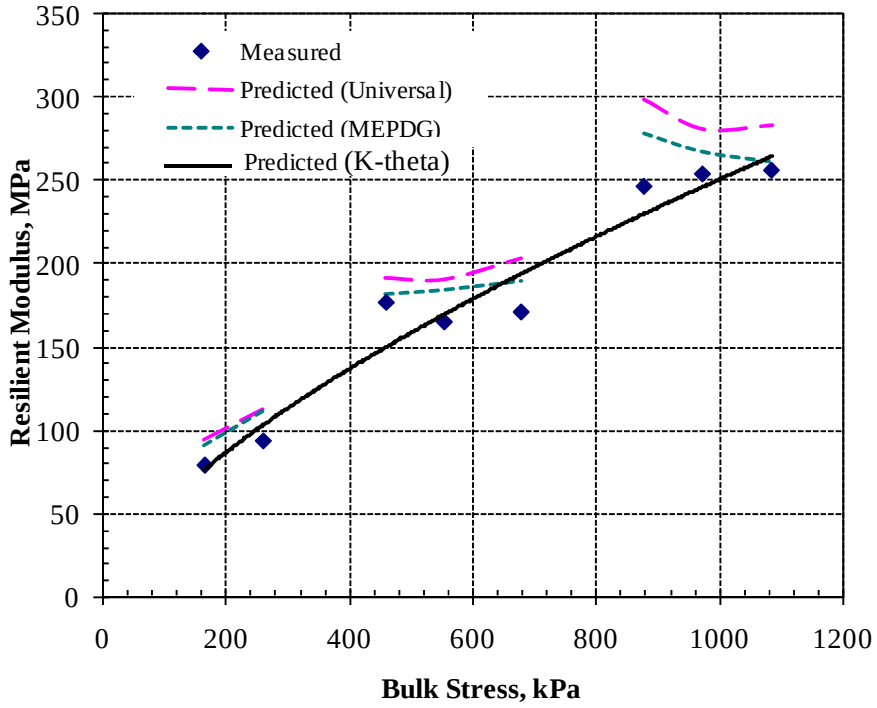

FIGURE 6.16 Performances of the SE-14 Oil sand Sample Resilient Modulus Models.

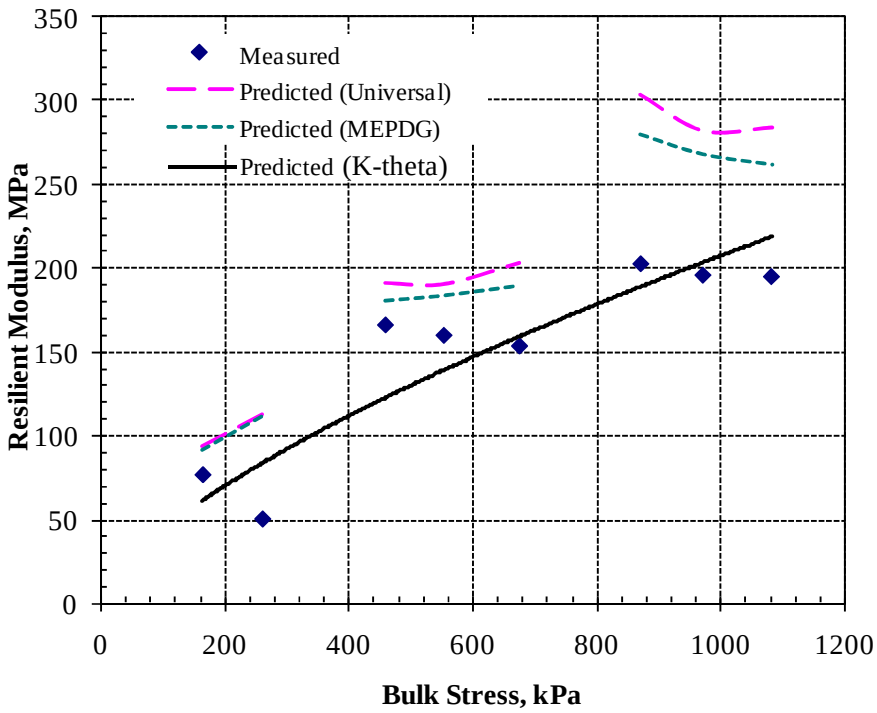

FIGURE 6.17 Performances of the AU-14 Oil sand Sample Resilient Modulus Models.

6.9 Summary

A newly developed repeated load triaxial test procedure was used to conduct tests on three types of oil sands with bitumen contents of 8.5%, 13.3% and 14.5% by weight at two temperatures and two load pulse durations. Results from the tests were used to develop phenomenological power models $\varepsilon_p = A*N^b$, for characterizing permanent strain accumulation in the oil sand materials. The statistical analyses showed that there was a strong correlation between model parameter A and the principal stress ratio (σ_1/σ_3), which could give the immediate sinkage at the first load application as function of the applied stress states/ratios. Using additional replicate test data, it was demonstrated that the developed permanent deformation models could reasonably predict permanent strain accumulations in the oil sand materials. When all the test data from the three oil sands were combined, unified permanent deformation models were successfully developed to account for applied principal stress states/ratios, temperature, bitumen content and oil sand gradation properties. In addition, the unified models were modified to include shear stress ratio to properly study the effect of shear strength in the field. Overall, the developed permanent deformation models can provide essential guidelines and practical predictive equations for estimating field sinkage and rutting potentials of oil sand materials under off-road haul trucks, shovels and other mining equipment.

The test results were also used to develop the parameters for the K-theta, the universal and the MEPDG models to characterize the resilient modulus behavior of the oil sand materials. Good model predictions of resilient modulus value in the low grade SE-09 sample did not result in favorable results for the high grade SE-14 and AU-14 samples.

The following conclusions can be derived from analyzing the test data:

1. The applied stress states have significant influence on permanent deformation accumulation in the three oil sand materials. As the deviator stress increased both the magnitude and the accumulation rate of the permanent deformation increased in all the three oil sand materials. Also, permanent strain accumulation rates generally decreased as the magnitude of the confining pressure increased. The accumulation of the permanent strains becomes higher as the confinement levels decreased and the applied principal stress ratios (σ_1/σ_3) increased. This implies

that permanent strains accumulated in the oil sand materials relate directly to deviator stress and inversely to confining pressure as reported by Morgan (1966) for granular materials.

2. Bitumen content, test temperature, and load pulse duration, all influenced permanent strain accumulation in the oil sand materials. At the same stress ratios, higher permanent deformation accumulations were observed in the high grades AU-14 and SE-14 samples than low grade SE-09 sample. Higher permanent deformations were also accumulated at 30^{o}C and load pulse duration of 0.5 seconds compared to the results at 20^{o}C and 0.1 second load pulse duration.
3. Resilient modulus increased with increasing confining pressure in all the oil sand samples. However, there was no significant effect of deviator stress on resilient modulus. The behavior of the oil sand samples appeared stress softening, especially in the high grade AU-14 sample in which resilient modulus generally decreased with increasing deviator stress. The resilient moduli of the three oil sand materials were generally higher at 20^{o}C than at 30^{o}C. This behavior is also observed in most bituminous materials in which stiffness gets higher at lower temperatures compared to high temperatures. There was statistically little or no significant difference between resilient modulus values at load pulse duration of 0.1 and 0.5 seconds. The was found to be in agreement with other researchers who reported that loading frequency or pulse duration had little or no effect on the resilient modulus of granular materials.
4. The K-theta model appears to give better predictions of resilient modulus for all the three oil sand materials. In addition to the K-theta model, only the universal model gave good prediction of resilient modulus for the low grade SE-09 oil sand material.

CHAPTER 7 SHEAR MODULUS OF FINE-GRAINED COHESIVE SOIL AND OIL SAND MATERIALS

7.1 Introduction

Shear modulus governs shear deformation characteristics by the extent of distortion in soils and other geomaterials under applied loads. Cyclic triaxial test has been the most commonly used one for measuring shear modulus in the laboratory. In this test, the radial stress is typically held constant while deviator stress is applied cyclically on the sample. The shear modulus obtained from the cyclic tests is evaluated from modulus of elasticity by assuming a representative Poisson's ratio for the soil. Results from cyclic triaxial tests have been mainly used to develop several empirical correlations of modulus and shear strain for soils. The most realistic shear loading, however, occurs when both varying confining and dynamic stresses are applied simultaneously on the sample. Obtaining such a loading condition in the laboratory would enable close simulation of the roll and bounce and rocking motions of construction and mining trucks and shovels in the field.

This chapter investigates the shear modulus characteristics of the fine-grained cohesive soil and three oil sand materials in the laboratory using a newly developed pure shear test procedure. The developed pure shear test procedure applies varying confining and dynamic stresses simultaneously on the specimen to determine shear modulus. Conventional type cyclic triaxial tests are also conducted on the oil sand samples to compare test results with the results obtained from the pure shear test procedures. The results of both tests are used to develop characterization models to correlate shear modulus with factors affecting field loading conditions. In addition to shear modulus, phase angles of the tested materials are also obtained from the test data.

7.2 Laboratory Testing

Pure shear tests were performed on the soil and three oil sand samples using Procedure D described in detail under section 3.5.8. In addition, cyclic tests were performed on the oil sand materials using the standard ASTM D3999 test procedure for determining shear modulus of soils using cyclic triaxial apparatus.

Specimens of the soil and oil sand samples were prepared in accordance with the sample preparation methods described in section 3.5.4. The laboratory testing involved applying varying frequencies of continuous sinusoidal load to the test specimen, and measuring shear stress and shear strain responses to directly obtain shear modulus properties. Table 7.1 summarizes the test program and testing conditions used to perform the pure shear tests. The cyclic triaxial tests were only performed at selected loading frequency of 2Hz and temperature of 20^{o}C for comparison purposes.

The UI-FastCell test setup was used to apply stresses on the soil specimens, and the RaTT cell setup was used for testing the oil sand specimens. The RaTT cell was specifically selected for the oil sand testing because of its temperature chamber and temperature transducer required for testing bituminous materials. A full factorial test matrix comprising 27 tests were conducted for the soil sample at three moisture states and one loading frequency. For the three oil sand samples, a total of 108 tests were conducted at two test temperatures and two loading frequencies.

TABLE 7.1 Shear Modulus Test Program and Loading Conditions

Soil Tests	
Sample ID	: CAT A-6
Loading Frequency (f)	: 5Hz
Test Temperature (T)	: 22^{o}C (room temperature)
Confining Stress (σ_3)	: 41.4, 69 and 138 kPa
Cyclic Stress (τ_{cyc})	: 20.7, 41.4, 69 and 138 kPa
Water Content (w)	: w = 11.3%, 14.3% and 17.3%.
Oil Sand Tests	
Sample ID	: SE-09, SE-14 and AU-14
Loading Frequency (f)	: 2 and 10Hz
Test Temperature (T)	: 20 and 30^{o}C
Confining Stress (σ_3)	: 41.4, 69, and 138 kPa
Cyclic Stress (τ_{cyc})	: 20.7, 41.4, 69 and 138 kPa
Bitumen content (w_b)	: w_b = 8.5% (SE-09); w_b = 13.3% (SE-14) and w_b = 14.5% (AU-14)

7.3 Test Data Analyses

The raw test data obtained included applied axial and confining stresses, and the measured specimen axial and radial strains. The applied shear stress and corresponding shear strain were computed from Equations 3.5a and 3.5b, and the shear modulus was computed from Equation 3.6.

To obtain the maximum shear stress and shear strain values, a generalized mathematical curve fit function given in Equation 3.8 was used to fit the sinusoidal loading test data obtained from the tests. Figures 7.1a and 7.1b are two typical plots of the raw test data. The figures represent typical test results for an oil sand sample at a loading frequency of 2Hz and 5 load cycles. In these figures shear stress and the corresponding shear strain are graphed with elapse time. The curve fit function presented in Equation 3.8, was used to perform least squared error regression analysis with Microsoft Excel Solver to calculate the amplitude of the sinusoidal pulse (Equation 3.9a) that represents peak (maximum) shear stress and strain. The parameters for computing the amplitude of the shear stress and shear strain curves were also used to determine phase angle of the samples (Equation 3.7c).

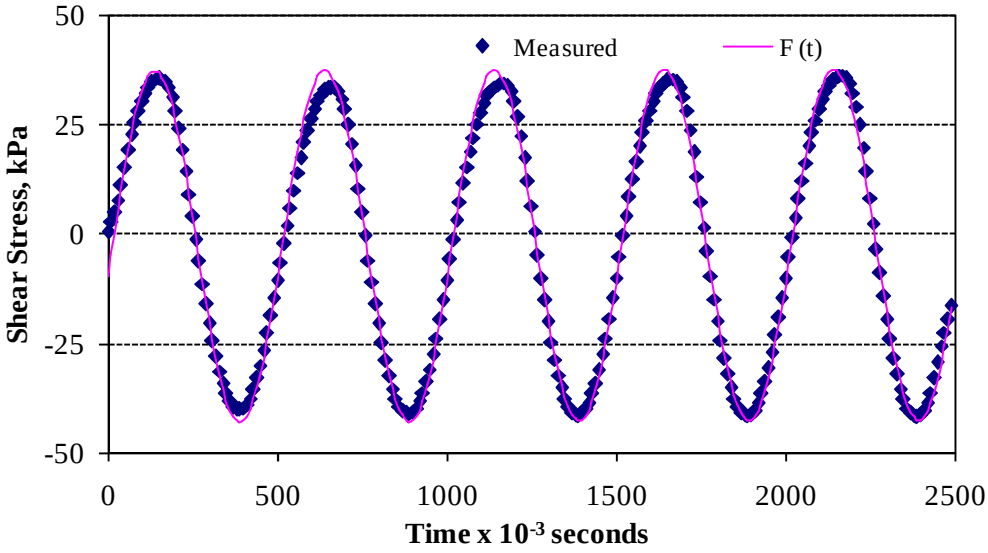

(a)

FIGURE 7.1a Raw Test Data for One Oil Sand Sample at 2Hz Frequency and 5 Load Cycles: (a) Shear Stress; (b) Shear Strain.

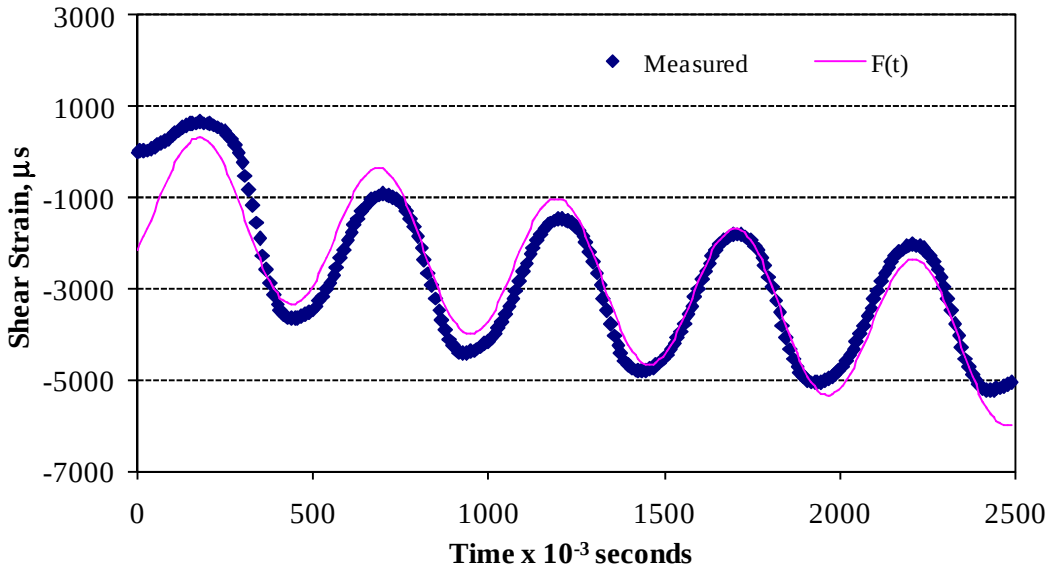

(b)

FIGURE 7.1b Raw Test Data for One Oil Sand Sample at 2Hz Frequency and 5 Load Cycles: (a) Shear Stress; (b) Shear Strain.

7.4 Analyses of Laboratory Test Results

7.4.1 Analyses of Fine-Grained Soil Test Results

The CAT A-6 soil test data were analyzed to obtain shear modulus and phase angle at the optimum water content (w_{opt} = 14.3%), and dry of optimum (w = 11.3%) and wet of optimum (w = 17.3%) moisture states. A single data set contains 250 stress-strain data points for one specimen. A total of 2,250 set of data points from 9 tests was obtained for the soil sample at each moisture state.

Table 7.2 lists a summary of the soil test results at the three moisture states. The shear modulus values at w = 17.3% are extremely low compared with the values at w = 11.3% and 14.3%. An average shear modulus measured at the optimum was found to be about 8 times the shear modulus at the wet of optimum moisture state. Also, the average shear modulus at dry of optimum moisture state is about 3.5 times the shear modulus at the optimum. Thus, a change in water content of 3% above or below the optimum resulted in a significant change in shear modulus of the soil sample. The shear modulus properties decrease with increasing applied cyclic stresses (see Table 7.2).

This trend was expected of CAT A-6 soil sample since fine-grained cohesive soils exhibit stress softening behavior under cyclic loading. Generally, the phase angle was lower at dry of optimum and higher at wet of optimum. At constant confining stress, the phase angle was found to increase with increasing cyclic stress.

TABLE 7.2 Stress States and Test Results for CAT A-6 Soil at Different Moisture States

Stress States (kPa)		Shear Modulus (MPa)			Phase Angle (Deg)		
σ_3	τ_{cyc}	w = 11.3%	w_{opt} = 14.3%	w = 17.3%	w = 11.3%	w_{opt} = 14.3%	w = 17.3%
40.4	20.7	118.3	50.5	7.5	13.8	21.4	31.4
40.4	40.4	91.9	23.0	4.2	14.5	24.2	32.1
69.0	20.7	145.3	62.3	9.0	15.6	22.1	38.2
69.0	40.4	106.6	30.3	4.9	16.9	22.6	43.8
69.0	69.0	64.4	14.4	5.2	17.5	23.1	45.5
138.0	20.7	273.9	166.6	23.1	11.3	17.2	31.4
138.0	40.4	221.5	112.1	10.1	12.0	21.3	37.7
138.0	69.0	173.1	69.6	7.1	13.8	22.2	41.3
138.0	138.0	89.0	24.0	7.2	16.9	25.0	56.7

7.4.1.1 Variation of Shear Modulus of CAT A-6 soil with Shear Strain

Figures 7.2 to 7.4 show variations of shear modulus properties with shear strains at different confining pressures for CAT A-6 soil at the three different water contents. Shear modulus typically decreases with increasing shear strain. At low shear strains, the shear modulus is extremely high compared to the low values at high strains. Also, the shear moduli generally decrease as the confining stresses decrease. A rapid decrease in shear modulus is observed at the high confining stress (σ_3 = 138 kPa) compared with the lower confining stresses. This behavior was observed at all the moisture states. This is an indication that high confining stresses significantly affect on shear modulus of the soil sample at various moisture levels.

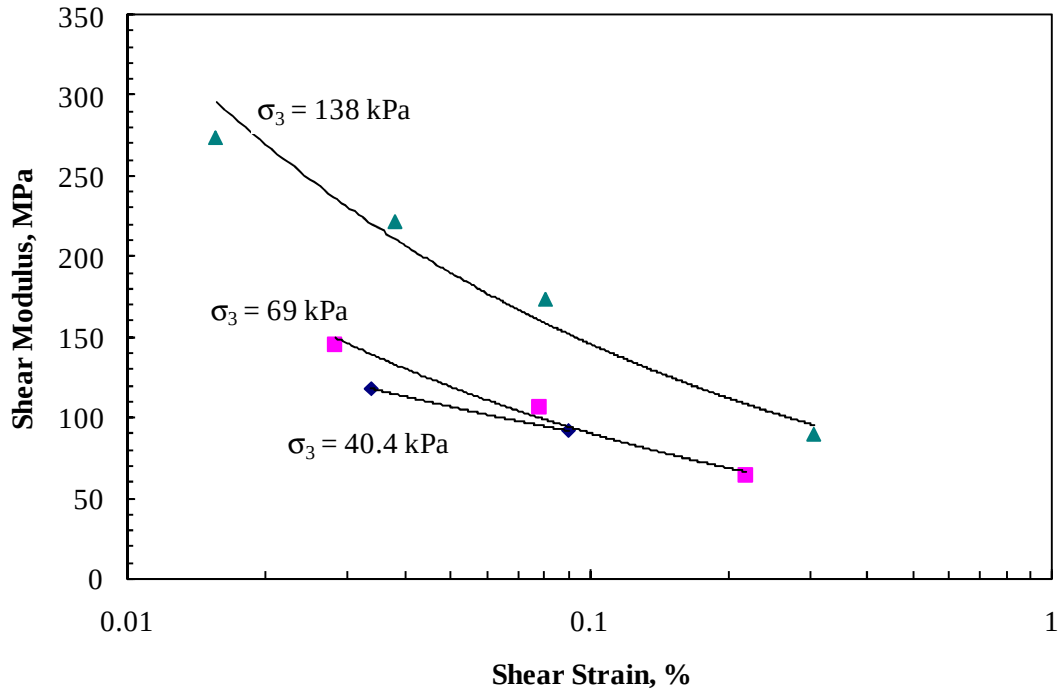

FIGURE 7.2 Variation of Shear Modulus with Shear Strain: CAT A-6 Soil at w = 11.3%.

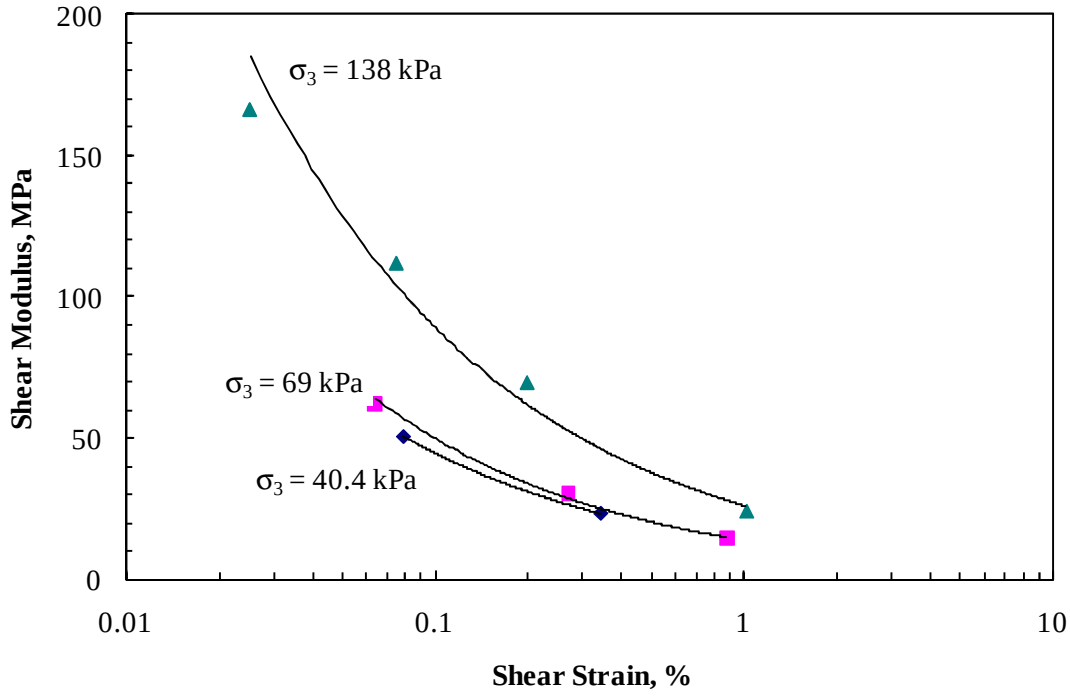

FIGURE 7.3 Variation of Shear Modulus with Shear Strain: CAT A-6 Soil at w_{opt} = 14.3%.

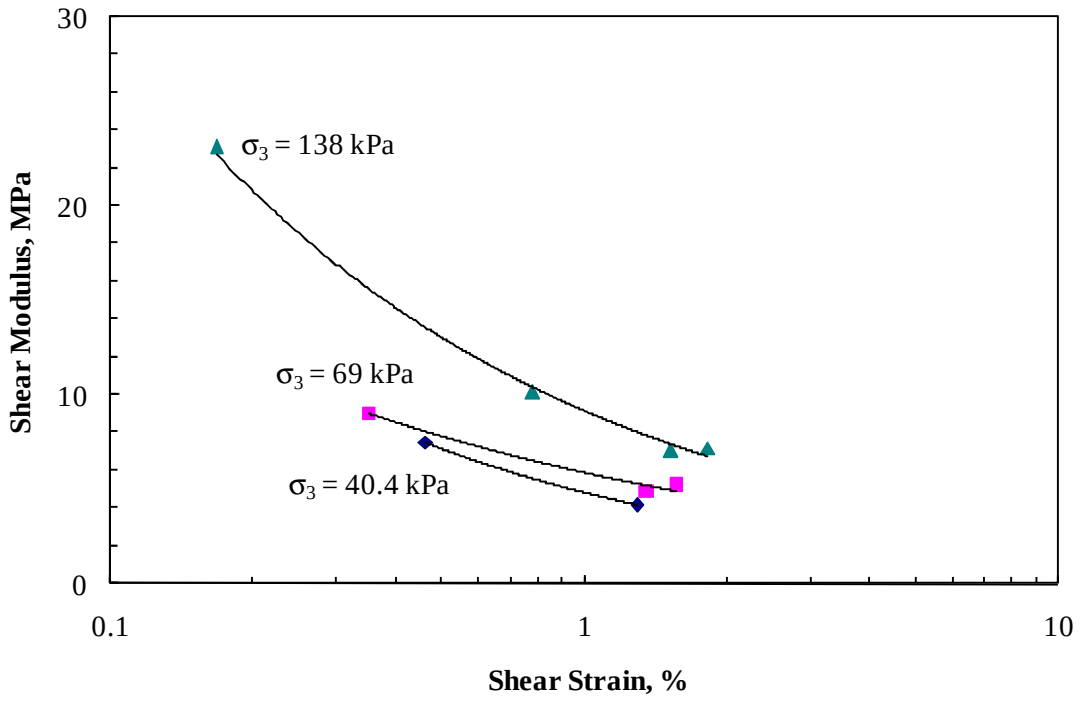

FIGURE 7.4 Variation of Shear Modulus with Shear Strain: CAT A-6 Soil at w = 17.3%.

7.4.2 Characterization of Pure Shear Modulus of CAT A-6 Soil

The maximum shear modulus G_{max} and the shear modulus ratio G/G_{max} or normalized shear modulus have generally been used to characterize the shear deformation characteristics at different strain levels (Hardin and black 1968, Seed and Idriss 1970, Kramer and 1996). At low strain levels below 0.001%, it is assumed that the soil shear modulus is equal to G_{max}, i.e., G/G_{max} is equal to one. In this study, the shear modulus reduction concept is used to characterize the soil material at the three moisture states. Several empirical equations have been proposed to compute of G_{max} of soils. However, these equations are based on strain levels less than 0.001%.

Assuming that the minimum shear strain is a good approximation for obtaining the maximum shear modulus from the test data, the maximum shear modulus G' obtained among all soil pure shear tests was used to normalize the shear moduli of the CAT A-6 soil sample at the various moisture states (G' = 273.9 MPa). Based on this approach, regression analyses were performed to develop relationships between the

normalized shear modulus and shear strain (γ). Figure 7.5 is a plot of normalized shear modulus against shear strain, and Equations 7.1 to 7.3 are empirical equations developed for the soil sample at the three moisture states. As seen from the graph, there is a large scatter of the results at w = 17.3%, although the R^2 value is comparable to the R^2 value at w = 11%. As expected, there is a general trend of shear modulus reduction as the shear strain increases at all the moisture states of the soil. Also, according to Equations 7.1 to 7.3, G/G' at all the three moisture states always decreases as γ increases.

$$\frac{G}{G'_{dry}} = 0.1646\,\gamma^{-0.3869} \text{ at w = 11.3\%:} \quad R^2 = 0.65 \tag{7.1}$$

$$\frac{G}{G'_{opt}} = 0.1015\,\gamma^{-0.5811} \text{ at w = 14.3\%:} \quad R^2 = 0.82 \tag{7.2}$$

$$\frac{G}{G'_{wet}} = 0.2976\,\gamma^{-0.5015} \text{ at w = 17.3\%:} \quad R^2 = 0.67 \tag{7.3}$$

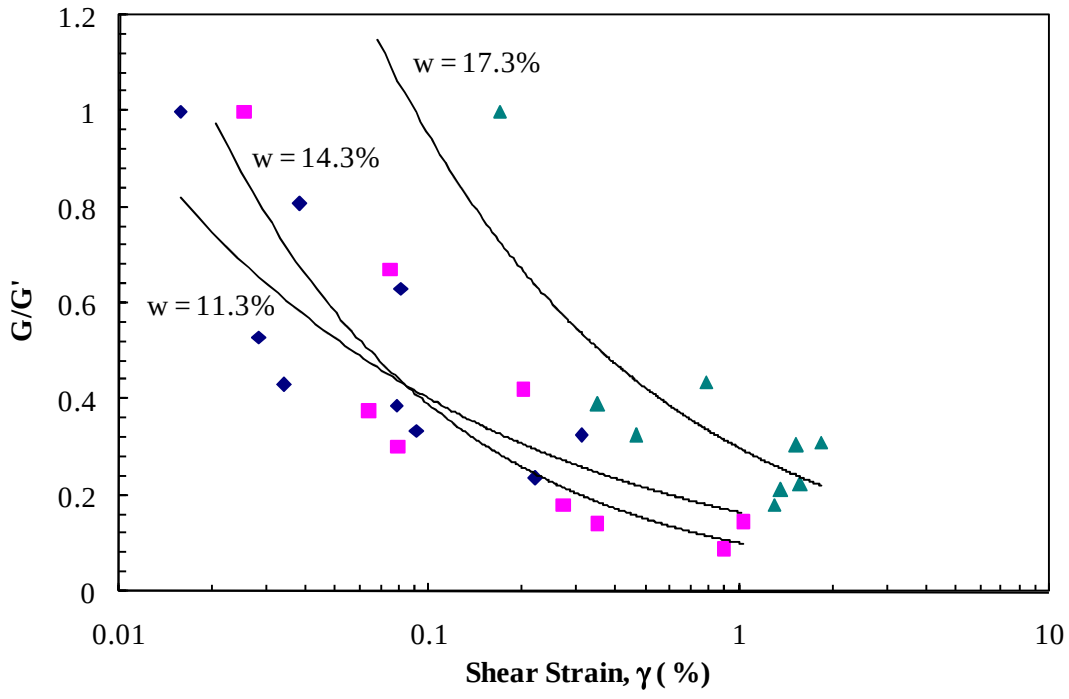

FIGURE 7.5 Normalized Shear Modulus against Shear Strain for CAT A-6 Soil.

7.4.3 Analyses of Oil Sand Test Results

The raw data obtained from the pure shear tests conducted on each oil sand sample generated about 4,500 data points at two loading frequencies at one test temperatures. Therefore, for the two test temperatures, a total of 9,000 data points obtained from the test matrix were used to analyze the properties of each oil sand sample. The analysis results include shear modulus and phase angle properties and the characterization models developed to describe the behavior of the oil sand materials. Tables 7.3 and 7.4 summarize the test results for SE-09, SE-14 and AU-14 oil sand samples at the two loading frequencies and two test temperatures. The shear moduli of SE-09 samples are generally higher than those of SE-14 and AU-14 samples at all the loading conditions. There is no significant difference between the shear modulus values of SE-14 and AU-14 although the shear moduli for SE-14 are generally higher than those of AU-14 samples. On the other hand, the phase angles of AU-14 and SE-14 samples are the highest and the phase angle of the SE-09 sample is the lowest.

Comparisons of the test results in these tables show that shear modulus is generally lower at 30^{o}C than at 20^{o}C for all the oil sand samples. Also, shear moduli were found to be lower at 2Hz than at10Hz for all the oil sand samples. The analyses of the test results show the average shear modulus at 20^{o}C was about 1.5 to 2 times of the shear modulus at 30^{o}C for the oil sand samples tested at the two loading frequencies. On the other hand, average shear modulus at 10Hz was about 2 to 3 times of the shear modulus at 2Hz for all the oil sand samples tested at the two test temperatures. Thus, the effect of reducing loading frequency is similar to the effect of increasing the test temperature. This behavior is typically observed for bituminous materials, in which stiffness increases at low temperatures and decreases at low frequencies. As listed in Tables 7.2 and 7.3, the shear moduli decrease with increasing applied cyclic stresses. This observation also supports the stress-softening behavior reported earlier in Chapter 6 for the oil sand samples.

TABLE 7.3a Stress States and Test Results for Oil Sand Samples at 10Hz and 20°C

Stress States (kPa)		Shear Modulus (MPa)			Phase Angle (Deg)		
σ_3	τ_{cyc}	SE-09	SE-14	AU-14	SE-09	SE-14	AU-14
40.4	20.7	86.2	51.2	37.3	31.7	34.8	44.7
40.4	40.4	63.3	47.7	35.6	39.2	41.8	47.5
69.0	20.7	158.1	116.4	89.3	29.7	31.4	37.3
69.0	40.4	99.1	74.0	60.6	36.6	40.1	46.4
69.0	69.0	77.4	68.9	54.2	42.2	44.3	51.8
138.0	20.7	298.0	222.5	214.5	20.7	25.3	22.4
138.0	40.4	212.5	133.2	121.5	26.7	30.2	34.2
138.0	69.0	170.9	119.1	108.0	34.1	37.6	42.7
138.0	138.0	104.8	95.5	91.8	37.8	43.3	50.6

TABLE 7.3b Stress States and Test Results for Oil Sand Samples at 10Hz and 30°C

Stress States (kPa)		Shear Modulus (MPa)			Phase Angle (Deg)		
σ_3	τ_{cyc}	SE-09	SE-14	AU-14	SE-09	SE-14	AU-14
40.4	20.7	50.7	38.0	16.7	28.8	33.2	42.6
40.4	40.4	28.2	27.8	15.6	37.9	38.4	47.5
69.0	20.7	102.2	74.7	54.0	25.7	28.2	33.5
69.0	40.4	52.2	43.1	31.3	33.0	35.6	43.3
69.0	69.0	31.5	34.3	24.5	36.4	36.6	46.1
138.0	20.7	272.4	194.6	163.1	20.2	18.7	25.4
138.0	40.4	167.5	112.8	74.4	24.3	27.8	36.8
138.0	69.0	111.0	80.3	49.1	30.4	36.7	42.8
138.0	138.0	48.6	49.9	32.3	40.4	41.5	44.7

TABLE 7.4a Stress States and Test Results for Oil Sand Samples at 2Hz and 20°C

Stress States (kPa)		Shear Modulus (MPa)			Phase Angle (Deg)		
σ_3	τ_{cyc}	SE-09	SE-14	AU-14	SE-09	SE-14	AU-14
40.4	20.7	41.6	15.8	15.9	31.4	32.3	47.7
40.4	40.4	20.7	10.5	8.4	37.2	35.9	52.3
69.0	20.7	94.4	53.2	40.5	28.8	32.0	38.8
69.0	40.4	34.2	23.7	20.3	34.8	35.0	45.4
69.0	69.0	22.9	17.8	16.2	41.9	41.3	48.9
138.0	20.7	232.5	158.8	128.7	23.5	23.6	20.6
138.0	40.4	131.7	66.1	61.4	31.2	32.0	42.3
138.0	69.0	62.7	38.9	36.6	37.5	41.1	45.2
138.0	138.0	39.7	30.6	24.9	49.6	58.4	58.7

TABLE 7.4b Stress States and Test Results for Oil Sand Samples at 2Hz and 30°C

Stress States (kPa)		Shear Modulus (MPa)			Phase Angle (Deg)		
σ_3	τ_{cyc}	SE-09	SE-14	AU-14	SE-09	SE-14	AU-14
40.4	20.7	23.4	14.5	7.3	29.8	31.5	30.9
40.4	40.4	11.0	10.0	6.8	33.6	31.8	32.2
69.0	20.7	72.7	39.5	23.1	24.3	28.7	33.7
69.0	40.4	21.6	15.4	11.7	33.0	32.7	36.2
69.0	69.0	15.8	13.0	9.9	40.3	37.4	37.0
138.0	20.7	219.6	129.5	124.6	22.8	20.1	18.8
138.0	40.4	116.4	56.9	34.9	28.2	30.7	33.5
138.0	69.0	41.8	28.0	24.6	35.8	38.1	40.6
138.0	138.0	25.7	22.1	19.3	37.3	49.3	41.2

7.4.3.1 Variation of Shear Modulus with Shear Strain

Figures 7.6 through 7.8 show the variations of shear moduli with shear strains measured at different confining pressures for the oil sand samples. In general, the shear modulus decreases as shear strain increases. At high confining stress (σ_3 = 138 kPa), the reduction in shear modulus is very rapid compared to the shear modulus reduction at the

low confining stress σ_3 = 40.4 kPa. Similar trends are observed for all the oil sand materials tested at different temperatures and different loading frequencies. A close observation at the modulus reduction curves shows that there is no significant modulus reduction when the shear modulus is less than 50 MPa. All of these trends occur at σ_3 = 40.4 kPa (low confining stress). Particularly, at 30°C the modulus reduction curves for all the samples at σ_3 = 40.4 kPa are almost flat or no change in shear modulus values occur with increasing shear strains. Thus, confining stress has considerable impact on the relationship between shear modulus and shear strain. The modulus reduction at the confining stress of 69 kPa appears to follow the same pattern for the three oil sand samples at all the loading conditions.

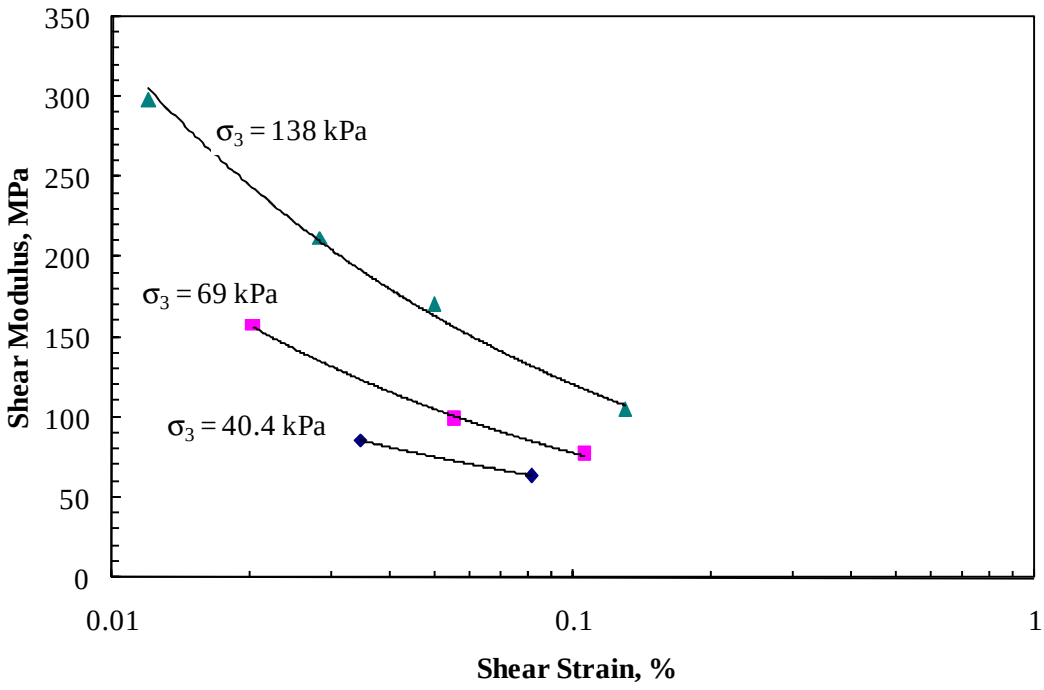

FIGURE 7.6a Variation of Shear Modulus with Shear Strain: SE-09 at 10Hz and 20°C.

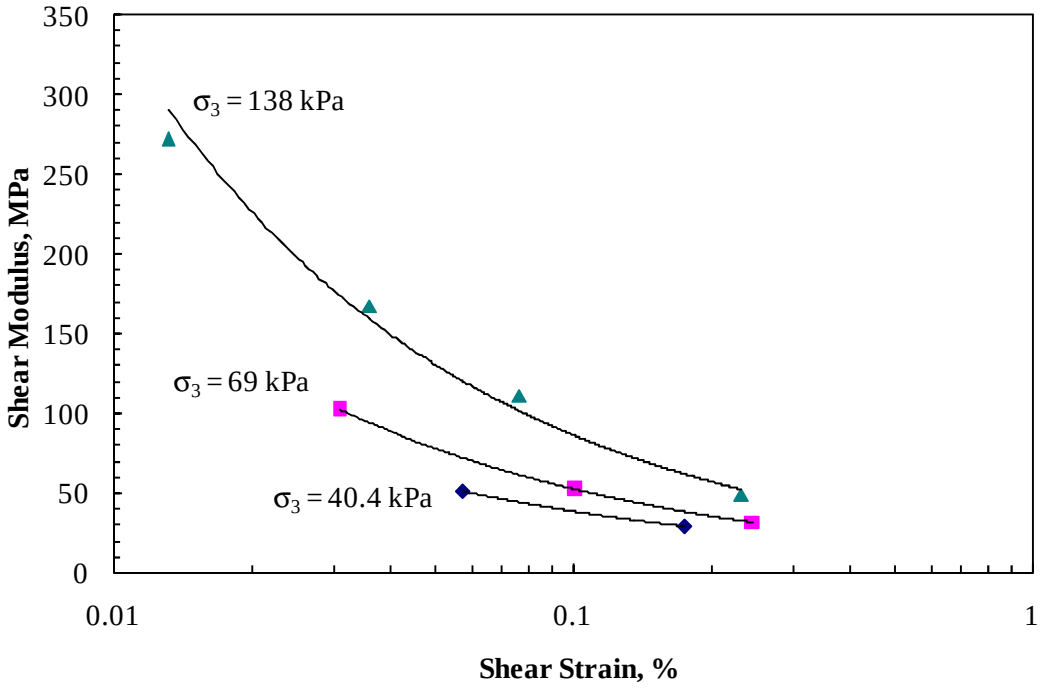

FIGURE 7.6b Variation of Shear Modulus with Shear Strain: SE-09 at 10Hz and 30°C.

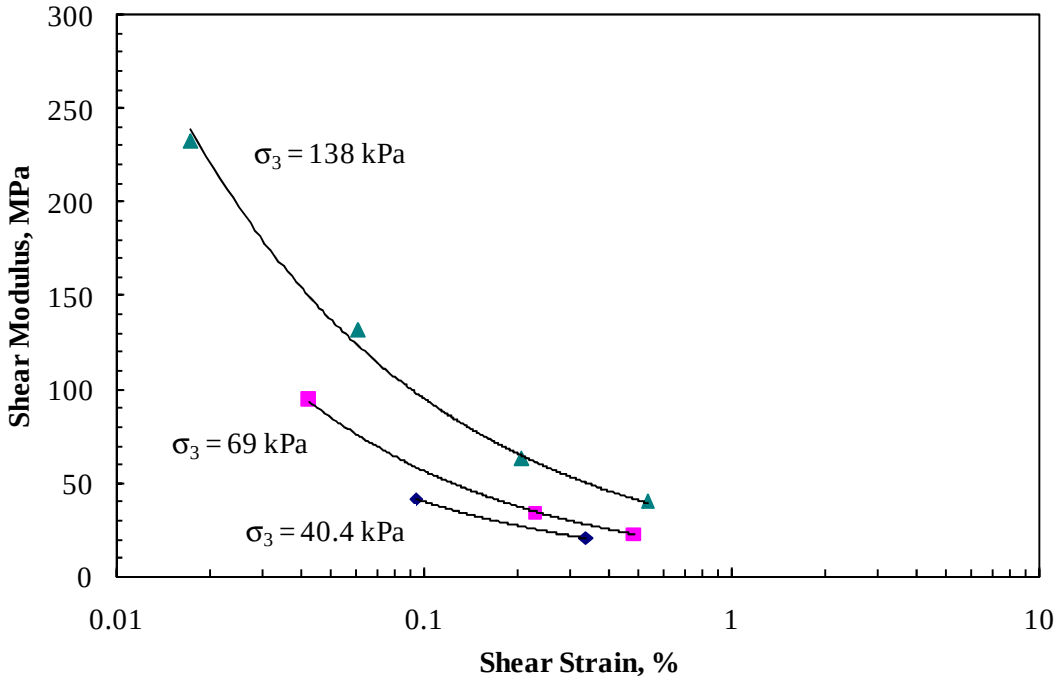

FIGURE 7.6c Variation of Shear Modulus with Shear Strain: SE-09 at 2Hz and 20°C.

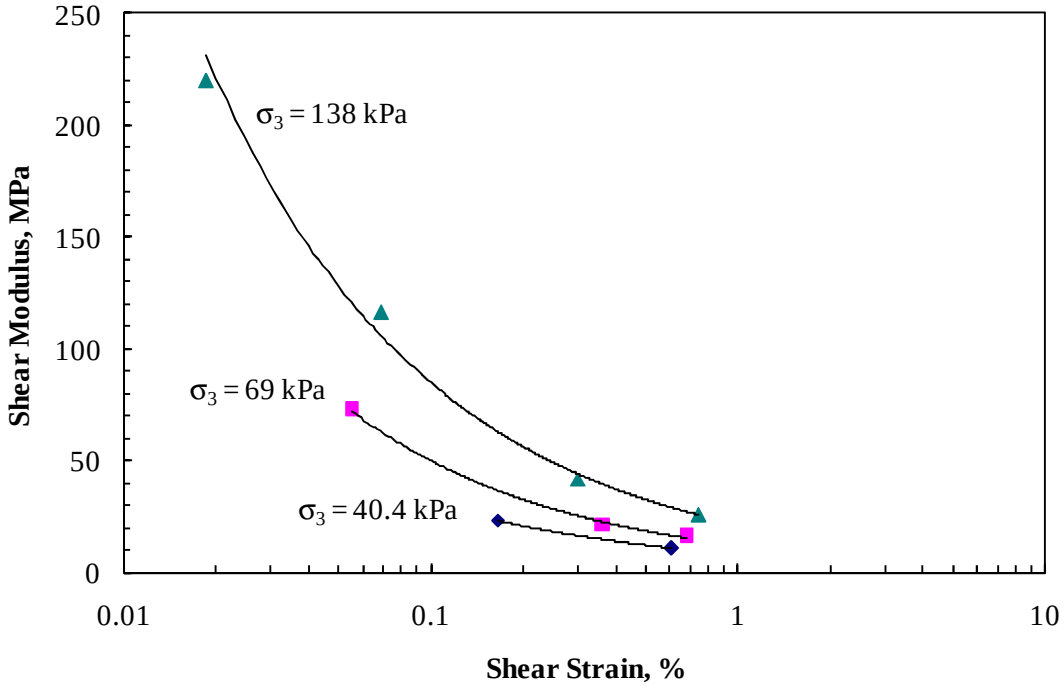

FIGURE 7.6d Variation of Shear Modulus with Shear Strain: SE-09 at 2Hz and 30°C.

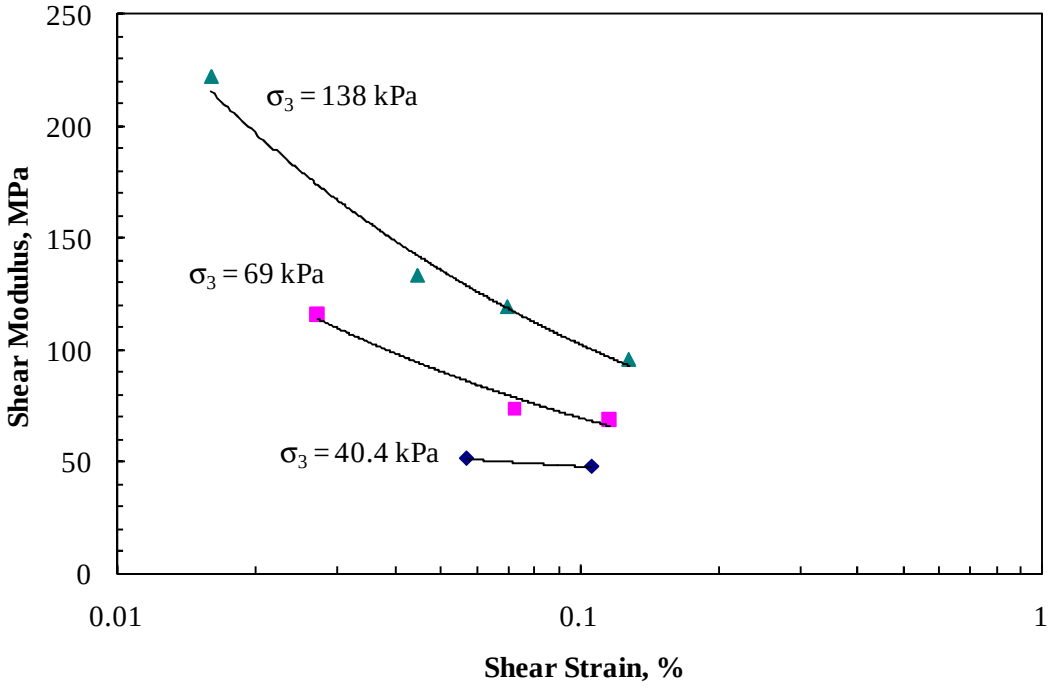

FIGURE 7.7a Variation of Shear Modulus with Shear Strain: SE-14 at 10Hz and 20°C.

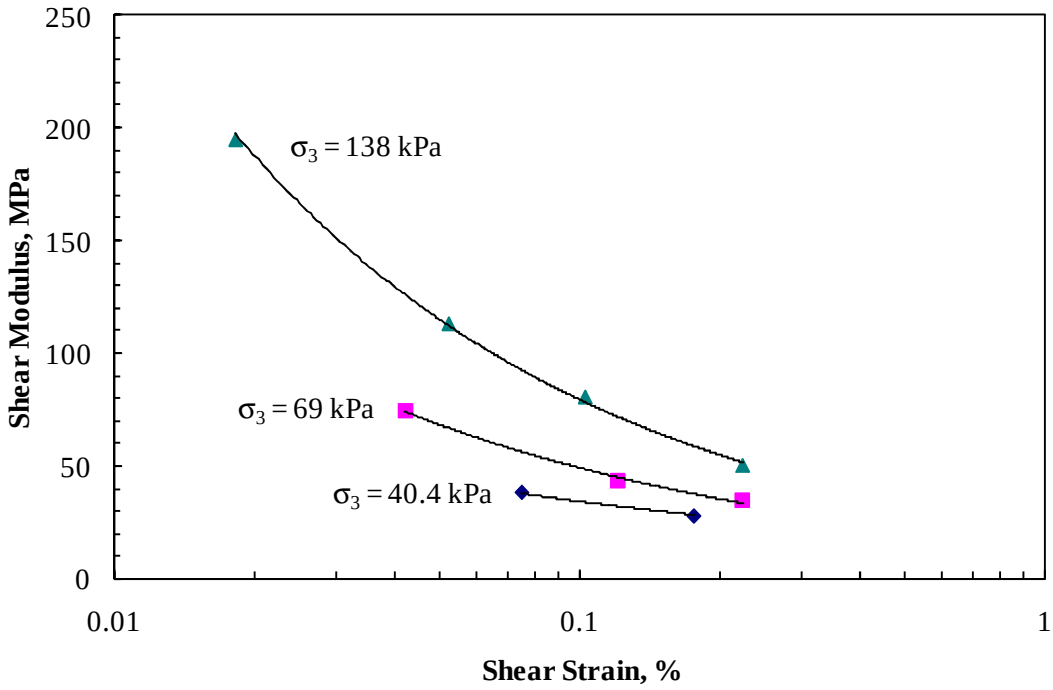

FIGURE 7.7b Variation of Shear Modulus with Shear Strain: SE-14 at 10Hz and 30°C.

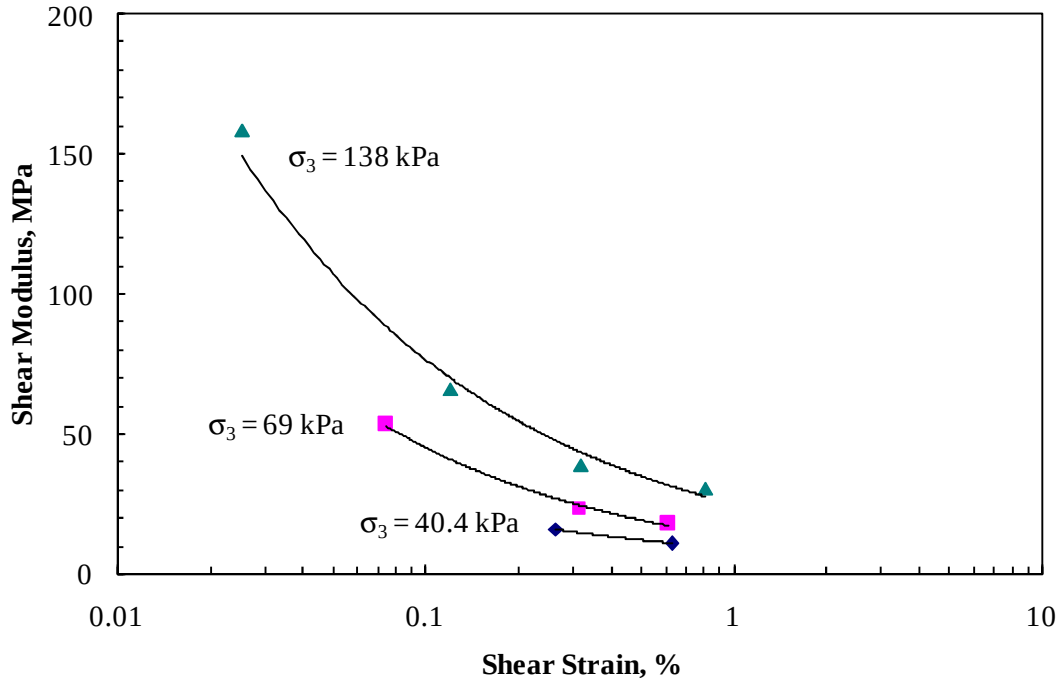

FIGURE 7.7c Variation of Shear Modulus with Shear Strain: SE-14 at 2Hz and 20°C.

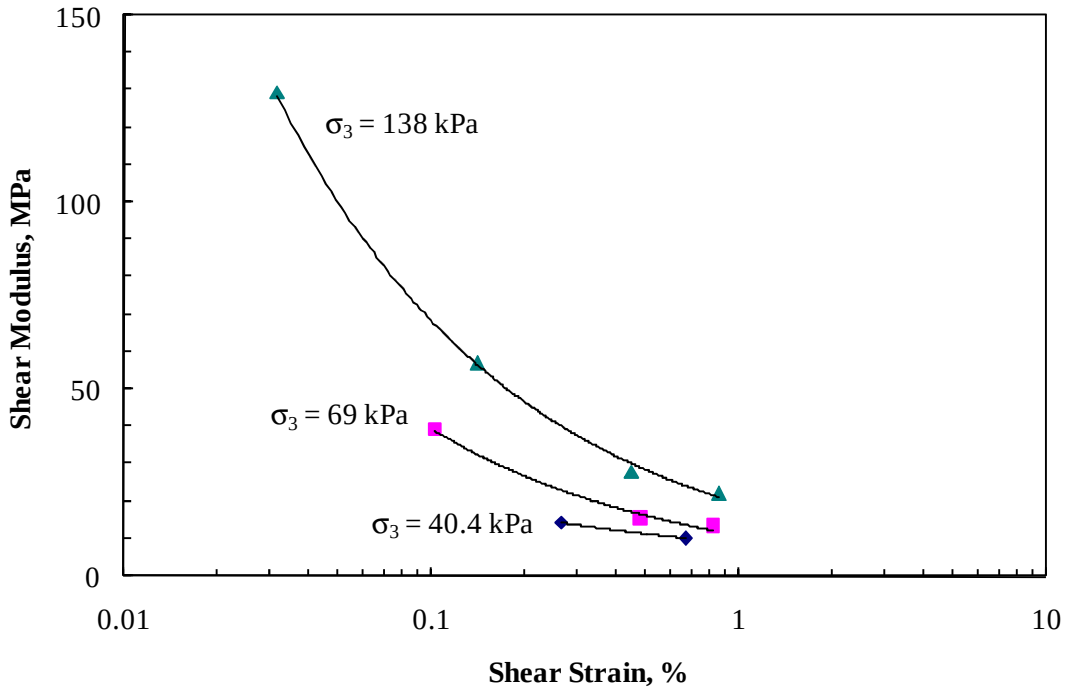

FIGURE 7.7d Variation of Shear Modulus with Shear Strain: SE-14 at 2Hz and 30°C.

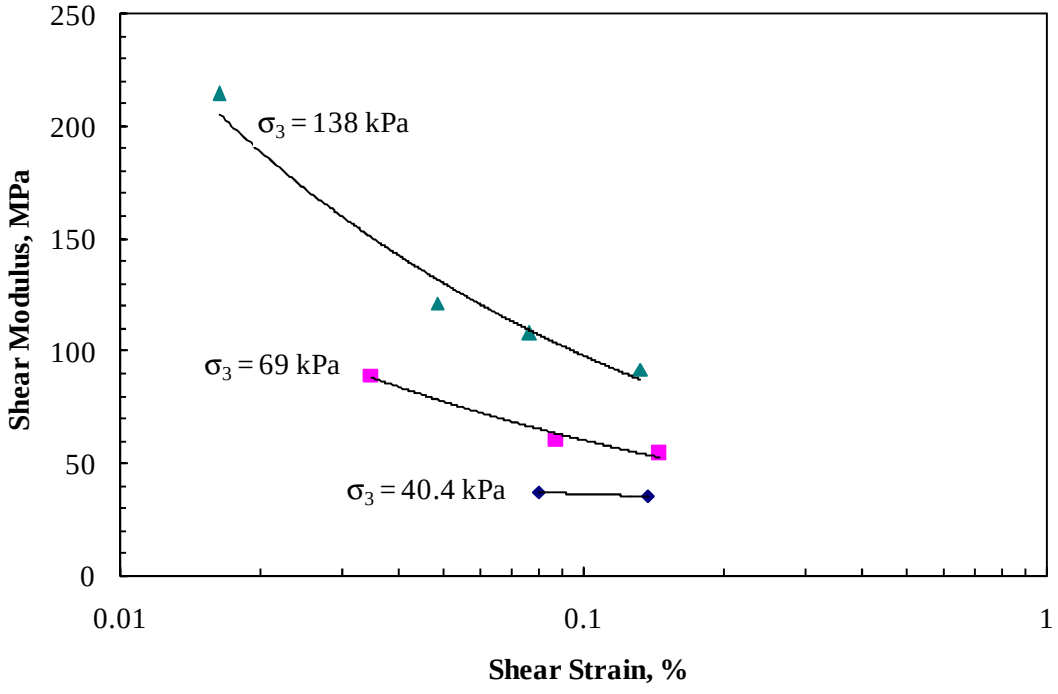

FIGURE 7.8a Variation of Shear Modulus with Shear Strain: AU-14 at 10Hz and 20°C.

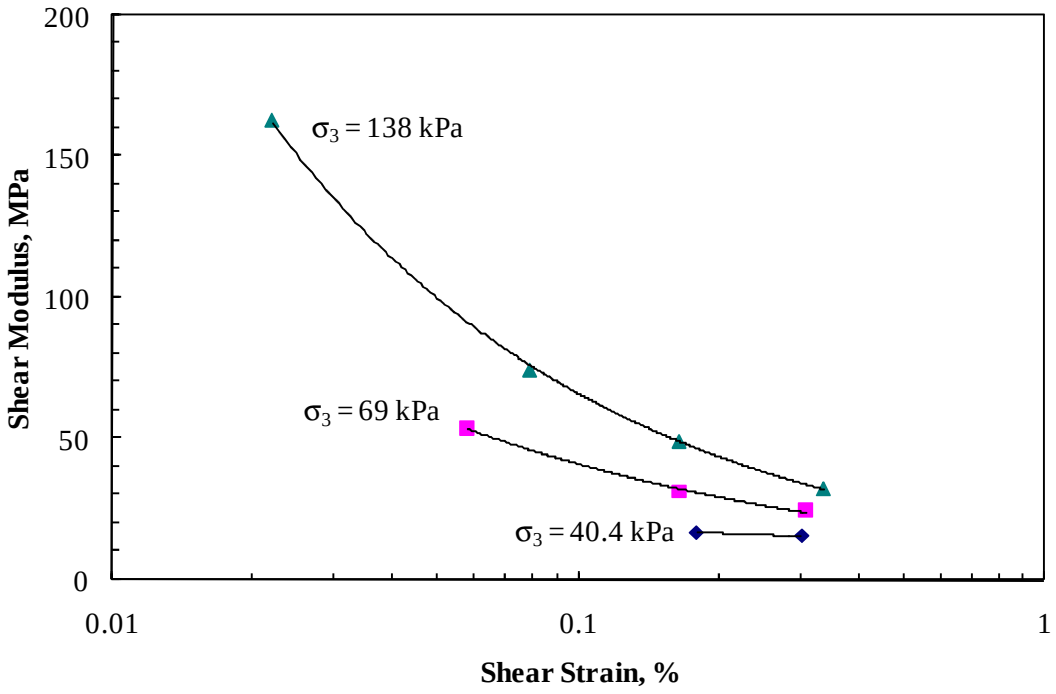

FIGURE 7.8b Variation of Shear Modulus with Shear Strain: AU-14 at 10Hz and 30°C.

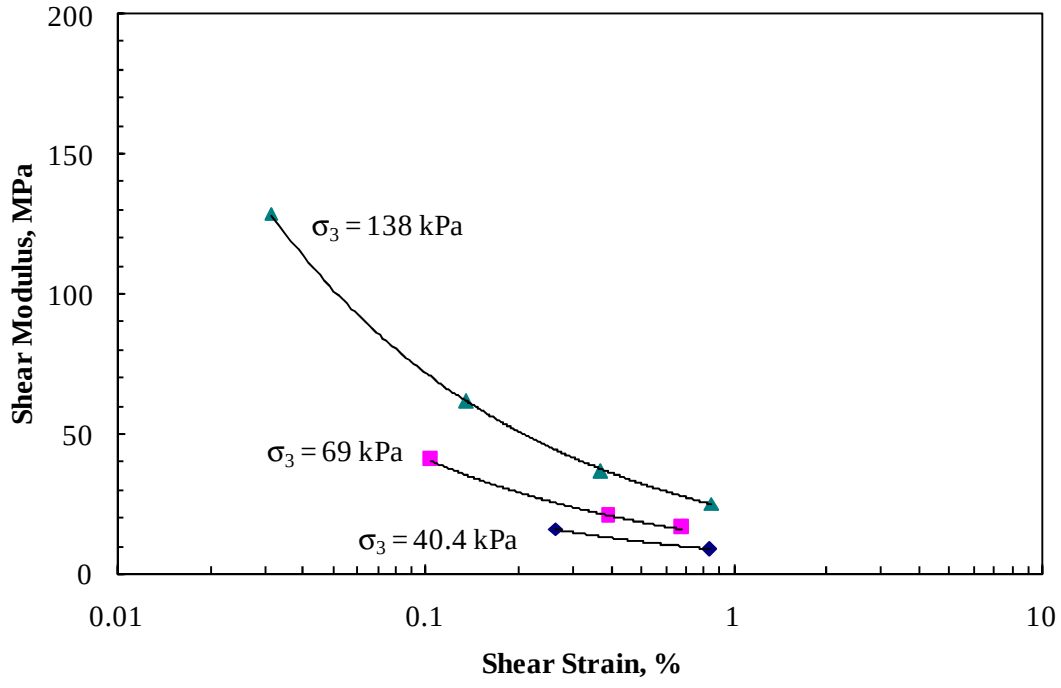

FIGURE 7.8c Variation of Shear Modulus with Shear Strain: AU-14 at 2Hz and 20°C.

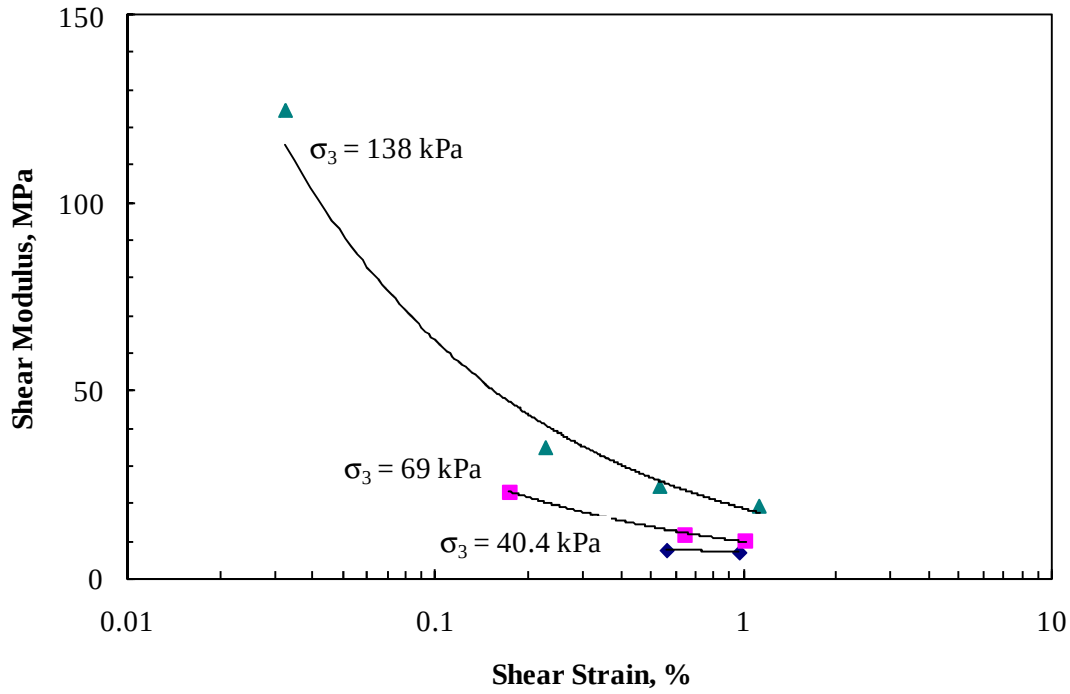

FIGURE 7.8d Variation of Shear Modulus with Shear Strain: AU-14 at 2Hz and 30°C.

7.4.4 Characterization of Pure Shear Modulus of Oil Sand Materials

7.4.4.1 Oil Sand Shear Modulus Reduction Curves

The shear modulus reduction curves have been used to model the relationship between a shear modulus and maximum shear modulus at a given strain level for soils, mostly at the low strain levels (< 0.001%). The modulus reduction concept used to model the CAT A-6 soil sample (section 7.4.2) is also employed for the oil sand samples. Figures 7.9 through 7.12 show the plots of normalized shear modulus G/G' against the shear strain γ for the oil sand samples at different loading frequencies and temperatures. It can be seen that data points for all the three oil sand samples fall within the specific range of a general trend, and there is little effect of temperature and loading frequency on the $G/G' - \gamma$ relations at low shear strains.

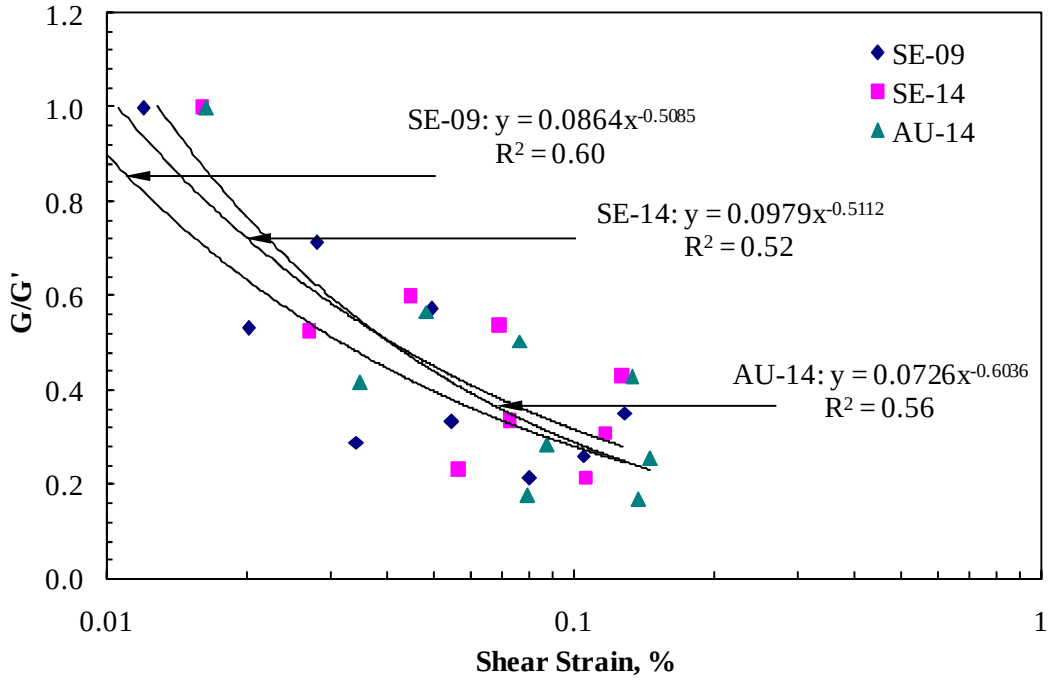

FIGURE 7.9 Normalized Shear Moduli of Oil Sands Samples against Shear Strain at 10Hz and 20°C.

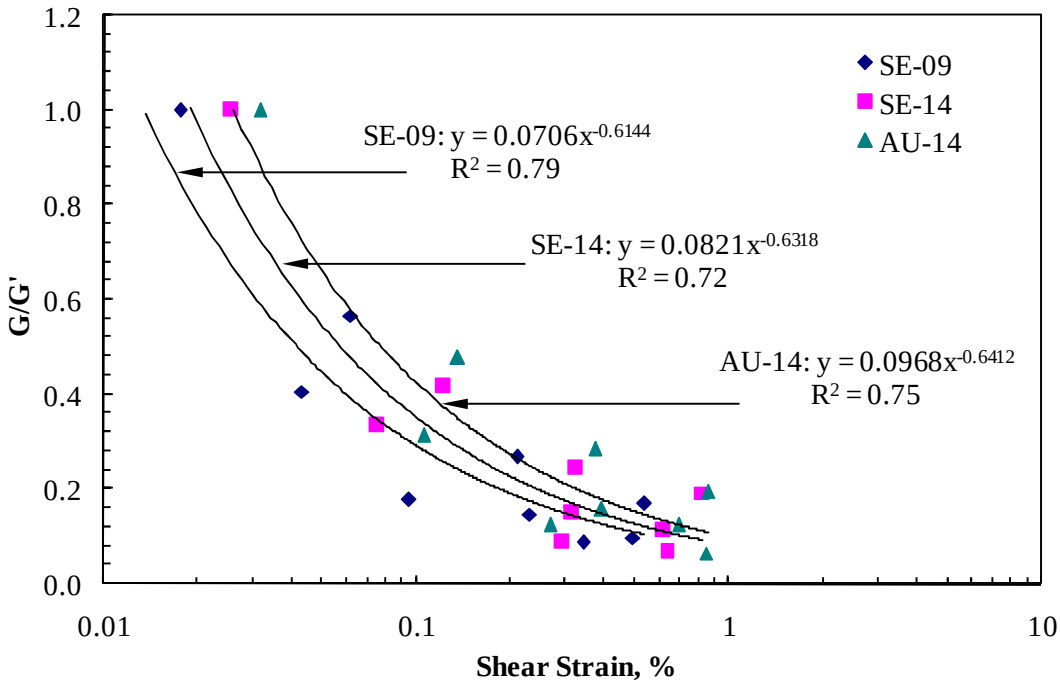

FIGURE 7.10 Normalized Shear Moduli of Oil Sand Samples against Shear Strain at 2Hz and 20°C.

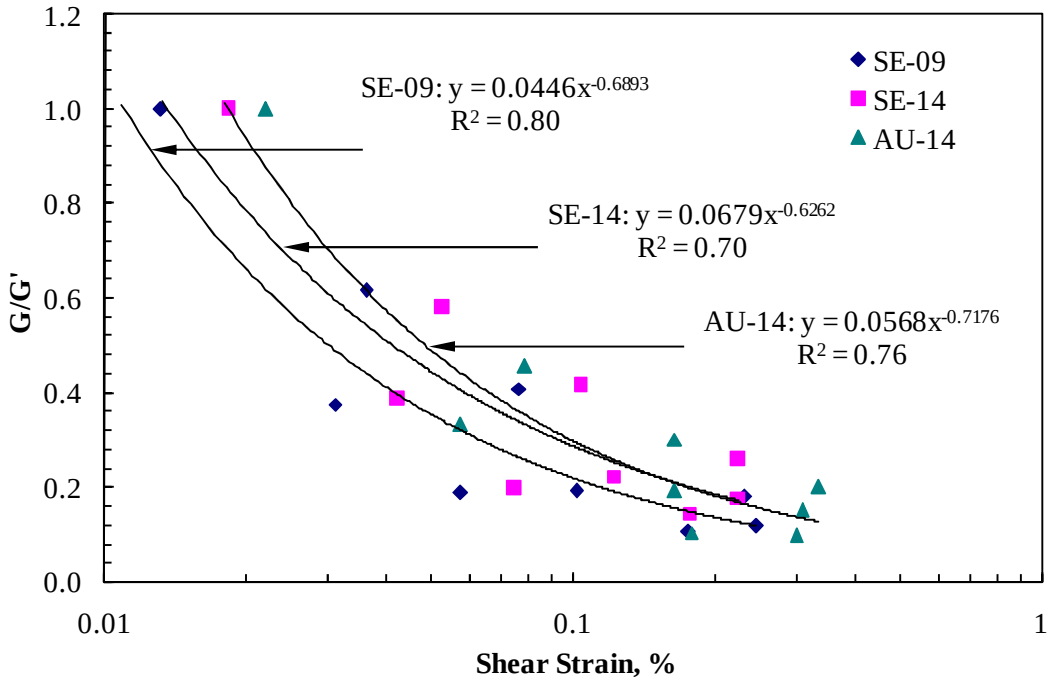

FIGURE 7.11 Normalized Shear Moduli of Oil Sand Samples against Shear Strain at 10Hz and 30°C.

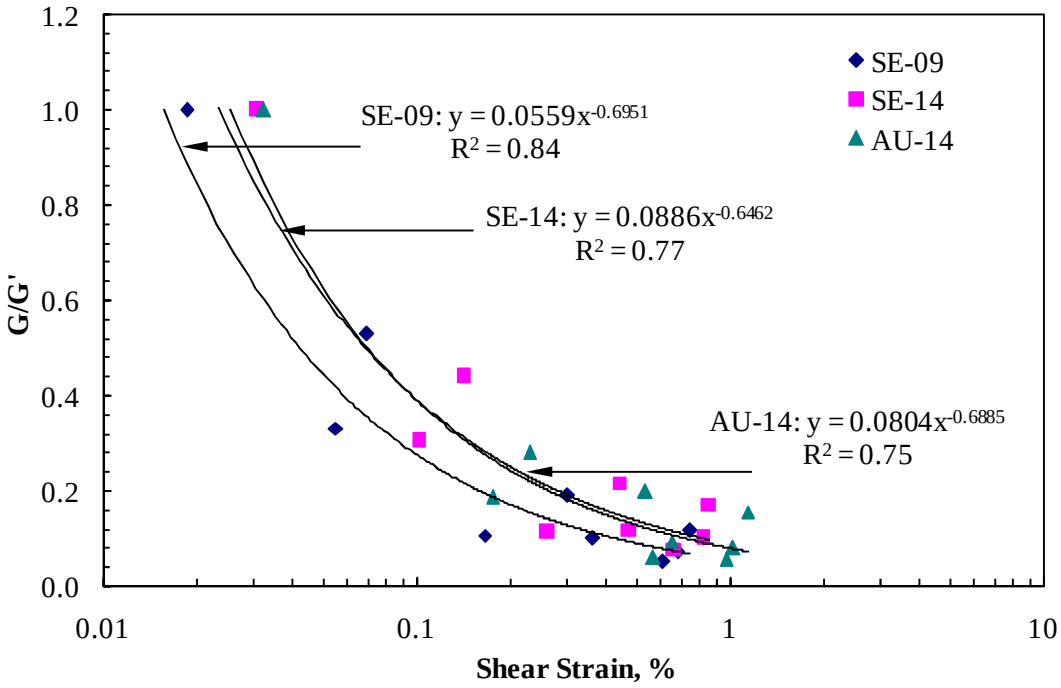

FIGURE 7.12 Normalized Shear Moduli of Oil Sand Samples against Shear Strain at 2Hz and 30°C.

Based on the observed similar trends and the regression constants shown in Figures 7.9 through 7.12, the combined data was used to perform regression analyses for the three oil sand samples. Figure 7.13 shows the normalized shear modulus (G/G') curve with $G' = 298.0$ MPa for combined test data, and Equations 7.4 through 7.7 are empirical correlations obtained from the regression analyses for the tested oil sand materials. A look at the shear strain exponents indicates that the stiffness of the three oil sand samples would be reduced more rapidly at 30°C and 2Hz than at 20°C and 10Hz. In other words, stiffness of the materials will be low at high temperature and low frequency.

$$\frac{G}{G'} = 0.0886\,\gamma^{-0.5242} \quad \text{at 10Hz and } 20^{o}\text{C}; \quad R^2 = 0.55 \tag{7.4}$$

$$\frac{G}{G'} = 0.0867\,\gamma^{-0.5954} \quad \text{at 2Hz and } 20^{o}\text{C}; \quad R^2 = 0.72 \tag{7.5}$$

$$\frac{G}{G'} = 0.0593\,\gamma^{-0.6482} \quad \text{at 10Hz and } 30^{o}\text{C}; \quad R^2 = 0.73 \tag{7.6}$$

$$\frac{G}{G'} = 0.0764\,\gamma^{-0.6472} \quad \text{at 2Hz and } 30^{o}\text{C}; \quad R^2 = 0.75 \tag{7.7}$$

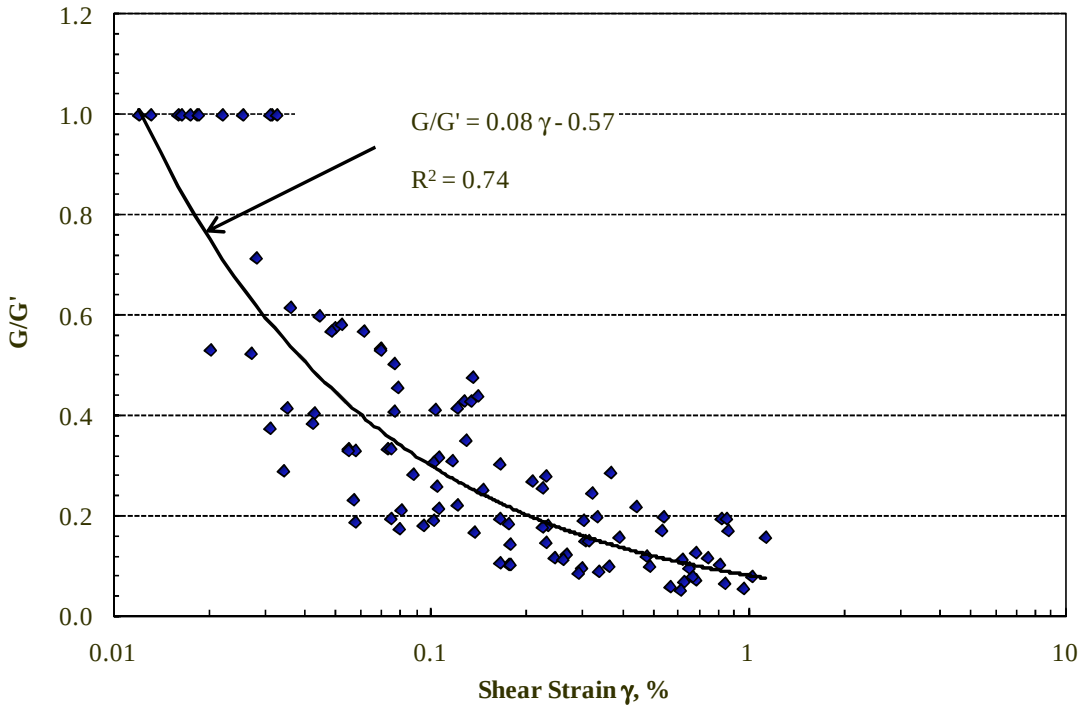

FIGURE 7.13 Normalized Shear Moduli against Shear Strain for Combined Data of Oil Sand Materials.

7.4.4.2 Development of Shear Modulus Characterization Models

Shear modulus models for soils have been primarily based on the modulus reduction curves. Although, these models have performed satisfactorily, they are mostly independent of stress and other loading conditions experienced by the soil material in the field. In this section, shear modulus models are developed for the three oil sand materials based on the applied stresses, the materials physical properties and testing conditions suspected to influence behavior in the field. An initial statistical analysis performed to determine variables that relate strongly with the shear modulus reveals that there was virtually no correlation between the oil sand gradation properties (Cu, Cc and D_{50}) and shear modulus ($R^2 < 0.1$). Also, shear modulus was found to be highly dependent on octahedral stress compared with instead of the applied cyclic and confining stresses. Similar to other characterization models developed in previous chapters, the power function was found to be most suitable for the oil sands shear modulus models.

Combined data sets obtained at all the loading conditions were used to study four models for characterizing the oil sand materials. As indicated earlier, a total of 9,000 data sets for each oil sand sample were used to develop the models. The SAS statistical software was used to perform multiple regression analyses on the data sets to obtain the model parameters. Table 7.5 lists the results of the analysis results, and the four shear modulus models studied for the oil sands. The differences in R^2 values indicate that the octahedral shear stress has a significant effect on the shear behavior. For instance, the R^2 value was improved by more than 200% when the octahedral shear stress term was included in model 2, compared to less than 15% increase when bitumen content and temperature were included in the models (see models 3 and 4). However, model 4 appears to be more realistic since it includes all the loading conditions necessary to describe shear modulus behavior of the oil sand materials in the field.

TABLE 7.5 Regression Models Studied for Pure Shear Modulus of Oil Sand Materials

Model 1 : $G = A \cdot \theta^{k_1}$

Model 2 : $G = A \cdot \theta^{k_1} \cdot \tau_{oct}^{k_2}$

Model 3 : $G = A \cdot \theta^{k_1} \cdot \tau_{oct}^{k_2} \cdot w_b^{k_3}$

Model 4 : $G = A \cdot \theta^{k_1} \cdot \tau_{oct}^{k_2} \cdot w_b^{k_3} \cdot T^{k_4}$

Model Parameters

Model	log A	k_1	k_2	k_3	k_4	R^2	*RMSE*
1	-0.492	0.866				*0.190*	*0.356*
2	-1.023	2.019	-1.592			*0.719*	*0.211*
3	0.112	2.021	-1.596	-1.059		*0.795*	*0.181*
4	1.762	2.029	-1.614	-1.059	-1.183	*0.865*	*0.147*

7.5 Comparison of Cyclic Triaxial and Pure Shear Test Results

As mentioned earlier, cyclic triaxial tests were also performed to compare test results to the newly developed pure shear tests. Specimens for the cyclic tests were subjected to the same stress conditions as the pure shear test specimens at the temperature of 20^{o}C and the loading frequency of 2Hz. A total of about 17,500 data points were obtained from the cyclic tests performed on the three oil sand samples.

Tables 7.6 compares shear modulus properties measured from cyclic triaxial (G) tests with those from the pure shear tests (G_{ps}). The shear moduli measured from the cyclic triaxial tests are higher than shear moduli measured from the pure shear tests. The average shear modulus from the cyclic triaxial test was about 1.8 to 2.7 times higher than the average value obtained from the pure shear test considering the data from all the three oil sand samples.

Note that the major difference between the cyclic triaxial and pure shear test procedures is such that in the pure shear tests, the confining stress is cycled in phase with the axial shear stress and the axial specimen deformations are generally larger due to the lack of a constant all-around confinement on the specimen. Therefore lower shear moduli are expected from the pure shear loading tests.

The test results of pure shear loading would better simulate haul trucks and shovel field loads, which at any time impose varying magnitudes of vertical, horizontal, and shear stresses in the oil sand materials during mining activities. It would be more conservative to characterize these materials by pure shear modulus since in the field oil sands experience induced dynamic loading in all directions.

Table 7.7compares the phase angles measured from pure shear tests to those obtained from cyclic triaxial tests. The phase angles obtained from the pure shear tests were higher in magnitude than those obtained from the cyclic triaxial tests. These results also suggest that oil sand materials become more viscous or less stiff under pure shear loading than cyclic triaxial loading conditions.

TABLE 7.6 Shear Moduli Compared from Pure Shear and Cyclic Triaxial Tests

Stress States (kPa)		G (MPa)			G_{ps} (MPa)		
σ_3	τ_{cyc}	SE-09	SE-14	AU-14	SE-09	SE-14	AU-14
40.4	20.7	89.0	72.9	41.5	41.6	13.7	15.9
40.4	40.4	39.1	34.3	20.3	20.7	10.5	8.4
69	20.7	155.3	122.5	76.3	94.4	53.2	40.5
69	40.4	84.6	69.1	36.4	34.2	23.7	20.3
69	69	36.2	34.3	21.0	22.9	17.8	16.2
138	20.7	314.0	259.5	195.8	232.5	158.8	128.7
138	40.4	234.9	187.8	131.1	131.7	66.1	61.4
138	69	149.6	117.7	66.5	62.7	38.9	36.6
138	138	40.5	37.6	25.1	39.7	30.6	24.9

TABLE 7.7 Phase Angles Compared from Pure Shear and Cyclic Triaxial Tests

Stress States (kPa)		δ (Deg)			δ_{ps} (Deg)		
σ_3	τ_{cyc}	SE-09	SE-14	AU-14	SE-09	SE-14	AU-14
40.4	20.7	31.3	33.5	35.7	31.4	32.8	47.7
40.4	40.4	34.2	36.3	37.1	37.2	35.9	52.3
69	20.7	27.9	30.2	33.2	28.8	32.0	38.8
69	40.4	30.5	33.5	35.0	34.8	35.0	45.4
69	69	33.6	35.3	36.3	41.9	41.3	48.9
138	20.7	24.1	23.4	25.3	23.5	23.6	20.6
138	40.4	26.6	27.7	29.6	31.2	32.0	42.3
138	69	27.9	30.3	33.4	37.5	41.1	45.2
138	138	32.5	33.7	34.1	49.6	58.4	58.7

Figures 7.14 through 7.16 show variations of shear moduli with shear strain obtained from the cyclic triaxial tests for the oil sand samples at the applied confining stresses. Similar trends in the results of the pure shear tests for the oil sand materials were obtained by the cyclic triaxial tests (see section 7.4.2.1), ie., there is a rapid reduction of shear modulus at high shear strains and confining stress of 138 kPa.

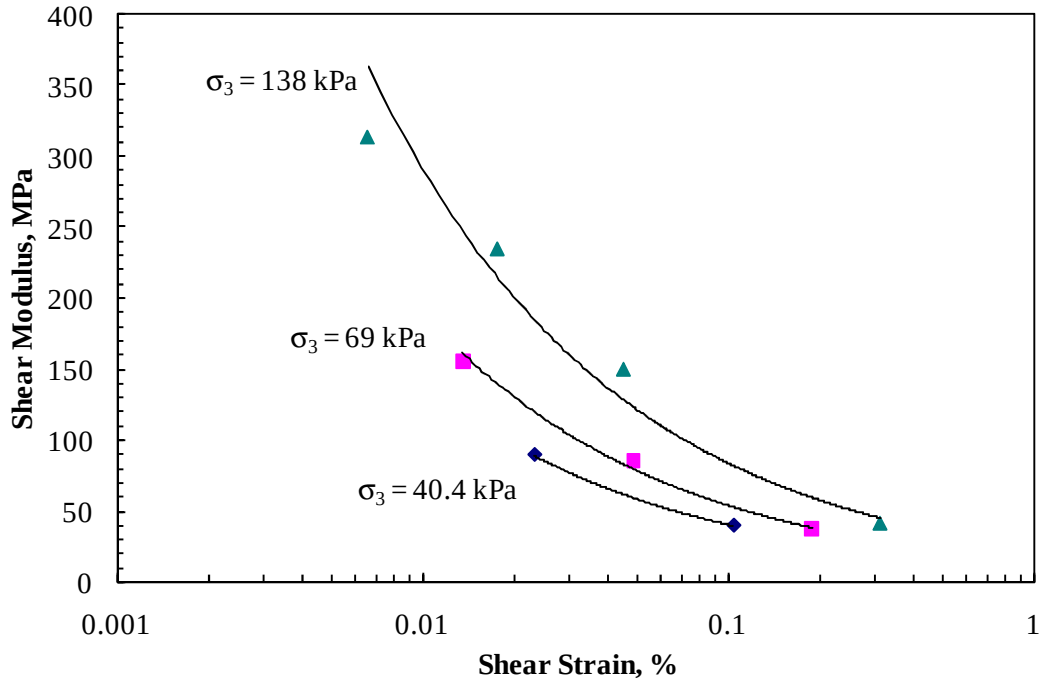

FIGURE 7.14 Variation of Shear Modulus with Shear Strain: Cyclic Triaxial (SE-09).

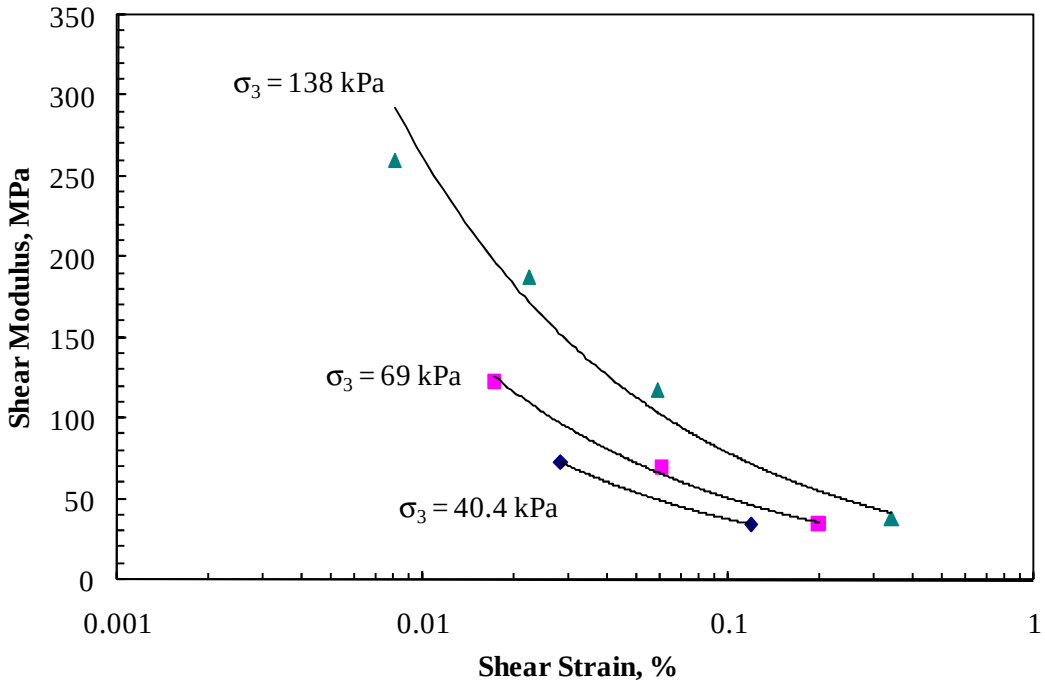

FIGURE 7.15 Variation of Shear Modulus with Shear Strain: Cyclic Triaxial (SE-14).

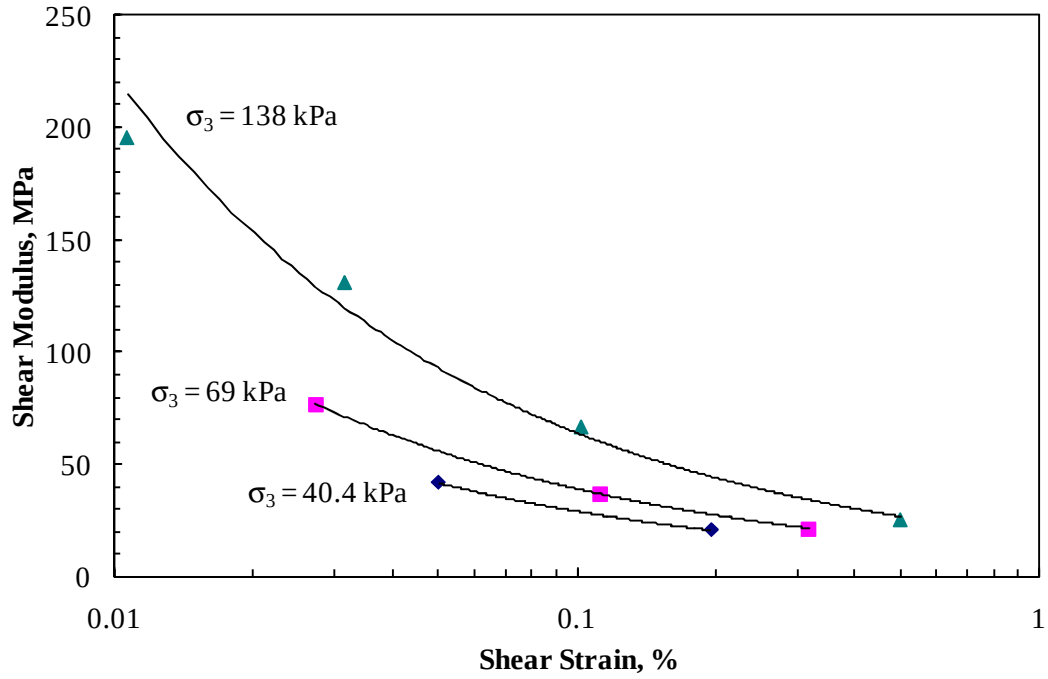

FIGURE 7.16 Variation of Shear Modulus with Shear Strain: Cyclic Triaxial (AU-14).

7.5.1 Correlating Shear Modulus from Cyclic Triaxial and Pure Shear Tests

Figures 7.17 to 7.19 show the correlations between the shear modulus properties obtained from pure shear and cyclic triaxial tests for all the three oil sand samples. Each data point in the figures represents the results of specimens tested at the same stress states for the two test procedures. Regression curve fits and 45-degree lines (lines of equality) are drawn in the data points to display the correlations between the shear modulus values obtained from cyclic triaxial and pure shear tests. It can be observed that the cyclic triaxial test predicts shear modulus by about 53 to 92% more than the pure shear test. It appears that there is close agreement only when shear modulus is quite low, i.e., less than 50 MPa. The test data in this region represent moduli under high cyclic stresses.

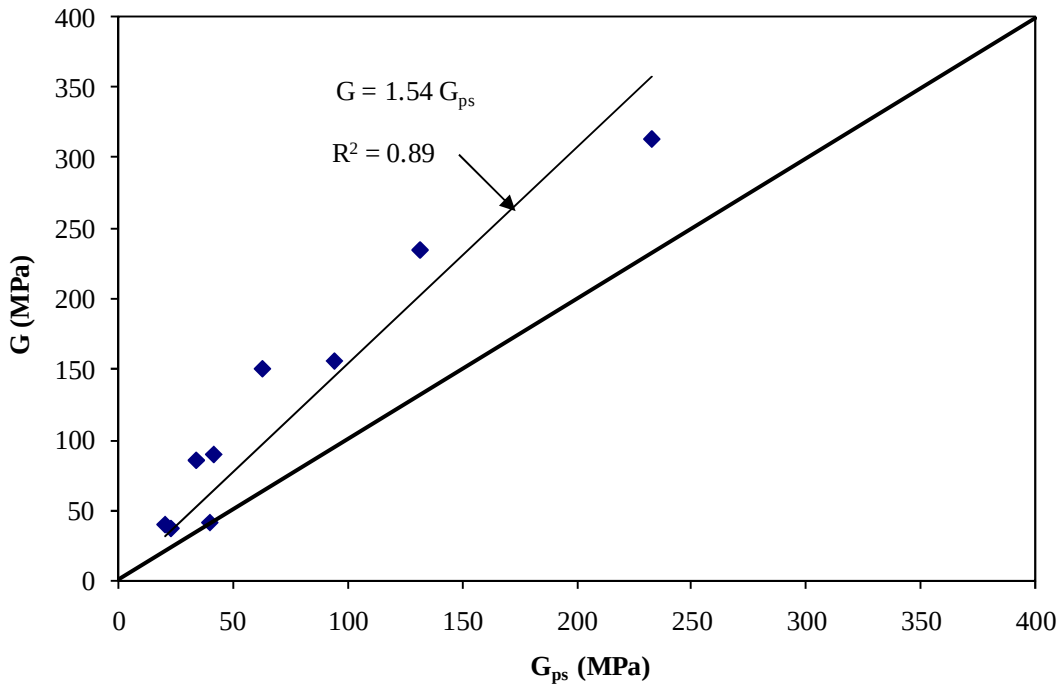

FIGURE 7.17 Comparison of Shear Moduli from Cyclic Triaxial and Pure Shear Tests for SE-09 Sample.

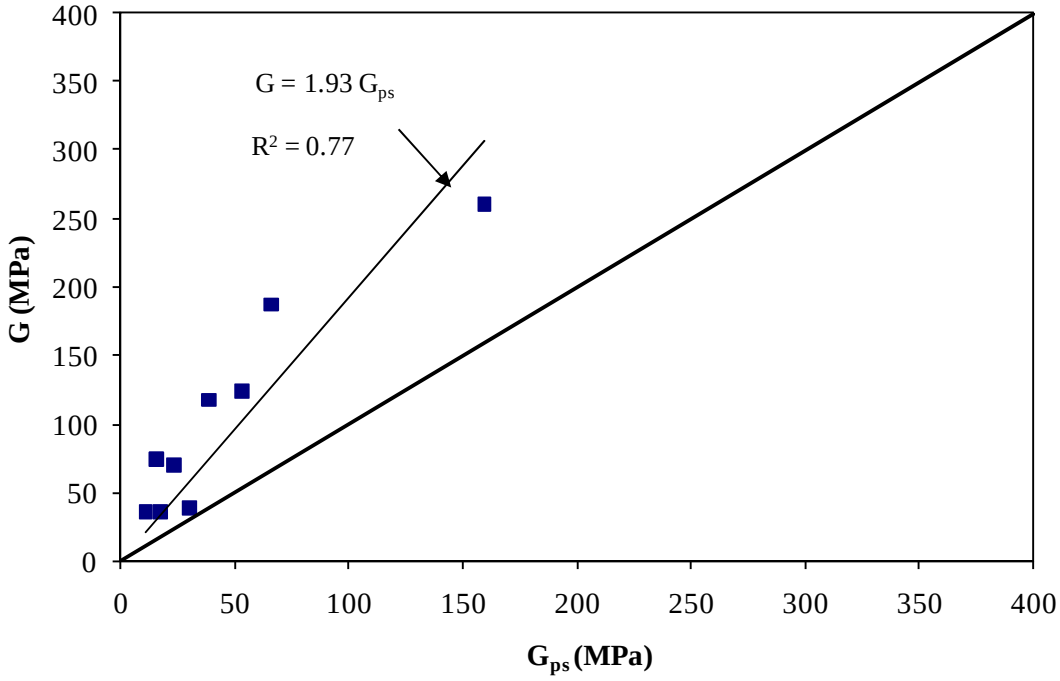

FIGURE 7.18 Comparison of Shear Moduli from Cyclic Triaxial and Pure Shear Tests for SE-14 Sample.

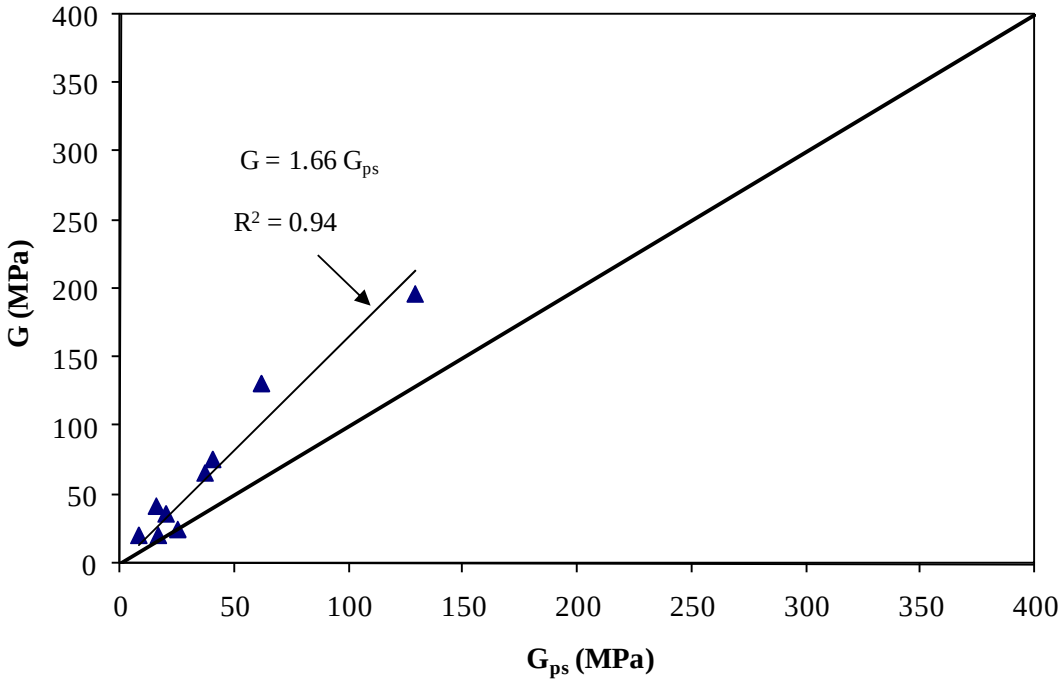

FIGURE 7.19 Comparison of Shear Moduli from Cyclic Triaxial and Pure Shear Tests for AU-14 Sample.

7.5.2 Characterization Models for Shear Moduli from Cyclic and Pure Shear Tests

Material characterization models were developed using both cyclic triaxial and pure shear data for selected testing conditions. Multiple regression analyses performed on pure shear test results in section 7.4.2 were also employed under this section. Table 7.8 compares the developed models and model parameters obtained from the cyclic and pure shear test data. The analyses show that pure shear modulus highly depends on octahedral shear stress. In contrast, the cyclic shear modulus depends more on bulk stress. This observation can be seen in the differences in R^2 values for models 1 and 2, and suggests that specimens experience higher dynamic loading in all directions under pure shear tests compared to only vertical dynamic stresses applied during cyclic triaxial tests. A comparison of R^2 values for the proposed models for both pure shear and cyclic triaxial tests indicate that model 3 would perform better than models 1 and 2. Moreover, the inclusion of bitumen content makes model 3 most suitable for describing behavior of the oil sand materials.

TABLE 7.8a Shear Modulus Models Developed from Pure Shear Test

Models for Pure Shear Modulus						
Model 1 : $G = A \cdot \theta^{k_1}$						
Model 2 : $G = A \cdot \theta^{k_1} \cdot \tau_{oct}^{k_2}$						
Model 3 : $G = A \cdot \theta^{k_1} \cdot \tau_{oct}^{k_2} \cdot w_b^{k_3}$						
Model	Model Parameters					
	log A	k_1	k_2	k_3	R^2	*RMSE*
1	-0.789	0.934			*0.263*	*0.321*
2	-1.435	2.119	-1.503		*0.859*	*0.143*
3	-0.160	2.114	-1.495	-1.192	*0.972*	*0.065*

TABLE 7.8b Shear Modulus Models Developed from Cyclic Triaxial Tests

Models for Cyclic Shear Modulus						
Model 1 : $G = A \cdot \tau_{oct}^{k_2}$						
Model 2 : $G = A \cdot \theta^{k_1} \cdot \tau_{oct}^{k_2}$						
Model 3 : $G = A \cdot \theta^{k_1} \cdot \tau_{oct}^{k_2} \cdot w_b^{k_3}$						
Model	Model Parameters					
	log A	k_1	k_2	k_3	R^2	*RMSE*
1	2.745	-0.680			*0.260*	*0.307*
2	-0.167	1.506	-1.311		*0.821*	*0.154*
3	0.857	1.507	-1.313	-0.955	*0.900*	*0.118*

In addition to the characterization models, regression analysis was also performed on the cyclic test results of the oil sand samples to develop correlations between normalized shear modulus and shear strain. Note that similar correlations have been developed for pure shear tests under the same testing conditions as the cyclic triaxial tests (Equations 7.4 to 7.7). Figure 7.20 shows normalized shear modulus graphed with shear stress with regression equation for the combined data of the three oil sand materials. Equation 7.8 is an empirical correlation between the normalized shear modulus and shear strain for the combined data.

$$\frac{G}{G'} = 0.054\,\gamma^{-0.584} \quad ; \quad R^2 = 0.82 \tag{7.8}$$

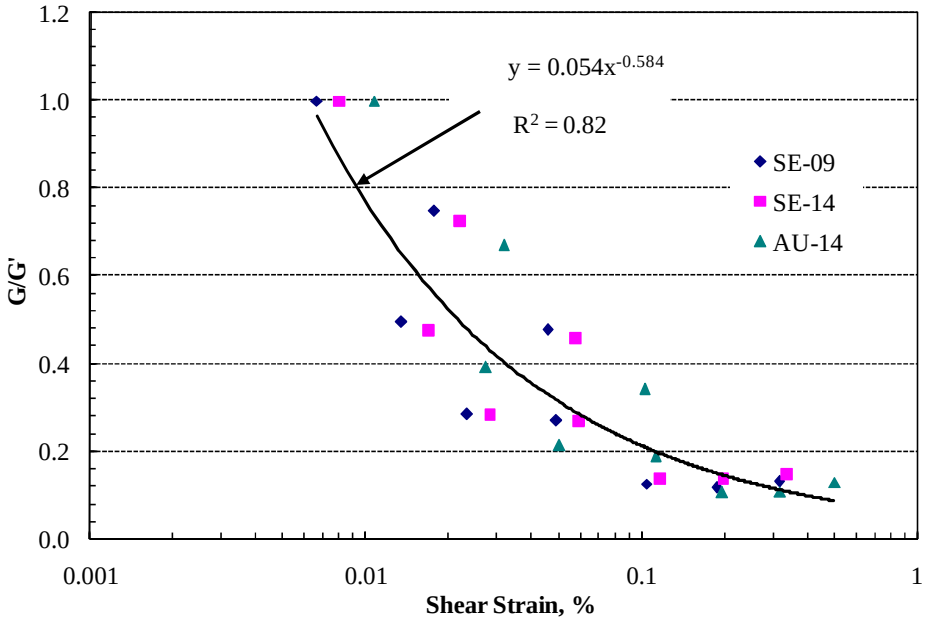

FIGURE 7.20 Normalized Shear Modulus for Oil Sand Samples - Cyclic Triaxial Test.

7.6 Summary

Shear modulus and phase angle properties of one fine grained-cohesive soil and three oil sand samples were investigated in the laboratory using a newly developed pure shear test procedure. The fine-grained soil sample was tested at three moisture states; optimum water content, w_{opt} = 14.3%, dry of optimum, w = 11.3% and wet of optimum, w = 17.3% with one loading frequency, and the oil sand samples with bitumen contents of 8.5%, 13.3% and 14.5%, were tested at two temperatures and two load frequencies. Results from these tests were used to develop regression equations and material characterization models for the soil and oil sand samples. The test results for the soil samples were used to obtain relationships between normalized shear moduli as a function of shear strain at the different water contents. For the oil sand samples, strong correlations were obtained between normalized shear moduli and shear strain at the test temperatures and loading frequencies. The various material characterization models developed for the oil sand samples indicate that the shear properties obtained from pure shear tests depend primarily on octahedral shear stress instead of bulk stress.

The coefficient of correlation values improved when temperature and loading frequency were also included in the model.

The standard cyclic triaxial test procedure was used to perform tests on the three oil sand samples at selected loading conditions to compare test results with the developed pure shear test. For the three oil sand samples, the average shear modulus measured by the cyclic triaxial procedure was in the range of 80 to more than 100% higher than average shear modulus measured by pure shear test procedure. Generally, the pure shear tests yielded higher phase angle values for all the oil sand samples than the cyclic triaxial tests. A combination of varying magnitudes of static and dynamic confining stresses applied in the pure shear test compared to constant confining stresses applied in the cyclic triaxial tests is suggested as the cause of the difference in the shear moduli values. Results from the cyclic triaxial tests were also used to develop material characterization models for the oil sand samples. For the cyclic triaxial tests, the material models show that shear modulus largely depends on bulk stress instead of octahedral shear stress. The following are the general conclusions drawn from the tests:

1. The average shear modulus of the soil sample at dry of optimum was about 3.5 times higher than at optimum water content, whereas the average shear modulus measured at the optimum was found to be about 8 times the shear modulus at wet of optimum moisture state. The phase angle at optimum was higher than dry of optimum and lower than wet of optimum. As observed in the previous chapters, an increase in water content of 3% above or below optimum had significant effects on the dynamic characteristics of the soil sample.
2. For the oil sand samples, the shear modulus values were generally lower at 30^{o}C than at 20^{o}C, and higher at 10Hz than 2Hz. This was expected since bituminous materials are less stiff at high temperatures and low loading frequencies. The SE-09 oil sand sample had the highest shear moduli and lowest phase angle values whereas the AU-14 sample had lowest shear moduli and highest phase angle properties. The shear modulus and phase angle values of SE-14 were comparable to AU-14 sample. However, the shear modulus of SE-14 sample was generally higher than shear modulus of the AU-14 sample.

CHAPTER 8 DAMPING RATIO AND DYNAMIC MODULUS OF FINE-GRAINED COHESIVE SOIL AND OIL SANDS

8.1 Introduction

Cyclic loading tests have been commonly used for studying dynamic properties such as damping ratio and dynamic modulus. The dynamic properties of the fine-grained cohesive soil and the oil sand materials were investigated under cyclic loading conditions in the laboratory for off-road construction and mining equipment. Damping ratio is a parameter used as a measure of the energy dissipated when a geomaterial is subjected to cyclic dynamic loading. On the other hand, dynamic modulus, obtained from the ratio of applied cyclic peak stress to the corresponding strain, is widely used to characterize behavior of bituminous materials. This chapter investigates damping ratio and dynamic modulus properties in an attempt to develop simple models to characterize the fine-grained soil and the three oil sand materials using a newly developed damping property test procedure presented in Chapter 3.

Laboratory tests on the soil sample were performed at three moisture states and three loading frequencies, and the oil sand tests were performed at two temperatures and three loading frequencies. The test data are then used to develop various characterization models for the soil and oil sand materials.

8.2 Laboratory Testing

Laboratory tests were performed on the soil and oil sand samples in accordance with the damping property test procedure (Procedure E) described in section 3.5.8. The tests involve applying various frequencies of continuous sinusoidal loading to the test specimen and measuring stress and strain responses to obtain damping ratio and dynamic modulus values. The test program and testing conditions are summarized in Table 8.1. The UI-FastCell test setup was used for applying stresses on the soil sample, and the RaTT cell setup was used for the oil sand samples. As mentioned in Chapter 7, the RaTT cell setup with an environmental chamber was used for the oil sand testing to apply loading at two temperatures. A full factorial test matrix comprising 45 tests were conducted for the soil sample at three moisture states and three load frequencies. The three moisture states were optimum, wet of optimum and dry of optimum water contents.

For the three oil sand samples a total of 72 tests conducted at test temperatures of 20°C and 30°C, and three loading frequencies constituted the test matrix.

TABLE 8.1 Damping Ratio Test Program and Loading Conditions

Soil Tests	
Sample ID	: CAT A-6
Test Temperature (T)	: 22°C (room temperature)
Loading Frequency (f)	: 2, 10 and 20Hz
Confining Stress (σ_3)	: 0, 41.4, 69 and 138 kPa
Deviator Stress (σ_d)	: 41.4 kPa
Water Content (w)	: optimum (w_{opt} = 14.3%); wet of optimum (w = 17.3%); and dry of optimum (w = 11.3%)
Oil Sand Tests	
Sample ID	: SE-09, SE-14 and AU-14
Test Temperature (T)	: 20 and 30°C
Loading Frequency (f)	: 2, 5, and 10Hz
Confining Stress (σ_3)	: 41.4, 69, and 138 kPa
Deviator Stress (σ_d)	: 41.4 kPa
Bitumen content (w_b)	: SE-09 (w_b = 8.5%); SE-14 (w_b = 13.3%) and AU-14 (w_b = 14.5%)

8.3 Data Analysis Procedure

The damping property raw test data include the time of loading, the applied stresses and the corresponding axial strains to evaluate damping ratio and dynamic modulus properties of the materials tested. Figures 8.1a and 8.1b show typical variations of axial stress and axial strain with time, at the loading frequency of 2Hz and 5 load cycles for an oil sand sample. Figure 8.2 also shows a typical plot of axial stress against axial strain that result in a hysteresis loop. The generalized mathematical curve fit function presented in Equation 3.8 was used to fit the raw test data to obtain parameters for computing damping ratio and dynamic modulus of the oil sand materials. Using Microsoft Excel Solver, a least squared error regression analysis was performed to determine the peak stresses and strains.

Dynamic modulus of the materials was calculated as the ratio of the peak stress to peak strain. The parameters for computing the amplitude of the stress and strain curves could also be used to determine phase angle of the materials. Phase angle is a measure of the viscous or elastic properties of viscoelastic materials.

The peak stress and strain values, and the area enclosed by the hysteresis loop (see Figure 8.2) were used for determining damping ratio of the materials. In this study, a generalized formula to compute an area of a polygon with *n* vertices was used to determine the area of the hysteresis loop. The formula is expressed as follows:

$$\text{Area} = \frac{1}{2} \sum_{i=1}^{n} (x_i y_{i+1} - x_{i+1} y_i) \qquad (8.1)$$

The hysteresis loop is closed by replacing x_{n+1} by x_1, and y_{n+1} by y_1. An average of the area determined from 5 hysteresis loops representing five load cycles was generally used for the computations. The damping ratio of the soil and oil sand samples at different loading conditions were computed using Equation 3.7. The results for the analyses are presented hereafter.

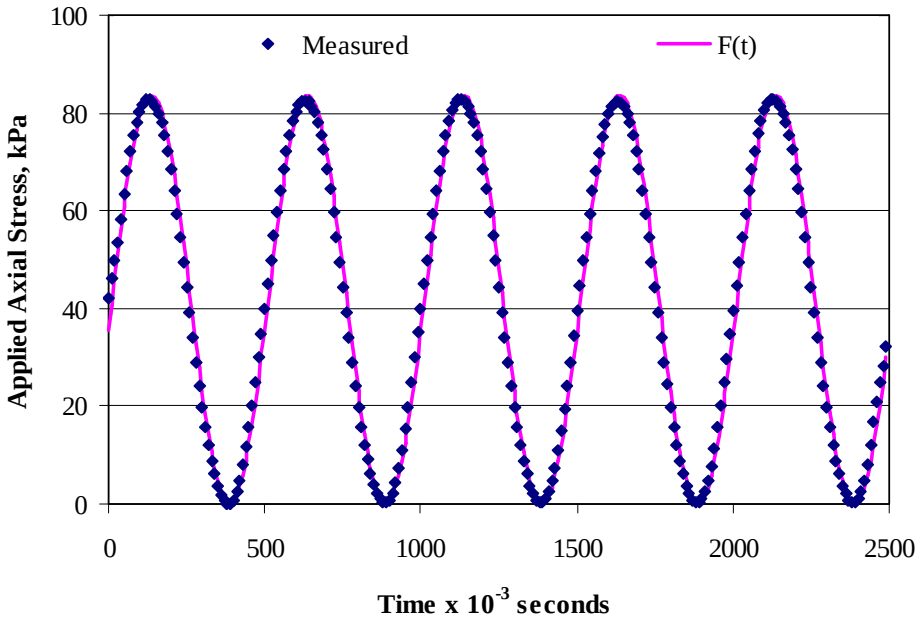

(a)

FIGURE 8.1a Variation of Stress with Time for Typical Test Results of Oil Sand Material.

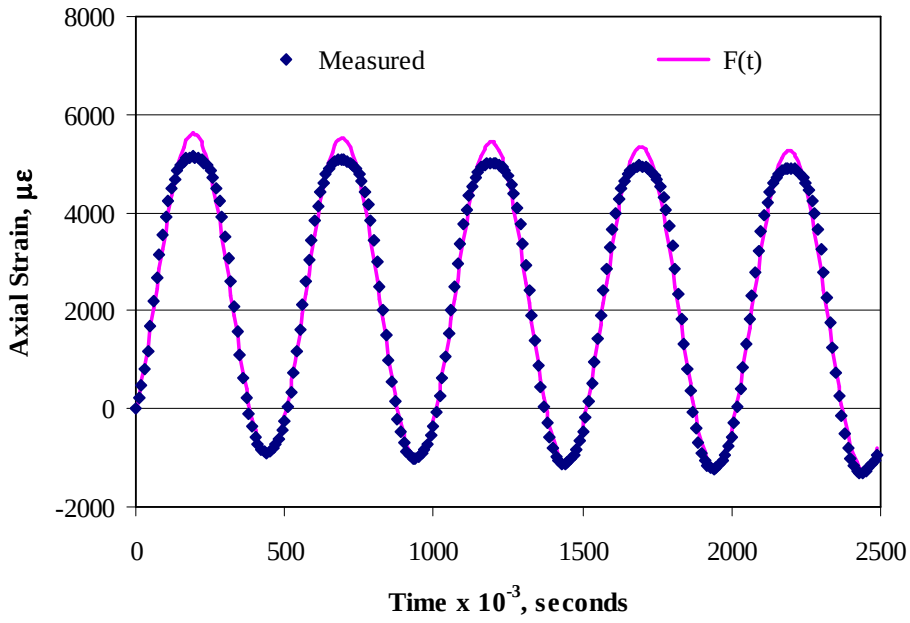

(b)

FIGURE 8.1b Variation of Strain with Time for Typical Test Results of Oil Sand Material.

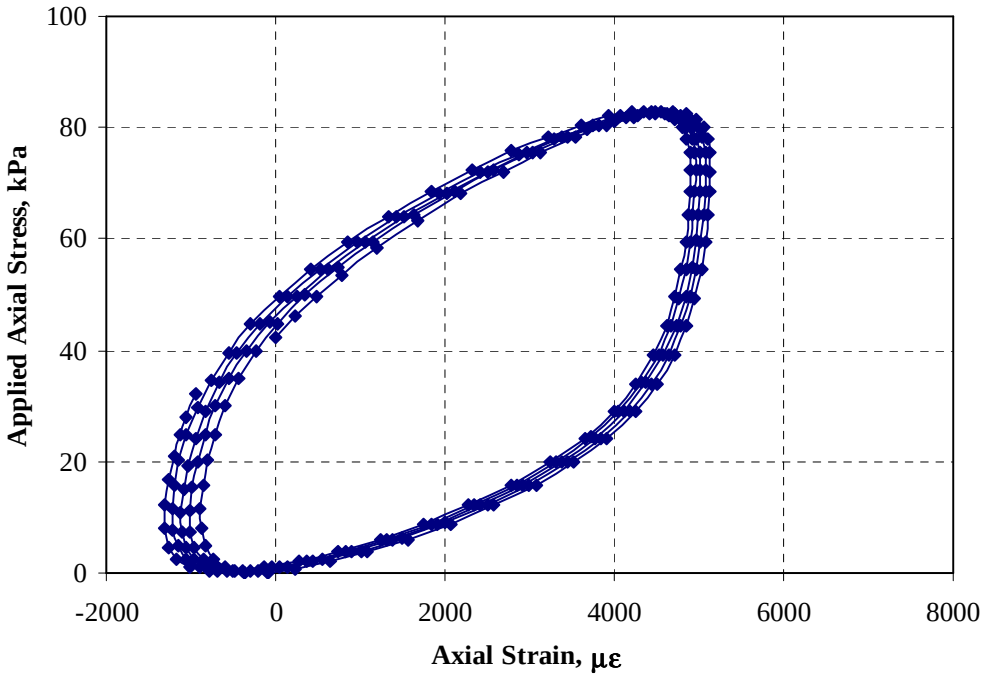

FIGURE 8.2 Typical Stress-Strain Hysteresis Loop for Oil Sand Material.

8.4 Analyses of Test Results

8.4.1 Analysis of Fine-Grained Soil Test Results

A total of about 3,750 sets of data points were obtained from 15 different test conditions at one moisture state. A single data set contains 250 stress-strain data points. Data analysis were performed for CAT A-6 soil at optimum (w_{opt} = 14.3%), dry of optimum (w = 11.3%) and wet of optimum (w = 17.3%). The dependency of damping ratio and dynamic modulus test results on the test loading conditions are listed in Tables 8.2 through 8.4 as obtained at the three moisture states. There is no significant difference between the damping ratio and dynamic modulus of the sample at loading frequencies 2, 10, and 20Hz when the moisture content is the same. The soil material is not viscoelastic, therefore the behavior was expected. However, at different moisture states, there was significant difference between the damping ratio and dynamic modulus of the soil sample. Damping ratio was found to be higher at wet of optimum and lower at dry of optimum. i.e., damping ratio increases with increasing water content in the CAT A-6 soil sample. This is reasonable since more energy dissipation is expected in the soil sample at the wet condition than in the dry state. On the other hand the dynamic modulus or stiffness of the sample was higher at dry of optimum and lower at wet of optimum. The average damping ratio of the soil sample at the optimum moisture was about 16% lower than the damping ratio at wet of optimum and 33% higher than at dry of optimum. On the other hand, the average dynamic modulus at the optimum moisture was about 40% higher than the dynamic modulus at wet of optimum and 31% lower than dry of optimum. The phase angle of the soil at optimum was generally lower than phase angle at wet of optimum and higher than dry of optimum. These properties did not change as the bulk stress increased. Note that the applied dynamic stress was constant at all the loading conditions. Therefore, the effect of bulk stress was the same as the effect of the applied confining stress.

TABLE 8.2 Summarized Damping Ratio Test Results for CAT A-6 Soil at w = 11.3%

Loading Frequency (f)	Bulk Stress (kPa)	Dynamic Modulus (MPa)	Damping Ratio (%)	Phase Angle (Deg.)
2	40.1	17.0	12.8	20.6
10	40.1	22.4	13.7	21.4
20	38.9	17.7	16.2	21.2
2	108.4	56.5	11.8	18.7
10	107.0	61.2	13.6	21.0
20	105.0	53.8	14.6	21.1
2	172.0	84.4	12.6	21.6
10	170.5	81.3	13.5	21.1
20	169.3	83.7	14.6	17.7
2	255.3	105.5	13.9	22.7
10	254.4	100.0	14.4	23.4
20	251.5	105.1	15.1	19.3
2	466.1	148.6	12.3	20.5
10	465.8	159.7	13.5	23.5
20	459.7	165.4	15.0	21.2

TABLE 8.3 Summarized Damping Ratio Test Results for CAT A-6 Soil at w_{opt} = 14.3%

Loading Frequency (f)	Bulk Stress (kPa)	Dynamic Modulus (MPa)	Damping Ratio (%)	Phase Angle (Deg.)
2	40.7	14.0	17.7	30.4
10	40.1	18.0	17.6	30.6
20	41.1	15.6	19.1	30.6
2	107.1	31.9	17.8	31.2
10	105.5	38.4	18.5	30.9
20	106.6	40.1	18.8	29.5
2	170.4	47.7	18.3	31.6
10	168.6	51.8	18.5	30.8
20	170.5	57.9	18.0	27.5
2	251.3	63.6	19.1	32.2
10	251.7	65.0	18.6	30.4
20	252.7	75.1	18.3	28.3
2	462.7	101.8	18.3	30.7
10	463.0	102.3	17.7	31.0
20	463.4	111.3	17.5	31.7

TABLE 8.4 Summarized Damping Ratio Test Results for CAT A-6 Soil at w = 17.3%

Loading Frequency (f)	Bulk Stress (kPa)	Dynamic Modulus (MPa)	Damping Ratio (%)	Phase Angle (Deg.)
2	40.9	9.7	21.5	33.8
10	40.9	13.0	21.9	33.8
20	40.2	15.0	23.2	33.6
2	113.3	24.6	20.8	33.8
10	109.1	25.1	20.7	33.3
20	106.0	26.9	24.6	35.5
2	175.6	33.5	20.8	34.0
10	171.9	36.0	20.6	33.0
20	170.3	39.4	22.7	33.0
2	258.7	43.2	22.2	33.6
10	255.8	48.7	20.9	33.9
20	254.3	54.3	22.0	33.3
2	469.9	65.8	22.6	33.1
10	463.9	72.6	21.6	33.8
20	462.3	82.2	21.2	31.3

8.4.1.1 Damping Ratio Variation with Axial Strain

Figure 8.3 show the variation of damping ratio of CAT A-6 soil with axial strain obtained at three moisture states. As the axial strain increases, damping ratio remains constant for the soil sample tested at all three moisture states. Thus, no correlation appears to exist between damping ratio of the soil sample and axial strain.

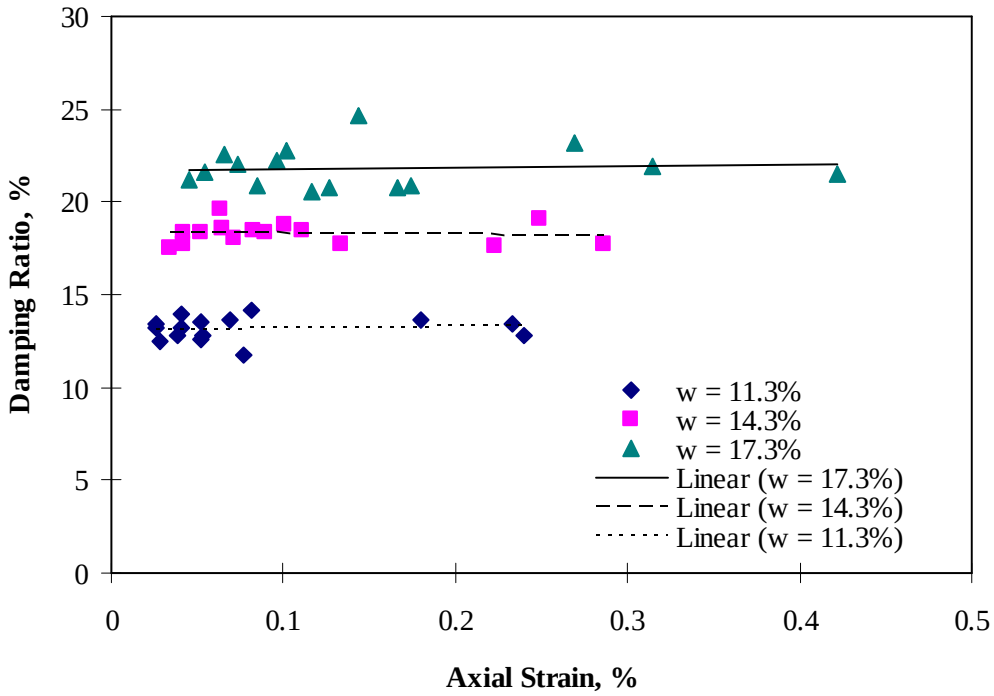

FIGURE 8.3 Variation of Axial Strain with Damping Ratio of CAT A-6 Sample.

8.4.1.2 Effect of Loading Frequency on Damping Ratio and Phase Angle

Figure 8.4 shows the effect of loading frequency on damping ratio of CAT A-6 soil sample tested at w = 11.3%, w_{opt} = 14.3% and w = 17.3% under different confining stresses. At one constant confining pressure damping ratio did not change when loading frequency increased. This observation was valid at all the three moisture states, which is in agreement with Vucetic and Dobry (1991) who found damping ratio was insensitive to the changes in the rate of loading (loading frequency) of the soil materials.

Figures 8.5 through 8.7 suggest that no correlation exist between the loading frequency and phase angle of the soil sample at all the three moisture levels. Like the damping ratio, the phase angle of the soil sample is higher at w = 17.3% and lower at w = 11.3%. It can be concluded that water content had a major influence on phase angle, whereas an increase in confining stress had no effect on phase angle at all the moisture states.

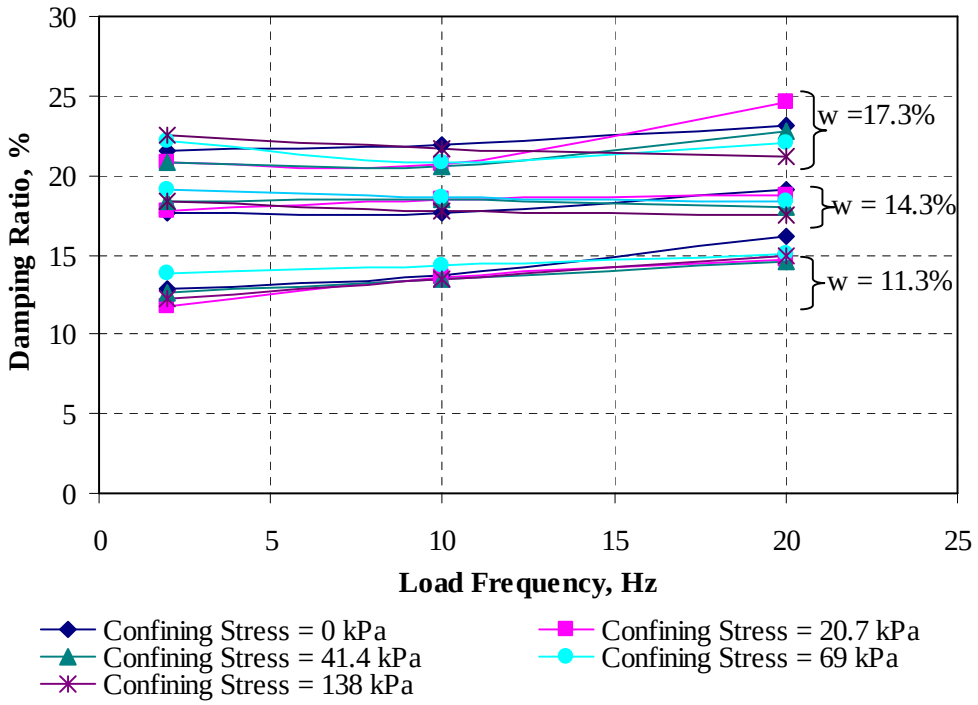

FIGURE 8.4 Effect of Loading Frequency on Damping Ratio for CAT A-6 Soil Sample.

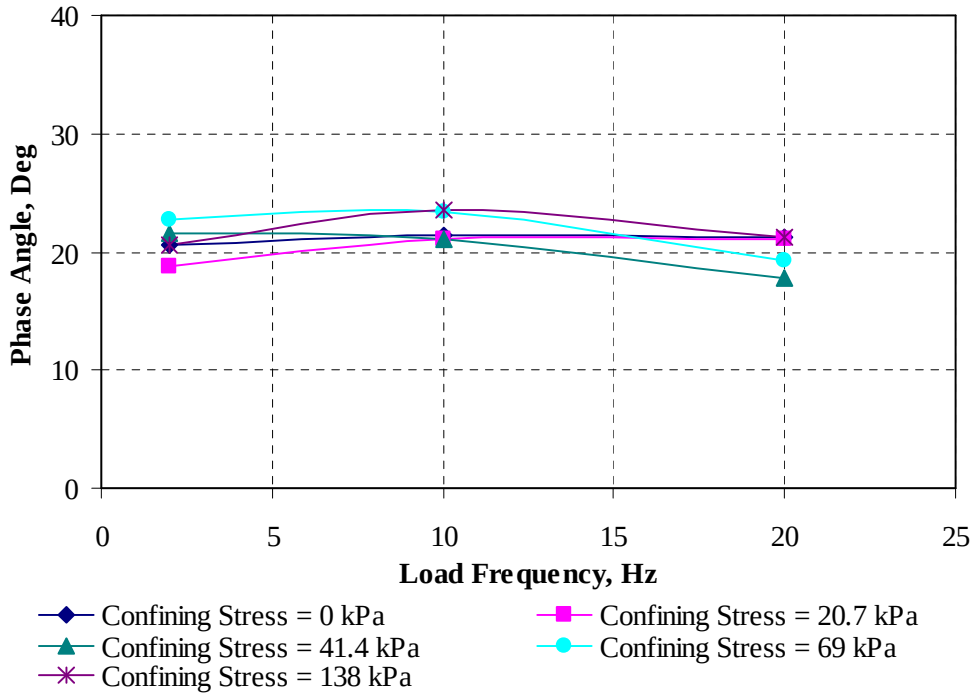

FIGURE 8.5 Effect of Loading Frequency on Phase Angle for CAT A-6 at w = 11.3%.

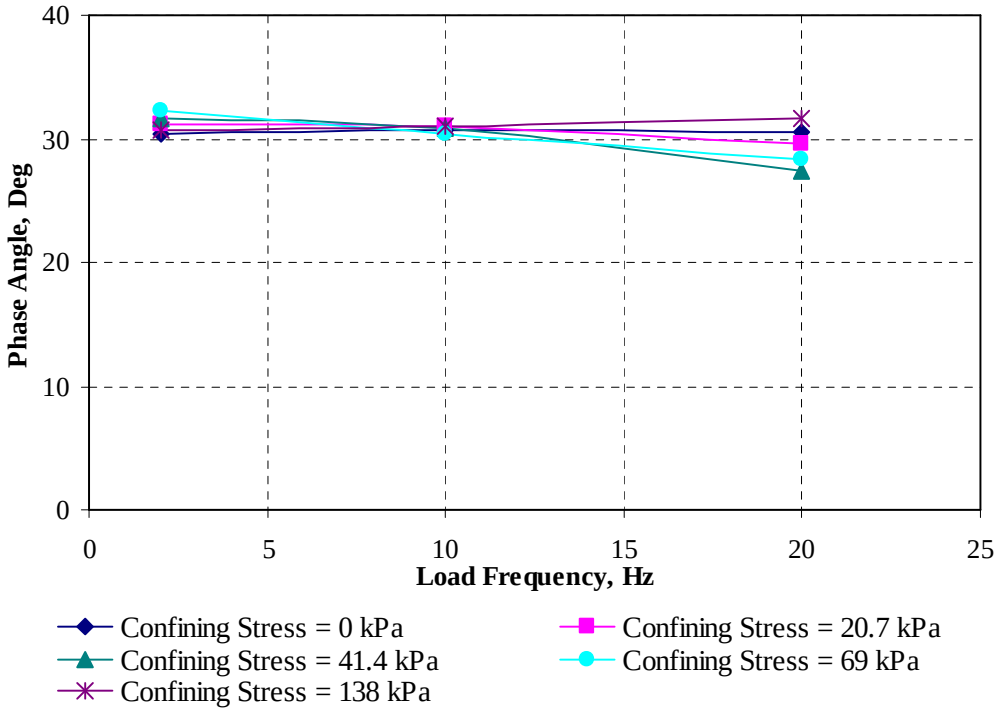

FIGURE 8.6 Effect of Loading frequency on Phase Angle for CAT A-6 at w_{opt} = 14.3%.

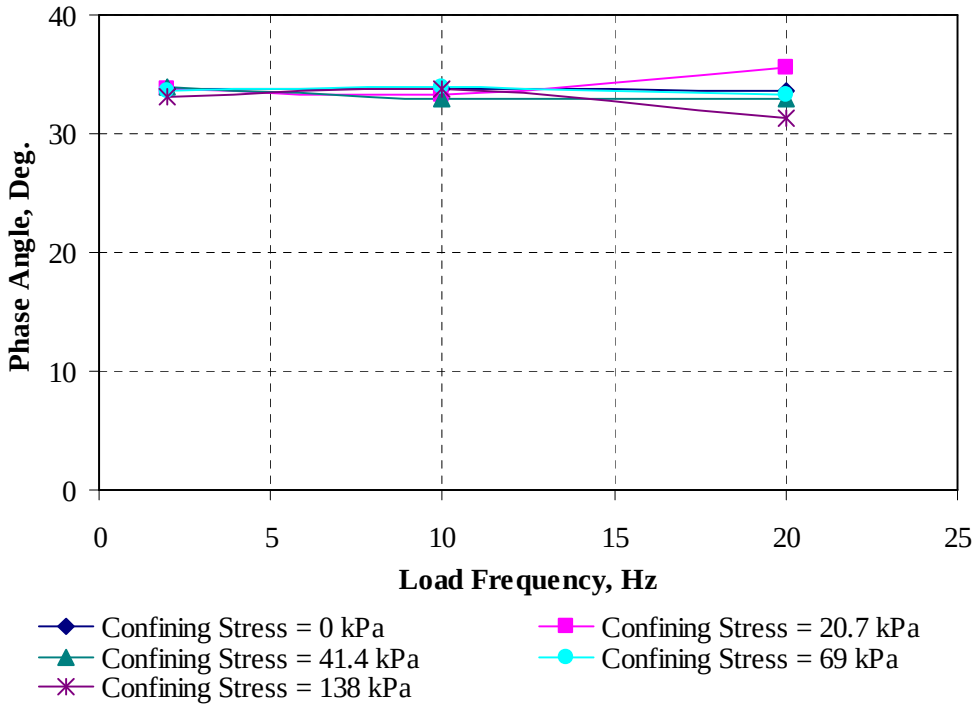

FIGURE 8.7 Effect of Loading frequency on Phase Angle for CAT A-6 at w = 17.3%.

8.4.1.3 Effect of Loading Frequency on Dynamic Modulus

As mentioned previously, dynamic modulus does not change as loading frequency increases from 2 to 20Hz, although there appears to be a slight increase in dynamic modulus at confining pressure of 138kPa. Figures 8.8 through 8.10 show the effect of loading frequency on the dynamic modulus of the CAT A-6 soil sample at w = 11.3%, w_{opt} = 14.3% and w = 17.3%. For the same loading frequency, the magnitude of the dynamic modulus decreases with an increase in water content, i.e., dynamic modulus is higher at w = 11.3% than w = 17.3% at all the loading frequencies.

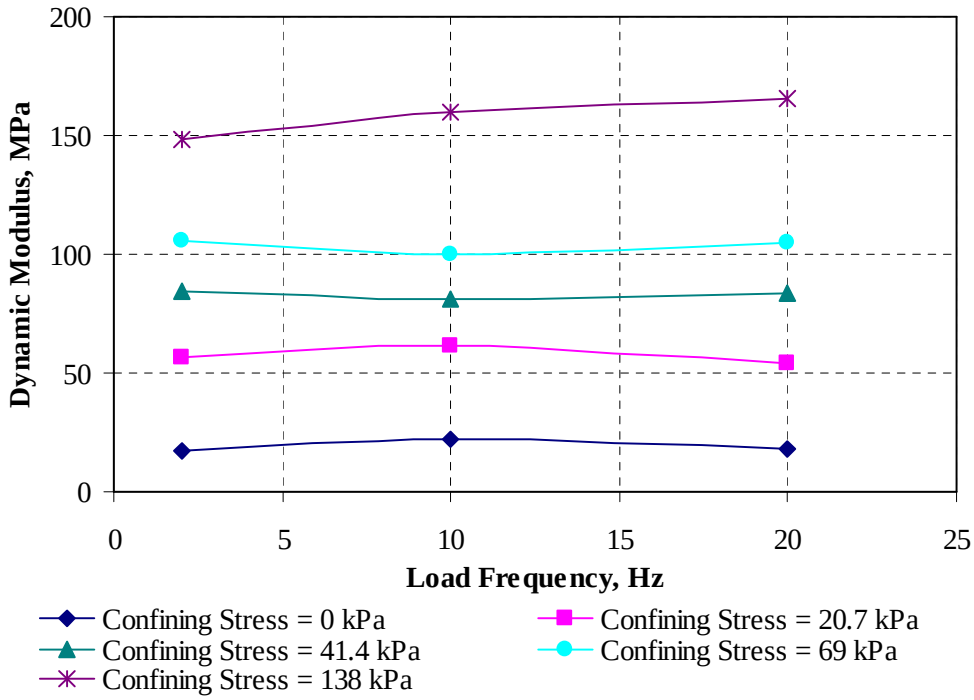

FIGURE 8.8 Effect of Loading Frequency on Dynamic Modulus at w = 11.3%.

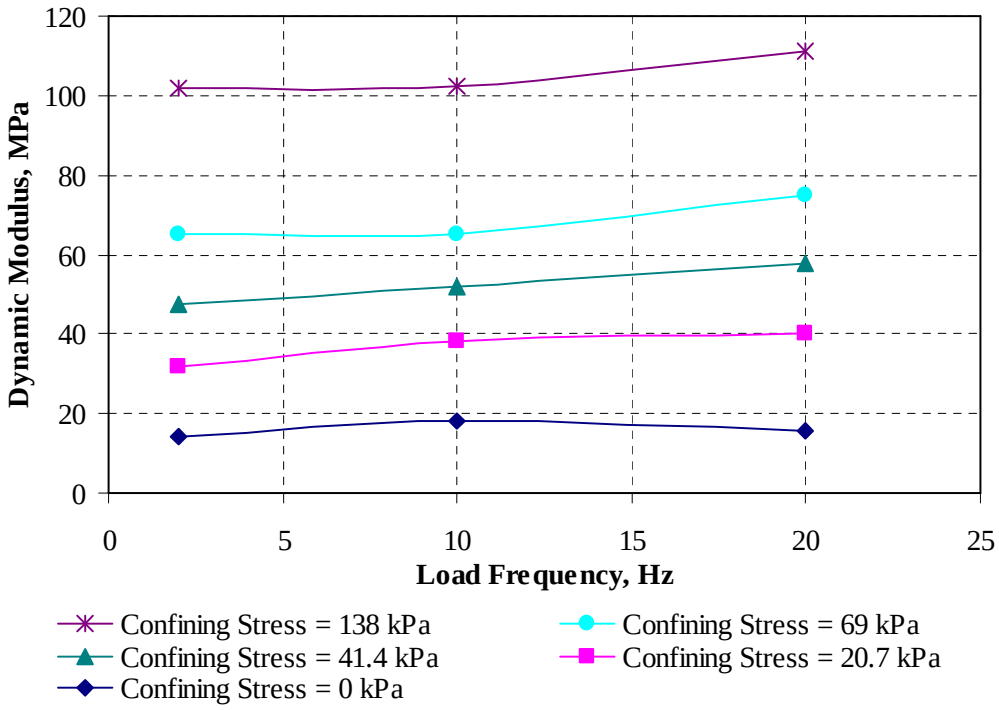

FIGURE 8.9 Effect of Loading Frequency on Dynamic Modulus w_{opt} = 14.3%.

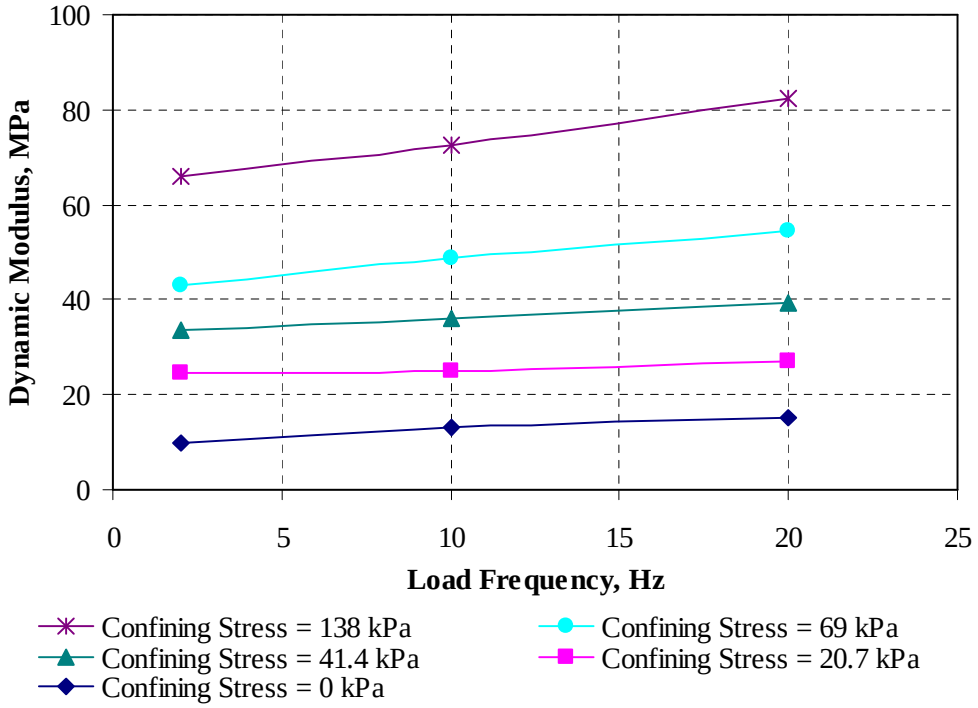

FIGURE 8.10 Effect of Loading Frequency on Dynamic Modulus at w = 17.3%.

8.4.1.4 Effect of Bulk Stress on Dynamic Properties of CAT A-6 Soil

Figure 8.11 shows the variation of dynamic modulus with bulk stress for CAT A-6 soil at w = 11.3%, w_{opt} = 14.3% w = 17.3%. The data points represent average dynamic modulus values obtained for loading frequencies of 2, 10, and 20Hz at the same confining or bulk stress. Recall that no significant difference was observed between the dynamic modulus values for the three loading frequencies at the same bulk modulus. Therefore, it is not unreasonable to use the average values to investigate the dynamic modulus behavior of the soil sample. Figure 8.11, shows that dynamic modulus of the soil sample is highly dependent on bulk stress at all the three moisture states.

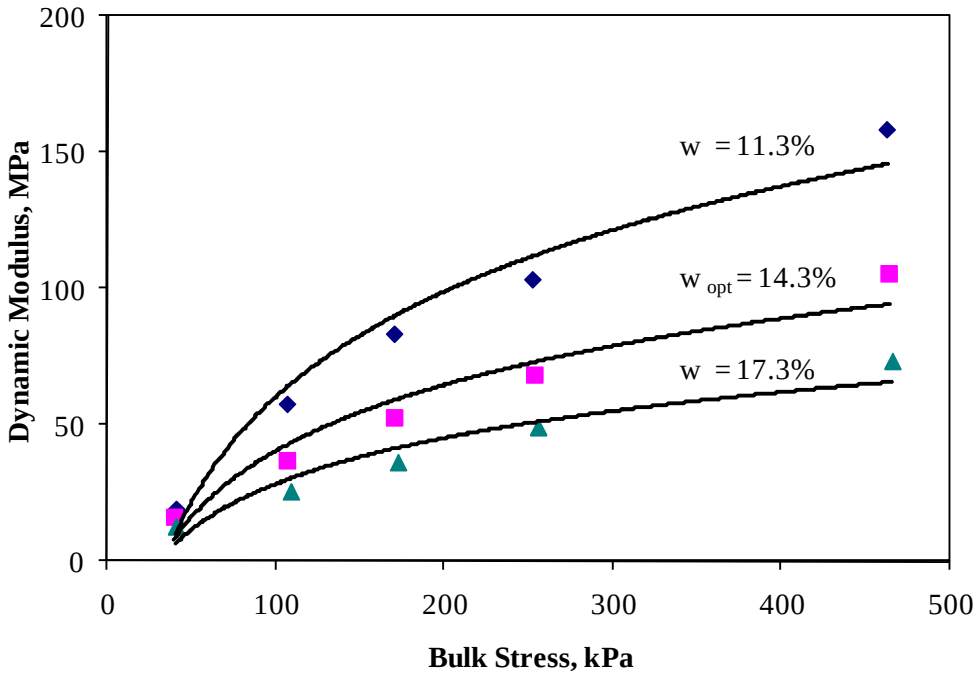

FIGURE 8.11 Variation of Dynamic Modulus of CAT A-6 Soil with Bulk Stress at three Moisture States.

From the test results presented in Figure 8.11, simple correlation analyses were conducted to establish dependency of the dynamic modulus and on bulk stress.

Generally, it was found that the logarithmic function was the best fit to describe the relationship between dynamic modulus and the applied bulk stress of the soil sample for the three moisture states. Equations 8.2 to 8.4 summarize the equations developed from regression analysis for the dynamic modulus.

$$\left|E^*\right| = 56\ ln\ (\theta)\ -195 \qquad : R^2 = 0.96 \tag{8.2}$$

$$\left|E^*\right| = 35\ ln\ (\theta)\ -121 \qquad : R^2 = 0.94 \tag{8.3}$$

$$\left|E^*\right| = 24\ ln\ (\theta)\ -84 \qquad : R^2 = 0.93 \tag{8.4}$$

where, θ = bulk stress, $\left|E^*\right|$ = dynamic modulus.

These equations show the qualitative effect of bulk stress on the dynamic modulus of when the soil sample is at optimum and 3% below or above the optimum water content. Note that these equations are valid when bulk stress is greater than 40.4 kPa (6 psi).

8.4.2 Analysis of Oil Sands Test Results

The test data for the damping properties consist of about 6,000 data points for one oil sand sample obtained from 12 stress-strain conditions and 2 test temperatures. Thus, a single data set for one oil sand sample at one test temperature comprises of 250 stress-strain data points. The analyses included damping ratio, dynamic modulus and phase angle computations and material characterization models developed to describe the behavior of oil sand materials.

Tables 8.5 through 8.7 summarize the test results for SE-09, SE-14 and AU-14 oil sand samples tested at the two test temperatures and three loading frequencies. Detailed discussions of the effects of applied total stress or bulk stress, and other loading conditions, such as temperature and frequency, on the dynamic properties of the oil sand materials are presented in subsequent subsections. The damping ratios of all the oil sands tested were generally higher at 30^{o}C than at 20^{o}C, while the dynamic moduli were higher at 20^{o}C than at 30^{o}C. The AU-14 sample had the highest damping ratios and the SE-14

sample had the lowest damping ratios. On the average, the damping ratios of AU-14 were about 47% higher than those of SE-09 at both test temperatures. On the other hand, the average dynamic moduli of SE-09 sample were about 2.5 times of the average dynamic moduli of the AU-14 sample. No significant differences were found between damping ratio and dynamic modulus of the AU-14 and SE-14 samples. The major differences between the modulus values occurred at a confining pressure of 138 kPa when the SE-14 had typically lower moduli. At the same time, the phase angles of the AU-14 sample were comparable to those of SE-14 sample. Generally the phase angles of the AU-14 sample were the highest, and the SE-09 phase angles were the lowest.

TABLE 8.5 Damping Property Test Results for SE-09 Oil Sand Sample

f (Hz)	Temperature = 20°C				Temperature = 30°C			
	θ (kPa)	$\|E^*\|$ (MPa)	D (%)	δ (Deg.)	θ (kPa)	$\|E^*\|$ (MPa)	D (%)	δ (Deg.)
2	164.4	54.1	26.0	30.3	164.3	19.8	32.7	36.2
5	164.1	87.8	25.0	29.3	164.0	28.6	33.8	35.8
10	163.8	110.4	25.3	29.9	163.7	34.2	34.4	36.4
2	248.4	171.2	13.4	14.9	248.2	77.3	23.8	22.1
5	248.1	189.7	15.9	17.8	248.0	103.5	26.1	29.8
10	247.9	205.1	18.2	21.0	247.8	112.4	27.7	29.9
2	458.3	287.1	9.2	12.0	458.2	224.5	14.4	20.0
5	457.6	308.1	12.1	14.7	457.5	235.2	17.0	20.8
10	456.1	327.5	13.7	15.0	455.9	246.4	19.6	20.7
2	666.9	373.3	8.0	10.5	666.8	311.4	11.7	17.0
5	666.2	411.5	10.0	12.5	667.4	340.0	12.1	16.3
10	667.1	502.5	9.6	14.7	666.1	414.2	10.9	16.7

θ = bulk stress, $|E^*|$ = dynamic modulus, D = damping Ratio, and δ = phase angle.

TABLE 8.6 Damping Property Test Results for SE-14 Oil Sand Sample

f (Hz)	Temperature = 20°C				Temperature = 30°C			
	θ (kPa)	$\|E^*\|$ (MPa)	D (%)	δ (Deg.)	θ (kPa)	$\|E^*\|$ (MPa)	D (%)	δ (Deg.)
2	164.6	15.9	33.0	39.4	172.0	8.6	35.3	42.4
5	164.2	27.2	34.3	40.9	165.9	12.1	35.1	42.8
10	164.4	43.5	33.1	42.7	166.6	16.3	36.5	45.3
2	248.2	52.2	25.6	31.0	253.8	12.6	29.8	33.7
5	247.9	66.6	27.2	33.0	249.4	20.5	32.4	34.7
10	249.0	93.3	26.2	32.2	251.2	32.1	33.6	35.8
2	459.1	161.8	14.2	15.6	463.2	35.6	23.8	23.5
5	458.5	176.8	16.0	18.9	459.6	54.2	24.4	24.4
10	458.2	206.9	16.7	20.5	458.7	111.6	21.7	29.7
2	668.9	263.3	9.8	12.6	671.9	91.1	18.5	18.3
5	667.9	286.7	11.3	14.4	667.4	124.8	17.6	18.3
10	666.1	343.2	11.9	18.4	667.8	240.8	14.2	18.8

TABLE 8.7 Damping Property Test Results for AU-14 Oil Sand Sample

f (Hz)	Temperature = 20°C				Temperature = 30°C			
	θ (kPa)	$\|E^*\|$ (MPa)	D (%)	δ (Deg.)	θ (kPa)	$\|E^*\|$ (MPa)	D (%)	δ (Deg.)
2	173.9	12.9	35.6	40.4	172.0	11.1	40.7	42.0
5	174.1	25.1	36.6	42.1	173.1	12.4	40.5	44.2
10	173.1	45.0	35.7	41.7	172.4	20.1	40.7	43.2
2	254.9	30.6	29.0	35.9	253.7	17.3	36.5	32.6
5	252.9	56.0	32.0	38.3	254.5	22.5	37.2	39.0
10	253.7	106.9	27.6	32.6	254.5	36.7	38.0	38.5
2	462.1	184.5	14.1	16.3	461.9	63.4	22.5	25.4
5	462.0	217.2	15.2	17.0	461.6	86.9	23.2	29.4
10	462.0	241.2	16.0	16.0	461.2	139.7	23.2	30.1
2	670.4	296.4	9.5	11.0	670.3	161.4	18.5	16.1
5	670.1	316.6	11.8	12.5	669.0	180.7	19.7	17.7
10	668.8	334.3	13.7	12.0	666.4	252.6	16.3	17.3

θ = bulk stress, $|E^*|$ = dynamic modulus, D = damping Ratio, and δ = phase angle.

8.4.2.1 Effect of Loading Frequency and Bulk Stress on Damping Ratio

A summary of the effects of loading frequency and bulk stress on damping ratio of the three oil sand materials is presented in Tables 8.5 to 8.7. Bulk stress was used in the analysis since the deviator stress was kept constant during the testing. At a constant bulk stress, there was little or no difference between the damping ratios measured at the three loading frequencies 2, 5 and 10Hz. This observation is clearly presented in Figures 8.12 to 8.14. The figures also show the effect of loading frequency on damping ratio of SE-09, SE-14 and AU-14 oil sand samples at 20^{o}C and at 30^{o}C. At a constant confining stress there is no apparent difference between damping ratio values obtained at the three loading frequencies. Therefore, it was reasonable to use average values to study the combined effect of bulk stress and bitumen content on damping ratio for the three oil sand materials. Figures 8.15a and 8.15b show the effect of bulk stress and bitumen content on damping ratio for the oil sand materials tested at 20^{o}C and at 30^{o}C.

The trends observed in these figures show that damping ratios of the oil sand materials decrease in proportion with bulk stress. As bulk stress increases, damping ratio typically decreases in all the three samples at both test temperatures. The probable explanation is that the oil sand materials become stiffer as bulk stress increases to result in less energy dissipation. Moreover, under constant confining stress and loading frequency, damping ratio of the oil sand materials at 20^{o}C was lower than at 30^{o}C. This is expected because at 20^{o}C, the oil sand material, being viscoelastic, would dissipate less energy compared to 30^{o}C. The AU-14 sample (w_b = 14.5%) generally had higher damping ratios while SE-09 sample (w_b = 8.5%) had the lowest damping ratio. Also, the AU-14 generally had higher damping ratios than SE-14 sample (w_b = 13.3%) did although the difference appeared to be minimal. Generally, it appears that the amount of bitumen content had an effect on the damping ratio of the oil sand materials.

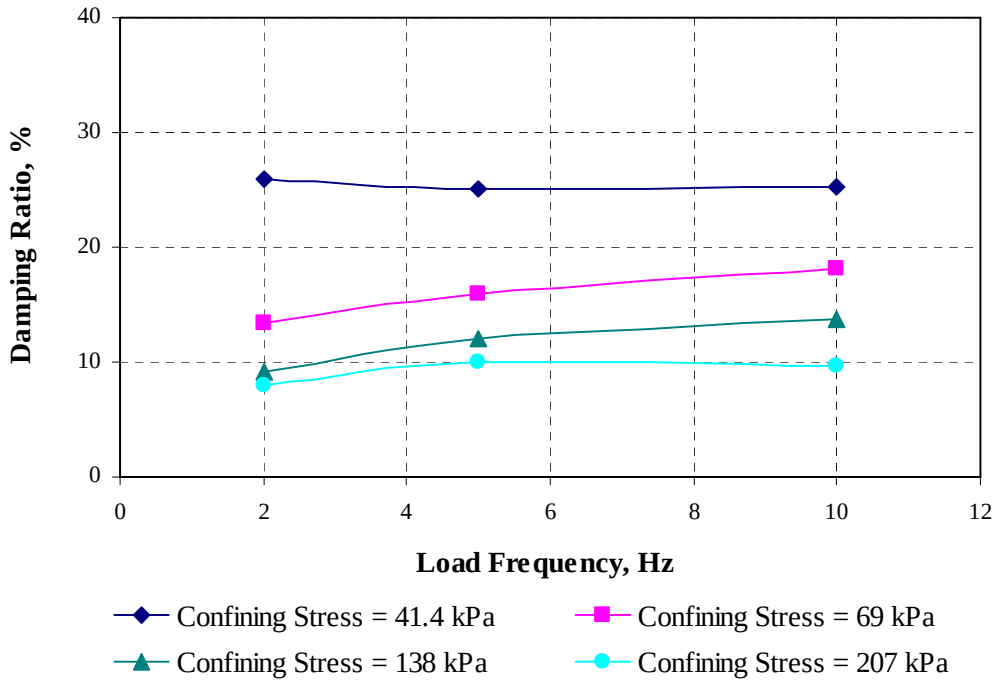

(a) Temperature = 20°C

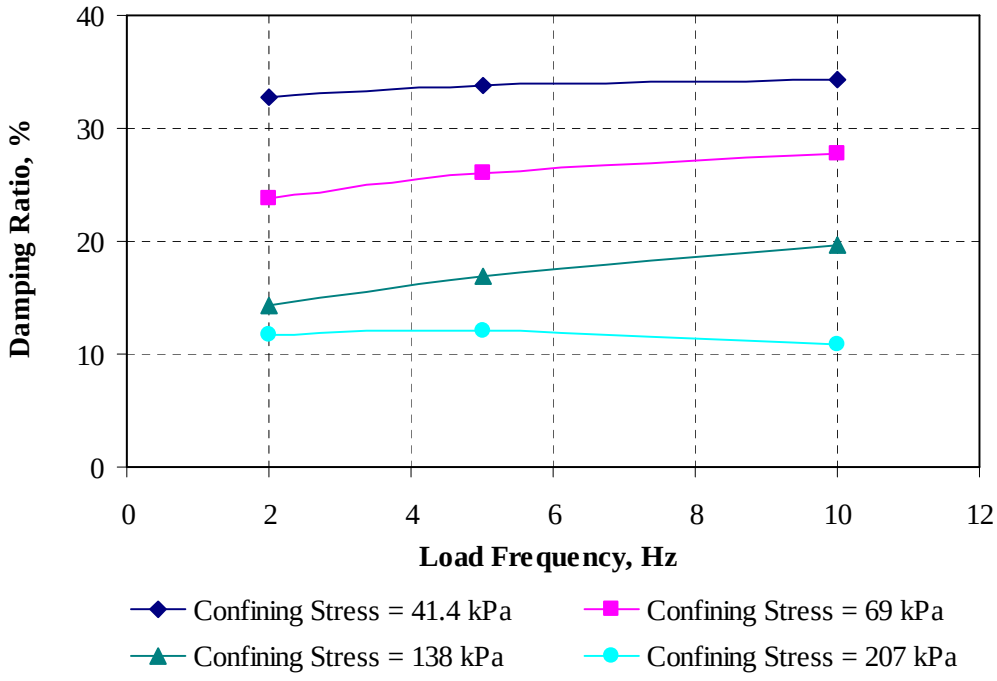

(b) Temperature = 30°C

FIGURE 8.12 Effect of Loading Frequency on Damping Ratio for SE-09.

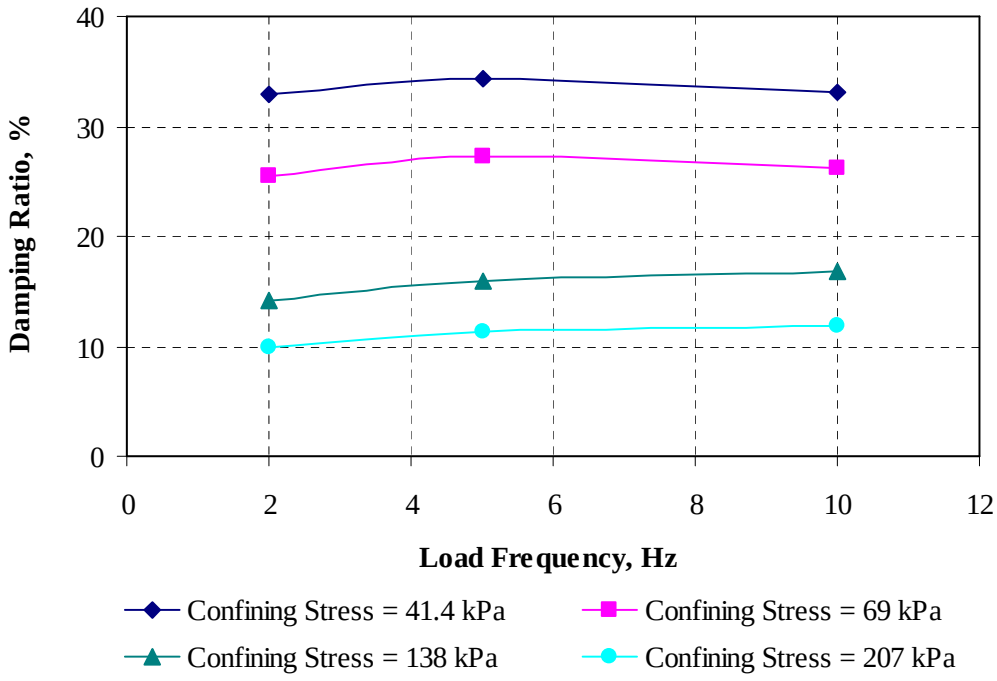

(a) Temperature = 20°C

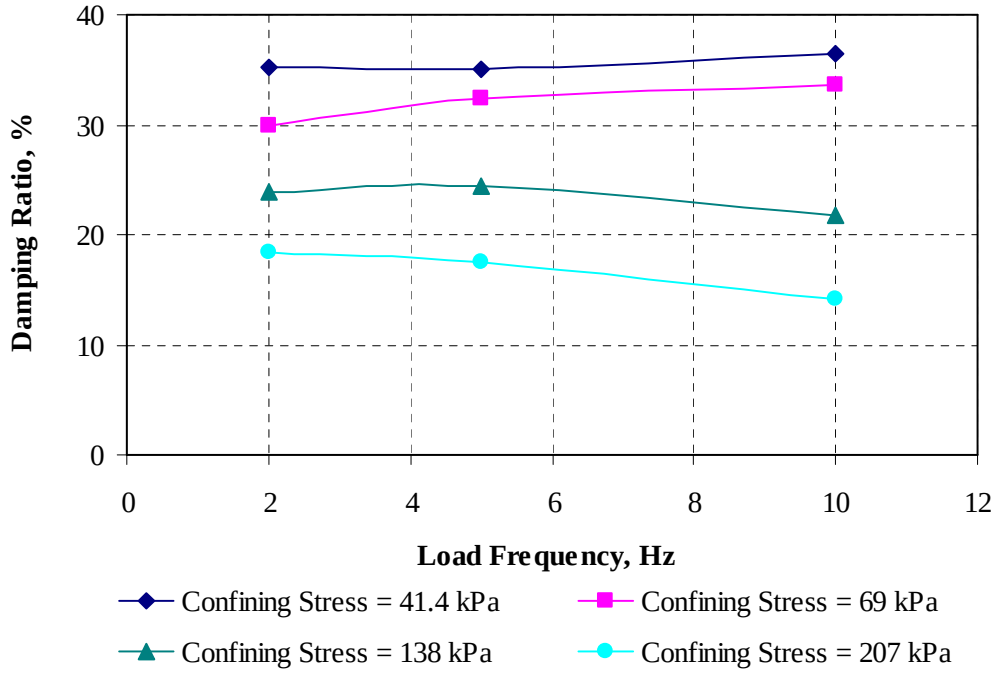

(b) Temperature = 30°C

FIGURE 8.13 Effect of Loading Frequency on Damping Ratio for SE-14.

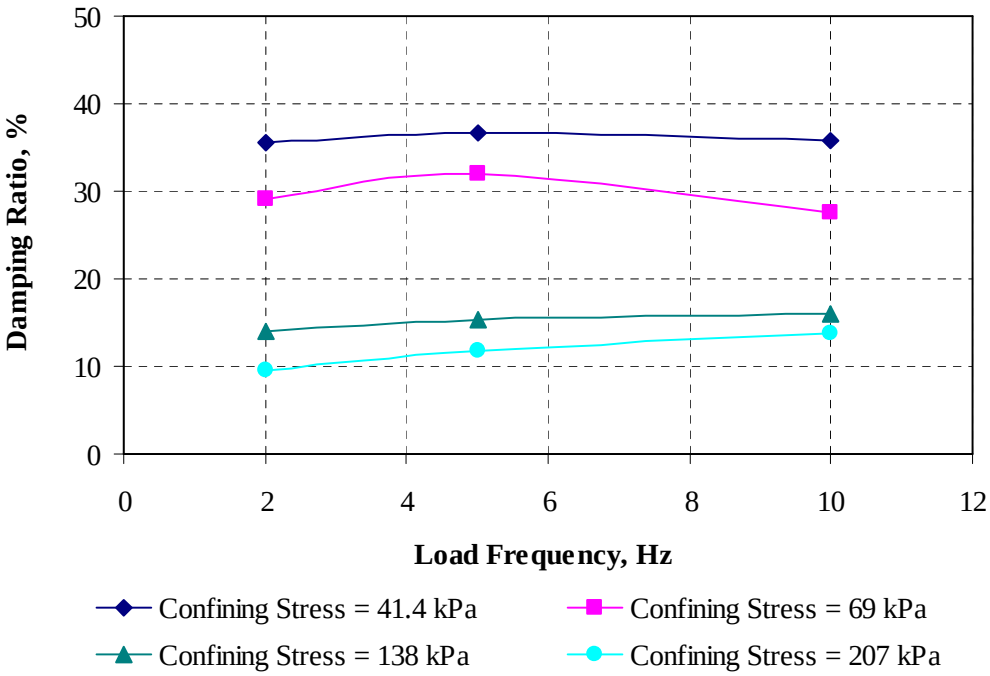

(a) Temperature = 20°C

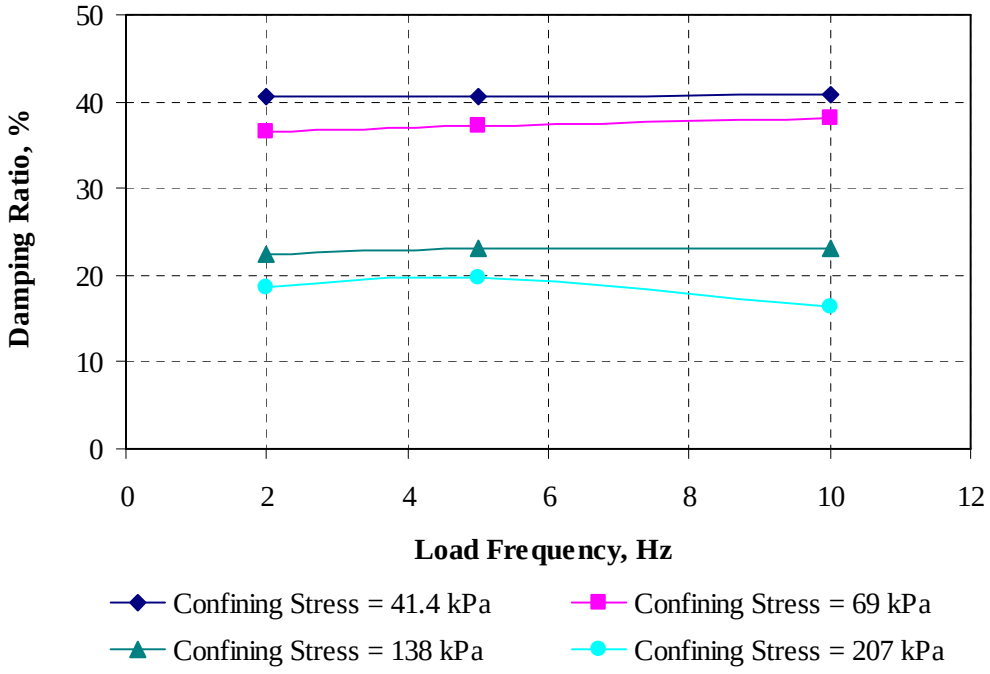

(b) Temperature = 30°C

FIGURE 8.14 Effect of Loading Frequency on Damping Ratio for AU-14.

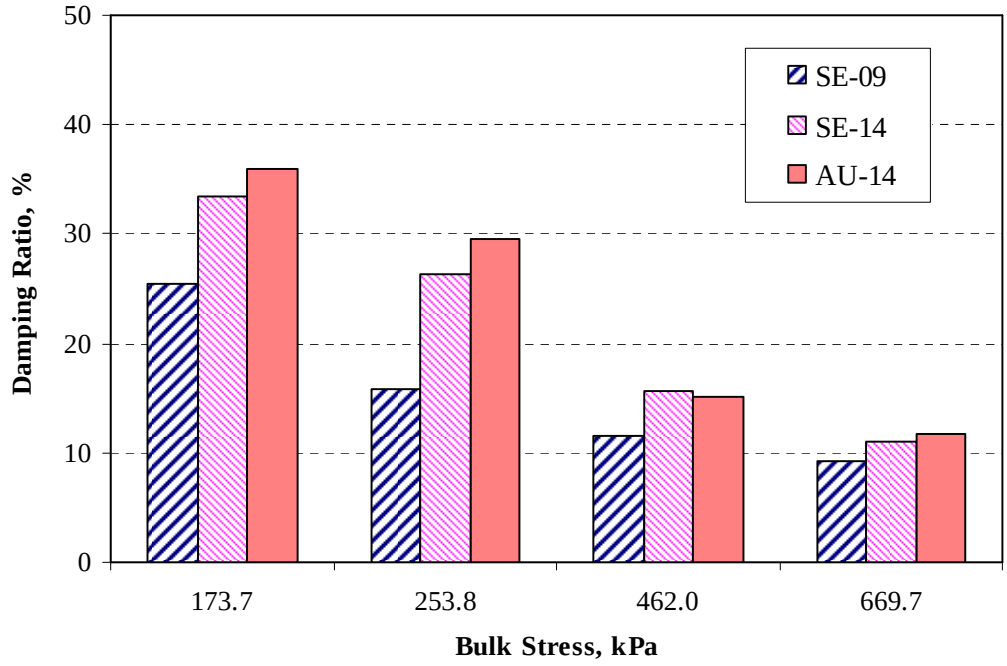

(a) Temperature = 20°C

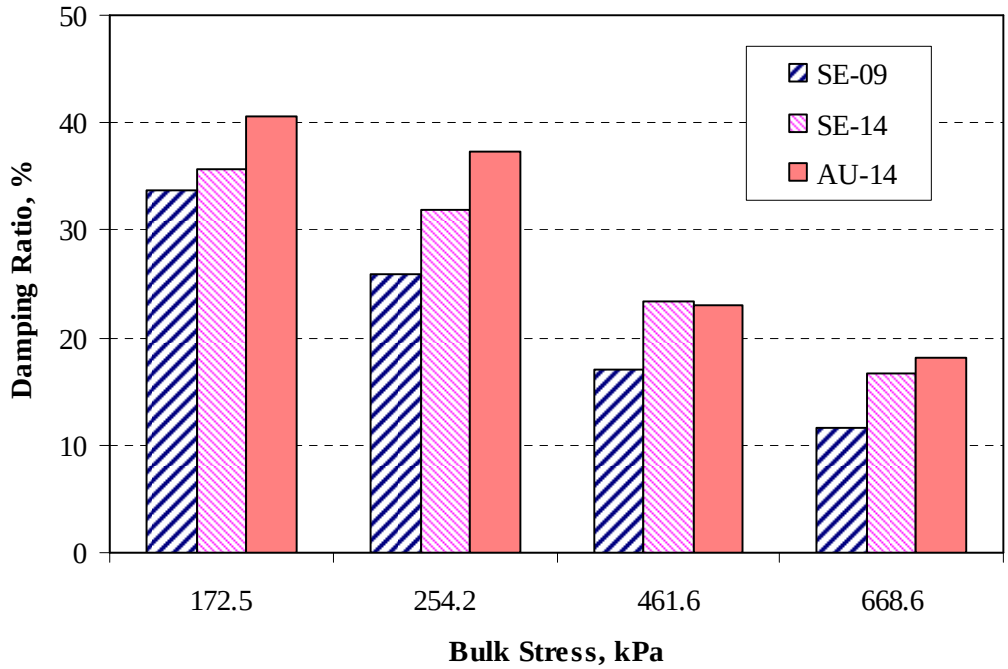

(b) Temperature = 30°C

FIGURE 8.15 Effect of Bulk Stress on Damping Ratio for Oil Sand Samples.

8.4.2.2 Damping Ratio Variation with Axial Strain of Oil Sand Samples

Figures 8.16 through 8.18 show damping ratio as a function of axial strains recorded at 20°C and at 30°C for the oil sands. In these figures, the regression equations are provided for each oil sand sample at the two test temperatures. The correlations were obtained from the combined data for each oil sand at 20°C and at 30°C. The results indicate that strong relationships generally exist between damping ratio and axial strain (high R^2 values in the range of 0.7 to 0.92). Generally, damping ratio increases with the increase in axial strain. Considerable scatter exists in the data, especially after 0.1% axial strain, but the effect of strain on damping ratio is still apparent.

At axial strains less than 0.1%, there is a rapid increase in damping ratio for the three oil sand materials. However, at axial strains greater than 0.1%, the damping ratio values become essentially constant for all the materials. These trends suggest that there could be major difference between damping ratio of oil sand material at specific strain values. However, no definite conclusion for the observed trends can be made. It appears energy dissipation might be constant at high strain levels, compared to the relatively lower ones.

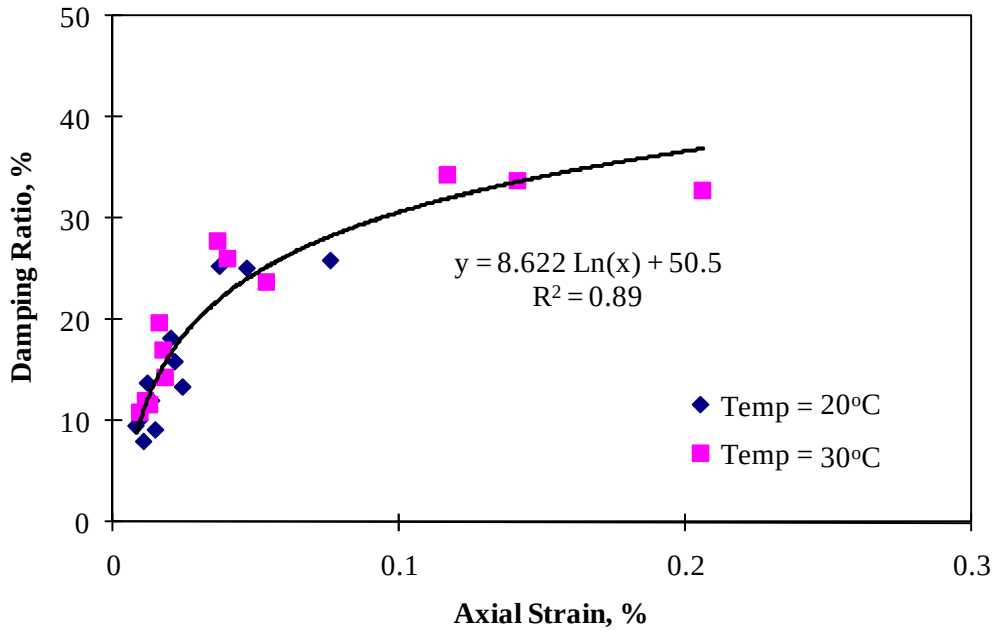

FIGURE 8.16 Damping Ratio Varying with Axial Strain for SE-09 Oil Sand Sample.

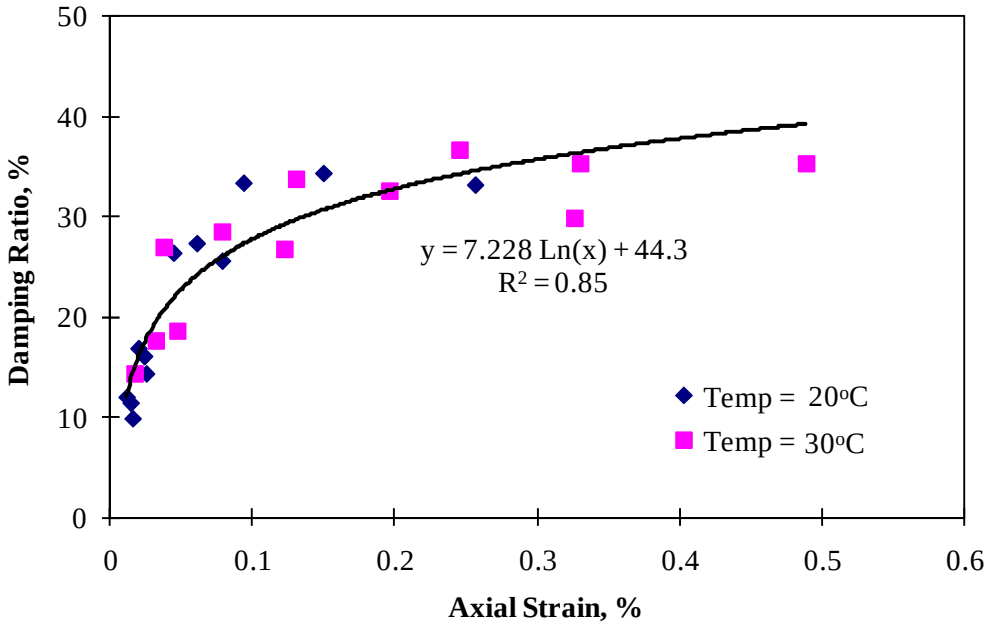

FIGURE 8.17 Damping Ratio Varying with Axial Strain for SE-14 Oil Sand Sample.

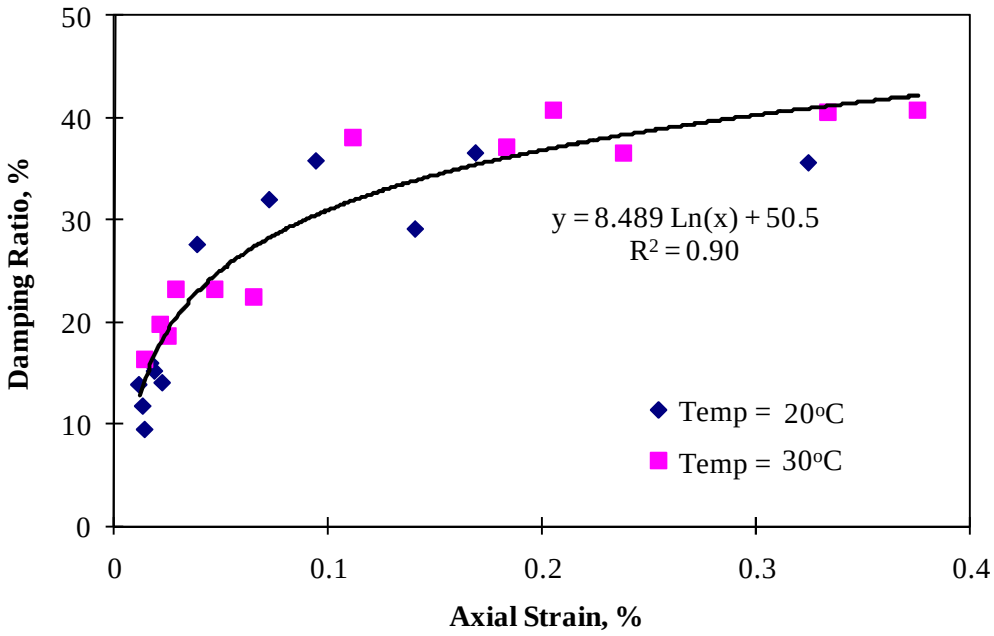

FIGURE 8.18 Damping Ratio Varying with Axial Strain for AU-14 Oil Sand Sample.

8.4.2.3 Effect of Loading Frequency on Dynamic Modulus

Figures 8.19 to 8.21 show the measured dynamic modulus results for the three oil sand samples as a function of loading frequency at 20°C and at 30°C. For the same loading frequency, the magnitude of the dynamic modulus in general decreases with an increase in temperature. Also, at the same test temperature, the magnitude of the dynamic modulus generally increases with an increase in the loading frequency although in some instances the increase appears not to be significant. For example, such an increase was rather high in the SE-14 and AU-14 materials at 30^{o}C and high confining stress states. An average increase of 40% in dynamic modulus was observed in the SE-09 sample when the loading frequency increases from 2 to 10Hz. Under the same conditions, there was more than 70% increase in the dynamic modulus values for both SE-14 and AU-14 samples. Clyne, et al. (2003) reported a similar effect on the stiffness of bituminous materials at increasing loading frequency.

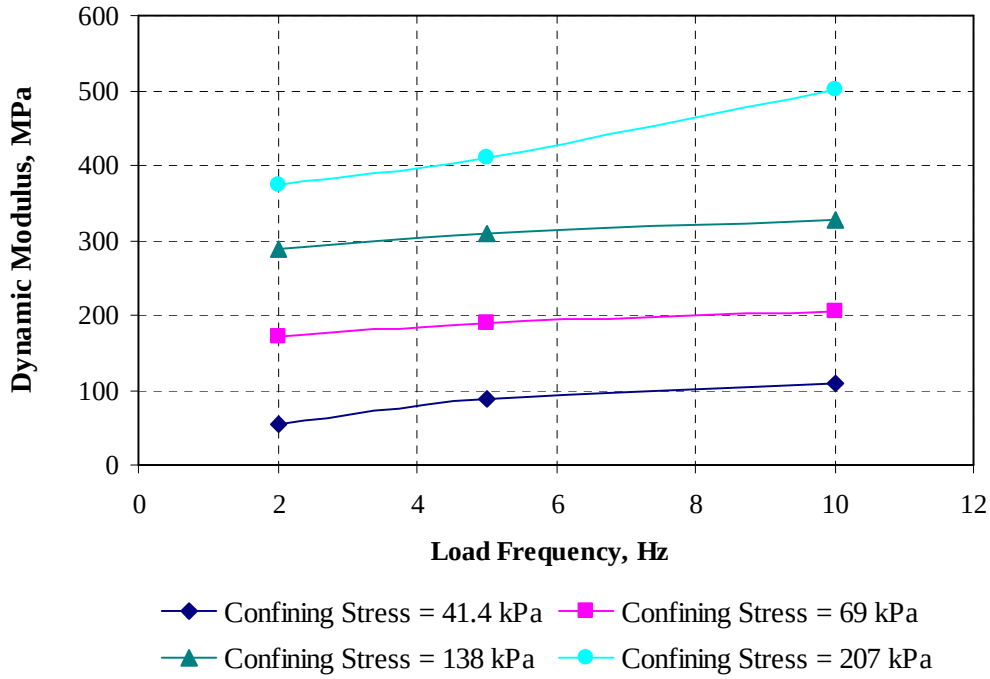

(a) Temperature = 20°C

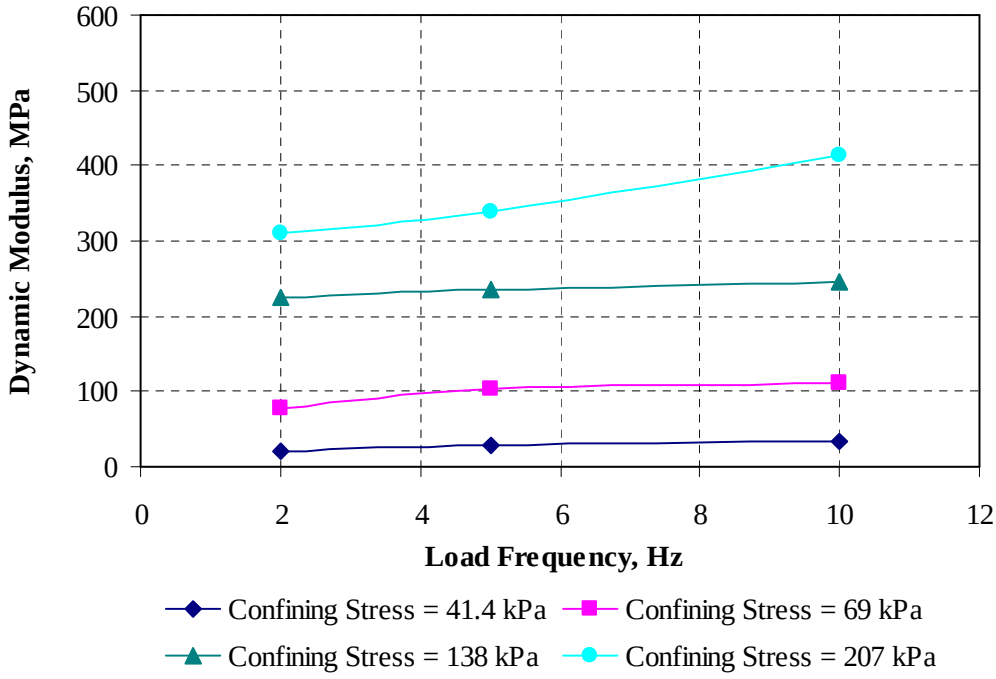

(b) Temperature = 30°C

FIGURE 8.19 Effect of Loading Frequency on Dynamic Modulus for SE-09.

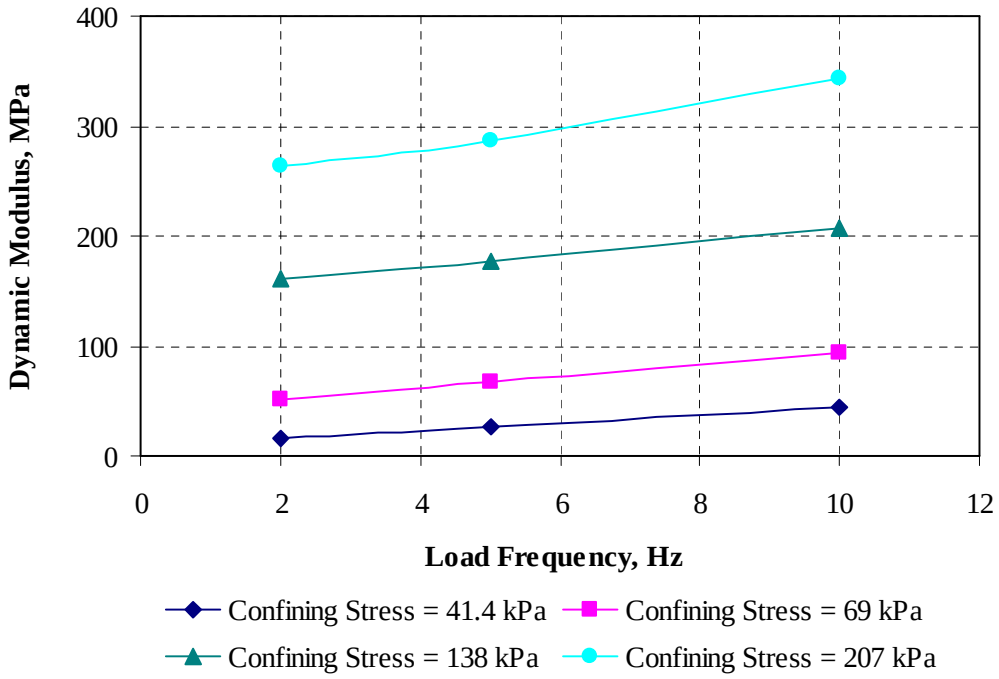

(a) Temperature = 20°C

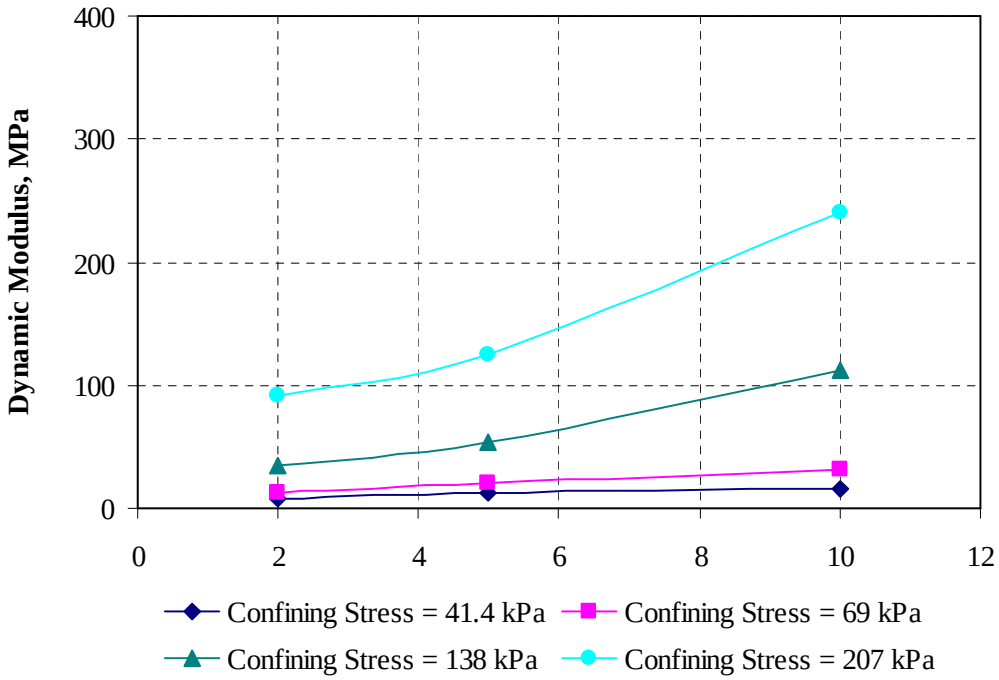

(b) Temperature = 30°C

FIGURE 8.20 Effect of Loading Frequency on Dynamic Modulus for SE-14.

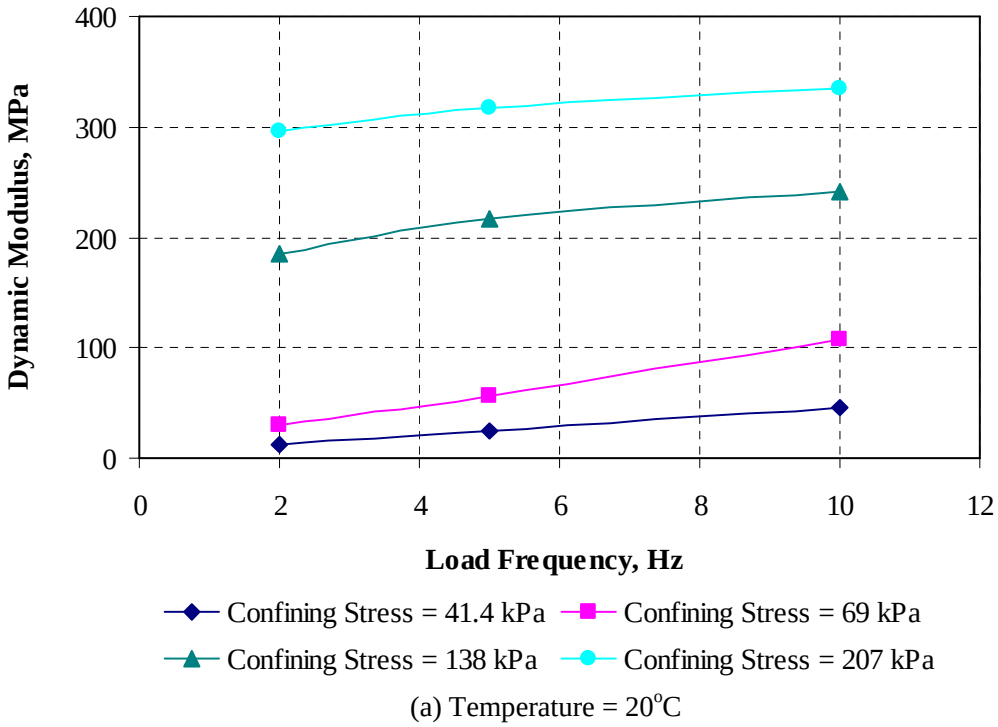

(a) Temperature = 20°C

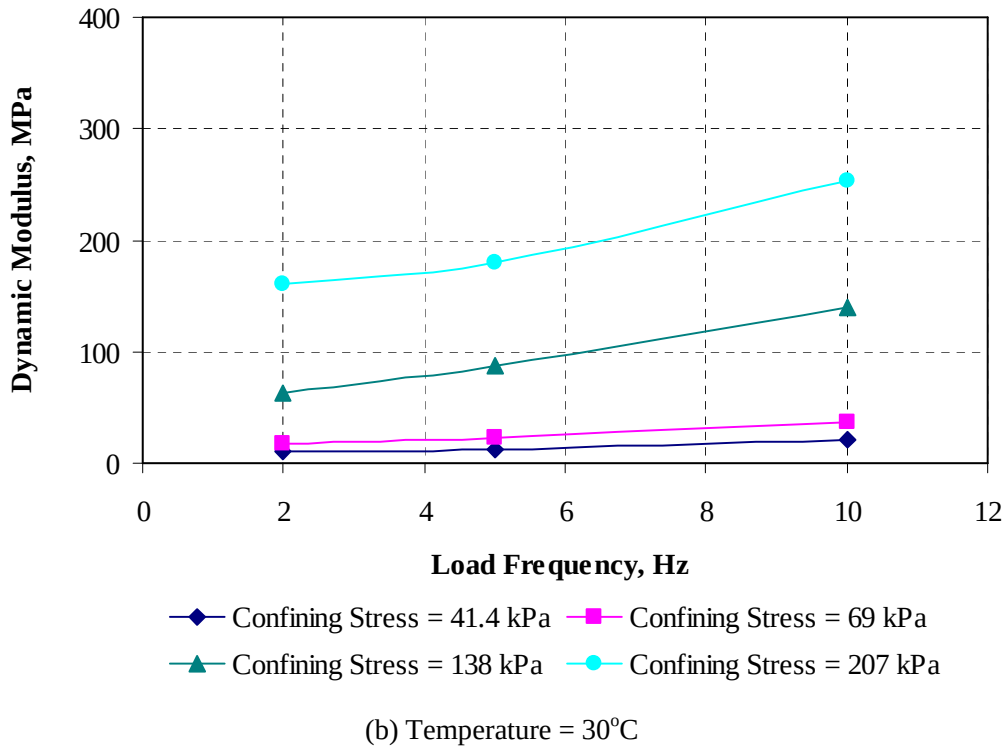

(b) Temperature = 30°C

FIGURE 8.21 Effect of Loading Frequency on Dynamic Modulus for AU-14.

8.4.2.3 Effect of Bulk Stress on Dynamic Modulus

Figures 8.22 through 8.24 show the effect of bulk stress on dynamic modulus observed at the three loading frequencies and two test temperatures. The dynamic moduli of the oil sand samples generally increase in proportion to the bulk stress. This is typical of geomaterials in which stiffness increases with increasing confining or bulk stress. As such, the dynamic moduli of all the oil sand materials at 20^{o}C were higher in magnitude than the values at 30^{o}C. This is consistent with general research findings on asphalt materials, which show high dynamic modulus values measured at low temperatures when compared to the low values at high temperatures.

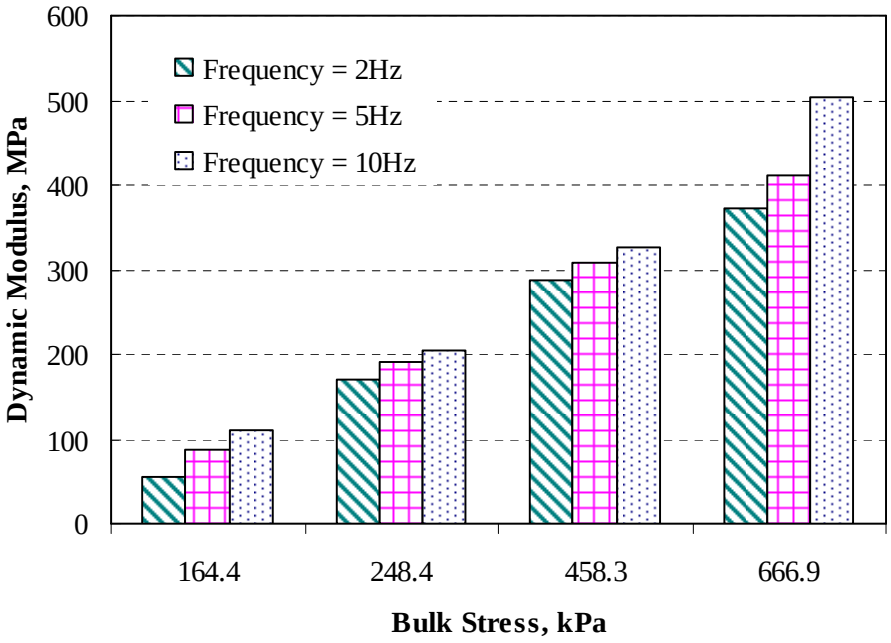

(a) Temperature = 20°C

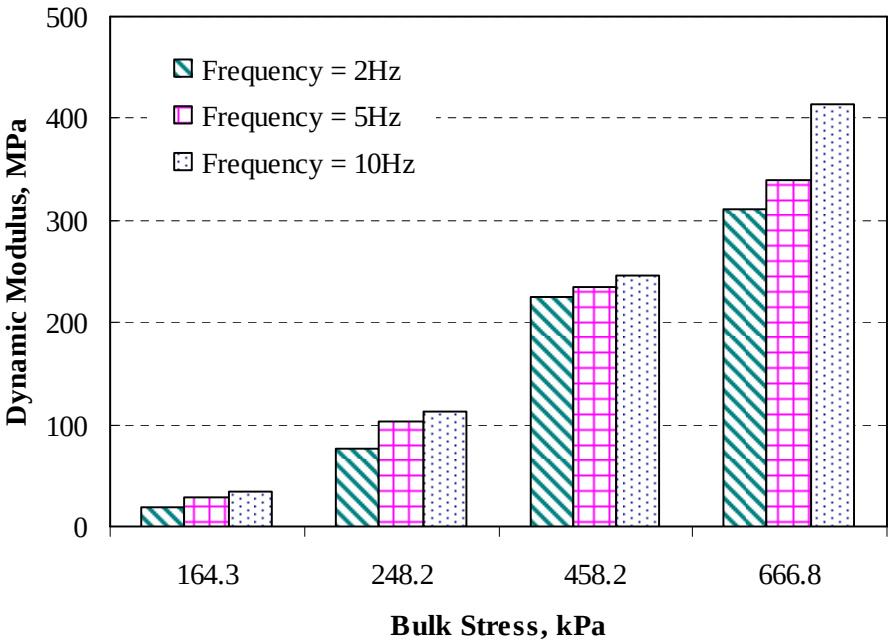

(b) Temperature = 30°C

FIGURE 8.22 Effect of Bulk Stress on Dynamic Modulus for SE-09.

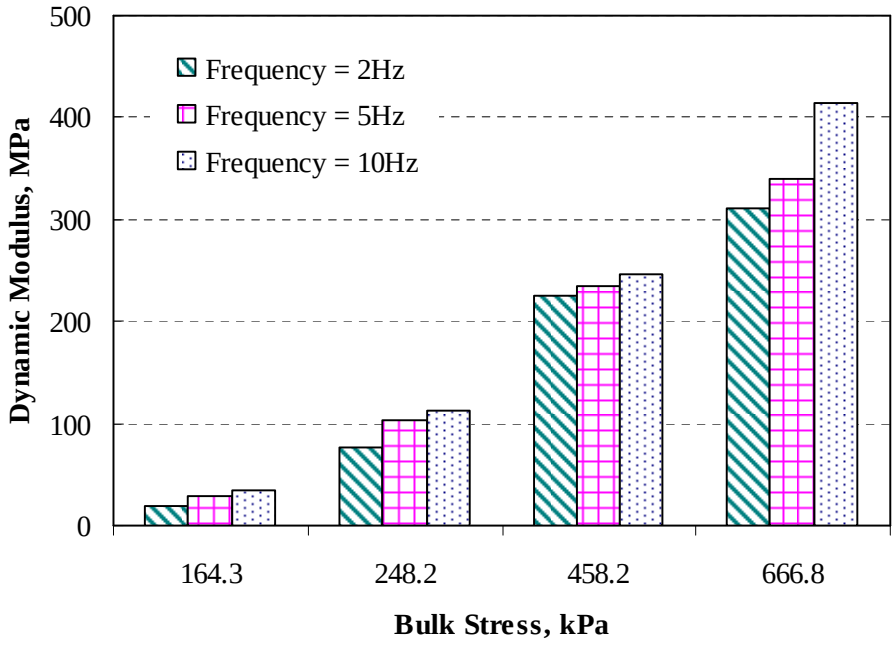

(a) Temperature = 20°C

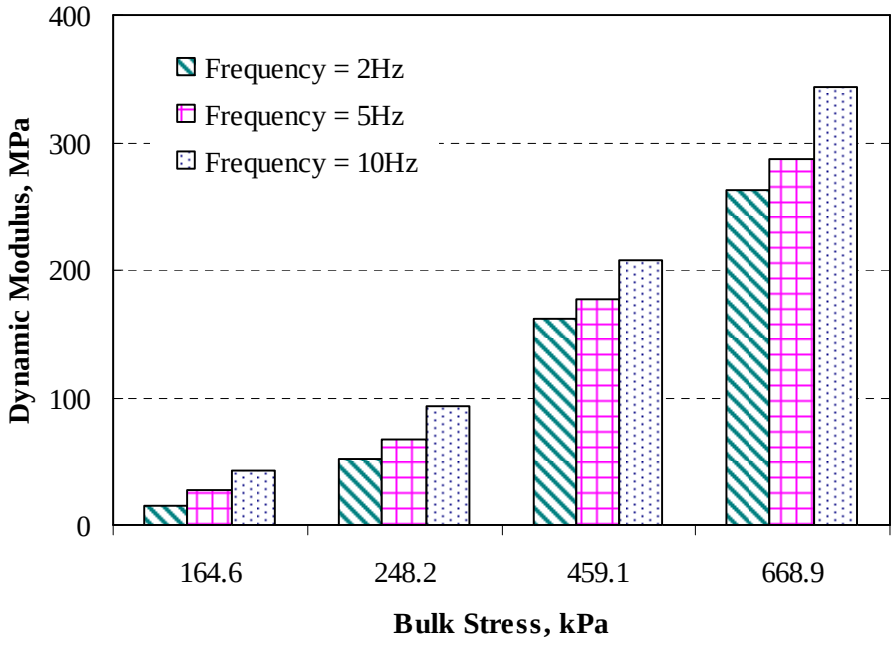

(b) Temperature = 30°C

FIGURE 8.23 Effect of Bulk Stress on Dynamic Modulus for SE-14.

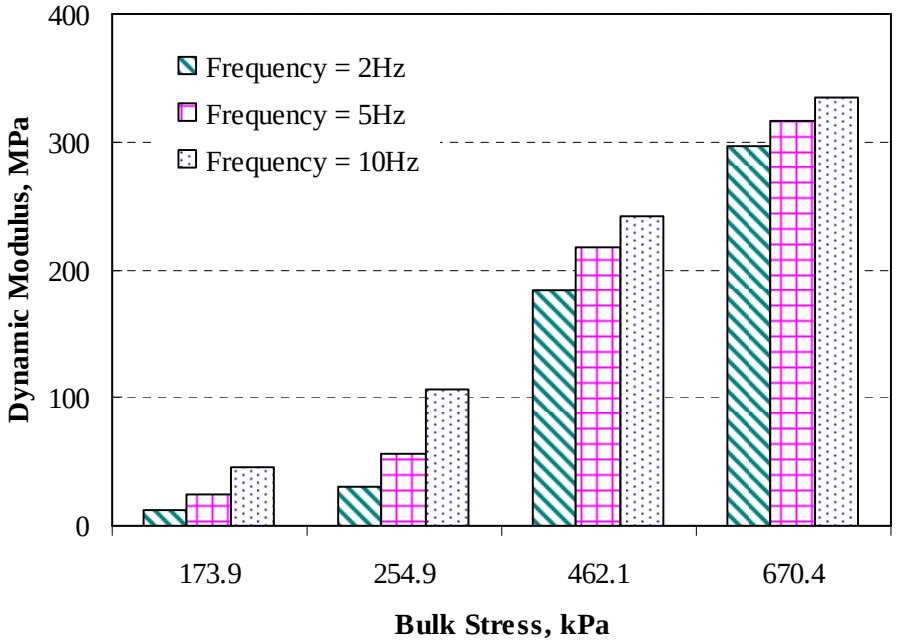

(a) Temperature = 20°C

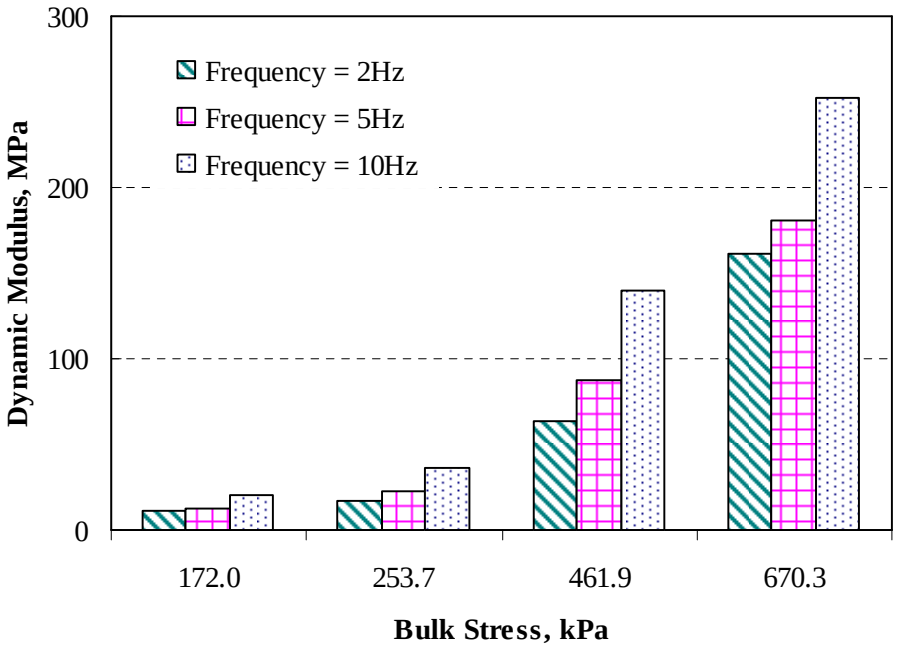

(b) Temperature = 30°C

FIGURE 8.24 Effect of Bulk Stress on Dynamic Modulus for AU-14.

8.4.2.4 Effect of Loading Frequency on Phase Angle

Figures 8.25 through 8.27 show the variations of phase angles of the three oil sand materials with loading frequency at various confining stresses at 20°C and at 30°C. For all the three oil sand materials, loading frequency has in general, little effect on the phase angle. Under the same test conditions, the phase angles of all the oil sand materials are higher at 30°C than at 20°C. This is also observed in asphalt mixtures with higher phase angles obtained at higher temperatures than lower temperatures. Generally, at the same loading frequency, the phase angle values of the oil sands are much larger at lower confining stresses.

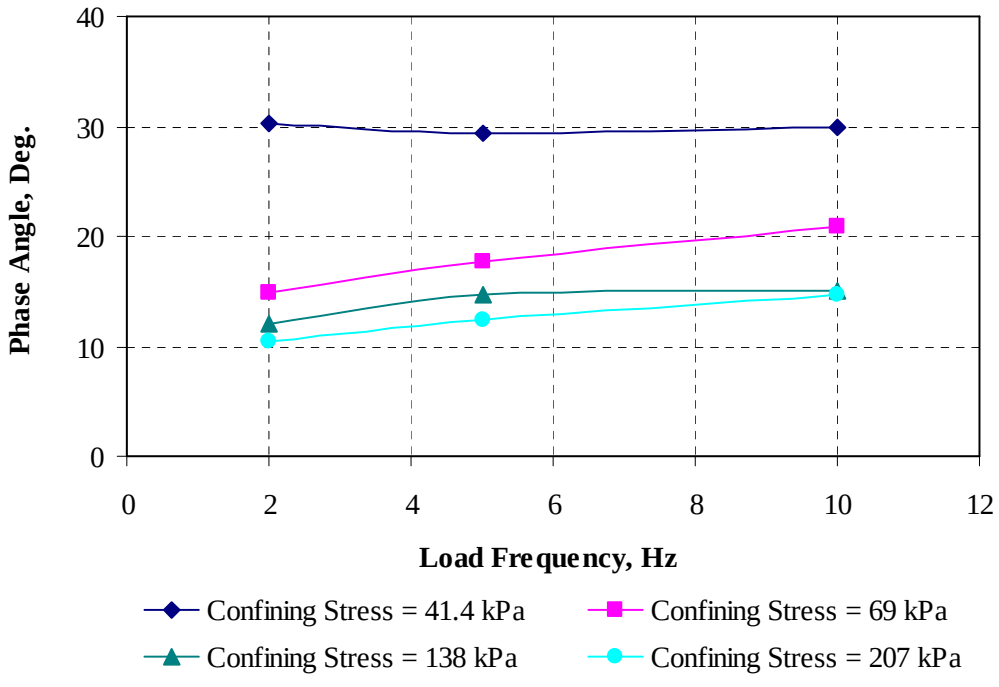

(a) Temperature = 20°C

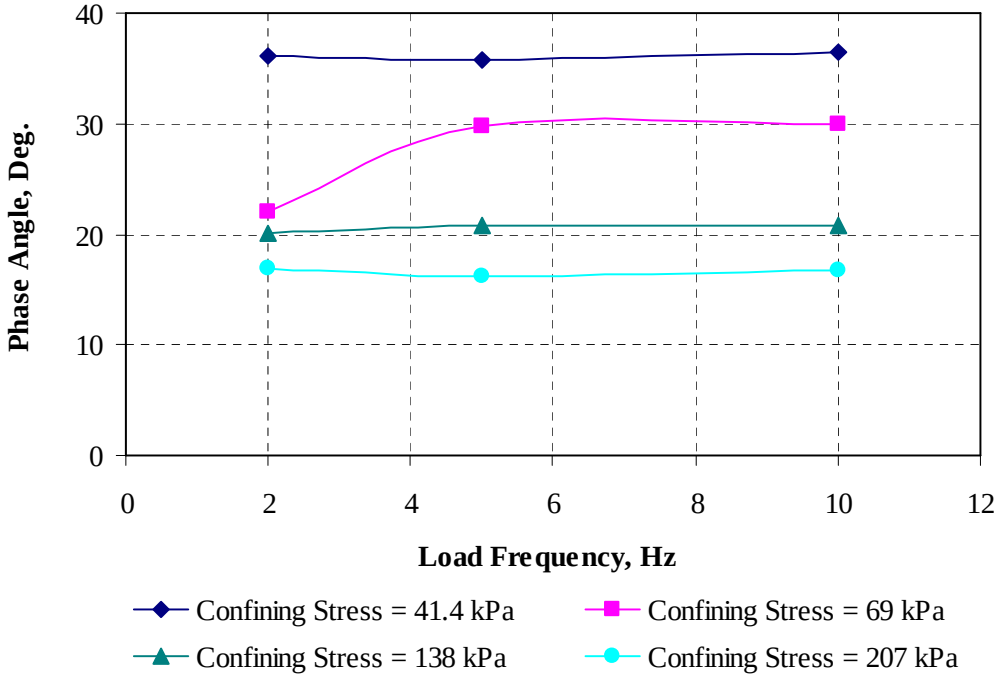

(b) Temperature = 30°C

FIGURE 8.25 Effect of Loading Frequency on Phase Angle for SE-09.

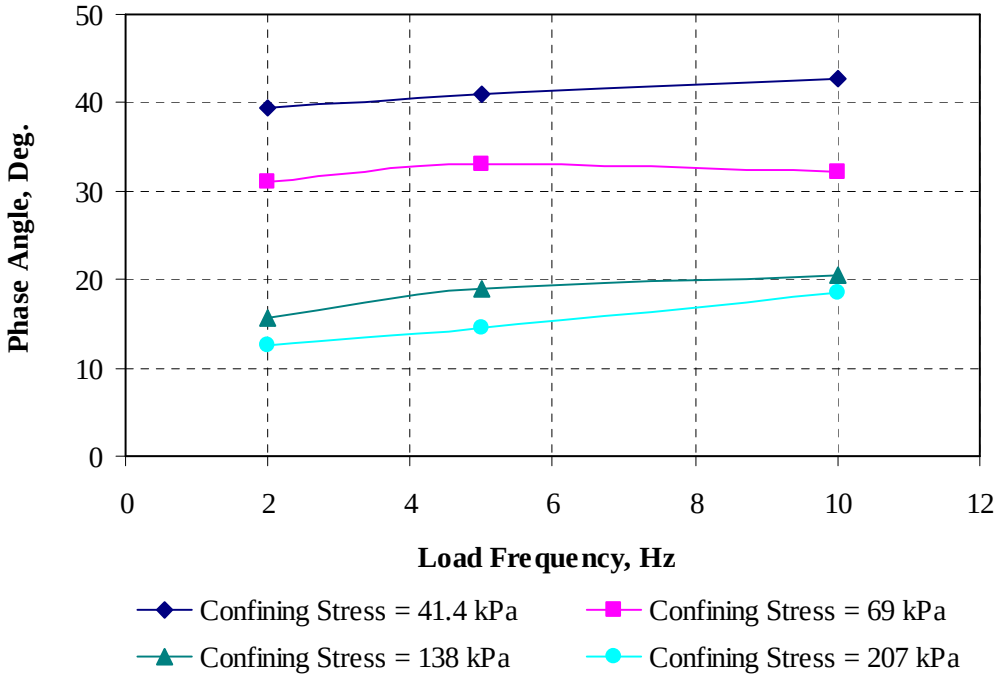

(a) Temperature = 20°C

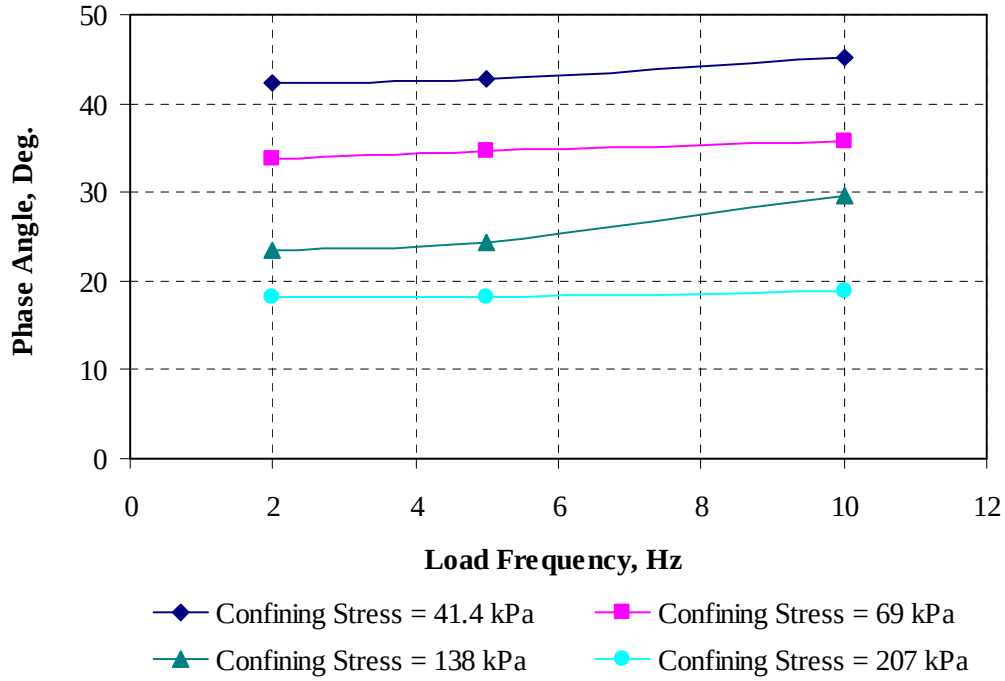

(b) Temperature = 30°C

FIGURE 8.26 Effect of Loading Frequency on Phase Angle for SE-14.

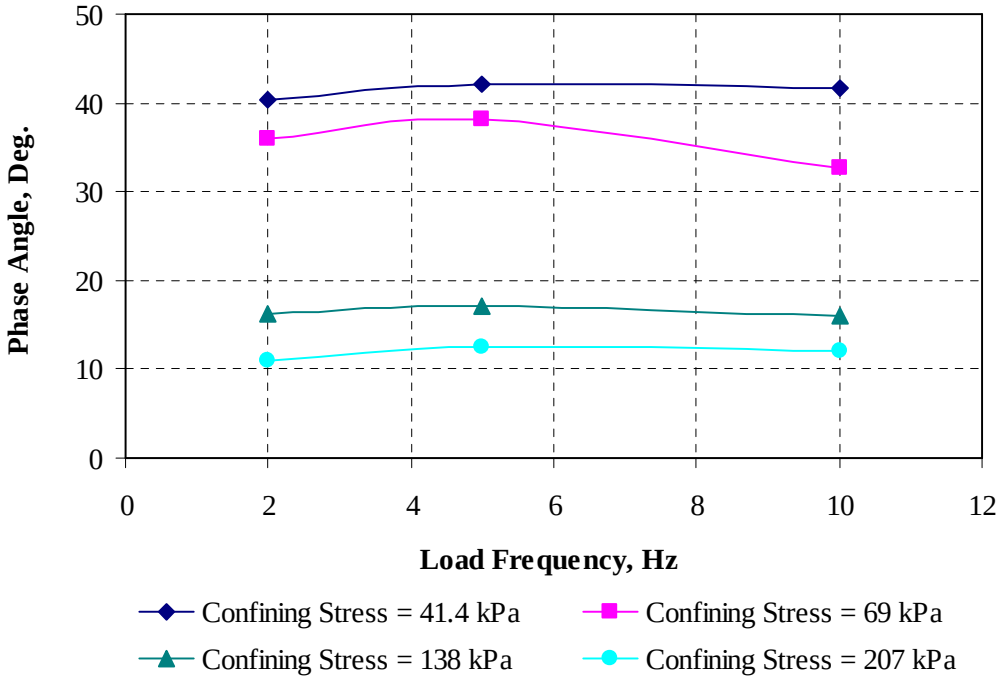

(a) Temperature = 20°C

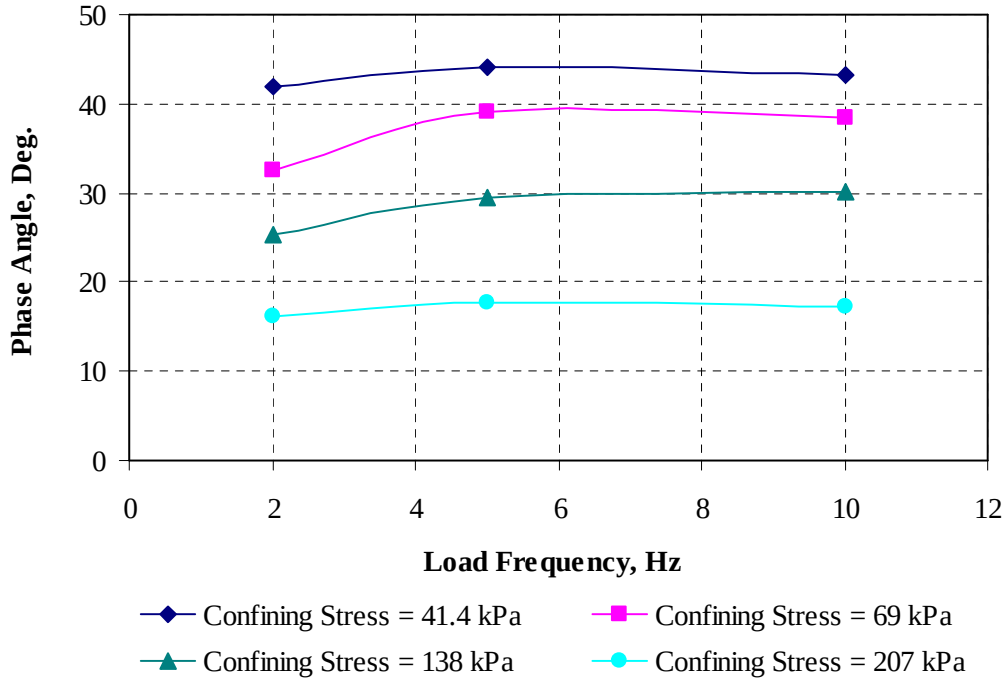

(b) Temperature = 30°C

FIGURE 8.27 Effect of Loading Frequency on Phase Angle for AU-14.

8.4.3 Characterization Models for the Oil Sand Materials

8.4.3.1 Statistical Analyses and Model Development

All the 6,000 data points generated for each oil sand sample at the two test temperatures were used for developing material characterization models. To model the dynamic behavior under the test conditions described in this chapter, there was a need to include all the important controlling variables in the model development. The main variables considered for the model development included the applied stress states, the test loading conditions and three gradation properties (Cu, Cc and D_{50}) of the oil sand materials. However, it was found that both dynamic modulus and damping ratio have little correlation with all the three gradation properties ($R^2 < 0.1$). Therefore, the applied stress states, temperature and bitumen content were mainly used for modeling the oil sands. A close examination of the test results obtained for the three oil sand materials at the different test conditions indicate that the individual databases of the three oil sand materials could be combined for the analyses. The SAS software package was used to perform nonlinear multiple regression analyses to establish characterization models for the oil sand materials.

Tables 8.8 and 8.9 summarize the dynamic modulus and damping ratio models developed for the oil sands and gives the model parameters obtained from the stepwise multiple regression analyses. All the models produced significantly high correlation coefficients (R^2) from the analyses. The inclusion of temperature and bitumen content in model 3 made it more comprehensive for field loading conditions and improved the goodness of the regression fit. As a result, model 3 has been selected to be more suitable for investigating the behavior of oil sand materials.

TABLE 8.8 Regression Models Studied for Dynamic Modulus of Oil Sand Materials

Model	Dynamic Modulus (MPa)
1	$\lvert E^* \rvert = A \cdot \theta^{k_1}$
2	$\lvert E^* \rvert = A \cdot \theta^{k_1} \cdot w_b^{k_2}$
3	$\lvert E^* \rvert = A \cdot \theta^{k_1} \cdot w_b^{k_2} \cdot T^{k_3}$

Model	Model Parameters					
	Log A	k_4	k_5	k_6	R^2	*RMSE*
1	-2.355	1.701			*0.644*	*0.298*
2	-1.539	1.713	-0.070		*0.780*	*0.236*
3	0.993	1.715	-0.070	-1.826	*0.887*	*0.170*

TABLE 8.9 Regression Models Studied for Damping Ratio of Oil Sand Materials

Model	Damping Ratio (%)
1	$D = A \cdot \varepsilon_1^{k_4}$
2	$D = A \cdot \varepsilon_1^{k_4} \cdot \theta^{k_5}$
3	$D = A \cdot \varepsilon_1^{k_4} \cdot \theta^{k_5} \cdot T^{k_6}$

Model	Model Parameters					
	Log A	k_4	k_5	k_6	R^2	*RMSE*
1	1.811	0.364			*0.830*	*0.083*
2	2.274	0.278	-0.228		*0.855*	*0.077*
3	1.902	0.213	-0.341	0.409	*0.878*	*0.071*

8.4.3.2 Master Curves and Sigmoidal Models for Oil Sand Samples

The master curve-sigmoidal function analytical approach for estimating dynamic modulus of asphalt materials at different temperatures and loading frequencies was explored to analyze the oil sand test data. Since the current oil sand research focused on determining material properties at temperatures of 20°C and 30°C and loading frequencies of 2, 5, and 10Hz, the master curves were based on only the selected temperatures and loading frequencies.

At different confining stresses, master curves were obtained to determine dynamic modulus of the oil sand materials at the test temperatures using temperature shift factors. Separate master curves were constructed for individual oil sand samples using the two test temperatures and three loading frequencies at different confining stresses. A nonlinear least square regression technique was used to fit the data with sigmoidal function defined in Equation 8.5. Using the time-temperature superposition principle, test data were then shifted horizontally relative to the temperature 30^{o}C. Detailed construction of master curves and corresponding shift factor has been well documented in the Mechanistic-Empirical Pavement Design Guide (NCHRP 1-37A 2004).

$$\log\left|E^{*}\right| = \delta + \frac{\alpha}{1+e^{\beta - \gamma \log f_r}} \tag{8.5}$$

where,

$\left|E^{*}\right|$ = dynamic modulus;

f_r = reduced frequency defined in Equation 8.6;

$\delta + \alpha$ = minimum modulus value;

β, γ = parameters describing the shape of the sigmoidal function.

Note that δ in Equation 8.5 is not related to phase angle. The parameter γ influences the steepness of the function (rate of change between minimum and maximum) and β is the horizontal position of the turning point. Parameters δ and α depend on aggregate gradation, binder content, and air void content, whereas β and γ depend on the characteristics of the asphalt binder and the magnitude of δ and α (NCHRP 1-37A 2004).

$$\log f_r = \log f + \log a(T) \text{ or } a(T) = \frac{f_r}{f} \tag{8.6}$$

where, a(T) = shift factor as a function of temperature, f = loading frequency at any temperature and T = test temperature.

Using Equation 8.6, the reduced frequency at the reference temperature can be calculated for any frequency at any temperature. The dynamic modulus can then be calculated from Equation 8.5 using the reduced frequency. The shift factor defines the amount of shift at a given temperature. In this study, The Williams-Landel-Ferry (WLF) equation for master curve construction was used to determine the shift factors for the master curves. The WLF equation was used because of the moderate test temperatures, i.e., 20^{o}C and 30^{o}C for this study. The WLF equation is expressed as follows:

$$\log a_T = -\frac{C_1 (T - T_{ref})}{C_2 + T - T_{ref}} \tag{8.7}$$

where, C_1 and C_2 are constants, T_{ref} = the reference temperature and a_T = the shift factor, which is expressed as a function of temperature of interest, T.

Table 8.10 summarizes the sigmoidal model parameters for the three oil sand samples and Figures 8.28 through 8.30 show master curves developed for the three oil sand samples at different confining stresses. At the various confining stresses, the upper range of the sigmoidal function approaches asymptotically to the maximum value of the dynamic modulus of the oil sand materials. On the other hand, at higher loading frequencies, the dynamic modulus starts to approach a limiting equilibrium value in all the oil sand materials. Thus, the sigmoidal function captures the effects of loading conditions of the oil sand materials. The shift factors for the master curves of individual oil sand samples are presented in Table 8.11.

TABLE 8.10 Model Parameters for the Master Curves for the Oil Sands

σ_3 (kPa)	δ	α	β	γ
SE-09 Sample				
41.4	1.240	0.960	2.982	-2.242
69	-7.945	10.452	-2.654	-0.462
138	2.248	0.532	1.621	-0.627
207	2.303	1.754	2.349	-0.769
SE-14 Sample				
41.4	0.486	4.818	2.541	-0.833
69	-2.079	5.518	-0.259	-0.335
138	1.106	1.210	1.708	-2.838
207	1.784	0.733	2.943	-4.198
AU-14 Sample				
41.4	1.035	0.723	6.332	-5.792
69	0.900	4.879	3.020	-1.148
138	1.649	0.742	2.519	-3.145
207	2.188	0.329	5.093	-5.649

TABLE 8.11 Shift Factors Developed for Dynamic Modulus Master Curves

Confining Stress (kPa)	SE-09		SE-14		AU-14	
	20°C	30°C	20°C	30°C	20°C	30°C
41.4	1.068	0	0.658	0	0.400	0
69	1.807	0	1.216	0	0.582	0
138	1.594	0	1.060	0	0.979	0
207	0.431	0	0.788	0	0.906	0

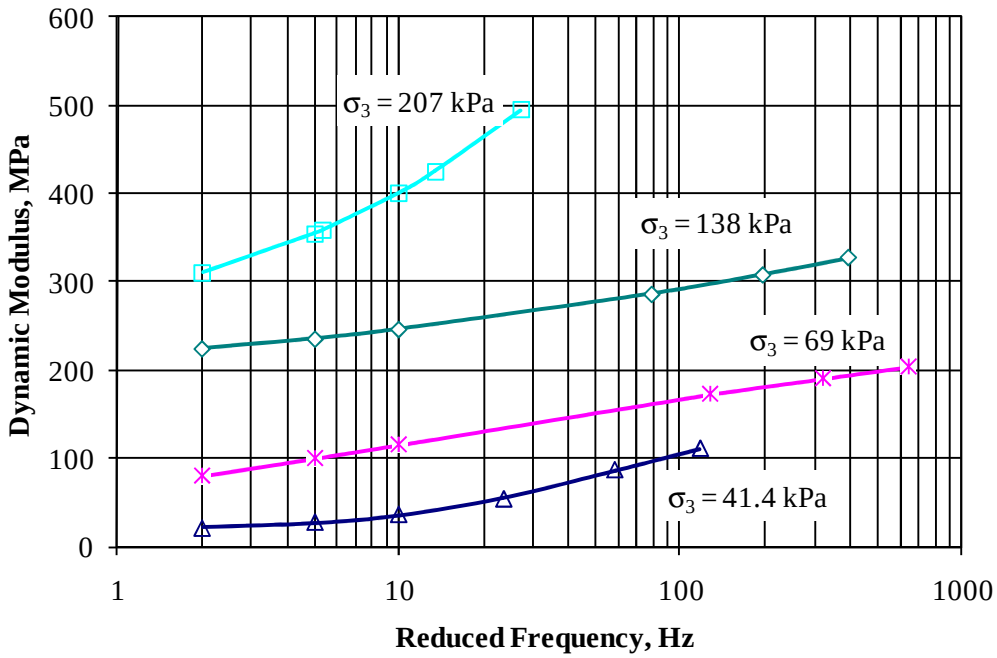

FIGURE 8.28 Master Curves for SE-09 Oil Sand Sample.

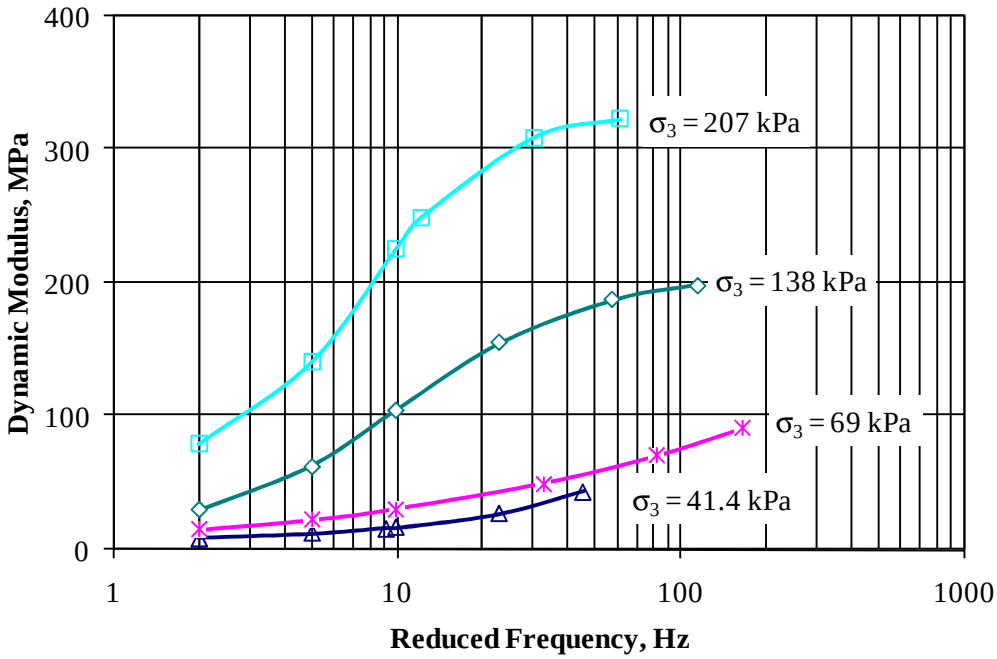

FIGURE 8.29 Master Curves for SE-14 Oil Sand Sample.

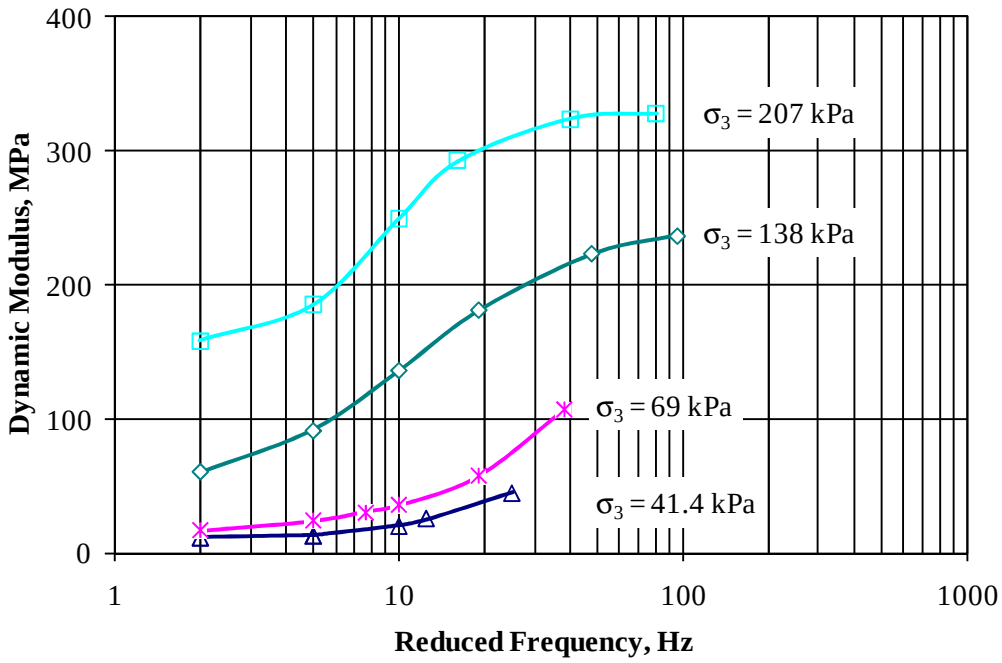

FIGURE 8.30 Master Curves for AU-14 Oil Sand Sample.

8.5 Summary

A newly developed damping property test procedure was used to investigate damping ratio, dynamic modulus and phase angle of one fine-grained cohesive soil and three oil sand samples in the laboratory. The fine-grained soil samples were tested at optimum, dry of optimum and wet of optimum, and at three loading frequencies. The test results were used obtain empirical equations of damping ratio and dynamic modulus of the soils as functions of bulk stress and axial strain. The oil sand samples had bitumen contents of 8.5%, 13.3% and 14.5%, and they were tested at two temperatures and three load frequencies. For the oil sand samples material characterization models were developed for damping ratio and dynamic modulus using the applied bulk stress, axial strain, temperature, and bitumen content as the independent variables. Also, the sigmoidal function for asphalt materials was employed to develop models for the oil sand samples. High coefficient of correlation values obtained for the models developed for the oil sand samples implied that the models would perform well in the field.

The following conclusions can be drawn from this chapter:

1. The average damping ratio of the soil sample tested at optimum content was about 16% lower than the average damping ratio at wet of optimum, and 33% higher than the average damping ratio at dry of optimum. On the other hand, the average dynamic modulus at optimum was about 40% higher than the average dynamic modulus at wet of optimum, and 31% lower than dry of optimum. The average phase angle of the soil at optimum was generally lower than the average phase angle at wet of optimum and higher than dry of optimum.
2. The damping ratios of all the oil sand samples were generally higher at 30^{o}C than at 20^{o}C, while the dynamic moduli were higher at 20^{o}C than at 30^{o}C. The AU-14 sample had the highest damping ratio, and the SE-14 sample had the lowest damping ratio. On the average, the damping ratios of AU-14 were about 47% higher than those of SE-09 at both test temperatures. On the other hand, the average dynamic moduli of SE-09 sample were about 2.5 times of the average dynamic moduli of the AU-14 sample. No significant differences were found between damping ratio and dynamic modulus of the AU-14 and SE-14 samples. At the same time, the phase angles of the AU-14 sample were comparable to those of SE-14 sample. Generally the phase angles of the AU-14 sample were the highest, and the phase angles of SE-09 were the lowest.
3. There was essentially no significant effect of loading frequency on damping ratio, phase angle and dynamic modulus of the soil sample at all the moisture states. Thus, the single most important parameter that affected the behavior of the soil sample was water content. Similarly, for the oil sand samples, there was little or no significant effect of loading frequency on damping ratio and phase angle. However, as loading frequency increased, the dynamic modulus of the oil sand samples increased. The test temperature and bitumen content of an oil sand had a major influence on the dynamic modulus and damping ratio of oil properties.

CHAPTER 9 SUMMARY, FINDINGS AND RECOMMENDATIONS

9.1 Summary and Conclusions

Large capacity off-road haul trucks and shovels, and other construction and mining equipment are often faced with rutting and sinkage, and other mobility (trafficability) problems during routine operations on certain fine-grained cohesive soils and naturally deposited oil sands. The existing laboratory test procedures and material characterization models are inadequate to address the dynamic loading behavior of these materials. A better understanding and proper modeling of strength and deformation behavior of the fine-grained soils and oil sand materials under static and dynamic loadings would result in less rutting and sinkage, and improved trafficability.

This research focused on developing laboratory test procedures to better characterize behavior of fine-grained soils and oil sand materials under field loading conditions of large capacity off-road construction and mining equipment. Overall, five newly developed and improved test procedures were established as a suite of tests to determine strength, stiffness and damping properties as well as permanent deformation characteristics of one fine-grained soils and three oil sand materials. Each test procedure was used to establish a comprehensive laboratory testing program to determine the engineering properties of the fine-grained soil sample, CAT A-6 soil, at moisture state chosen at the optimum moisture content, 3% below the optimum, and 3% above the optimum, and the three types of oil sand materials, SE-09, SE-14 and AU-14 with bitumen contents of 8.5%, 13.3% and 14.5% by weight, respectively. The test results provided extensive database of friction angle and cohesion strength properties, bulk modulus, shear modulus, resilient modulus, dynamic modulus, damping ratio, and permanent deformation properties for the soil and oil sand samples. Each database was analyzed to develop material property correlations and characterization models that incorporated loading conditions such as applied stress states, loading frequencies, test temperatures and oil sand bitumen contents as variables. Generally, the majority of the relationships established between the soil properties and the loading conditions were of empirical nature. The main reason is that only one sample of fine-grained soil was tested at this stage. On the other hand, material characterization models that considered field loading conditions were developed for three different oil sand samples having different

bitumen contents and sand types. The characterization models will be useful for describing field behavior of oil sand materials.

The newly developed and improved test procedures successfully applied static and dynamic stress states representative of field loading of off-road construction and mining equipment and provided static and dynamic material properties for one fine-grained soil and three types of oil sand materials. The range of material properties determined suggest that the test procedures could potentially serve as guidelines for the future development of standard test protocols for fine-grained cohesive soils and oil sand materials under typical loading conditions of construction and mining equipment. Moreover, the material property correlations and models developed may be used as practical predictive equations to estimate the strength and stiffness properties of fine-grained soils and oil sands, and predict the amount of rutting and sinkage in oil sand materials under typical field loading conditions.

The following lists specific findings and conclusions drawn from the study.

- A comprehensive literature review indicated that the dynamic behavior of fine-grained cohesive soils and oil sand materials under construction and mining equipment have not been studied extensively in the laboratory. Research on these materials has traditionally focused on obtaining laboratory stress-strain test data to describe shear strength and elastic behavior of oil sands. Based on the data collected in these studies, confining pressure, peak stress or strain, friction angle and cohesion are the material properties used for modeling the strength and elastic behavior.
- The single most important parameter that affected strength, stiffness and damping behavior of the soil tested (CAT A-6 soil) was moisture content. The strength and stiffness properties generally increased for the 3% dry of optimum condition and decreased for the 3% wet of optimum. There was essentially no significant effect of loading frequency on damping ratio, phase angle and dynamic modulus of the soil sample at the three moisture states. The damping ratio values of the CAT A-6 soil increased with increasing moisture content.
- Bitumen contents of the oil sand materials in general affected stiffness and permanent deformation properties. The Suncor Energy low grade oil sand sample

(SE-09) with bitumen content of 8.5% was found to be the stiffest sample, whereas the Aurora high grade oil sand sample (AU-14) with bitumen content of 14.5% generally appeared as the softest. The amount of bitumen content appears to be the main factor that explains the difference observed in the permanent deformation trends for the oil sands. The SE-09 sample, with the lowest bitumen content, had the lowest permanent strain accumulation, whereas AU-14 sample with the highest bitumen content generally had the highest accumulation of permanent strain. The effect of bitumen content on the material properties of the Suncor Energy high grade oil sand sample (SE-14) with bitumen content of 13.3% appear to be similar to Aurora high grade oil sand sample.

- The test temperature, loading frequency and applied stress states significantly affected the laboratory determined material properties of the oil sands. The modulus generally decreased with increasing temperature and decreasing loading frequency, whereas damping ratio increased with increasing temperature. However, there was little or no significant effect of loading frequency on damping ratio and phase angle of the oil sand materials. Also, no significant effect of temperature was found on the shear strength properties of the oil sand samples. The applied stress states had significant influence on permanent deformation accumulation in the three oil sand materials. As the deviator stress increased, both the magnitude and the accumulation rate of the permanent deformation increased in all the three oil sand materials. Also, permanent strain accumulation rates generally decreased as the magnitude of the confining pressure increased. Thus, permanent strains accumulated in the oil sand materials related directly to deviator stress and inversely to confining pressure. Applied principal stress ratios (σ_1/σ_3) more significantly influenced permanent deformation and the rate of accumulation than the applied deviator and confining stresses. The permanent strains became larger as the confinement levels decreased and the principal stress ratios increased.
- The oil sand materials and fine-grained cohesive soils appeared to have similar stress softening modulus behavior. The shear modulus and resilient modulus generally decreased as the applied deviator stress increased. On the other hand,

the stiffness trends of oil sand materials under different temperatures and loading frequencies were typical of asphalt materials.

- The newly developed pure shear loading test procedure provided lower shear modulus values than the results obtained from the standard cyclic triaxial test procedure. Therefore, pure shear test appears to be more conservative for characterizing shear modulus compared with the standard cyclic triaxial test.
- Since cylindrical test specimens did not undergo shear failures in triaxial testing, the direct shear test procedure was more applicable for determining shear strength properties of oil sand materials than triaxial shear testing.

9.2 Recommendations for Future Research

Based on the findings of this research study, the following recommendations are made for further research:

1. For fine-grained soils, the study was limited to one type of soil sample. It is important to include different types of cohesive soils and develop additional characterization models to evaluate their field loading behavior. Further laboratory studies can consider fine-grained cohesive soils at different density levels to evaluate density effect on dynamic material properties. There is a need to perform permanent deformation tests to predict sinkage or rutting potential in the soils.
2. There is a need to investigate the rheological properties of bitumen in oil sand materials. Particularly, further study to determine viscosity of the three oil sand materials at the test temperatures is recommended. Results from such a study can provide additional verification of stiffness behavior exhibited by the oil sand materials. It will also provide additional knowledge on the effect of bitumen contents on the material properties of the oil sands.
3. The effectiveness of the developed laboratory test procedures should be validated through expanded test program to include additional soil and oil sand samples. For instance, the laboratory test program could be performed under several loading conditions to verify the repeatability of test results. In particular, temperature effect on oil sand behavior need further study.

4. Further validation and verification of the models can be accomplished using the results of additional laboratory tests and field test, which can be performed on fine-grained soils and oil sand samples obtained from several construction and oil sand mining fields.
5. Further studies are recommended for shear strength testing of oil sand materials using triaxial testing condition. This time, samples could be tested at different loading rates to observe the shear strength properties.

REFERENCES

Adu-Osei, A. *Characterization of Unbound Granular Layers in Flexible Pavements.* PhD dissertation. Texas A & M University, 2000.

Agar, J.G., Morgenstern, N.R., and Scott, J.D. Shear Strength and Stress-Strain Behavior of Athabasca Oil Sand at Elevated Temperatures and Pressures. *Canadian Geotechnical Journal,* Vol. 24, 1987, pp. 1-10.

Agar, J.G., Morgenstern, N.R., and Scott, J.D. Geotechnical Testing of Alberta Oil Sands at Elevated Temperatures and Pressures. *Proc., 24th U.S. Symposium on Rock Mechanics,* June 1983, pp. 795-806.

Alavi, S.H. *Viscoelastic and Permanent Deformation Characteristics of Asphalt-Aggregate Mixes Tested as Hollow Cylinders and Subjected To Dynamic Axial and Shear Loads.* PhD Thesis, University of California, Berkeley, CA, 1992.

Al-Qadi, I.L and Rivera-Ortiz, L.A. Use of Gravel Properties to Develop Arrester Bed Stopping Model. Journal of Transportation Engineering Vol. 117, N0. 5, 1991, pp. 566-584.

American Society for Testing and Materials, Annual Book of ASTM Standards. Vol. 04.03, 2004.

Anochie-Boateng, J., Tutumluer, E., and Salami, M.R. Laboratory Evaluation of Subgrade Soils for a New Airport Runway. *Proc., 11th Annual Great Lakes Geotechnical /Geoenvironmental Conference, on Advances in Characterizing and Engineering Problem Soils,* Purdue University, West Lafayette, IN, May 23, 2003.

Barksdale, R.D. Compressive Stress Pulse Times in Flexible Pavements for Use in Dynamic Testing. In *Highway Research Record 345,* HRB, National Research Council, Washington, D.C., 1971, pp 32-44.

Barksdale, R.D. Laboratory Evaluation of Rutting in Base course Materials. *Proc., 3rd International Conference on Structural Design of Asphalt Pavements,* 1972, pp. 161-174.

Barksdale, R.D. Practical Application of Fatigue and Rutting Tests on Bituminous Base Mixes. *Association of Asphalt Paving Technologists,* St. Paul, MN, 1987, pp. 115-159.

Barksdale, R.D. Rutting of Pavement Materials. Report, School of Engineering, Georgia Institute of Technology, Atlanta, GA, 1973.

Barksdale, R.D. Test Procedures for Characterizing Dynamic Stress-Strain Properties of Pavement Materials. *Transportation Research Board Special Report 162,* 1975, pp. 1-40.

Bejarano, M.O., and Thompson, M.R. S*ubgrade Soil Evaluation for the Design of Airport Flexible Pavements.* Technical Report, DOT 95-C-001, Federal Aviation Administration, September 1999.

Bekker, M.G. Introduction to Terrain-Vehicle Systems. The University of Michigan Press, Ann-Arbor, 1969.

Bekker, M.G. *Off the road Locomotion, the Mechanics of Vehicle Mobility*. The University of Michigan Press, Ann-Arbor, 1960.

Bekker, M.G. *Theory of Land Locomotion, the Mechanics of Vehicle Mobility*. The University of Michigan Press, Ann-Arbor, 1956.

Bernstein, R. Probleme zur experimentellen Motorpflugmechanik. Der Motorwagen 16, 1913.

Boateng-Poku, Y., and Drumm, E.C. Hyperbolic Model for the Resilient Modulus Response of Fine-Grained Soils. Geotechnical Special Publication No.24, American Society of Civil Engineers, 1989.

Boyce, J.R. A Non-Linear Model for Elastic Behavior of Granular Materials under Repeated Loading. *International Symposium on Soils under Cyclic and Transient Loading,* Swansea, 1980.

Boyce, J.R. *The Behavior of a Granular Material under Repeated Load*. Ph.D Thesis. University of Nottingham, Department of Civil Engineering, 1976.

Brown, S.F. The Characterization of Cohesive Soils for Flexible Pavement Design. In Proceedings, *7th European Conference on Soil Mechanics and Foundation Engineering*, Vol. 2, 1979, pp. 15-22.

Brown, S.F., and Hyde, A.F.L. The Significance of Cyclic Confining Stress in Repeated Triaxial Testing of Granular Material. *Transportation Research Record S37*, TRB, 1975, pp. 49-58.

Button, J.W., Epps, J.A., and Gallaway, B.M. Properties of Bituminous Binders Derived from Oil Shale and Tar Sands. *7th Interamerican Conference on Materials Technology*, Mexico, D.F., 1981, pp. 697-703.

Cameron, R., and Lord, E. R. F. Compaction Characteristics of Athabasca Tar Sand and its Suitability as a Backfill Material. *Proc., 4th International Conference on Heavy Crude and Tar Sands*, Edmonton, Alberta, Vol. 3, 1988, pp. 107-115.

Carpenter, S., and Vavrik, W. Repeated Triaxial Testing during Mix design for Performance Characterization. In *Transportation Research Record 1767*, TRB, National Research Council, Washington, D.C., 2001, pp. 76-84.

Caterpillar Performance Handbook, 36th ed., Caterpillar Inc., Peoria, Illinois, 2006.

Chang, F.K., and Brown, S.F. Significance of Principal Stress Rotation in Pavements. *Proc., 13th International Conference on Soil Mechanics and Foundation Engineering*, Delhi, Vol. 4, 1984, pp. 1823-1826.

Chatterji, P.K., Smith, L.B., and Insley, A.E. Construction of Saline Creek Tunnel in Athabasca Oil Sand. *Canadian Geotechnical Journal*, Vol. 16, 1979, pp. 90-106.

Clyne, T. R., Li, X., Marasteanu, M. O., and Skok, E. L. Dynamic and Resilient Modulus of MN DOT Asphalt Mixtures. Report No. MN/RC-2003-09, 2003, Minnesota Department of Transportation, Minneapolis, MN.

Curtis, B., Crockford, B., and Lytton, R. Comparison of Alternative Test Methods for Predicting Asphalt Concrete Rut Performance. *Proc., 44th Annual Conference of Canadian Technical Asphalt Association*, Vol. XLVL, 1999, pp. 405-434.

Dawson, R.F., Sego, D.C., and Pollock, G.W. Freeze-Thaw Dewatering of Oil Sands Fine Tails. *Canadian Geotechnical Journal*, Vol. 36, December 1999, pp. 587-598.

Duncan, J.M. Hyperbolic Stress-Strain Relationships. *In Proc., of the Workshop on Limit Equilibrium, Plasticity, and Generalized Stress-Strain in Geotechnical Engineering*, McGill University, May 28-30, 1980, pp. 443-460.

Duncan, J.M., and Chang, C-Y. Nonlinear Analysis of Stress and Strain in Soils. *Journal of the Soil Mechanics and Foundations Division,* ASCE, Vol. 96, No. SM5, September, 1970, pp. 1629-1653.

Dusseault, M.B. Sample Disturbance in Athabasca Oil Sand. *The Journal of Canadian Petroleum Technology,* Vol. 19, No. 2, 1980, pp. 85-92.

Dusseault, M.B. Stress and Volume Changes in Gas-Saturated Very Dense Sands. *1st International Conference on the Future of Heavy Crude Oils and Tar Sands,* 1981, pp. 312-320.

Dusseault, M.B. Stress State and Hydraulic Fracturing in the Athabasca Oil Sands. *Journal of Canadian Petroleum Technology,* Vol. 16, 1977, pp. 19-27.

Dusseault, M.B. The Behavior of Hydraulically Induced Fractures in Oil Sands. *13th Canadian Rock Mechanics Symposium,* Vol. 22, 1980, pp. 36-41.

Dusseault, M.B. Undrained Volume and Stress Change Behavior of Unsaturated Very Dense Sands. *Canadian Geotechnical Journal,* Vol.16, 1979, pp. 627-640.

Dusseault, M.B., and Hans, R.V.D. Unconsolidated Sand Sampling in Canadian and Venezuelan Oil Sands. *2nd International Conference on the Future of Heavy Crude Oils and Tar Sands,* Caracas, Venezuela, February 1-17, 1982.

Dusseault, M.B., and Morgenstern, N. R. Shear Strength of Athabasca Oil Sands. *Canadian Geotechnical Journal,* Vol. 15, 1978b, pp. 216-238.

Dusseault, M.B., and Morgenstern, N.R. Characteristics of Natural Slopes in the Athabasca Oil Sands. *Canadian Geotechnical Journal,* Vol. 15, 1978a, pp. 202-215.

Fredlund, D.G., Bergan, A.T., and Wong, P.K. Relation between Resilient Modulus and Stress Conditions for Cohesive Subgrade Soils. *Transportation Research Record 642*, TRB, 1977, pp. 73-81.

Garg, N. and Thompson, M. R. *Mechanistic-Empirical Evaluation of the Mn/Road Low Volume Road Test Sections.* Final Project Report, Civil Engineering Studies, Transportation Engineering Series No. 96, University of Illinois Urbana-Champaign, Urbana, IL, 1998.

Garg, N., and Thompson, M.R. Triaxial Characterization of Mn/ROAD Granular Materials. In *Transportation Research Record 1577*, TRB, National Research Council, Washington, D.C., 1977, pp. 27-36.

Gould J.S., Nanagiri, Y.V., Mallick, R.B., Petruccelli, J.D., and Crockford, W.C. An Evaluation of use of Rapid Triaxial Test in Quality Control of Hot mix Asphalt (HMA). In *Transportation Research Record*, TRB 2003 Annual Meeting CD-ROM.

Hardin, B.O., and Black, W.L. Vibration Modulus of Normally Consolidated Clay. *Journal of Soil Mechanics and Foundation Engineering Division,* ASCE, Vol. 94 (SM2), 1968, pp. 353-369.

Hardin, B.O., and Drnevich, V.P. Shear Modulus and Damping in Soils: Design Equation and Curves. *Journal of Soil Mechanics and Foundation Engineering Division,* ASCE, Vol. 98 (SM7), 1972, pp. 667-691.

Harnisch, C., Lach, B., Jakobs, R. Troulis, M., and Nehls, O. A New Tyre-Soil Interaction Model for Vehicle Simulation on Deformable Ground. *Vehicle System Dynamics*, Vol. 43, Supplement, 2005, pp. 384-394.

Hicks, R. G., and Monismith, C. L. Factors Influencing the Resilient Response of Granular Materials. *Highway Research Board Record No. 345*. Washington D. C., 1971, pp. 15-31.

Hicks, R.G. Factors Influencing the Resilient Properties of Granular Materials. Ph.D. Thesis, University of California, Berkley, 1970.

Hovland, J.H. Mechanics of Wheel-Soil Interaction. Prepared for NASA Headquarters, Washington, D.C., Under NASA Grant NGR 05-003-406, April 1973.

Hsu, T.R., Chen, G.G., and Gong, Z.L. Technique for the Measurement of Dynamic Mechanical Properties of Oil Sands. *The Journal of Canadian Petroleum Technology*, Vol.24, No. 3, 1985, pp. 63-68.

Huang, Y.H. *Pavement Analysis and Design.* 1st Edition, Prentice Hall, Englewood Cliffs, NJ, 1993.

Ishibashi, I., and Sherif, M.A. Soil Liquefaction by Torsional Simple Shear Device. *Journal of Geotechnical Engineering*, ASCE, Vol. 100, No. GT8, 1974, pp. 871-888.

Janbu, N. Soil Compressibility as Determined by Oedometer and Triaxial Tests. *Proc., European Conference on Soil Mechanics and Foundations Engineering,* Wiesbaden, Germany, Vol. 1, 1963, pp. 9-25.

Janosi, Z., and Hanamoto, B. The Analytical Determination of Drawbar Pull as a Function of Slip, For Tracked Wheels in Deformable Soils. *Proc., of the 1st International Conference,* Mechanics of Soil-Vehicle System, Turin, Italy, 1961.

Joseph T.G., Sherif-Abadi A.D. & Shi N. A Broken Material Approach to Modeling Oil Sand under Dynamic Load. *Presentation in Calgary at CIM conference,* 2003.

Joseph, T.G. Oil Sands Reactions to Cable Shovel Motion," *CIM Bulletin,* Vol. 95, No. 1064, 2002b, pp. 62-64.

Joseph, T.G. OsEIP: The Oil Sands-equipment Interactions Program. *CIM Bulletin,* Vol. 95, No. 1064, 2002a, pp. 58-61.

Joseph, T.G. *Physical, Static and Inferred Dynamic Loaded Properties of Oil Sand.* Progress Report Phase I, CAT/0405, 2004.

Joseph, T.G. *Physical, Static and Inferred Dynamic Loaded Properties of Oil Sand.* Progress Report, Phases II, & III (Final Report), CAT/0405, 2005.

Khedr, S. Deformation Characteristics of Granular Base Course in Flexible Pavements. In *Transportation Research Record 1043*, TRB, National Research Council, Washington, D.C., 1985.

Kim, I. T. *Permanent Deformation Behavior of Airport Flexible Pavement Base and Subbase Courses.* PhD dissertation. University of Illinois, Urbana, 2005.

Kim, I.T., Tutumluer, E. Field Validation of Airport Pavement Granular Layer Rutting Predictions. In *Transportation Research Record: Journal of Transportation Research Board, No. 1952,* National Research Council, Washington D.C., 2006, pp 48-57.

Kondner, R.L. Hyperbolic Stress-Strain Response: Cohesive Soils. *Journal of the Soil Mechanics and Foundations Division,* ASCE, Vol. 89, No. SM1, February, 1963, pp. 115-143.

Kosar, K. M., Scott J. D., and. Morgenstern, N. R. Testing to Determine the Geotechnical Properties of Oil Sands. *Proc., 38th Annual Technical Meeting of Petroleum Society of CIM, Innovation and Optimization: Everyone's Challenge*, June 1987, 16 pages.

Kraft, D.C., Luming, H., and Hoppenjans, J.R. *Aircraft Landing Gear-Soils Interaction and Floatation Criteria, Phase II.* Technical Report, AFFDL-TR-69-76, Air force Flight Dynamics Laboratory, Wright-Patterson AFB, Ohio, November 1969.

Kramer, S.L. *Geotechnical Earthquake Engineering.* Prentice Hall, Upper Saddle River, NJ 07458, 1996.

Ladd, D., and Ulery, H., Jr. *Aircraft Ground Floatation Investigation.* Technical Documentary Report, AFFDL-TDR-66-43, Part I, Air force Flight Dynamics Laboratory, Wright-Patterson AFB, Ohio, August, 1967.

Lade, P.V., and Nelson. Modeling the Elastic Behavior of Granular Materials. International Journal for Numerical and Analytical Methods in Geomechanics, Vol. 11, 1987, pp. 521-542.

Lashine, A.K., Brown, S.F., and Pell, P.S. *Dynamic Properties of Soils.* Report No. 2, University of Nottingham, Nottingham, England, 1971.

Lekarp, F., Isacsson, U., and Dawson, A. Permanent Strain Response of Unbound Aggregates. *Journal of Transportation Engineering*, Vol. 126, No.1, 2000, pp. 76-83.

Leung, S.K., Kry, P.R., and Wong, R.C.K. Visualization of Deformation in Unconsolidated Athabasca Oil Sand. *Proc., International Heavy Oil Symposium*, Calgary, Alberta, Canada, No. 200093, June 1995, pp. 637-645.

Li, P., and Chalaturnyk, R.J. Geomechnanical Model of Oil Sands. *SPE International Thermal Operations and Heavy Oil Symposium*, Calgary, Alberta, Canada, November, 2005, pp. B453-B457.

Lord, E. R.F., and Cameron, R. Compaction characteristics of Athabasca Tar Sand. *38th Canadian Geotechnical Conference*, Edmonton, AB, Canada, 1985, pp. 359-368.

Lord, E. R.F., and Cameron, R. Compaction characteristics of Athabasca Tar Sand and its Suitability as a Backfill Material. I*nternational Conference on Heavy Crude and Tar Sands*, Edmonton, AB, Canada, Paper No.3, 1988, pp. 107-115.

Loulizi, A., Al-Qadi, I.L., Lahouar, S., and Freeman, T.E. Measurement of Vertical Compressive Stress Pulse in Flexible Pavements and Its Representation for Dynamic Loading Tests. In *Transportation Research Record 1816*, Washington, D.C., 2002, pp. 125-136.

Maccarini, M. A Comparison of Direct Shear Box Tests with Triaxial Compression Tests for a Residual Soil. Geotechnical and Geological Engineering, Vol. 11, 1993, pp. 69-80.

Maclaurin, E. B. The use of mobility numbers to describe the in-field tractive performance of pneumatic tires. *Proc., of the 10th International ISTVS Conference*, Kobe, Japan, August 20-24, 1990, pp. 177-186.

Maclaurin, E. B. The use of mobility numbers to predict the tractive performance of wheeled and tracked vehicles in soft cohesive soils. *Proc., of the 7th European ISTVS Conference*, Ferrara, Italy, 8-10. October 1997:391-398.

Macmillan, R. H. The Mechanics of Tractor - Implement Performance, *Theory and Worked Examples*, Textbook for Students and Engineers, University of Melbourne, October 2002, http://www.eprints.unimelb.edu.au

McRae, J.L. Theory for Predicting Performance of a Wheel in Soft Soil. Miscellaneous Paper No. 4-870, U.S. Army Engineers Waterways Experiment Station, Vicksburg, Mississippi, February 1965. *Paper Summarized in Journal of Terramechanics*, Vol. 4, No. 3, 1967.

Monismith, C.L., Ogawa, N., and Freeme, C.R. Permanent Deformation Characteristics of Subgrade Soils Due to Repeated Loading. In *Transportation Research Record 537*, TRB, National Research Council, Washington, D.C., 1985.

Moossazadeh, J., and Witzack, M.W. Prediction of Subgrade Moduli for Soil that Exhibits Nonlinear Behavior. In *Transportation Research Record 810*, TRB, National Research Council, Washington, D.C., 1981, pp. 9-17.

Morgan, J.R. The Response of Granular Materials to Repeated Loading. *Proceedings, 3rd Conference, Australian Road Research Board*, Sydney, 1966, pp. 1178-1192.

Morgenstern, N.R., and Scott, J.D. Oil Sand Geotechnique. *Geotechnical News*, 1997, pp. 102-106.

Morgenstern, N.R., Fair, A.E., and McRoberts, E.C. Geotechnical Engineering beyond Soil Mechanics – A Case Study. *Canadian Geotechnical Journal,* Vol. 25, August 1988, pp. 637-661.

Mossop, G.D. Geology of Athabasca Oil Sands. *Science,* Vol. 207, January 1980, pp. 145-152.

NCHRP 1-26. Calibrated Mechanistic Structural Analysis Procedure for Pavements. *Final Report, Phase 1,* Transportation Research Board, National Research Council, Washington D.C., 2000.

NCHRP 1-37A. *Development of the 2002 Guide for the Design of New and Rehabilitated Pavement Structures:* Phase II, 2004.

NCHRP 1-37A. Development of the Mechanistic-Empirical Design Guide of New and Rhabilitated Pavement Structures. http://www.trb.org/mepdg/guide.htm, 2004.

O'Reilly, M.P., and Brown, S.F. *Cyclic Loading of Soils: From Theory to Design.* Department of Civil Engineering, University of Nottingham, Blackie and Son Ltd., 1991.

Quabin, B.S., Kaliakin, V.N., and Martin, J.P. Variable Bulk Modulus Constitutive Model for Sand. Journal of Geotechnical and Geoenvironmental Engineering, 2003, pp. 158-162.

Reece, A.R. Curve Fitting Technique in Soil Vehicle Mechanics. Journal of Terramechanics, Vol.1, No. 2, 1964, pp. 44-55.

Richmond, L.D., DeBord, K.G., and Fuller, J.R. *Aircraft Dynamic Load from Substandard Landing Sites.* Phase I, Interim Technical Report D6-16190, The Boeing Company, Renton, Washington, November, 1965.

Round, G.F. Shear Strength of McMurray Oil Sands. *The Canadian Mining and Metallurgical Bulletin,* Vol. 53, No. 576, 1960, pp. 233-238.

Saarilahti, M. *Soil Interaction Model: Manual 1.* Seltra-Documentation of the Computer Programme for Calculating of the Trafficability of Terrain and the Mobility of Forest Tractors. University of Helsinki May 2002.

Samieh, A. M., and Wong, R.C.K. Deformation of Athabasca oil sand in Triaxial Compression Tests at Low Effective Stresses under Varying Boundary Conditions. *Canadian Geotechnical Journal,* Vol. 34, 1997, pp. 985-990.

Samieh, A. M., and Wong, R.C.K. Modeling the Responses of Athabasca Oil Sand in Triaxial Compression Tests at Low Pressure. *Canadian Geotechnical Journal,* Vol. 35, 1998, pp. 395-406.

Sasitharan, S., Robertson, P.K., Sego, D.C., and Morgenstern, N.R. Collapse Behavior of Sand. *Canadian Geotechnical Journal,* Vol. 30, March 1993, pp. 569-577.

Scott, J. D., and Hsu, T. R. Measurements of Thermophysical and Mechanical Properties of Oil Sands. *Proc., Tar Sand Symposium,* Jackson, Wyoming, July 7-10, 1986, 14 pages.

Scott, J.D., and Kosar, K.M. Geotechnical Properties of Athabasca Oil Sands. *Proc., WRI-DOE Tar Sand Symposium,* Vail, Colorado, June 26-29, 1984, 32 pages.

Scott, J.D., and Kosar, K.M. Design of Hot Foundations on Oil Sands. *Proc., Canadian Geotechnical Conference,* 1985, pp. 111-121.

Scott, J.D., and Kosar, K.M. Thermal Expansion of Oil Sands. *Proc., Forum on Subsidence due to Fluid Withdrawal,* Checotah, Oklahoma, USA, 1983 pp. 46-57.

Scott, J.D., Dusseault, M.B., and Carrier III, W.D. Behavior of the Clay/Bitumen/Water Sludge System from Oil Sands Extraction Plants. *Journal of Applied Clay Science,* Vol.1, March 1985, pp 207-218.

Scott, J.D., Robertson, P.K., and Wong, E.P. Development of a High Stress and Temperature Laboratory System to Measure Seismic velocities in Oil Sands. *Proc., Canadian Geotechnical Conference,* 1991, pp. 48/1-9.

Seed, H.B. Soil Liquefaction and Cyclic Mobility Evaluation for Level Ground during Earthquakes. *Journal of Geotechnical Engineering,* ASCE, Vol. 105, No. GT2, 1979, pp. 201-255.

Seed, H.B., and Idriss, I.M. *Soil Moduli and Damping Factors for Dynamic Response Analyses.* Report EERC 70-10. Earthquake Engineering Research Center, University of California, Berkeley, CA, 1970.

Settari, A., Ito, Y., Fukushima, N., and Vaziri, H. Geotechnical Aspects of Recovery Processes in Oil Sands. *Canadian Geotechnical Journal,* Vol. 30, 1993, pp. 22-33.

Seyhan, U and Tutumluer, E. Anisotropic Modular Ratios As Unbound Aggregate Performance Indicators. *Journal of Materials in Civil Engineering,* 2002, pp. 1-8.

Seyhan, U. *Characterization of Anisotropic Granular Layer Behavior in Flexible Pavements.* PhD dissertation. University of Illinois, Urbana, 2002.

Smith, W.S., and Nair, K. Development of Procedures for Characterization of Untreated Granular Base Course and Asphalt-Treated Base Course Materials. FHWA, FHWA-RD, 1973, pp. 61-74.

Sousa, J.B., and Monismith, C.L. Dynamic Response of Paving Materials. *Transportation Research Record 1136*, TRB, 1987, pp. 57-68.

Standard Specifications for Transportation Materials and Methods of Sampling and Testing, 22nd ed. AASHTO, Washington, D.C., 2002.

Sweere, G.T.H. *Unbound Granular Bases for Roads.* PhD dissertation. University of Delft, Delft, The Netherlands, 1990.

Tao, J. G., Wang, L., Deng, Z. Q., Gao, H. B., and Quan, Q. Q. Mechanical Analysis and Measurement of Parameters of Wheel-Soil Interaction for a Lunar Rover. *Journal of Physics: Conference Series,* Vol. 48, No. 1, 2006, pp. 1222-1226.

Terzaghi, K., and Peck, R. B. *Soil Mechanics in Engineering Practice, 2nd ed.* Wiley, New York, 1967.

Thompson, M.R. Important Properties of Base and Subgrade Materials. *Proc., Conference on Crushed Stone and Street Construction and Reconstruction,* National Crushed Stone Association, 1984a.

Thompson, M.R. Subgrade Stability. In *Transportation Research Record 705*, TRB, National Research Council, Washington, D.C., 1979.

Thompson, M.R., and Nauman, D. Rutting Rate Analyses of the AASHO Road Test Flexible Pavements. In *Transportation Research Record 1384*, TRB, National Research Council, Washington, D.C., 1993.

Thompson, M.R., and R.P. Elliott. ILLI-PAVE Based Response Algorithms for Design of Conventional Flexible Pavements. In *Transportation Research Record 1043,* TRB, National Research Council, Washington, D.C., 1985, pp. 50-57.

Thompson, M.R., and Robnett, Q.L. Resilient Properties of Subgrade Soils. *Transportation Engineering Journal,* ASCE, Vol. 105, No. TE1. 1979.

Tseng, K.-H. and Lytton, R.L. Prediction of Permanent Deformation in Flexible Pavements. Implication of Aggregates in the Design, Construction, and Performance of Flexible Pavements, ASTM STP 1016, H.G. Schreuders and C.R. Marek, Editors, American Society of Testing and Materials, Philadelphia, 1989, pp. 154-172.

Turnage, G. W. *Performance of soils under tire loads. Application of Test Results to Tire Selection for Off-Road Vehicles.* US Army Waterways Experiment Station, Report No. 6. Technical Report No. 3-666, 1972c.

Tutumluer, E. *Predicting Behavior of Flexible Pavements with Granular Bases*. PhD Thesis, Georgia Institute of Technology, Atlanta, GA, 1995.

Tutumluer, E., and Seyhan, U. Laboratory Determination of Anisotropic Aggregate Resilient Moduli using a New Innovative Test Device. In *Transportation Research Record: Journal of Transportation Research Board, No. 1687*, National Research Council, Washington D.C., 1999, pp 13-21.

Tutumluer, E., and Thompson, M.R. Anisotropic Modeling of Granular Bases in Flexible Pavements. In *Transportation Research Record 1577*, TRB, National Research Council, Washington, D.C., 1997a, pp. 18-26.

Tutumluer, E., and Thompson, M.R. Granular Base Moduli for Mechanistic Pavement Design. *Proc., ASCE Airfield Pavement Conference*, Seattle, WA, August, 1997b, pp. 33-47.

Universal Testing Machine (UTM) Reference Manuals, Industrial Process Controls Ltd., (IPC) Melbourne, Australia, 1988.

Uzan, J. Characterization of Granular Materials. In *Transportation Research Record 1022*, TRB, National Research Council, Washington, D.C., 1985, pp. 52-59.

Uzan, J., Witczak, M.W., Scullion, T., and Lytton, R.L. Development and Validation of Realistic Pavement Response Models. *In Proceedings of the 7th International Conference on Asphalt Pavements,* Nottingham, UK, Vol. 1, 1992, pp. 334-350.

Vesic, A.B., Clough, G.W. Behavior of Granular Material under High Stresses. Journal of the Soil Mechanics and Foundation Division, Vol. 3, No. 94, 1968, pp. 661-668.

Walters, D.A., and Wong, R. C. K. Mechanical Characterization of an Oil Sand Fracture. *2nd North American Rock Mechanics Symposium*, Montreal, Quebec, Canada, June 1996, Vol. 2, pp.1383-1390.

Walters, D.A., and Wong, R. C. K. The Hydraulic and Mechanical Response of an Oil Sand Fracture under a Varying Confining Pressure. *Canadian Geotechnical Journal*, Vol. 36, 1999, pp. 262–271.

Wong, J.Y. Terramechanics and Off-Road Vehicles. Amsterdam, The Netherlands: *Elsevier Science Publishers B.V.*, 1989.

Wong, J.Y. *Theory of Ground Vehicles.* 3rd ed., John Wiley & Sons, Inc., New York, 2001.

Wong, J.Y., Garber, M., and Preston-Thomas, J. Theoretical Prediction and Experimental Substantiation of Ground Pressure Distribution and Tractive Performance of Tracked Vehicles. *Proc., Institute of Mechanical Engineers,* Part D, Transport Engineering, Vol. 198, No. D15, 1984.

Wong, R. C. K. Mobilized Strength Components of Athabasca Oil Sand in Triaxial Compression. *Canadian Geotechnical Journal*, Vol. 36, 1999, pp. 718-735.

Wong, R. C. K. Sand Production in Oil Sand under Oil Foamy Flow. *The Journal of Canadian Petroleum Technology*, Vol.42, No. 3, 2003, pp. 56-61.

Wong, R. C. K. Strength of Two Structured Soils in Triaxial Compression. *International Journal for Numerical and Analytical Methods in Geomechanics,* John Wiley and Sons Ltd., New York, N.Y, 2001, pp. 131-153.

Wong, R. C. K. Stress-Strain Response of Cold Lake Oil Sands. *Canadian Geotechnical Journal*, Vol. 30, 1993, pp. 220-235.

Wong, R. C.K. Strain-Induced Anisotropy in Fabric and Hydraulic Parameters of Oil Sand in Triaxial Compression. *Canadian Geotechnical Journal*, Vol. 40, April 2003, pp. 489-500.

Wong, R.C.K. Effect of Oil Sands Core Disturbance Induced by Gas Exsolution on Geotechnical and Hydraulic Properties Measurements. *The Journal of Canadian Petroleum Technology*, Vol. 44, No. 9, 2005, pp. 44-50.

AUTHOR'S BIOGRAPHY

Joseph Kojo Anochie-Boateng was born in Kumasi, Ghana to Mr. Simon Kofi Barimah-Boateng and Madam Agnes Adwoa Nyarko Fordjour. He received his Bachelor of Science degree in Civil Engineering from University of Science and Technology, Ghana in 1994. After his undergraduate studies, he worked with Wahome Steel Company, a leading steel manufacturing and construction company in West Africa, for five years. During this period, he supervised the design and construction of several steel structures for manufacturing companies and government agencies in Ghana. In January 2000, he relocated to the United States of America to pursue advanced studies in Civil Engineering. He completed a Master of Science in Civil Engineering with emphasis in Structures at North Carolina A & T State University, Greensboro in spring 2002. At North Carolina A & T State University, he was involved in Federal Aviation Administration (FAA) research on material selection and design of a new runway at Piedmont Triad International airport in Greensboro, North Carolina between Summer 2001 and Spring 2002. He evaluated the engineering properties of fourteen subgrade soils and three FAA base and subbase materials for the new runway. In Fall 2002, he began his doctoral studies at the University of Illinois at Urbana-Champaign Civil Engineering program with emphasis in Transportation Facilities Engineering. Under the guidance of Dr. Erol Tutumluer he performed several researches on transportation materials for highway and airport pavements. In addition, he performed extensive research studies on bituminous sand materials for Caterpillar Inc. Following completion of his Ph.D., he will begin work for the Council for Scientific and Industrial Research (CSIR) in South Africa as researcher of its Transportation Infrastructure Engineering research area. The North Carolina Board of Examiners for Engineers and Surveyors certified Joseph as Professional Engineer Intern in December, 2001.